Multi-Panel CLT Shearwalls: Experimental Assessment, Analytical Development, and Design Considerations

by

Mohammad Masroor

Thesis submitted to the University of Ottawa

in partial fulfillment of the requirements for the degree of

Doctor of Philosophy

in Civil Engineering

Under the auspices of the Ottawa-Carleton Institute for Civil Engineering

Department of Civil Engineering

Faculty of Engineering

University of Ottawa

Abstract

Analysis and design of Cross-Laminated Timber (CLT) walls under gravity loads have been outlined in the Canadian timber design standard with an adequate amount of details. The methods for designing shearwalls to resist lateral loads have not yet been fully developed, with only concepts being adopted, based on generalized capacity-based design concepts and definitions of yielding and non-yielding components. Several studies have focused on developing analytical expressions and design approaches for multi-panel CLT shearwalls, assuming angle brackets only behave in shear to prevent sliding, while ignoring compression zone effects in CLT panels. These assumptions may simplify the analysis, but they are not practical, especially since contemporary angle brackets are available on the market with uplift capacities comparable to those of hold-down connections.

This study aimed to investigate the lateral behaviour of multi-panel CLT shearwalls and provided practical and comprehensive analytical expressions and design procedures for this type of structure. The analysis aimed to integrate the effects of all boundary connections, including hold-downs, angle brackets, panel-to-panel connections, and compression zones, into the analysis. On the basis of the developed analytical expressions, a capacity-based design procedure was proposed, which promoted rocking behaviour and optimized energy dissipation in the shearwall system. A novel yield hierarchy among various connections was introduced, and expressions for associated over-strength factors are proposed. For multi-storey applications, an approach which ensures uniform energy dissipation along the structure height and limits soft-storey failures was also presented. Experimental tests were conducted at the connection level to study the performance of conventional connections used in CLT shearwalls and to obtain their associated mechanical properties. Furthermore, the performance of multi-panel CLT shearwalls was investigated by conducting wall-level experimental tests to investigate the kinematic modes and establish levels of resistance and deflection. Numerical models were developed to verify the mathematical accuracy of the proposed analytical and design expressions. Also, to validate the proposed analytical expressions, they were compared against the numerical models, as well as the wall-level experimental tests. The results showed a reasonable match between the different approaches in terms of the general shape of the curves and kinematic behaviour.

Acknowledgements

This study would not have been possible without the help and contributions of many individuals who have continued to be supportive and helpful over the course of my Ph.D. program. It is with pleasure that I extend my very first thanks to my supervisor, Dr. Ghasan Doudak, for all of his support and guidance over the past few years. The encouragement, ideas, and contributions of his expertise have illuminated many difficulties I have encountered and have helped me learn to lead the process in the most efficient manner possible. I would also like to acknowledge my colleague and friend, Dr. Daniele Casagrande. Without his continuous supervision and support this study could not have been completed.

My sincere appreciation is extended to the technical officers in the structural lab at the University of Ottawa, Dr. Muslim Majeed and Dr. Gamal Elnabelsya, who helped me enormously with their constructive ideas and advice concerning the experimental tests conducted during my studies. Also, I would like to thank Mr. Luc Cloutier and his colleagues in the Civil Engineering department for their kind assistance.

I have had the privilege of working with an excellent research team in the timber field. I would like to thank everyone who helped and collaborated with me to achieve the highest level of accuracy in the lab. My sincere thanks to Mohammadreza Khajehpour, Dario Markovinovic, Antoine Bérubé, Dalu Xing, and all my friends and colleagues.

I would like to acknowledge Nordic structures company from Montreal, Canada, and Rothoblaas from Italy for providing the CLT panels and steel connections and fasteners. These were used for connection and shearwall level experimental tests.

I would like to thank my family for their continued support and encouragement. My last, but not least, thanks go to my beloved wife for her support and patience during the most difficult times of my studies. All of this would not have been possible without her encouragement and light in the heart. I dedicate this thesis to you, my dearest Sepideh.

Table of Contents

List of Tables

List of Figures

List of symbols and notations

ASTM American society for testing and materials

CD Capacity-based design

CLT cross-laminated timber

CoV Coefficient of variation

EEEP Energy equivalent elastic-plastic

C_h ratio of the bending moment strength of the wall when the hold-down yields after yielding of the vertical joints while angle brackets remain elastic, $M_{r,h}^c$, to the applied moment due to lateral load, M_f

$C_{sw,j}$ over-capacity coefficient of the LLRS at storey j

$C_{sw,min}$ over-capacity coefficient of the weakest storey

D_{EEEP} ductility ratio obtained using EEEP simulation

$D_{trilinear}$ ductility ratio obtained using trilinear simulation

E_0 longitudinal CLT layers modulus of elasticity

E_{90} transverse CLT layers modulus of elasticity

$E_{eff,1}$ the effective moduli along the horizontal direction of CLT panels

$E_{eff,2}$ the effective moduli along the vertical direction of CLT panels

$E_{f,j}$ action due to the seismic load at storey j

$E_{f,ND}$ action affecting the non-dissipative element

E_g action due to the gravity load

$E_{r,ND}$ strength of the non-ductile elements

EI_{eff} elastic effective bending stiffness of the CLT panels

F concentrated lateral force applied on the top of the wall

F_j lateral horizontal load distributed in the j^{th} panel

F_{max} maximum load on load-displacement curves

$F_{y,EEEP}$ yield load on load-displacemenet curves based on EEEP simulation

$F_{y,trilinear}$ yield load on load-displacement curves based on trilinear simulation

F_u ultimate load on load-dispalcement curves

G equivalent shear deformation of CLT panels

G_{mean} shear modulus in-plane of laminations

K_{V,P_κ} lateral stiffness of the shearwall at point P_κ for $\kappa = [1: n_a + 2]$

$\widetilde{M}$ dimensionless moment ratio

M_f design bending moment due to the lateral load

$M_{f,j}^{i}$ bending moment acting at the bottom of shearwall i at storey j

M_q contribution of the stabilizing moment induced by the uniform vertical load

$M_{r,a}^{el}$ bending moment strength of the shearwall associated with the angle brackets yielding first, while all other connections remain elastic

$M_{r,c}^{el}$ bending moment strength of the shearwall associated with the point of yielding of the vertical joints, while all other connections remain elastic

$M_{r,h}^{el}$ bending moment strength of the shearwall associated with the point of yielding of the the hold-down, while all other connections remain elastic

$M_{r,a}^{c}$ bending moment strength of the shearwall associated with the point of yielding of the angle brackets, after the vertical joints have yielded while the hold-down remains elastic

$M_{r,h}^{c}$ bending moment strength of the shearwall associated with the yielding of the hold-down, after the vertical joints have yielded while the angle brackets remain elastic

$M_{r,j}^{i}$ bending moment strength of shearwall i at storey j, oriented parallel to the seismic shear force direction

$M_{y,x}$ yield bending moment in the horizontal direction to define macro elements

$M_{y,z}$ yield bending moment in the vertical direction to define macro elements

$\theta_{u,x}$ ultimate rotation in the horizontal direction to define macro elements

$\theta_{u,z}$ ultimate rotation in the vertical direction to define macro elements

$R_{C,1}$ the vertical reaction at the rotation point of the first panel

R_D design strength of the dissipative elements

$R_{D,5^{th}}$ 5^{th} percentile of dissipative elements' strength distribution

$R_{D,95^{th}}$ 95^{th} percentile of dissipative elements' strength distribution

R_{ND} design strength of the non-dissipative elements

$R_{D,an}$ strength of dissipative elements obtained from analytical models

$R_{c,5^{th}}$ 5^{th} percentile of the strength distribution of a connection in a vertical joint

$R_{c,an}$ strength of a connection in a vertical joint obtained from analytical models

$R_{c,95^{th}}$ 95^{th} percentile of the strength distribution of a connection in a vertical joint

$R_{c,x^{th}}$ x^{th} percentile of the strength distribution of a connection in a vertical joint

$R_{h,5^{th}}$ 95^{th} percentile of hold-down's strength distribution

$R_{h,an}$ hold-down's strength obtained from analytical models

$R_{h,y^{th}}$ y^{th} percentile of hold-down's strength distribution

R_{P_0} activation force

R_{P_κ} inelastic lateral capacity of the shearwall at point P_κ for $\kappa = [1: n_a + 2]$

$T_{f,j}$ internal force in each fastener in the panel-to-panel connections used for joining panel j to $j + 1$

$T_{h,x}$ horizontal force in the hold-down

$T_{h,z}$ uplift force in the hold-down

$T_{s,x,i,j}$ horizontal force in the i^{th} angle bracket from the centre of rotation placed in panel j

$T_{s,z,i,j}$ uplift force in the i^{th} angle bracket from the centre of rotation placed in panel j

$T_{s,z,i}^{P_\kappa}$ uplift force in the i^{th} angle bracket at point P_κ for $\kappa = [1: n_a + 2]$

$T_{h,z}^{P_\kappa}$ uplift force in the hold-down at point P_κ for $\kappa = [1, 2]$

V_f design shear load due to the lateral load

$V_{f,j}$ total seismic shear load at the bottom of storey j

$V_{f,w}$ shear force applied on the wall at the point where the hold-down starts yielding

$V_{r,a}^{el}$ elastic shear strength of the shearwall associated with the angle brackets

$V_{r,a}^{c}$ total shear strength of the shearwall associated with the angle brackets

$V_{f,CLT}$ shear force acting on each CLT panel

$V_{r,CLT}$ shear strength of each CLT panel

W_{ext} external work in the system

W_{int} internal work in the system

W_{total} total potential energy in the system

b length of individual panel

$d_{y,s,x}$ yielding displacement of the angle brackets in the horizontal direction (shear)

$d_{y,s,z}$ yielding displacement of the angle brackets in the vertical direction (uplift)

$d_{y,c}$ yield displacement of fasteners in the vertical joints

$d_{y,h,x}$ yielding displacement of the hold-down in the vertical direction (uplift)

$d_{y,h,z}$ yield displacement of the hold-down in the horizontal direction (shear)

$d_{u,s,x}$ ultimate displacement of the angle brackets in the horizontal direction (shear)

$d_{u,s,z}$ ultimate displacement of the angle brackets in the vertical direction (uplift)

$d_{u,f}$ ultimate displacement of fasteners in the vertical joints

$d_{u,h,x}$ ultimate displacement of the hold-down in the horizontal direction (shear)

$d_{u,h,z}$ ultimate displacement of the hold-down in the vertical direction (uplift)

h height of the panels

$k_{e,EEEP}$ elastic stiffness obtained using EEEP simulation

$k_{e,trilinear}$ elastic stiffness obtained using trilinear simulation

k_f elastic stiffness of a fastener in the vertical joint

$\tilde{k}$ dimensionless stiffness ratio

$k_{s,x}$ elastic stiffness of an angle bracket in the horizontal direction (shear)

$k_{s,z}$ elastic stiffness of an angle bracket in the vertical direction (uplift)

$k_{h,x}$ elastic stiffness of a hold-down in the horizontal direction (shear)

$k_{h,z}$ elastic stiffness of a hold-down in the vertical direction (uplift)

k_v vertical contribution of hold-down and angle brackets in the total potential energy

k_v' contribution of the connections' stiffness in the rotation of panels

k'_{v,P_κ} contribution of the connections' stiffness in the uplift of panels at point P_κ for $\kappa = [1: n_a + 2]$

m number of panels in the shearwall

n_f number of fasteners per vertical joint

n_l number of laminations in CLT panels

n_s number of angle brackets used in the length of each panel

q uniform vertical load applied on the top of the wall

$\tilde{q}$ dimensionless uniform vertical load

$r_{s,x}$ yield strength of angle brackets in the horizontal direction (shear)

$r_{s,z}$ yield strength of angle brackets in the vertical direction (uplift)

r_f yield strength of fasteners in the vertical joints

$r_{h,x}$ yield strength of hold-down in the horizontal direction (shear)

$r_{h,z}$ yield strength of hold-down in the vertical direction (uplift)

t tottal thickness of CLT panels

t_0 total thicknesses of the longitudinal layers of CLT panels

t_{90} total thicknesses of the transverse layers of CLT panels

t_{mean} the average thickness of layers in CLT panels

$t_{a,z,i}^{P_\kappa}$ increase in the uplift force of the i^{th} angle bracket from point $P_{\kappa-1}$ to P_κ for $\kappa = [1: n_a + 2]$

$t_{h,z}^{P_2}$ increase in the hold-down's uplift force at point P_2

v_j vertical displacement of panel j at the rotation point for $j = [1: m]$

$v_{F,max}$ displacement corresponding the maximum load on load-displacement curve

$v_{y,EEEP}$ displacement corresponding the yield load using EEEP method

$v_{y,trilinear}$ displacement corresponding the yield load using trilinear method

v_u displacement corresponding the ultimate load on envelope curves

w the average of the edge distance and spacing between stress relief and the width of the CLT laminates

x^{th} percentile of dissipative element's strength related to ensuring of yielding of vertical joints before the hold-down

y^{th} percentile of dissipative element's strength related to ensuring of elastic angle brackets

$x_{\varphi=0}$ parameter studied when the vertical contribution of angle bracket is neglected

$x_{\varphi>0}$ parameter studied when the vertical contribution of angle bracket is considered

Δ_{P_0} lateral displacement due to sliding at the activation force (i.e., P_0)

Δ_{P_κ} lateral displacement at the top of the wall due to the rocking and sliding at point P_κ for $\kappa = [1: n_a + 2]$

Δ_r lateral displacement at the top of the wall due to the rocking

$\Delta_{r,s}$ lateral displacement at the top of the wall due to the rocking and sliding

Δ_s lateral displacement due to the sliding

Δ_{s,P_κ} lateral displacement due to the sliding at point P_κ for $\kappa = [3: n_a + 2]$

$\Delta_{sh,j}$ shear deformation in the j^{th} panel

Δ_b bending deformation in CLT panels

Δ_{total} total lateral displacement due to the rocking, sliding and shear deformation

$\emptyset$ variable considering the effect of multiple angel brackets used in sensitivity analysis

α coefficient incorporating the effect of multiple angle brackets used in the length of panels

β coefficient incorporating the effect of compression zone in the panels

γ_M partial material factor

γ_{Rd} over-strength factor

γ_{an} The ratio between $R_{D,5^{th}}$ and R_{an}

$\gamma_{r,a}$ over-strength factor to ensure that angle brackets remain elastic

$\gamma_{r,h}$ over-strength factor to ensure that vertical joints yield prior to hold-down

$\gamma_{r,ND}$ over-strength factor to protect non-dissipative elements

γ_{sc} The ratio between $R_{D,95^{th}}$ and $R_{D,5^{th}}$

ε_1 lower limit of the ratio between the over-capacity coefficient at storey j (with $j \geq 2$) and that at storey $j-1$

ε_2 upper limit of the ratio between the over-capacity coefficient at storey j (with $j \geq 2$) and that at storey $j-1$

δ_{P_κ} increase in the total lateral displacement from point $P_{\kappa-1}$ to P_κ for $\kappa = [2: n_s + 2]$

$\xi(x)$ ratio of the studied parameter x

η_1 the ratio of the distance between the center of rotation of the first panel and the hold-down to the length of each panel (b)

η_2 the ratio of the distance between the bottom of the wall and the position of the lateral load actuor to the height of the wall

ρ_s ratio incorporating the effect of multiple angle brackets in the limit expression of CP kinematic region

τ_i parameters used to define SW system of equations for $i = [1: 8]$

ϑ angle of rotation of the panels

φ angle bracket's vertical stiffness ratio

Chapter 1 - Introduction

1.1. General

Cross-Laminated Timber (CLT) is an engineered wood product consisting of multiple layers of lumber which are typically attached together using adhesive, and where longitudinal and transverse layers are placed perpendicular to one another, as shown in Figure 1-1.

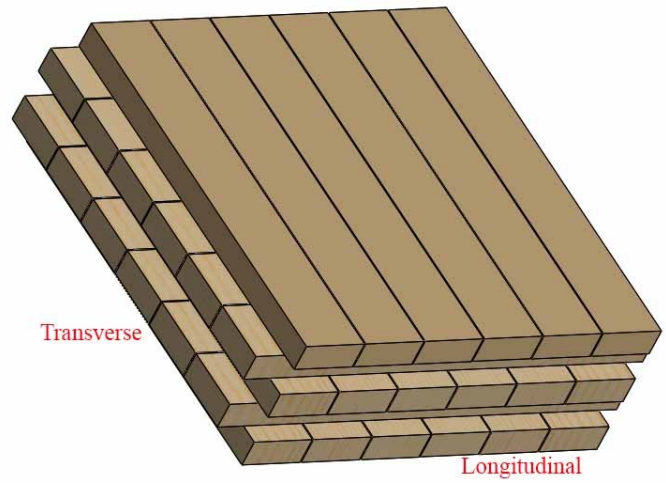

Figure 1-1: CLT layout

CLT is primarily manufactured and used as panels, allowing for use in floor and wall applications. Due to their excellent structural performance, including high in-plane and out-of-plane strength and stiffness, they have become a valuable contender in low- and medium-rise buildings, resisting both gravity and lateral loads. CLT presents another key advantage in terms of sustainability, as it emits fewer greenhouse gases during the production and construction process than other conventional building materials (Himes & Busby, 2020; Myllyviita et al., 2021). Furthermore, the prefabrication process allows considerably faster on-site installation and less waste materials.

CLT buildings can be categorized into two general construction types: (1) balloon-frame, in which wall panels span along multiple storeys and, in some cases, throughout the height of the building, and (2) platform-type, in which wall panels span only one storey between floor slab elements. The latter is currently the only construction type permitted in the

Canadian timber design standard (CSA O86-19, 2019). It includes a requirement to promote more efficient connection engagement through limiting aspect ratios between 4:1 and 2:1. The benefits of platform-type could be attributed to the engagement of more connections involved in resisting loads and dissipating energy at each storey and easier transportation and construction. There is a need for further research to compare the two systems, particularly with regards to connection engagement and energy dissipation under seismic loads.

In high wind and seismic regions, CLT shearwalls are typically relied upon to resist both gravity and lateral loads. Experimental investigations of the behaviour of CLT shearwalls subjected to lateral in-plane loading have revealed that the wall assembly exhibits rigid-body deformation in the CLT panels, due to their high in-plane rigidity, while non-linearity is principally achieved in the connections (e.g., Ceccotti et al., 2013; Hristovski et al., 2018). This emphasizes the importance of connections behaviour and their contribution to the strength, stiffness and ductility of the wall assembly and the building as a whole. Such connections consist of panel-to-panel connections that connect the individual CLT panels together, hold-downs, which are typically placed at the ends of the shearwall or openings to resist the uplift force, and angle brackets with the capability to resist the shear force from the wall to the foundation or floor below (Figure 1-2).

Within platform type construction, two CLT shearwall configurations can be identified, as shown in Figure 1-2: (a) monolithic, consisting of single CLT panels; (b) multi-panel, consisting of multiple CLT panels, attached together using panel-to-panel or vertical joint connections. Multi-panel wall configuration is particularly desired in North America, particularly in seismic regions, due to the ability to employ lateral resistance and seismic energy dissipation contributed by panel-to-panel connections.

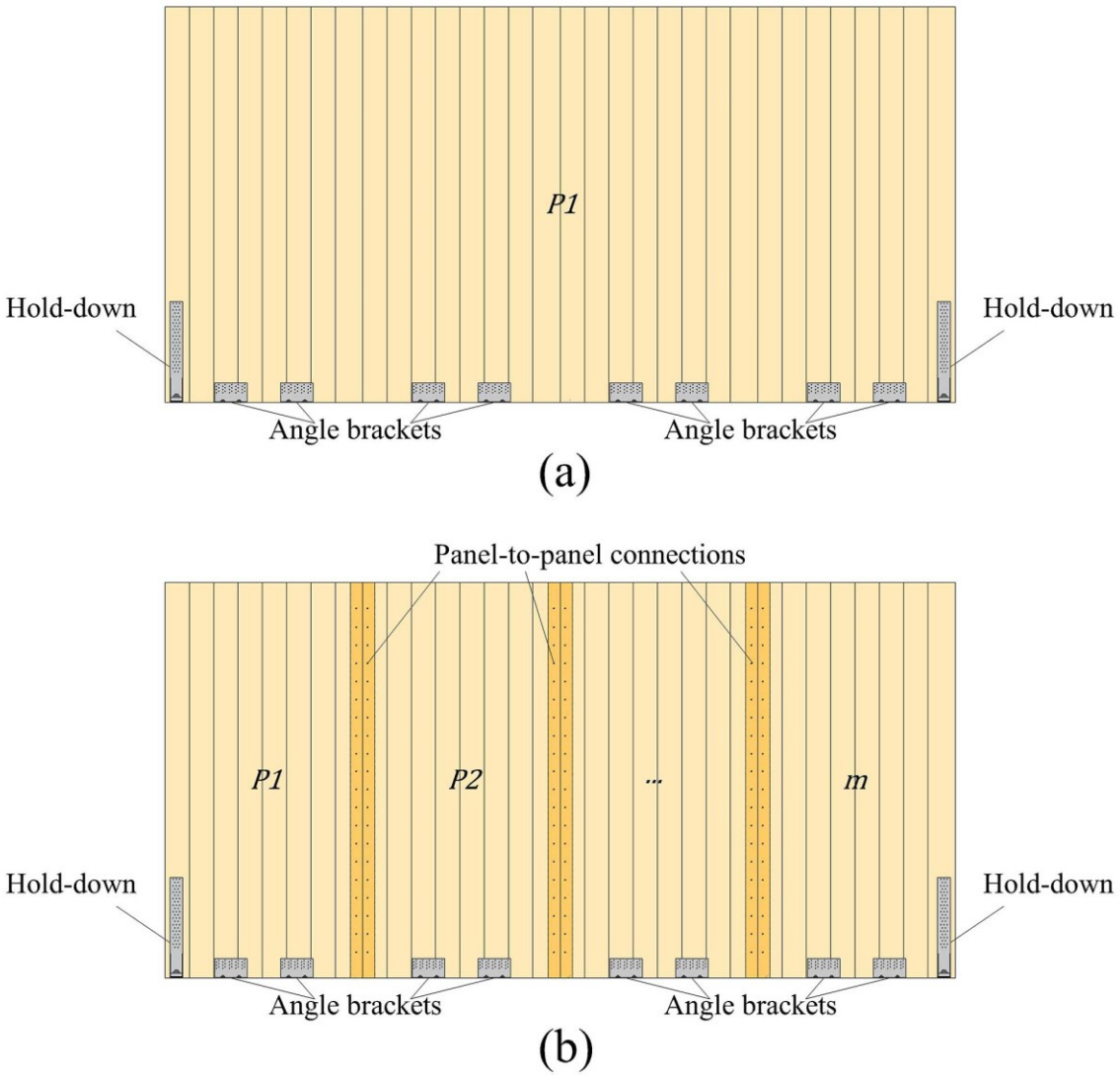

Figure 1-2: CLT shearwall configurations: (a) monolithic; (b) multi-panel

1.2. Motivation

The analysis and design procedures for CLT shearwalls under gravity loads have already been outlined with reasonable details in the Canadian timber design standards (CSA O86-19, 2019), however, methodologies for lateral load design still lack development. Although some general provisions, mainly based on a hierarchy of failure among various components in the shearwall assembly, have been enacted, no clearly defined design method currently exists for multi-panel CLT shearwalls in the various design standards (CSA O86-19, 2019;

EN 1995-1-1:2004/A2, 2013; NDS, 2018). Consequently, simplistic analysis assumptions, based on static methods, or comprehensive modelling techniques involving sophisticated 3-D finite element models, are commonly used by designers.

The majority of the available information on CLT shearwalls focuses on single panel walls (e.g., Lukacs et al., 2019), while only limited studies have been conducted on developing analytical expressions and design approaches for multi-panel CLT shearwalls. Casagrande et al. (2018) and Nolet et al. (2019) developed elastic and plastic models, respectively, for single-storey multi-panel CLT shearwalls in the rocking mode using the minimum potential energy method. These studies developed expressions for wall capacity, rotation, displacement, and stiffness. The authors assumed that only hold-down and panel-to-panel connections contribute to rocking behaviour, whereas angle brackets only behave in shear to prevent sliding. Also, the compression zone effect in CLT panels was ignored. Although these assumptions help simplify the analysis, they may not be practical since modern angle brackets available on the market, such as angle brackets with relatively thick washer plates (e.g., Pozza et al., 2018; D'Arenzo et al., 2019), have uplift capacities comparable to those achieved in hold-down connections. Also, incorporating the contribution of the compression zone into the analytical expressions describing the shearwall behaviour is lacking.

The concept of Capacity-based Design (CD) has been incorporated into structural design provisions to avoid brittle failure modes, especially in seismic design, where energy dissipation is paramount to life safety. Using this approach approach, selected components are predetermined to behave as dissipative zones and the sequence of yielding and failure in the building elements is established to ensure that non-dissipative zones are capacity protected (e.g., Paulay & Priestly, 1992). The sequence of yielding and failure is determined by introducing over-strength factors, to capacity protect non-dissipative elements when energy dissipative components reach a desired level of inelastic displacement. Although the CD philosophy has been the agreed upon principle to establish general design methodologies for seismic design, the applicability of such approach to timber buildings, especially those consisting of Cross Laminated Timber (CLT) shearwalls, has lacked analytical expressions that depend on the structural type (i.e., platform- or

balloon framing) and failure mechanisms. Due to wood's brittle nature, particularly in flexure, tension, and shear, energy dissipation is required through yielding of mechanical connectors. Additionally, the selection of the dissipative zones should ensure a global behaviour and ductility consistent with the behaviour factor used to reduce elastic design forces.

Although some research efforts have been made to develop analytical procedures to describe the behaviour of multi-panel CLT shearwalls, there are still some shortcomings in the current state of knowledge respecting the development of a comprehensive method that adequately considers the effect of all the connections involved in the assembly. The proposed research project focuses on investigating the lateral behaviour of multi-panel CLT shearwalls and provides practical and comprehensive analytical expressions and design procedures. The aim is to incorporate the effect of all boundary connections into the analytical procedure. This includes the bi-directional effect of hold-downs and angle brackets, as well as compression zones. Research objectives, methods, and limitations are presented in the next sections.

1.3. Research objectives

The main objective of the current research project is to develop a comprehensive design provision for multi-panel CLT shearwalls subjected to lateral load. The key objectives are as follows:

1. Evaluate the contribution of angle brackets in the vertical direction (uplift) to the behaviour of CLT shearwalls through sensitivity analyses.
2. Develop a detailed analytical and design approach, including the bi-directional behaviour of angle brackets and compression zones.
3. Develop a CD approach following requirements such as yielding hierarchy and wall kinematic modes to ensure sufficient energy-dissipation and ductility for design in a seismic region.
4. Define different over-strength factors and their respective strength percentiles to ensure the yield hierarchy and protect the non-dissipative elements.
5. Evaluate the cyclic behaviour of the connections and investigate the effect of strength degradation and low-cyclic fatigue on wall behaviour.

6. Evaluate the performance of various configurations of single-story multi-panel CLT shearwalls, including strength, stiffness, ductility, ultimate failure, and kinematic modes, as well as their mechanical properties.
7. Verify the mathematical accuracy of the developed expressions and CD proposal.
8. Validate the developed expressions against experimental tests and numerical models.

1.4. Methodology and limitations

The following methodology is employed in order to achieve the research objectives:

1. Conduct a detailed literature review on CLT shearwalls with respect to experimental investigations, analytical and design developments, and numerical modeling.
2. Review the available clauses in CSA O86-19 concerning CLT shearwall seismic design.
3. Conduct experimental tests on different conventional connections used in CLT shearwalls subjected to monotonic and cyclic loads to investigate their behaviour and obtain their associated mechanical properties.
4. Conduct experimental tests on different configurations of multi-panel CLT shearwalls subjected to monotonic lateral loads. Different configurations were investigated with varying connections' configuration, panels' size and number, and gravity load. This was done to examine various conditions affecting the shearwall behaviour and proposed expressions.
5. Conduct numerical modeling by adopting the connections properties obtained from connection-level tests and compare the results against the developed expressions and wall-level experimental tests.

The limitations of the current study are as follows:

1. Analytical expressions were developed for single-storey shearwalls, and as such the effect of floors, including the connections between floors and walls, was neglected. To allow for the use of equations for multi-storey applications, elastic design and

CD expressions were defined with respect to bending and shear loads. These equations are suitable for platform-type constructions, while more research on

2. The idealized elastic-perfectly-plastic properties of connections were adopted in models. While this assumption aimed to simplify equation complications, it was inevitable that there would be some discrepancy.
3. The shearwall-level experimental tests were conducted on single-storey walls, consistent with the developed equations. Thus, investigations and comparisons between analytical expressions, numerical models, and wall-level experimental tests are valid for single-storey applications.
4. The connections used in experimental tests were limited to one type of hold-down and angle brackets, while using two nailing patterns, fully and partially nailed, as well as three different dowel-type fasteners used as panel-to-panel connections.

1.5. Structure of thesis

Chapter 1 presents research problem definitions, objectives, and limitations.

Chapter 2 introduces a detailed literature review of studies related to CLT shearwalls. This includes analytical and design developments, CD developments, experimental tests on connections, CLT shearwalls and buildings.

Chapter 3 presents the development of analytical approaches in the elastic and inelastic ranges, in which the bi-directional action of angle brackets and hold-down and impact of compression zones in CLT panels are included. The results of sensitivity analysis to study the contribution of angle brackets' uplift action to CLT shearwall resistance and deflection are also highlighted.

Chapter 4 introduces the design approach for multi-storey CLT shearwall applications subjected to lateral load, as well as CD proposal considering the developed expressions in Chapter 3.

Chapters 5 and 6 present experimental tests on connections and CLT shearwalls, respectively. They include the procedure and details, results analysis, behaviour investigations, and mechanical properties.

Chapter 7 presents the mathematical verification of the developed expressions and CD proposal, as well as their validation against experimental tests and numerical models.

Chapter 8 summarizes the research findings and proposes the future research topics.

Appendix A presents detailed results and test set-ups for the experimental connection tests.

Appendix B summarizes the details of test set-ups used for CLT shearwall level experimental tests and the results of mesh sensitivity analysis used for numerical modelling.

Appendix C presents the results obtained from various analyses to show the applicability of interpolation between different kinematic modes.

Chapter 2 - Literature review

2.1. General

In this section, an analysis of the state-of-the-art on the mechanical behaviour of CLT shearwalls is presented, including a literature review of experimental tests conducted at building, shearwall and connection levels. An overview is presented of developed analytical and design approaches for CLT shearwalls subjected to wind and earthquake loads. Additionally, advancements made to establish CD approaches for CLT shearwalls are investigated. Finally, an overview is provided of the current Canadian timber structural design standard (CSA O86-19, 2019) concerning lateral design and CD of CLT shearwalls.

2.2. CLT shearwalls: experimental investigations

2.2.1. Building level tests

SOPHIE project was the first comprehensive testing campaign conducted on CLT buildings. Experimental tests were carried out on single-storey (M. P. Lauriola & C. Sandhaas, 2006) and three-storey (A. Ceccotti & M. Follesa, 2006) buildings consisting of narrow CLT panels anchored to a steel foundation by conventional connections similar to what was used in light frame timber and connected to one-another by partially threaded screws. The lateral loads were applied using a pseudo-dynamic actuator and shaking table for the single- and three-storey buildings, respectively. It was observed that damages were limited to the connections, and it was concluded that the buildings could withstand several seismic load applications. The CLT panels behaved mostly as rigid bodies, and connections provided ductility and energy dissipation in the assembly. It was also concluded that the yield hierarchy among energy dissipative connections could significantly contribute to ductility in the assembly. Particularly, panel-to-panel connections used in multi-panel CLT shearwalls contributed significantly to providing ductility and energy-dissipation in the system. Shake table experimental tests were also conducted on a seven-storey building consisting of CLT panels connected using partially threaded screw connections and anchored to the steel foundation or CLT floor below through angle brackets and innovative hold-downs with a relatively thick steel plate thickness (10 mm thickness) fastened with 6 mm lag screws (Ceccotti et al., 2013). Those hold-downs were designed to resist higher

uplift and shear forces and provided more ductility than conventional types, particularly compared to the previously mentioned campaigns where the hold-downs were suitable for light frame timber shearwalls. No brittle failure was observed in the CLT panels after load applications composed of 10 severe earthquakes. After each load application, minor repairs or replacements of connections were made. Failure of connections was determined to be ductile, including fastener bending and embedment crushing failure.

Flatscher & Schickhofer (2015) conducted shake table tests on a three-storey CLT building composed of monolithic single-panel walls, as part of the SERIES testing campaign. Lower deflections and inter-storey drifts were observed compared to the three-storey building tested under the SOFIE project (A. Ceccotti & M. Follesa, 2006), while a decrease in energy dissipation was reported due to the absence of panel-to-panel connections. This emphasized the better seismic behaviour of multi-panel CLT shearwalls and the significant role of panel-to-panel connections in providing ductility in CLT shearwalls and the building as a whole. The hold-down connections were the same as those used by A. Ceccotti & M. Follesa, (2006) which were designed and mostly used in light frame timber. The authors reported an average uplift (tension) resistance of the hold-downs around 51 kN, which seems significantly lower than the newer generations available on the market, those designed more specifically for CLT shearwalls (e.g., *European Technical Approval ETA-11/0086*, 2018).

Popovski & Gavric (2016) performed experimental full-scale tests on a two-storey CLT building composed of narrow panels attached together using half-lap joints with self-tapping screws. In total, one monotonic and four cyclic loading tests were conducted. No severe damage to CLT panels was observed after each test, indicating the failure mechanism in the nails fastening angle brackets to the CLT shearwalls due to the interaction of sliding and uplift deformations. That showed the interaction between the angle brackets used under such loads, and its impact on CLT shearwall failure. Consistent with previous test campaigns, it was observed that building resistance and ductility derived predominantly from panel-to-panel connections and mechanical brackets used to anchor CLT shearwalls to the base (e.g., angle brackets and hold-downs).

Yasumura et al. (2016) conducted experimental tests on a two-storey CLT building with additional dead loads on both storeys. Cyclic lateral loads were applied at the second storey level. Two configurations were investigated, one with monolithic walls (single panel) and the other with narrow panels (multi-panel). Smaller hold-downs than previous studies were used on each side and one angle bracket in the middle of each segment. It was concluded that the building with a monolithic wall possessed significantly higher lateral stiffness while lower ductility than those composed of multi-panel walls. No global instability was observed, while failure in the corners of monolithic walls openings and in the connections for the multi-panel walls were reported.

Blomgren et al. (2019) tested a two-story building consisting of two-panel CLT shearwalls, CLT floor, and a glulam gravity frame. An innovative and replaceable connection system was utilized, including panel-to-panel connections and a center anchor. The results showed that the CLT shearwall system achieved the expected behaviour and remained stable even during severe earthquakes. It was shown that damaged components and connections in CLT shearwall system can be replaced after an earthquake.

The following is a summary of the main outcomes and observations resulting from full-scale experimental tests of buildings constructed with CLT shearwalls:

- CLT panels behave like rigid bodies. The deformation occurring in panels (bending and shear) appeared insignificant compared to the total lateral deflection of the panels.
- In light of the previous point, connections are primarily responsible for resisting lateral loads and providing ductility and energy dissipation.
- Multi-panel CLT shearwalls appeared to behave more ductile than monolithic walls due to the engagement of panel-to-panel connections and their flexibility, while monolithic walls exhibited more stiffness.
- In most experimental tests, the hold-downs used were suitable for light frame timber shearwalls and were not designed primarily for CLT shearwalls. Thus, they lacked cases with new generations of hold-downs (e.g., European Technical Approval ETA-11/0086, 2018) or innovative hold-down connections with enhanced seismic performance (e,g., Dires & Tannert, 2022).

- The interaction between shear and uplift in one experimental campaign was discussed, which affected ultimate failure and wall behaviour.

2.2.2. Shearwall level tests

Popovski et al. (2010) conducted experimental tests on CLT shearwalls using varying wall configurations, including the number of panels and storeys, construction method (i.e., platform- or balloon-type), and connections. Different mechanical anchors were used to anchor the walls to the base, such as one type of hold-down, two types of angle brackets, and two proprietary timber rivets. The study showed that deformation in connections contributed mostly to walls' lateral displacement while CLT panels' deformations (bending and shear) appeared negligible. Particularly, panel-to-panel connections significantly impacted walls' ability to deflect as well as dissipate energy under seismic loads. Multi-panel shearwalls also provided lower stiffness, but better seismic performance than monolithic walls. The seismic behaviour of the wall was improved when hold-downs were used on both sides. It was also observed that adding gravity loads resulted in increased resistance and stiffness.

Gavric et al. (2015) and Flatscher et al. (2015) tested CLT shearwalls with conventional connections subjected to monotonic and cyclic lateral loads. Different connection configurations and the number of panels (single- and two-panel) were investigated. Relatively flexible hold-down and angle brackets were utilized compared to more recent generations of mechanical anchors. The impact of using more angle brackets to resist both uplift and shear and adding gravity loads appeared to be significantly high on walls resistance and stiffness. It was observed that panel-to-panel connections contributed significantly to the performance and ductility of the shearwalls, where using relatively fewer joints resulted in lower stiffness and slightly lower resistance while achieving higher ductility. It also appeared that ultimate failures consistently occurred in hold-downs or angle brackets due to their relatively lower ultimate displacement than panel-to-panel connections. The performance of CLT walls, particularly the two-panel configurations, was heavily affected by the panel-to-panel connections stiffness. It was found that by increasing their stiffness by incorporating more connections and/or stiffer fasteners, the wall performed as a single panel and all panels except for the last one left the ground with

one global center of rotation, while by utilizing relatively flexible panel-to-panel connections each panel behaved as an individual wall with distinct rotational centers. As such, two kinematic modes were defined, Single-Wall (SW) associated with relatively stiff panel-to-panel connections and Coupled-Panel (CP) associated with relatively flexible panel-to-panel connections.

Hristovski et al. (2013 & 2018) conducted shake table tests on a CLT wall system composed of two primary walls oriented parallel to the load excitation, and two orthogonal walls and a CLT floor to provide lateral support. The primary walls were attached to the reinforced concrete foundation using angle brackets to resist uplift and shear loads. A gravity load of 9.6 tons was applied to the CLT floor to simulate three-storey mass. Two wall configurations were tested, namely monolithic and two-panel walls. Consistent with previous test campaigns, it was reported that the system with two-panel shearwalls dissipated more seismic energy and provided more ductility than monolithic shearwalls due to the contribution of panel-to-panel connections.

Several research efforts have been made on testing CLT shearwalls using novel connections (D'Arenzo et al., 2021; Hashemi et al., 2017; Loo, Kun, et al., 2014; Moroder et al., 2018; Sarti et al., 2016). Compared to conventional connections, the results highlighted improvements in seismic performance such as greater energy dissipation, load resistance, and deformability. More details are available in the associated references, which are outside the scope of this research.

The summary of the main outputs and observations from wall-level experimental tests consisting of CLT panels is as follows:

- Deformation of connections significantly contributed to the top lateral displacement of the shearwalls, while deformation of CLT panels appeared to have a negligible impact.
- Panel-to-panel connections showed significant contributions to ductility and energy dissipation in the shearwalls.
- The mechanical anchors attaching walls to the base, such as hold-downs and angle brackets, consistently failed.

- It was found that the stiffness and resistance of the walls were improved by using more angle brackets that resist uplift and shear, hold-downs at the ends of the wall, as well as by adding gravity loads to the walls.
- CLT shearwall performance was significantly influenced by panel-to-panel connections' stiffness. Relatively flexible panel-to-panel connections resulted in more ductility, lower stiffness, and a kinematic mode where each panel behaved as an individual wall with a separate center of rotation (CP behaviour). Relatively stiff panel-to-panel connections led to less ductility, increased stiffness, and a kinematic mode where the wall behaved like a single panel with one global center of rotation (SW behaviour).
- Experimental tests on CLT shearwalls with conventional connections were limited to single and two-panel configurations and used relatively flexible hold-down and angle brackets.

2.2.3. Connection level tests

Extensive experimental tests were carried out under the SERIES and SOFIE projects on various conventional connections used in CLT shearwalls, including hold-downs and angle brackets, and different fasteners used as panel-to-panel connections, such as self-tapping screws (e.g., Gavric et al. 2015a & 2015b, Flatscher et al. 2015). The hold-down and angle brackets used belonged to a first generation of connections adopted directly from light-frame shearwall systems to be used in low-rise CLT buildings with little-to-no technological advancements. Tests on mechanical anchors subjected to uplift tension force showed that hold-down connections exhibited reasonable energy dissipation and ductile behaviour, while angle brackets failed in nail withdrawal or bolt pull-through when CLT floor or steel base were used, respectively. Contrarily, when subjected to horizontal shear force, angle brackets acted ductile, whereas hold-downs exhibited elastic and undesirable behaviour due to their rotation. A relatively small number of nails (partially nailed) was intentionally selected in the hold-downs to prevent failure in the steel bracket while achieving failure in the nails and enhanced ductility by engaging their flexibility. This approach, however, resulted in reduced resistance and stiffness. Low cycle fatigue appeared insignificant on both hold-down and angle brackets under shear and uplift. Panel-

to-panel connections with a diameter of 8 mm and different lengths were tested and exhibited more ductile and energy dissipation than mechanical anchors under uplift, represented by fastener yielding and wood crushing. Low cycle fatigue appeared insignificant for panel-to-panel connections, which can be attributed to large fastener diameters.

Tomasi & Smith (2015) conducted experimental tests on different types of conventional angle brackets and various fasteners to investigate their performance under horizontal shear forces. Angle brackets with long width parallel to the force and more nails exhibited higher resistance and stiffness than smaller angle brackets commonly used to anchor light frame shearwalls. However, the smaller angle brackets exhibited more ductility. It was highlighted that the geometry of angle brackets and their methods of attachment to the base could significantly impact their performance and mechanical properties. The authors investigated these aspects and provided recommendations to improve angle bracket performance under shear loads.

Casagrande et al., (2016) performed experimental tests on conventional connections used in timber buildings adopted to seismic regions. Mechanical properties were estimated, including maximum and yield resistances and displacements, stiffness, and ductility. Different connections were tested subjected to cyclic load patterns, such as hold-downs and angle brackets, as well as various fasteners in different diameters, lengths, and penetration angles (i.e., orthogonal, or inclined) as panel-to-panel connections. Orthogonal panel-to-panel connections exhibited more ductility than inclined ones. Lower ductility was observed for hold-downs and angle brackets compared to panel-to-panel connections. One type of angle bracket with a relatively thick washer subjected to uplift tension loads, showed increased strength, stiffness, and ductility than conventionally used angle brackets without washers. This highlighted their ability to resist such loads additional to their initial load-resisting purpose (shear).

Hossain et al., (2016 & 2019) conducted monotonic and reversed cyclic tests on panel-to-panel connections consisting of self-taping screws with a diameter of 8 mm under shear in different joint configurations, such as inclined and orthogonal penetrations. Mechanical

properties and connection behaviour were assessed. Reasonable ductility was observed in monotonic tests, whereas it decreased slightly under reversed cyclic tests.

Although hold-downs and angle brackets are primarily designed to resist uplift and shear loads, respectively, they are inevitably exposed to both loads. Experimental test results on these mechanical brackets under both uplift and shear have highlighted that the interaction between the loads significantly affects the behaviour and mechanical properties of mechanical anchors (Pozza et al., 2017; Pozza, Ferracuti, et al., 2018; Pozza, Saetta, et al., 2018; Liu & Lam, 2018, 2019; Liu et al., 2020). The studies indicated that different magnitudes of load in one direction could affect the performance of connections in the other direction. This can be interpreted as connections acting weaker than they were designed to carry pure load in one direction only. It is therefore necessary to account for this effect in order to avoid overestimating the resistance of the connections.

Several experimental investigations were conducted on innovative connections used in CLT shearwalls to improve seismic energy dissipation and ductility, such as slip friction connectors (e.g., Loo, Quenneville, et al., 2014), damping hold-down (e.g., Wrzesniak et al., 2016), X-RAD (e.g., Polastri et al., 2018), hollow steel tubes (e.g., Schneider et al., 2018), internal perforated steel plates (e.g., Dires & Tannert, 2022). The results highlighted better seismic performance and improved ductile behaviour and failure compared to conventional connections used in CLT shearwalls.

The summary of main outputs and observations from connections level experimental tests used in CLT shearwalls can be highlighted as follows:

- Conventional fasteners used as panel-to-panel connections exhibited more ductility than hold-down and angle brackets.
- Experimental tests on hold-down and angle brackets designed for light frame timber shearwalls showed relatively low resistance.
- The impact of low cycle fatigue appeared insignificant for hold-down and angle brackets under different load directions (shear and uplift).

- The impact of low cycle fatigue on conventional fasteners used for panel-to-panel connections, particularly small diameter dowel type fasteners, was not investigated in the literature as only one size of relatively large fastener diameter was tested.
- Experimental tests on angle brackets under shear showed that the geometry of brackets and the type of attachment to the base could significantly affect their performance and mechanical properties.
- Various studies showed that the interaction between shear and uplift has a significant impact on the behaviour and mechanical properties of hold-down brackets and angle brackets.

2.3. CLT shearwalls: Analytical and design development

The studies conducted to develop analytical and design approaches for CLT shearwalls are reviewed in this section. Seismic design proposals are also discussed, including CD proposals, which involve different requirements to ensure sufficient energy dissipation in CLT shearwalls.

2.3.1. Analytical approaches for CLT shearwalls

Casagrande et al., (2016) developed an analytical approach for one-storey timber shearwalls, including light frame timber and CLT, based on static equilibrium, to determine the wall's lateral displacement and strength. The developed model considered the contribution of gravity load and a compression zone equal to 90% of the total wall length. Validation of the proposed model was done against experimental tests to show the applicability of the expressions to predicting the mechanical properties of the walls.

A state-of-the-art review was presented on analytical approaches to analyze single-panel CLT shearwalls, including expressions related to shearwall lateral strength and stiffness (Lukacs et al., 2019). The presented approaches were developed based on the assumption of rigid-body behaviour of CLT panels and using static equilibrium. A comparison was made between the highlighted approaches and experimental test results on CLT shearwalls to validate their applicability. The results indicated diverse outputs for strength and stiffness, mostly underestimated results with a few overestimations. Those approaches that

included the vertical (uplift) contribution of angle brackets showed more accurate predictions than those that excluded it.

Gavric et al. (2015c) proposed an analytical approach for analyzing single- and two-panel CLT shearwalls, using moment equilibrium, where the bi-directional effect of hold-down and angle brackets was implemented separately without incorporating their interaction effect. Mechanical properties of connections were implemented by employing tri-linear simulations. The comparison between the analytical approach and the experimental tests showed that the proposed analytical method may under- or over-estimate shearwall behaviour in different practical cases. The reasons indicated neglecting the bi-directional interaction of angle brackets in the models and their plasticization in uplift during experimental tests, which led to excessive sliding and a reduction in the wall's maximum strength.

Flatscher & Schickhofer (2016) established an iterative displacement-based method limited to single-panel and two-panel CLT shearwalls, by which rotation, displacement and internal forces in connectors can be determined. The connections were defined as panel-to-panel connections and hold-downs that operated only in shear and uplift, respectively, as well as angle brackets with an interaction effect between shear and uplift. The authors validated the analytical model against experimental tests on various shearwall configurations by varying the size and number of panels, connection configurations, and gravity load. The results highlighted a reasonable match in predicting wall mechanical properties.

Casagrande et al. (2018) developed an elastic analytical approach for single-storey multi-panel CLT shearwalls using the minimum potential energy method. The energy induced in the system through connections and lateral and gravity loads was minimized. This was done to obtain expressions calculating internal forces in the connections, shearwall top lateral displacement and elastic strength. The authors proposed equations to predict shearwall kinematic modes, for CP when all the panels remain in contact with the ground, SW when only the last panel is on the ground, and Intermediate (IN) which is a case between CP and SW with some panels remaining in contact with the ground. The proposed analytical expressions were verified against numerical models with high accuracy showing

their mathematical correctness. The developed expressions were limited to unidirectional hold-downs, resisting uplift, and angle brackets, resisting shear, and did not include the compression zone effect.

Nolet et al. (2019) extended the study by Casagrande et al. (2018) to incorporate the elastic-perfectly plastic properties of connections. Various yield and failure modes were investigated for different kinematic modes. This comprehensive study revealed the significant contribution of the connections' mechanical properties, such as yield and failure strengths and displacements, to the shearwall's lateral behaviour and ductility. The authors developed expressions and force-displacement curves associated with each possible kinematic mode in both elastic and plastic regions, based on different yield and failure hierarchies in connections. Consistent with Casagrande et al. (2018), the developed approach was limited to uni-directional hold-down and angle brackets, and did not include the compression zone effect. The assumption of elastic-perfectly plastic connections could also cause discrepancies if the real load-displacement curves of the connections are not accurately represented by this idealistic model.

D'Arenzo, Schwendner, et al. (2021) developed an analytical procedure for CLT multi-panel shearwalls including the interaction effect of the floor above. The proposed expressions were validated against numerical models showing a reasonable match in terms of lateral stiffness, bending moment and base shear. Results highlighted that the interaction effect improved the rocking stiffness of the shearwall and often changed the kinematic mode from CP to SW.

The summary of the main outputs and observations from analytical developments for CLT shearwalls is as follows:

- Several approaches were developed for single-panel CLT shearwalls using static equilibrium. The comparisons against experimental tests revealed that including the uplift contribution of angle brackets led to better predictions. The complexity of analytical expressions seemed lower than multi-panel CLT shearwalls, in which panel-to-panel connections should be incorporated, and different kinematic modes can be achieved.

- Comparisons between the developed expressions for two-panel CLT shearwalls and experimental tests showed some discrepancies. These can be attributed to idealizing the mechanical properties of connections and not considering the interactive properties of hold-down and angle brackets in resisting uplift and shear.
- Elastic and elastoplastic analytical approaches were developed for multi-panel CLT shearwalls using minimum potential energy method. The expressions were limited to uni-directional behaviour of hold-down and angle brackets and did not include the compression zone. Also, the mechanical properties of connections were modelled using elastic-perfectly plastic simulation.
- Analytical methods including the interaction between CLT walls and the floors above were developed. It was revealed that this added contribution could improve the rocking performance of CLT shearwalls and change the kinematic modes, such as from CP to SW.

2.3.2. Seismic design approaches for CLT shearwalls

Gavric et al. (2013) proposed a CD approach, defining dissipative connections, such as fasteners, in which a plastic hinge is developed, and non-dissipative elements, such as CLT panels and mechanical brackets and anchoring bolts attached to the base. It was proposed that panel-to-panel connections resisting shear and hold-downs resisting uplift force be defined as dissipative connections, while angle brackets remain elastic to minimize sliding. Shahnewaz et al. (2017) proposed a CD approach for a one-storey single-panel CLT shearwall attached to the base using distributed angle brackets.

Research efforts in Europe contributed to the development of a comprehensive CD approach to be included in the next generation of Eurocode 8 (Follesa et al., 2015, 2018; Fragiacomo et al., 2019). The authors categorize buildings composed of CLT shearwalls into two ductility levels as follows:

1. Medium ductility, which refers to buildings made of single panel or multi-panel shearwalls that behave monolithically (i.e., as a SW), and where hold-downs and angle brackets provide limited ductility to the shearwalls.

2. High ductility, which refers to buildings made with CLT shearwalls consisting of multiple panels in which panel-to-panel connections are designed to yield and provide ductility and energy dissipation in the shearwall, and where CP behaviour is the dominant kinematic mechanism.

Casagrande et al. (2019) developed a CD approach for light frame timber and multi-panel CLT shearwalls, in which design expressions and requirements were proposed for each ductility class, including associated over-strength factors to design non-dissipative elements. The approach limits to angle bracket and hold-down working in shear and uplift alone, respectively.

2.4. CLT shearwalls: CSA O86 review

Although several research efforts have been made towards developing analytical and design expressions for CLT shearwalls based on theoretical and experimental investigations, major wood structural standards worldwide have provided only some general guidance for lateral design and CD, and they lack analytical and design expressions and procedures (e.g., Eurocode 5, 2013; Eurocode 8, 2014; CSA O86-19, 2019).

According to CSA O86-19 (2019), the resistance of connections shall govern the strength behaviour of shearwalls. Seismic considerations were provided for ductility and over strength factors of $R_d \cdot R_0 = 3$, where earthquake energy should be dissipated in rocking behaviour through the connections, while wall sliding is minimized. In general, energy dissipation in connections used in timber structural members occurs through yielding in small diameter fasteners and/or embedment crushing in wood. Dissipative connections must meet the following requirements:

1. *Connections shall be designed so that a yielding mode governs the resistance.*
2. *Connections shall be at least moderately ductile in the directions associated with the rocking rigid body motions of CLT panels.*
3. *Connections shall possess sufficient deformation capacity under the force and displacement demands that are induced in them to allow for the CLT panels to develop rocking motion.*

The Standard does not provide more details on how to satisfy the requirements above. It is vague about how to ensure yielding in connections (requirement 1) and what is the minimum required ductility ratio value to define a connection as moderately ductile (requirement 2). However, standard commentary (*Wood Design Manual- Commentary CSA O86-19*, 2020) recommends using a minimum ductility ratio of 3.0, based on ASTM E2126 (2019) standard, to ensure sufficient energy dissipation in connections.

Concerning the third requirement, the standard requires CP behaviour to be predominant to ensure the engagement of panel-to-panel connections and sufficient energy dissipation. Although standard does not present any procedure to satisfy that, another requirement is provided concerning the aspect ratio of each shearwall segment (i,e., the ratio of height to width) to facilitate the development of rocking motion. The range of aspect ratio shall be in between 2:1 and 4:1. The lower limit (2:1) is to ensure rocking motion develops, while the greater limit (4:1) ensures the lateral resistance of the shearwall is optimized since greater aspect ratio leads to lower resistance when rocking mode governs.

The standard categorizes two types of connections as energy dissipative: (1) panel-to-panel connections and (2) angle brackets in uplift only. It can be interpreted that the standard does not allow angle brackets to yield in shear while permitting a ductile behaviour in uplift. However, it is unclear how yielding in uplift is achievable while neglecting its interaction with shear.

Despite providing the requirements and categorization mentioned earlier, no clear explanation or expressions were provided to achieve them. This resulted in confusion among engineers dealing with designing CLT shearwalls under lateral and seismic loads.

2.5. Summary and observations

This chapter provides an overview of the current research efforts on CLT shearwalls. Several studies investigated CLT shearwall behaviour through experimental tests at different construction levels. Analytical and design provisions related to the seismic design of CLT shearwalls were also presented.

According to the experimental results, CLT panels behave like rigid bodies, while connections mainly dissipate energy and resist lateral forces. It was shown that the

behaviour of the connections and their mechanical properties could significantly impact the shearwall's performance.

The review of the literature reveals that although several analytical methods were proposed for multi-panel CLT shearwalls, they adopted certain assumptions that might significantly affect shearwall behaviour and mechanical properties. These assumptions include neglecting the bi-directional contribution of angle brackets to shearwall rocking and the effect of the compression zone. Additionally, a comprehensive approach including such contributions lacks the analytical expressions to ensure CD requirements are achieved.

The literature lacks experimental tests at connection-level on new generations of connections available on the market designed more specifically for CLT shearwalls. Further, the effect of low cyclic fatigue on panel-to-panel connections was not investigated with different fastener diameters. There is also a gap in experimental tests on CLT shearwalls pertaining to multi-panel applications, particularly more than two-panel walls, and the use of new generations of connections. The developed analytical approaches were also not validated against experimental tests on multi-panel CLT shearwalls.

Chapter 3 - Analytical model development

3.1. General and definitions

The review of the available literature in Chapter 2 highlighted the need to develop a comprehensive analytical method for multi-panel CLT shearwalls, in which the bi-directional behaviour of angle brackets and hold-downs is considered. This approach is achieved in this study by building on existing models found in the literature (Casagrande et al., 2018; Nolet et al., 2019) and contributing to specific gaps in knowledge. Examples of contributions in the proposed model include considering the contribution of multiple angle brackets along the wall length, bi-directional contribution of both the hold-down and angle brackets, as well as accounting for the effect of compression zone in the CLT panel.

Figure 3-1 shows the investigated shearwalls and the placement of the connections used in this study. A hold-down is assumed at the ends of the shearwall, and equally spaced angle brackets connecting each wall panel to the floor below are placed along the panel length. The shearwall consists of m panels connected to each other using panel-to-panel connections. The shearwalls are assumed to be subjected to a vertical uniformly distributed gravity load, q, and a concentrated lateral load, F, with constant values.

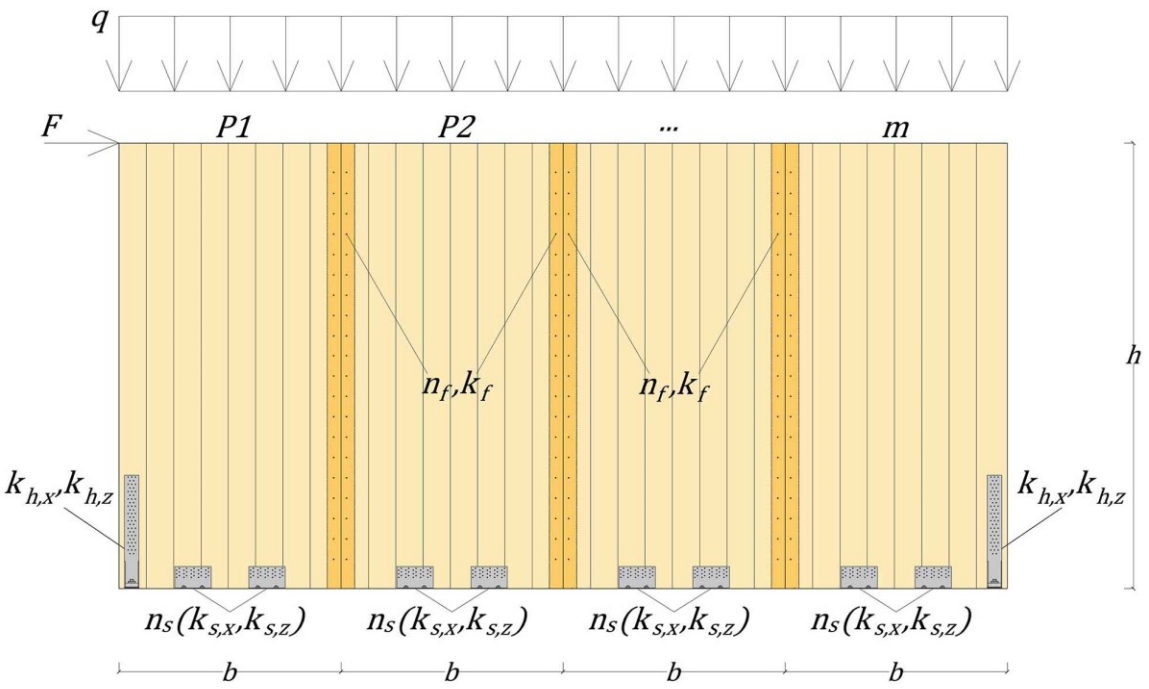

Figure 3-1: Multi-panel CLT shearwalls with typical connection and loading configuration

The hold-down connectors in this model are assumed to resist both vertical (uplift) and horizontal (shear) loads. n_f fasteners in each panel-to-panel connection are used to connect the panels together, and n_s equally spaced angle brackets, capable of resisting both uplift and shear, are considered. The stiffness of the hold-down in the vertical and horizontal directions and the stiffness of the panel-to-panel connections are denoted $k_{h,z}$, $k_{h,x}$ and k_f, respectively. The angle brackets are assigned horizontal and vertical stiffness of $k_{s,x}$ and $k_{s,z}$, respectively.

Four contributions can be considered in the determination of the lateral displacement of a CLT shearwall, including bending and shear deformations of the panels and rocking and sliding of the shearwall (Figure 3-2). Experimental tests highlighted that rocking and sliding have the highest contribution to the total lateral displacement, and CLT panels behave almost like rigid bodies (e.g., Ceccotti et al., 2013; Flatscher & Schickhofer, 2015; Gavric et al., 2015; Popovski & Gavric, 2016). However, shearwalls with large openings or high aspect ratios of panels could undergo significant bending and shear deformations (e.g., Casagrande, Fanti, et al., 2021).

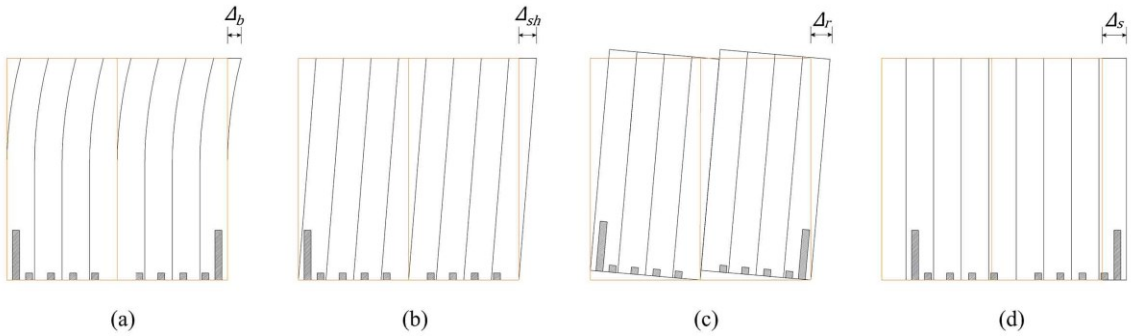

Figure 3-2: Contributions of lateral displacement of CLT shearwalls: bending (a); shear (b); rocking (c); sliding (d)

Based on the mechanical properties of connectors and the applied loads, three kinematic behaviours can be defined (Figure 3-3): 1) CP, where one center of rotation for each panel is attained, 2) SW, where only one global point of contact for the entire wall is attained, and 3) IN, which represents a special case, where only some panels are in contact with the ground.

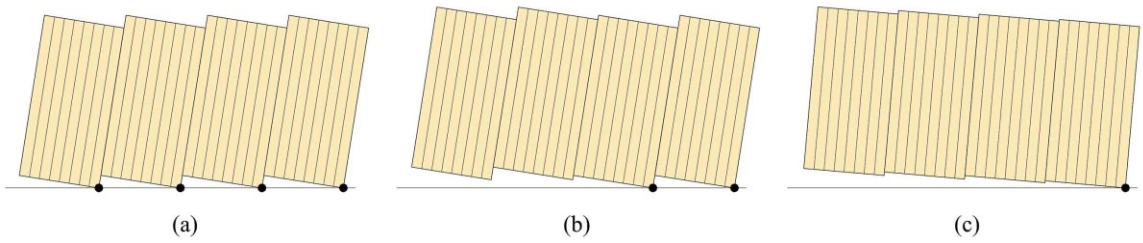

Figure 3-3: CLT shearwall kinematic modes: (a) CP; (b) IN; (c) SW

The general assumptions used in the development of the proposed approach are:

- CLT panels are assumed to be rigid elements for investigating the kinematic behaviour.
- The same horizontal displacement is assumed for all points at the top and bottom of the shearwall due to the in-plane diaphragm behaviour of the floor elements.

The first assumption is attributed to the high in-plane stiffness in the diaphragm as well as the connection between the CLT floor and the shearwall. With regard to the second assumption, the contribution from panel deformation has been found to be relatively small. As such assuming the panels to be perfectly rigid is a reasonable approximation based on

experimental results (e.g., Ceccotti et al., 2013; Popovski & Gavric, 2016). It should be noted that the contribution from panel deformation may be significant for certain wall configurations, such as panels with very high aspect ratios, and walls with openings. In those cases, the flexure and shear deformation of the panels can be considered independently of the rocking and sliding deformations. Methods that account for such contributions are readily available in the literature (e.g., Brandner et al., 2017a). Furthermore, experimental investigations of CLT shearwalls (e.g., Flatscher et al., 2015; Gavric et al., 2015) have shown that the centers of rotation of the wall segments may not be located at the corner of each panel due to the presence of a compressive zone in the panel. This effect is incorporated in the proposed model by assuming a reduced panel length equal to $b \cdot \beta$ in the CP behaviour (Figure 3-4). By setting β to unity, such contributions may be neglected.

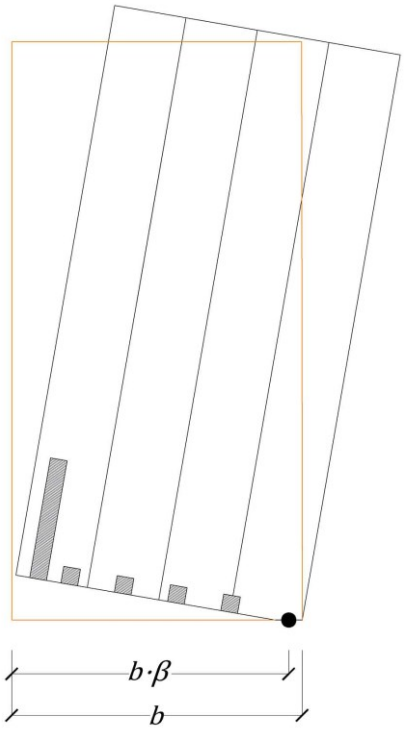

Figure 3-4: The reduced length of panel considering the compression zone

The analytical method is established for CP and SW behaviour using the minimum potential method applying small angle assumptions in the panels. The total potential

energy, W_{total}, is defined as the sum of the internal and external work, W_{int} and W_{ext}, as shown in Equation (3-1).

$$W_{total} = W_{int} - W_{ext} \tag{3-1}$$

3.2. Elastic analytical method

3.2.1. Coupled-Panel behaviour

The analytical variables in the CP case include the horizontal displacement due to panel sliding, denoted as Δ_s, and the angle of rotation of the panels, defined as ϑ, which is equal for all panels due to the diaphragm constraint (Figure 3-5). The connectors are defined as elastic springs, where the hold-downs are assumed to resist uplift and shear, panel-to-panel connections resist the shear force transferred between panels, and the angle brackets are considered as two springs along the bottom edge of the wall panels.

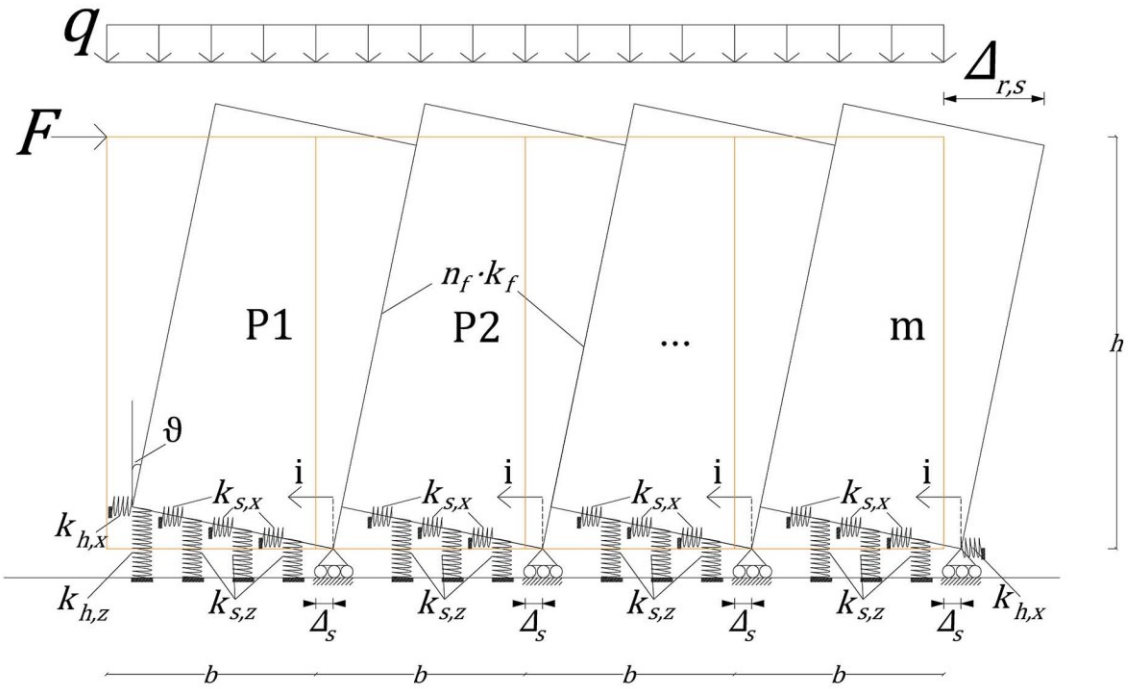

Figure 3-5: CP behaviour of multi-panel CLT shearwalls

The relationship between the vertical stiffness of the hold-down and the angle brackets is presented in Equation (3-2), where φ represents the angle brackets' vertical stiffness ratio. This equation expresses a measure of the contribution of angle brackets in the vertical

direction (uplift) and facilitates the comparison between including and excluding such contribution.

$$\varphi = \frac{k_{s,z}}{k_{h,z}} \tag{3-2}$$

The total contribution of the hold-down and angle brackets to the vertical stiffness, k_v, can be defined as shown in Equation (3-3), which was obtained using total potential energy. Equation (3-3) contains the flexibility of including multiple angle brackets by introducing the coefficient α, as expressed in Equation (3-4).

$$k_v = k_{h,z} \cdot (\beta^2 + \alpha \cdot \varphi \cdot m) \tag{3-3}$$

$$\alpha = \sum_{i=1}^{n_s} \left[\frac{i}{(n_s + 1)} + (\beta - 1) \right]^2 \tag{3-4}$$

Based on the model proposed in Figure 3-5, the total potential energy in CP behaviour is expressed, as shown in Equation (3-5). It should be noted that this equation includes the angle brackets' vertical stiffness (incorporated in k_v) and the sliding effect of the angle brackets and hold-downs, which are independent of the rocking motion. The contribution of the connectors' stiffness in rotation is denoted k'_v, and obtained using Equation (3-6), which combines the stiffness effect in the vertical direction of the hold-down and the angle brackets as well as the effect of the panel-to-panel connections.

$$\begin{aligned} W_{total} = {} & \frac{1}{2} \cdot b^2 \cdot \vartheta^2 \cdot k'_v + \left(\frac{1}{2} k_{s,x} \cdot n_s \cdot m + k_{h,x} \right) \cdot {\Delta_s}^2 \\ & - F \cdot (h \cdot \vartheta + \Delta_s) + \frac{q \cdot m \cdot b^2 \cdot (2 \cdot \beta - 1)}{2} \cdot \vartheta \end{aligned} \tag{3-5}$$

$$k'_v = k_v + (m - 1) \cdot n_f \cdot k_f \cdot \beta^2 \tag{3-6}$$

Based on the minimum potential energy method, the first derivative of the total potential energy with respect to rotation due to rocking, ϑ, and lateral displacement due to sliding alone, Δ_s, is set to zero, as shown in Equation (3-7) and (3-8), respectively.

$$\frac{\partial W_{total}}{\partial \vartheta} = 0 \rightarrow b^2 \cdot k'_v \cdot \vartheta + \frac{q \cdot m \cdot b^2 \cdot (2 \cdot \beta - 1)}{2} - F \cdot h = 0 \quad (3\text{-}7)$$

$$\frac{\partial W_{total}}{\partial \Delta_s} = 0 \rightarrow \left(k_{s,x} \cdot n_s \cdot m + 2 \cdot k_{h,x}\right) \cdot \Delta_s - F = 0 \quad (3\text{-}8)$$

By solving Equation (3-7), the rotation angle, ϑ, can be recovered, as shown in Equation (3-9). The lateral displacement due to sliding, Δ_s, can be recovered by solving Equation (3-8), as shown in Equation (3-10). Equation (3-10) indicates that wall sliding only depends on the horizontal stiffness of the angle brackets and hold-downs and is independent of the stiffness of other connectors.

$$\vartheta = \left[\frac{F \cdot h}{b^2} - \frac{q \cdot m \cdot (2 \cdot \beta - 1)}{2}\right] \cdot \frac{1}{k'_v} \quad (3\text{-}9)$$

$$\Delta_s = \frac{F}{k_{s,x} \cdot m \cdot n_s + 2 \cdot k_{h,x}} \quad (3\text{-}10)$$

The lateral displacement at the top of the wall, $\Delta_{r,s}$, is defined in Equation (3-11), by considering both rocking (Δ_r) and sliding (Δ_s) effects:

$$\Delta_{r,s} = \Delta_r + \Delta_s = \vartheta \cdot h + \Delta_s \quad (3\text{-}11)$$

The internal forces in the connectors can be obtained by multiplying the displacement by the stiffness of the associated connectors. The internal forces in the panel-to-panel connections, $T_{f,j}$, can be obtained using Equation (3-12) for panel j. The internal forces in all fasteners used in panel-to-panel connections are equal due to equal displacements in the joints when CP behaviour is achieved.

$$T_{f,j} = b \cdot \beta \cdot \vartheta \cdot k_f = \left[\frac{F \cdot h}{b^2} - \frac{q \cdot m \cdot (2 \cdot \beta - 1)}{2}\right] \cdot \frac{k_f \cdot b \cdot \beta}{k'_v}, \quad j = [1\!:\! m-1] \quad (3\text{-}12)$$

The uplift forces in the hold-down, $T_{h,z}$, and the i^{th} angle bracket away from the center of rotation of each panel (see Figure 3-5), $T_{s,z,i,j}$, can be expressed as presented in Equation (3-13) and (3-14), respectively. These equations are derived by multiplying the associated displacement with the stiffness of the connector.

$$T_{h,z} = b \cdot \beta \cdot \vartheta \cdot k_{h,z} = \left[\frac{F \cdot h}{b^2} - \frac{q \cdot m \cdot (2 \cdot \beta - 1)}{2}\right] \cdot \frac{k_{h,z} \cdot b \cdot \beta}{k'_v} \tag{3-13}$$

$$T_{s,z,i,j} = b \cdot \vartheta \cdot \left[\frac{i}{n_s + 1} + (\beta - 1)\right] \cdot \varphi \cdot k_{h,z}$$

$$= \left[\frac{i}{n_s + 1} + (\beta - 1)\right] \cdot \left[\frac{F \cdot h}{b^2} - \frac{q \cdot m \cdot (2 \cdot \beta - 1)}{2}\right] \cdot \frac{\varphi \cdot k_{h,z} \cdot b}{k'_v}, \tag{3-14}$$

$$i = [1{:}\, n_s], j = [1{:}\, m]$$

The horizontal forces in the hold-downs and each angle bracket can be calculated using Equations (3-15) and (3-16), respectively.

$$T_{h,x} = \Delta_s \cdot k_{h,x} = \frac{F \cdot k_{h,x}}{k_{s,x} \cdot m \cdot n_s + 2 \cdot k_{h,x}} \tag{3-15}$$

$$T_{s,x,i,j} = \Delta_s \cdot k_{s,x} = \frac{F \cdot k_{s,x}}{k_{s,x} \cdot m \cdot n_s + 2 \cdot k_{h,x}}, i = [1{:}\, n_s], j = [1{:}\, m] \tag{3-16}$$

Two criteria are required to be checked to ensure that CP elastic mode is achieved. The first criterion (which applies to all other kinematic behaviours) is that the panel rotation is positive. This implies that vertical load does not prevent rocking, as expressed in Equation (3-17). In this equation, the dimensionless uniform vertical load, $\tilde{q}$ [defined as $q \cdot m^2 \cdot b^2/(2 \cdot F \cdot h)$]

$$\vartheta > 0 \;\rightarrow\; \frac{F \cdot h}{b^2} > \frac{q \cdot m}{2} \;\rightarrow\; \tilde{q} < m \tag{3-17}$$

The second criterion is that the vertical reactions at the rotation points are positive (i.e., in compression), as outlined in Equation (3-18) for the first panel. This is considered for the first panel only since the other panels automatically meet the requirement when the reaction at the first panel is in compression and in contact with the ground. By establishing the dimensionless stiffness, $\tilde{k} = k_{h,z}/\left(n_f \cdot k_f\right)$, and after simplification, Equation (3-19) is obtained. In this equation, if the vertical contribution of the angle brackets is desired to be omitted, it can be done by setting φ equal to zero in the inequality. ρ_s is a coefficient that accounts for the contribution of the multiple angle brackets, as expressed in Equation (3-20).

$$R_{C,1} = k_{h,z} \cdot b \cdot \beta \cdot \vartheta + \sum_{i=1}^{n_s} b \cdot \vartheta \cdot \left[\frac{i}{n_s + 1} + (\beta - 1)\right] \cdot \varphi \cdot k_{h,z} - n_f \cdot T_{f,j} + q \cdot b \geq 0 \tag{3-18}$$

$$\tilde{k} \geq \frac{\beta \cdot \left\{1 - \frac{\tilde{q} \cdot [4 \cdot m \cdot \beta - (m + 2 \cdot \beta)]}{m^2}\right\}}{(\beta + \varphi \cdot \gamma_s) - \frac{\tilde{q} \cdot [m \cdot (\beta + \varphi \cdot \gamma_s) \cdot (2 \cdot \beta - 1) - 2 \cdot (\beta^2 + \alpha \cdot \varphi \cdot m)]}{m^2}} \tag{3-19}$$

$$\rho_s = \sum_{i=1}^{n_s} \left[\frac{i}{(n_s + 1)} + (\beta - 1)\right] \tag{3-20}$$

3.2.2. Single-Wall behaviour

For the SW behaviour, the vertical displacements of the individual panels are different, however, the displacements due to rotation and sliding are the same due to the diaphragm constraint (Figure 3-6). The variables in the SW behaviour include rotation, ϑ, vertical displacement of each panel at the point of rotation, v_j, and the sliding displacement, Δ_s.

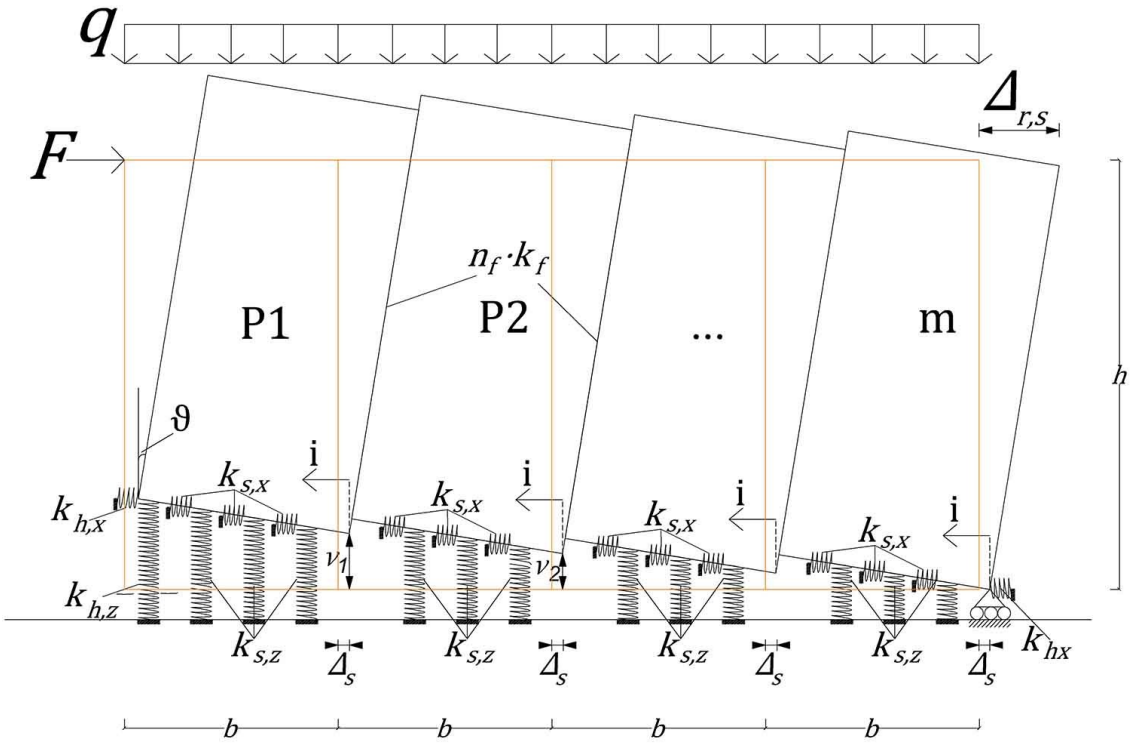

Figure 3-6: SW behaviour of multi-panel CLT shearwalls

Based on the deformed shape shown in Figure 3-6, the total potential energy of the wall assembly can be expressed, as shown in Equation (3-21).

$$\begin{aligned} W_{total} = \frac{1}{2}\cdot k_{h,z} & \\ & \cdot\left\{(v_1 + b\cdot\vartheta)^2 + \varphi \right. \\ & \left.\cdot\left[\alpha\cdot b^2\cdot\vartheta^2 + \sum_{j=1}^{m-1}\sum_{i=1}^{n_s}\left(v_j + \frac{i}{(n_s+1)}\cdot b\cdot\vartheta\right)^2\right]\right\} \\ +\frac{1}{2}\cdot n_f\cdot k_f\cdot & \left[(b\cdot\beta\cdot\vartheta - v_{m-1})^2 + \sum_{j=1}^{m-2}\left(b\cdot\vartheta + v_{j+1} - v_j\right)^2\right] + \frac{1}{2} \\ & \cdot\left(k_{s,x}\cdot n_s\cdot m + 2\cdot k_{h,x}\right)\cdot {\Delta_s}^2 \\ -F\cdot(h\cdot\vartheta + \Delta_s) + \frac{q\cdot b^2\cdot(2\cdot\beta + m - 2)}{2}\cdot\vartheta + & \ q\cdot b\cdot\sum_{j=1}^{m-1} v_j \end{aligned} \tag{3-21}$$

By minimizing the potential energy, the first derivative is set to zero. Equation (3-22) and (3-23) provide the first derivative of the vertical displacements at the rotation point of the first panel and the j^{th} panel, respectively, where $j = [2: m-1]$.

$$\begin{aligned} \frac{\partial W_{total}}{\partial v_1} = 0 \rightarrow k_{h,z}\cdot\left[v_1\cdot(1+\varphi\cdot n_s) + b\cdot\vartheta\cdot\left(1+\frac{\varphi\cdot n_s}{2}\right)\right] - n_f\cdot k_f & \\ \cdot(b\cdot\vartheta + v_2 - v_1) + q\cdot b = 0\,, \qquad j = 1 & \end{aligned} \tag{3-22}$$

$$\begin{aligned} \frac{\partial W_{total}}{\partial v_j} = 0 \rightarrow \varphi\cdot k_{h,z}\cdot n_s\cdot\left(v_j + \frac{b\cdot\vartheta}{2}\right) + n_f\cdot k_f\cdot\left(b\cdot\vartheta + v_j - v_{j-1}\right) - n_f & \\ \cdot k_f\cdot\left(b\cdot\vartheta + v_{j+1} - v_j\right) + q\cdot b = 0, \qquad j = [2: m-1] & \end{aligned} \tag{3-23}$$

The first derivative of the rotation, ϑ, is presented in Equation (3-24). It should be noted that the first derivative of the sliding displacement, Δ_s, outlined in Equation (3-25) is the same as that obtained in the CP case (Equation (3-8)), and is independent of the rotation and vertical displacement of panels at the point of rotation.

$$\frac{\partial L_{total}}{\partial \vartheta} = 0 \rightarrow b \cdot k_{h,z} \cdot \left\{ (v_1 + b \cdot \vartheta) + \varphi \cdot \left[\alpha \cdot b \cdot \vartheta + \frac{n_s}{2} \cdot \sum_{j=1}^{m-1} \left(v_j + \frac{2 \cdot n_s + 1}{n_s + 1} \cdot \frac{b \cdot \vartheta}{3} \right) \right] \right\} + b \cdot n_f \cdot k_f \cdot \left[\beta \cdot (b \cdot \beta \cdot \vartheta - v_{m-1}) + \sum_{j=1}^{m-2} (b \cdot \vartheta + v_{j+1} - v_j) \right] - F \cdot h + \frac{q \cdot b^2 \cdot (2 \cdot \beta + m - 2)}{2} = 0 \quad (3\text{-}24)$$

$$\frac{\partial W_{total}}{\partial \Delta_s} = 0 \rightarrow \left(k_{s,x} \cdot n_s \cdot m + 2 \cdot k_{h,x} \right) \cdot \Delta_s - F = 0 \quad (3\text{-}25)$$

By solving this system of equations (Equation (3-22)-(3-24)), unknowns, such as the vertical displacements at the rotation point of each panel, v_j, and the panel rotation, ϑ, can be determined. The outputs could be considerably complex, especially for a high number of panels. The system of equations is provided in the square $m \times m$ matrix format as shown in Equation (3-26), by which the rotation and the vertical displacement at the rotation point of each panel can be calculated. The sliding displacement, Δ_s, can be obtained by solving Equation (3-25), resulting in the same equation as that defined for the CP case (Equation (3-10)).

$$\begin{bmatrix} v_1 \\ v_2 \\ v_3 \\ \vdots \\ v_j \\ \vdots \\ v_{m-1} \\ v_m \end{bmatrix} = \begin{bmatrix} \tau_1 & \tau_2 & 0 & 0 & 0 & \dots & \dots & \dots & \dots & \dots & \dots & \dots & 0 & \tau_3 \\ \tau_2 & \tau_4 & \tau_2 & 0 & 0 & \dots & \dots & \dots & \dots & \dots & \dots & \dots & 0 & \tau_5 \\ 0 & \tau_2 & \tau_4 & \tau_2 & 0 & \dots & \dots & \dots & \dots & \dots & \dots & \dots & 0 & \tau_5 \\ \vdots & \ddots & \ddots & \ddots & \ddots & \ddots & \ddots & \ddots & \ddots & \ddots & \ddots & \ddots & \ddots & \vdots \\ 0 & 0 & 0 & 0 & 0 & \dots & \tau_2 & \tau_4 & \tau_2 & 0 & \dots & \dots & 0 & \tau_5 \\ \vdots & \ddots & \ddots & \ddots & \ddots & \ddots & \ddots & \ddots & \ddots & \ddots & \ddots & \ddots & \ddots & \vdots \\ 0 & 0 & 0 & 0 & 0 & \dots & \dots & \dots & \dots & \dots & \dots & \tau_2 & \tau_4 & \tau_5 \\ \tau_3 & \tau_5 & \tau_5 & \tau_5 & \tau_5 & \dots & \dots & \dots & \dots & \dots & \dots & \dots & \tau_5 & \tau_6 \end{bmatrix}^{-1} \times \begin{bmatrix} \tau_7 \\ \tau_7 \\ \tau_7 \\ \vdots \\ \tau_7 \\ \vdots \\ \tau_7 \\ \tau_8 \end{bmatrix}$$

(columns: 1 2 3 4 5 … j-1 j j+1 … … m-2 m-1 m)

$$\tau_1 = k_{h,z} \cdot (1 + \varphi \cdot n_s) + n_f \cdot k_f$$
$$\tau_2 = -n_f \cdot k_f \quad (3\text{-}26)$$

$$\tau_3 = k_{h,z} \cdot b \cdot (1 + \frac{\varphi \cdot n_s}{2}) - n_f \cdot k_f \cdot b$$
$$\tau_4 = k_{h,z} \cdot \varphi \cdot n_s + 2 \cdot n_f \cdot k_f$$
$$\tau_5 = 0.5 \cdot k_{h,z} \cdot \varphi \cdot b \cdot n_s$$
$$\tau_6 = b^2 \cdot k_{h,z} \cdot \left\{1 + \varphi \cdot \left[\alpha + \frac{(m-1) \cdot n_s \cdot (2 \cdot n_s + 1)}{6 \cdot (n_s + 1)}\right]\right\} + b^2 \cdot n_f \cdot k_f \cdot (m - 2 + \beta^2)$$
$$\tau_7 = -q \cdot b$$
$$\tau_8 = (F \cdot h) - \frac{q \cdot b^2 \cdot (2 \cdot \beta + m - 2)}{2}$$

Equations (3-27) expresses the internal forces in each fastener in panel-to-panel connections when $j = [1: m-2]$ and $j = m-1$, respectively. It should be noted that in the SW behaviour, fasteners located in the same panel have equal internal force, consistently with the CP case, however, the internal forces of the panel-to-panel connections between different panels are not equal.

$$T_{f,j} = k_f \cdot \left(b \cdot \vartheta + v_{j+1} - v_j\right), \qquad j = [1: m-2]$$
$$T_{f,j} = k_f \cdot (b \cdot \beta \cdot \vartheta - v_{m-1}), \qquad j = m-1 \tag{3-27}$$

The uplift force in the hold-down can be developed, as presented in Equation (3-28). The uplift force in the i^{th} angle bracket from the center of rotation in panel j, can be calculated using Equation (3-29). For the last panel ($j = m$), Equation (3-30) can be used given that v_m is equal to zero.

$$T_{h,z} = k_{h,z} \cdot (b \cdot \vartheta + v_1) \tag{3-28}$$

$$T_{s,i,j,z} = \varphi \cdot k_{h,z} \cdot \left(\frac{i}{n_s + 1} \cdot b \cdot \vartheta + v_j\right), \qquad i = [1: n_s], j = [1: m-1] \tag{3-29}$$

$$T_{s,i,j,z} = \varphi \cdot k_{h,z} \cdot \left[\frac{i}{n_s + 1} + (\beta - 1)\right] \cdot b \cdot \vartheta, \qquad i = [1: n_s], j = m \tag{3-30}$$

Similar to the case presented for CP behaviour, the horizontal forces in a angle bracket and hold-down can be obtained using Equations (3-15) and (3-16), respectively.

To illustrate the concept of the procedure for a simple system, an example is presented in Equations (3-31)-(3-33) for $m = 2$ and $n_s = 3$, and $\beta = 1$. In this case, v_2 is equal to zero since in SW behaviour $m - 1$ panels are displaced vertically at the rotation point, while

the last panel m is in contact with the ground. v_1 is the vertical displacement of the first panel at the rotation point, and ϑ is the rotation of the panels. The sliding displacement, Δ_s, can be obtained using Equation (3-10), by equating m to 2, as shown in Equation (3-33). The total lateral displacement at the top of the panels due to sliding and rotation, $\Delta_{r,s}$, can be obtained using Equation (3-11).

$$\vartheta = \frac{2 \cdot \{F \cdot h \cdot [k_{h,z} \cdot (6 \cdot \varphi + 2) + 2 \cdot n_f \cdot k_f] - q \cdot b^2 \cdot (4 \cdot n_f \cdot k_f + 3 \cdot \varphi \cdot k_{h,z})\}}{b^2 \cdot [\varphi \cdot k_{h,z}^2 \cdot (12 \cdot \varphi + 7) + k_{h,z} \cdot n_f \cdot k_f \cdot (31 \cdot \varphi + 16)]} \quad (3\text{-}31)$$

$$v_1 = \frac{-\{F \cdot h \cdot [k_{h,z} \cdot (6 \cdot \varphi + 4) - 4 \cdot n_f \cdot k_f] + q \cdot b^2 \cdot (8 \cdot n_f \cdot k_f + \varphi \cdot k_{h,z})\}}{b \cdot [\varphi \cdot k_{h,z}^2 \cdot (12 \cdot \varphi + 7) + k_{h,z} \cdot n_f \cdot k_f \cdot (31 \cdot \varphi + 16)]} \quad (3\text{-}32)$$

$$\Delta_s = \frac{F}{2 \cdot (3 \cdot k_{s,x} + k_{h,x})} \quad (3\text{-}33)$$

To ensure SW behaviour, the expression presented in Equation (3-34) needs to be satisfied, where the vertical displacement at the rotation point of panel $m-1$ is required to be positive. This means that all panels except the last one would lift and not maintain contact with the ground at the rotation point. This equation varies depending on the number of panels. An example is provided for $m = 2$ and $n_s = 3$ in Equation (3-35). This is done by equating the vertical displacement at the rotation point for panel $m-1$ (v_1) to zero. After simplification, this equation is rewritten, as shown in Equation (3-36).

$$v_{m-1} > 0 \quad (3\text{-}34)$$

$$F \cdot h \cdot [k_{h,z} \cdot (6 \cdot \varphi + 4) - 4 \cdot n_f \cdot k_f] + q \cdot b^2 \cdot (8 \cdot n_f \cdot k_f + \varphi \cdot k_{h,z}) < 0 \quad (3\text{-}35)$$

$$\tilde{k} < \frac{1 - \frac{\tilde{q}}{2}}{1 + \frac{\varphi}{2} \cdot \left(3 + \frac{\tilde{q}}{8}\right)}, \qquad for: m = 2, n_s = 3 \quad (3\text{-}36)$$

Appendix C Appendix C - presents the results of 10 different cases of multi-panel CLT shearwalls in IN kinematic mode to show the applicability of interpolation between proposed expressions for CP and SW against the results obtained from expressions for IN available in the literature (Casagrande et al., 2018). Acceptable accuracy was observed in all cases, indicating interpolation effectiveness. However, interpolation when the bi-

directional contribution of angle brackets and hold-downs is included, as proposed in this section, is not investigated since IN expressions are not developed.

3.3. Inelastic analytical method

The elastic approach described in Section 3.2 is extended to the inelastic behaviour, including the effect of bi-direction contribution of the angle brackets and hold-downs. Similar methodology has been successfully used to describe the behaviour of CLT shearwalls with multiple panels (Nolet et al., 2019), however these approaches omitted the vertical contribution of angle brackets and the horizontal effect of hold-downs. The developed methodology focuses on the CP behaviour, because it promotes rocking kinematic mode (CSA O86-19, 2019; Nolet et al., 2019). CP plastic behaviour occurs when panel-to-panel connections yield before angle brackets and hold downs.

The methodology outlined in this section assumes that the connectors behave as elastic-perfectly plastic, as shown in Figure 3-7. Although it is expected that some discrepancy could occur when the real properties of the connection are employed, this assumption reduces the complexity of analytical expressions and requirements. The method also allows for the development of closed-form expressions at different levels of load and displacement. In Chapter 7, section 7.5, the discrepancy attributed to this assumption is examined by providing examples of multi-panel CLT shearwalls in which experimental test results are compared with numerical models based on real load-displacement curves of connections and analytical expressions developed in the current section. The properties used are: r_f, r_{hz}, r_{hx}, r_{sz} and r_{sx}, representing the strength of the fasteners in the panel-to-panel connections, hold-downs in vertical and horizontal direction, and angle brackets in vertical and horizontal direction, respectively. Parameters d_y and d_u denote the yield and ultimate displacement of the connectors, respectively, with additional subscripts indicating the type of connector represented (i.e., f for fasteners in the panel-to-panel connections, hx and hz for hold-downs in horizontal and vertical directions, respectively, and sx and sz for angle brackets in the horizontal and vertical directions, respectively).

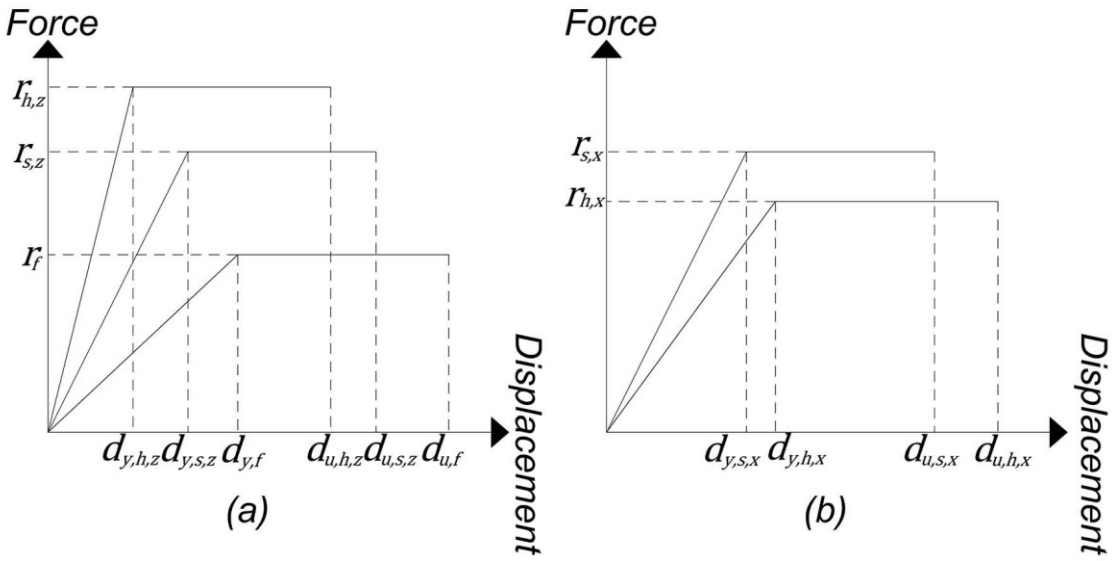

Figure 3-7: Elastic-perfectly plastic (bi-linear) curve of connections: (a) for hold-down and angle brackets in uplift and panel-to-panel connection in shear; (b) for hold-down and angle brackets in shear

The interaction between the vertical and horizontal direction in the angle brackets and hold-downs can be expressed in the circular domain, demonstrated in Equations (3-37) and (3-38), respectively (*European Technical Assessment ETA-06/0106*, 2016; Izzi et al., 2018). In these equations, $T_{s,z,i}$ and $T_{s,x,i}$ are the internal forces in the angle bracket i from the center of rotation and $T_{h,z}$ and $T_{h,x}$ are the internal forces in the hold-downs.

$$\left(\frac{T_{s,z,i}}{r_{s,z}}\right)^2 + \left(\frac{T_{s,x,i}}{r_{s,x}}\right)^2 \leq 1.0, \qquad i = [1{:}\, n_s] \tag{3-37}$$

$$\left(\frac{T_{h,z}}{r_{h,z}}\right)^2 + \left(\frac{T_{h,x}}{r_{h,x}}\right)^2 \leq 1.0 \tag{3-38}$$

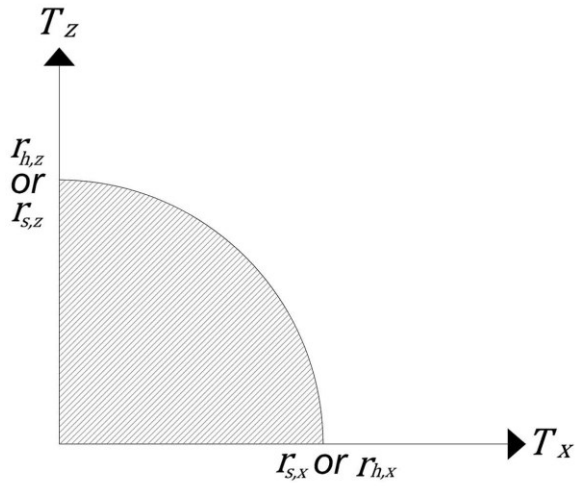

Figure 3-8: The circular domain defined for angle brackets and hold-downs as shown in Figure 3-7

The behaviour of the CLT shearwall in the elastic and inelastic regions is described in a generalized form in Figure 3-9. In this figure, P_0 represents the activation point at which the wall starts to rotate, corresponding to lateral force, R_{P_0}, and displacement, Δ_{P_0}. Points P_1 and P_2 represent the yielding of fasteners in panel-to-panel connections and hold-down, respectively. Points P_3 to P_{n_s+2} represent the yielding order of the angle brackets starting from the last angle bracket away from the centre of rotation of each panel. The expression for the ultimate displacement of the shearwall is not established due to the uncertainty associated with the contribution of sliding and rotation after the yielding of all connections.

In the analytical procedure, a verification is made using Equations (3-37) and (3-38) to ensure that the angle brackets and hold-down remain elastic at required levels. This verification is particularly important for the angle brackets because when they start yielding, the wall is no longer capable of resisting additional horizontal loads, and consequently, it will proceed to slide until the ultimate failure of them is reached.

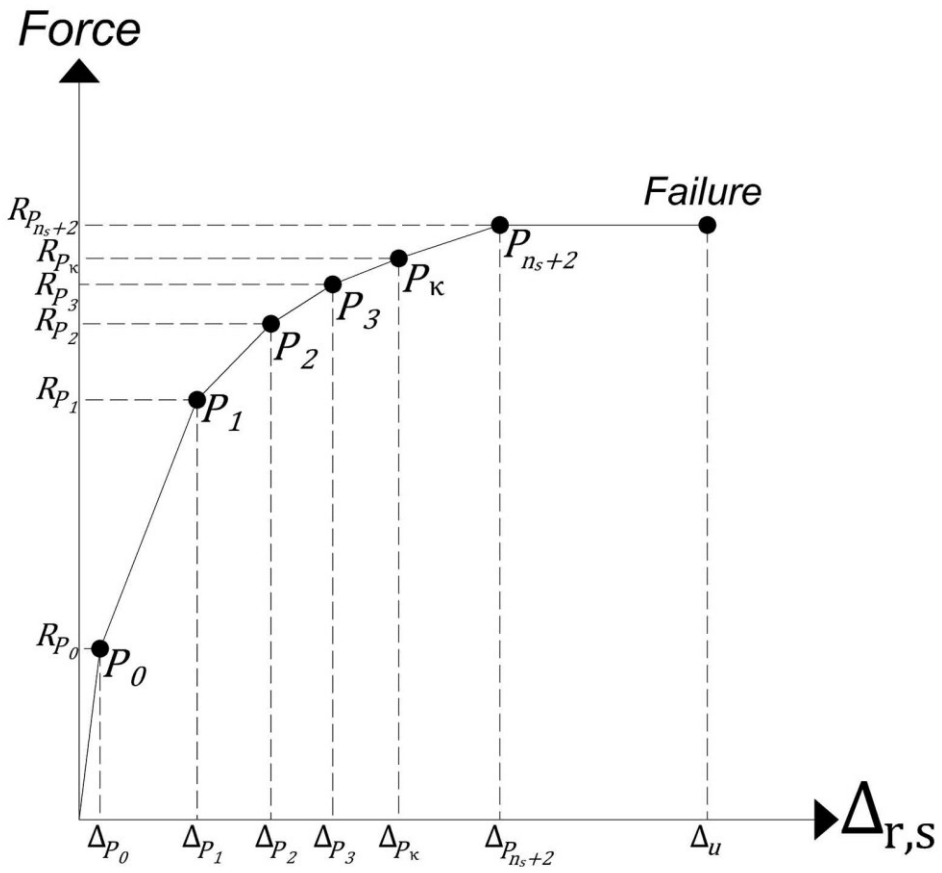

Figure 3-9: The inelastic curve of multi-panel CLT shearwalls in CP-CP behaviour

3.3.1. Expressions for P_0

The activation force, R_{P_0}, is defined as the lateral force at which the gravity load is overcome, and the panels start to rotate. The value of R_{P_0} can be obtained using Equation (3-39).

$$R_{P_0} = \frac{q \cdot m \cdot b^2 \cdot (2 \cdot \beta - 1)}{2 \cdot h} \tag{3-39}$$

At the activation force, the lateral displacement, Δ_{P_0}, is presented in Equation (3-40), using Equation (3-10). Upon reaching the activation force, there is no rotation in the panels, so the lateral displacement is caused only by sliding. Equations (3-41) and (3-42) are used to verify whether angle brackets and hold-downs remain elastic. These equations are derived by setting the vertical component of the angle brackets and hold-downs, T_{sz} and T_{hz}, in Equations (3-37) and (3-38) equal to zero, since there is no rotation or uplift in the panels.

$$\Delta_{P_0} = \frac{R_{P_0}}{k_{s,x} \cdot m \cdot n_s + 2 \cdot k_{h,x}} \tag{3-40}$$

$$\left(\frac{T_{s,x}}{r_{s,x}}\right)^2 < 1 \rightarrow \left[\frac{R_{P_0} \cdot k_{s,x}}{r_{s,x} \cdot \left(k_{s,x} \cdot m \cdot n_s + 2 \cdot k_{h,x}\right)}\right] < 1 \tag{3-41}$$

$$\left(\frac{T_{h,x}}{r_{h,x}}\right)^2 < 1 \rightarrow \left[\frac{R_{P_0} \cdot k_{h,x}}{r_{h,x} \cdot \left(k_{s,x} \cdot m \cdot n_s + 2 \cdot k_{h,x}\right)}\right] < 1 \tag{3-42}$$

3.3.2. Expressions for P_1

The lateral force associated with the yielding of the fasteners in the panel-to-panel connection, denoted P_1 in Figure 3-9, is expressed in Equation (3-43). This expression is obtained by equating the elastic force in panel-to-panel connections, defined in Equation (3-12), with the yield capacity of the fasteners in the panel-to-panel connections, r_f. In this equation, $k'_{v,P_1} = k_v + (m-1) \cdot n_f \cdot k_f \cdot \beta^2$, where k_v can be obtained from Equation (3-3).

$$R_{P_1} = \left(r_f \cdot \frac{k'_{v,P_1} \cdot b}{k_f \cdot h \cdot \beta}\right) + R_{P_0} \tag{3-43}$$

The associated lateral displacement due to the sliding and rocking, Δ_{P_1}, can be determined using Equations (3-44), based on the elastic displacement of the wall in the CP behaviour, obtained from Equation (3-11). In Equation (3-44), K_{V,P_1} is the lateral stiffness of the shearwall at point P_1, obtained as $k'_{v,P_1} \cdot b^2/h^2$.

$$\begin{aligned}\Delta_{P_1} &= \left[\frac{R_{P_1} \cdot h^2}{b^2} - \frac{q \cdot m \cdot (2 \cdot \beta - 1) \cdot h}{2}\right] \cdot \frac{1}{k'_{v,P_1}} + \frac{R_{P_1}}{\left(k_{s,x} \cdot m \cdot n_s + 2 \cdot k_{h,x}\right)} \\ &= \frac{R_{P_1} - R_{P_0}}{K_{V,P_1}} + \frac{R_{P_1}}{\left(k_{s,x} \cdot m \cdot n_s + 2 \cdot k_{h,x}\right)} \\ &= d_{y,f} \cdot \frac{h}{b \cdot \beta} + \frac{R_{P_1}}{\left(k_{s,x} \cdot m \cdot n_s + 2 \cdot k_{h,x}\right)}\end{aligned} \tag{3-44}$$

The internal uplift forces in the angle brackets and hold-down at the point of yielding of the angle brackets, $T_{s,z}^{P_1}$ and $T_{h,z}^{P_1}$, are presented in Equations (3-45) and (3-46), respectively.

These equations are based on the elastic uplift load in the angle brackets and hold-down and where F is replaced by the associated lateral load at this point, equal to R_{P_1}.

$$T_{s,z,i}^{P_1} = \left[\frac{i}{n_s+1} + (\beta-1)\right] \cdot \left[\frac{R_{P_1} \cdot h}{b^2} - \frac{q \cdot m \cdot (2 \cdot \beta - 1)}{2}\right] \cdot \frac{\varphi \cdot k_{h,z} \cdot b}{k'_{v,P_1}}, \quad i = [1{:}\, n_s] \tag{3-45}$$

$$T_{h,z}^{P_1} = \left[\frac{R_{P_1} \cdot h}{b^2} - \frac{q \cdot m \cdot (2 \cdot \beta - 1)}{2}\right] \cdot \frac{k_{h,z} \cdot b \cdot \beta}{k'_{v,P_1}} \tag{3-46}$$

At this point, the angle brackets and hold-downs remain in the elastic region if the interaction expressions outlined in Equation (3-47) and (3-48) are satisfied. These equations are based on the general interaction equation (i.e., Equations (3-37) and (3-38)), while replacing the associated internal forces using the equations provided in section 3.2.1.

$$\left(\frac{T_{s,z,i}^{P_1}}{r_{s,z}}\right)^2 + \left[\frac{R_{P_1} \cdot k_{s,x}}{r_{s,x} \cdot \left(k_{s,x} \cdot m \cdot n_s + 2 \cdot k_{h,x}\right)}\right]^2 < 1.0, \qquad i = [1{:}\, n_s] \tag{3-47}$$

$$\left(\frac{T_{h,z}^{P_1}}{r_{h,z}}\right)^2 + \left[\frac{R_{P_1} \cdot k_{h,x}}{r_{h,x} \cdot \left(k_{s,x} \cdot m \cdot n_s + 2 \cdot k_{h,x}\right)}\right]^2 < 1.0 \tag{3-48}$$

3.3.3. Expressions for P_2

The increase in the internal hold-down force from P_1 to P_2, $t_{h,z}^{P_2}$, can be obtained by replacing F in the internal force of hold-down with the associated increase in lateral force, $R_{P_2} - R_{P_1}$. The lateral load capacity of the shearwall at point P_2, representing the yield point of the hold-down, is denoted R_{P_2}. In Equation (3-49), k'_{v,P_2} is equal to k_v, since the panel-to-panel connections have yielded and are no longer contribute to the wall stiffness. It is noteworthy to mention that the effect of uniform load q is not considered in the equations developed subsequently, since such effect has already been taken into account in the equations at points P_1 and P_0.

$$t_{h,z}^{P_2} = \left[\frac{\left(R_{P_2} - R_{P_1}\right) \cdot h}{b}\right] \cdot \frac{k_{h,z}}{k'_{v,P_2}} = \frac{\left(R_{P_2} - R_{P_1}\right) \cdot h \cdot \beta}{b \cdot (\beta^2 + \alpha \cdot \varphi \cdot m)} \tag{3-49}$$

By equating the interaction expression for the hold-down at P_2 to 1, as shown in Equation (3-50), the lateral capacity at this level, R_{P_2}, can be obtained. The solution to this equation is cumbersome and is more suitable for use in the development of software solutions, especially for higher numbers of panels. The associated uplift force in the hold-down, $T_{h,z}^{P_2}$, is equal to the sum of $T_{h,z}^{P_1}$ and $t_{h,z}^{P_2}$.

$$\left(\frac{T_{h,z}^{P_2}}{r_{h,z}}\right)^2 + \left[\frac{R_{P_2} \cdot k_{h,x}}{r_{h,x} \cdot \left(k_{s,x} \cdot m \cdot n_s + 2 \cdot k_{h,x}\right)}\right]^2 = 1.0 \tag{3-50}$$

The increase in lateral displacement from P_1 to P_2, δ_{P_2}, can be determined using Equation (3-51). This equation is based on the elastic displacement obtained in the CP behaviour, Equation (3-11), by replacing the lateral load, F, with the associated increase in lateral load capacity, $R_{P_2} - R_{P_1}$. Finally, the lateral displacement at P_2 due to sliding and rocking is presented in Equation (3-52), which can be obtained by summing the lateral displacement at P_1, Δ_{P_1}, and the increase in lateral displacement, δ_{P_2}. The lateral stiffness of shearwalls at P_2, K_{V,P_2}, is defined as $k'_{v,P_2} \cdot b^2/h^2$.

$$\begin{aligned}\delta_{P_2} &= \left[\frac{\left(R_{P_2} - R_{P_1}\right) \cdot h^2}{b^2}\right] \cdot \frac{1}{k'_{v,P_2}} + \frac{R_{P_2} - R_{P_1}}{\left(k_{s,x} \cdot m \cdot n_s + 2 \cdot k_{h,x}\right)} \\ &= \frac{R_{P_2} - R_{P_1}}{K_{V,P_2}} + \frac{R_{P_2} - R_{P_1}}{\left(k_{s,x} \cdot m \cdot n_s + 2 \cdot k_{h,x}\right)}\end{aligned} \tag{3-51}$$

$$\Delta_{P_2} = \Delta_{P_1} + \delta_{P_2} = d_{y,f} \cdot \frac{h}{b \cdot \beta} + \frac{R_{P_2} - R_{P_1}}{K_{V,P_2}} + \frac{R_{P_2}}{\left(k_{s,x} \cdot m \cdot n_s + 2 \cdot k_{h,x}\right)} \tag{3-52}$$

To ensure that the fasteners in the panel-to-panel connections do not reach their ultimate displacement at or before P_2, Equation (3-53) is required to be satisfied.

$$d_{y,f} + \frac{b \cdot \beta}{h} \cdot \frac{R_{P_2} - R_{P_1}}{K_{V,P_2}} < d_{u,f} \tag{3-53}$$

The increase in internal uplift force in the i^{th} angle bracket from P_1 to P_2, $t_{s,z}^{P_2}$, is presented in Equation (3-54):

$$t_{s,z,i}^{P_2} = \left[\frac{i}{n_s+1} + (\beta - 1)\right] \cdot \left[\frac{\left(R_{P_2} - R_{P_1}\right) \cdot h^2}{b^2}\right] \cdot \frac{\varphi \cdot k_{h,z} \cdot b}{k'_{v,P_2} \cdot h}$$
$$= \left[\frac{i}{n_s+1} + (\beta - 1)\right] \cdot \frac{\left(R_{P_2} - R_{P_1}\right) \cdot h \cdot \varphi}{b \cdot (\beta^2 + \alpha \cdot \varphi \cdot m)}, \qquad i = [1{:}\, n_s] \tag{3-54}$$

At this point, the vertical uplift load in the angle brackets is obtained as the sum of Equation (3-54) and (3-45). Also, the horizontal load in the angle bracket can be obtained using Equation (3-16). Equation (3-55) is used to check that the angle brackets remain in the elastic region. It is only required to check the last angle brackets from the centre of rotation of each panel ($i = n_s$).

$$\left(\frac{T_{s,z,i}^{P_1} + t_{s,z,i}^{P_2}}{r_{s,z}}\right)^2 + \left[\frac{R_{P_2} \cdot k_{s,x}}{r_{s,x} \cdot \left(k_{s,x} \cdot m \cdot n_s + 2 \cdot k_{h,x}\right)}\right]^2 < 1.0, \;\; i = [1{:}\, n_s] \tag{3-55}$$

3.3.4. Expressions for P_{κ}

Equation (3-56) represents the increase in the uplift forces in the angle brackets after the yielding of the panel-to-panel connections and the hold-down. The increase in the vertical uplift force in the angle brackets from $P_{\kappa-1}$ to P_{κ}, is denoted as $t_{s,z,i}^{P_{\kappa}}$, where κ is equal to $[3{:}\, n_s + 2]$. Equation (3-57) represents the contribution to stiffness of those angle brackets that remain elastic in the uplift direction at P_{κ}, $k'_{v,P_{\kappa}}$. In this equation, c is equal to $(n_s + 3) - \kappa$.

The increase in angle brackets' uplift force from $P_{\kappa-1}$ to P_{κ}, $t_{s,z,i}^{P_{\kappa}}$, can be obtained using Equation (3-56), where $\kappa = [3{:}\, n_s + 2]$. Equation (3-57) represents the contribution of not yielded angle brackets at P_{κ}, $k'_{v,P_{\kappa}}$. In these equations, c stands for the number of angle brackets remaining elastic in each panel at P_{κ}, which is equal to $(n_s + 3) - \kappa$. It is noteworthy to mention that the yielding of angle brackets starts from the last angle bracket away from the center of rotation since the magnitude of the uplift force is higher than other angle brackets.

$$t_{s,z,i}^{P_{\kappa}} = \left[\frac{i}{n_s+1} + (\beta - 1)\right] \cdot \left[\frac{\left(R_{P_{\kappa}} - R_{P_{\kappa-1}}\right) \cdot h}{b^2}\right] \cdot \frac{\varphi \cdot k_{h,z} \cdot b}{k'_{v,P_{\kappa}}}, \qquad i = [1{:}\, c] \tag{3-56}$$

$$k'_{v,P_{\kappa}} = k_{h,z} \cdot \varphi \cdot m \cdot \sum_{i=1}^{c} \left[\frac{i}{(n_s + 1)} + (\beta - 1) \right]^2 \tag{3-57}$$

In order to determine the yield point of the associated angle brackets, Equation (3-58) is obtained by equating the interaction equation (i.e., Equation (3-37)) to 1. The associated lateral capacity, $R_{P_{\kappa}}$, can be obtained by solving this equation, however similar to Equation (3-50), the solution to this equation is cumbersome and does not lend itself to reasonable simple expressions, especially for higher numbers of panels.

$$\left(\frac{T_{s,z,c}^{P_1} + t_{s,z,c}^{P_2} + \sum_{x=3}^{\kappa} t_{s,z,c}^{P_x}}{r_{s,z}} \right)^2 + \left\{ \frac{1}{r_{s,x}} \cdot \left[\frac{R_{P_2} \cdot k_{s,x}}{(k_{s,x} \cdot m \cdot n_s + 2 \cdot k_{h,x})} + \sum_{x=3}^{\kappa} \frac{(R_{P_x} - R_{P_{x-1}}) \cdot k_{s,x}}{m \cdot k_{s,x}(n_s + 3 - x) + k_{h,x}} \right] \right\}^2 = 1.0 \tag{3-58}$$

The increase in the lateral displacement from $P_{\kappa-1}$ to P_{κ}, $\delta_{P_{\kappa}}$, can be derived based on the same procedure as described in Equation (3-51), by considering the associated increase in the lateral load capacity, as expressed in Equation (3-59). The lateral displacement due to sliding and rocking, $\Delta_{P_{\kappa}}$, can be calculated using Equation (3-60), which is the sum of the total lateral displacement at $P_{\kappa-1}$, and the increase in the displacement from $P_{\kappa-1}$ to P_{κ}, obtained using Equation (3-59). $K_{V,P_{\kappa}}$ is defined as $k'_{v,P_{\kappa}} \cdot b^2/h^2$.

$$\begin{aligned} \delta_{P_{\kappa}} &= \left[\frac{(R_{P_{\kappa}} - R_{P_{\kappa-1}}) \cdot h^2}{b^2} \right] \cdot \frac{1}{k'_{v,P_{\kappa}}} + \frac{R_{P_{\kappa}} - R_{P_{\kappa-1}}}{k_{s,x} \cdot m \cdot c + k_{h,x}} \\ &= \frac{R_{P_{\kappa}} - R_{P_{\kappa-1}}}{K_{V,P_{\kappa}}} + \frac{R_{P_{\kappa}} - R_{P_{\kappa-1}}}{k_{s,x} \cdot m \cdot c + k_{h,x}} \end{aligned} \tag{3-59}$$

$$\Delta_{P_{\kappa}} = \Delta_{P_{\kappa-1}} + \delta_{P_{\kappa}} = \Delta_{P_{\kappa-1}} + \frac{R_{P_{\kappa}} - R_{P_{\kappa-1}}}{K_{V,P_{\kappa}}} + \frac{R_{P_{\kappa}} - R_{P_{\kappa-1}}}{k_{s,x} \cdot m \cdot c + k_{h,x}} \tag{3-60}$$

At P_{κ}, it is required to ensure that the fasteners in the panel-to-panel connections have not reached their respective ultimate displacements by satisfying Equation (3-61).

$$d_{y,f} + \frac{b \cdot \beta}{h} \cdot \sum_{i=2}^{\kappa} \frac{R_{P_i} - R_{P_{i-1}}}{K_{V,P_i}} < d_{u,f} \tag{3-61}$$

To ensure that the hold-down connections do not reach their ultimate displacement at P_{κ}, Equation (3-62) needs to be satisfied. In this equation, $\Delta_{s,P_{\kappa}}$ and $D_{z,P_{\kappa}}$ are the sliding and uplift displacements in the hold-down, respectively, as presented in Equations (3-63) and (3-64).

$$\left(\frac{D_{z,P_{\kappa}}}{d_{u,h,z}}\right)^2 + \left(\frac{\Delta_{s,P_{\kappa}}}{d_{u,h,x}}\right)^2 < 1 \tag{3-62}$$

$$\Delta_{s,P_{\kappa}} = \frac{R_{P_2}}{\left(k_{s,x} \cdot m \cdot n_s + 2 \cdot k_{h,x}\right)} + \sum_{i=3}^{\kappa} \frac{R_{P_i} - R_{P_{i-1}}}{k_{s,x} \cdot m \cdot (n_s + 3 - i) + k_{h,x}} \tag{3-63}$$

$$D_{z,P_{\kappa}} = d_{y,f} + \frac{b \cdot \beta}{h} \cdot \sum_{i=2}^{\kappa} \frac{R_{P_i} - R_{P_{i-1}}}{K_{V,P_i}} \tag{3-64}$$

It is required to ensure that the last angle bracket from the centre of rotation of each panel, which has the highest uplift force, does not reach its ultimate displacement, as presented in Equation (3-65). This equation is expected to be checked for values of κ greater than 3, since for values equal or less than 3, the angle brackets would not have started to yield.

$$\left\{\left[\frac{n_s}{n_s + 1} - (1 - \beta)\right] \cdot \frac{D_{z,P_{\kappa}}}{d_{u,s,z} \cdot \beta}\right\}^2 + \left(\frac{\Delta_{s,P_{\kappa}}}{d_{u,s,x}}\right)^2 < 1 \tag{3-65}$$

3.4. Shear deformation in CLT panels

The CLT panels have so far been assumed as rigid bodies and as such their shear deformation has been ignored in the development of the proposed model. The shear deformation contribution of the panels can be independently calculated and then incorporated into the total lateral deformation equation containing the lateral displacements due to rocking and sliding (Casagrande, Rossi, Tomasi, et al., 2016). The shear deformation of panel j, $\Delta_{sh,j}$, can be calculated using the expression presented in Equation (3-66). In this equation, F_j is the lateral load in the j^{th} panel, G is the equivalent shear modulus, as outlined in Equation (3-67) (Brandner et al., 2017a), and t is the thickness of CLT panels. G_{mean} is the shear modulus in-plane of laminations, n_l is the number of laminations, w is the average of the edge distance and spacing between stress relief and the width of the CLT

laminates. g_1 and g_2 are the coefficients that vary depending on the number of laminations, as summarized in Table 3-1.

$$\Delta_{sh,j} = \frac{F_j \cdot h}{G \cdot t \cdot b}, \qquad j = [1:m] \tag{3-66}$$

$$G = \frac{G_{mean}}{1 + 6 \cdot y_t \cdot \left(\frac{t_{mean}}{w}\right)^2} \tag{3-67}$$

Where, $y_t = g_1 \cdot \left(\frac{t_{mean}}{w}\right)^{g_2}$ & $t_{mean} = \frac{t}{n_l}$

Table 3-1: The values of g_1 and g_2 for different number of laminations (Brandner et al., 2017a)

Number of layers	**3-ply**	**5-ply**	**7-ply**
$\boldsymbol{g_1}$	0.53	0.43	0.39
$\boldsymbol{g_2}$	-0.79	-0.79	-0.79

3.5. Bending deformation in CLT panels

The bending deformation of CLT panels can be calculated independently using elastic theory since the panels act elastically due to the high in-plane stiffness, as can be obtained using Equation (3-68).

$$\Delta_b = \frac{F_j \cdot h^3}{3 \cdot EI_{eff}} \tag{3-68}$$

Where, EI_{eff} represents the elastic effective bending stiffness of the CLT panels. The value of EI_{eff} can be calculated using Equations (3-69).

$$EI_{eff} = m \cdot \left(E_0 \cdot t_0 \cdot \frac{b^3}{12} + E_{90} \cdot t_{90} \cdot \frac{b^3}{12}\right) \tag{3-69}$$

Where, E_0 and E_{90} are longitudinal (vertical layers) and transverse (horizontal layers) modulus of elasticity, respectively, and t_0 and t_{90} refer to the total thicknesses of the longitudinal and transverse layers, respectively.

3.6. Investigations on the contribution of bi-directional behaviour of angle brackets

3.6.1. Kinematic consistency regions of lateral behaviour

The kinematic regions, depicting areas where different kinematic modes govern the behaviour of the wall, are plotted using the consistency (limit) expressions provided in Equations (3-19) and (3-34) for the CP and SW behaviours, respectively. The IN region can be obtained as the area between CP and SW behaviours. The graphs are based on dimensionless vertical load, $\tilde{q}$, and dimensionless stiffness, $\tilde{k}$, allowing for the representation of different properties of connectors and applied loads. The angle bracket stiffness ratio, φ, is considered for discrete values of 0, 0.5 and 1. An example of such representation is demonstrated in Figure 3-10, for shearwalls consisting of 4 and 6 panels with one angle bracket at the middle of each panel (i.e., $n_s = 1$), while also neglecting the compression zone (i.e., $\beta = 1$) for simplicity.

As expected, when the bi-directional effect of the angle brackets is considered in the analysis, especially for relatively stiff angle brackets in the vertical direction (i.e., large values of φ), more panels are likely to maintain contact with the ground, resulting in less displacements and rotations. Comparing Figure 3-10(a) (depicting 4 panels) to Figure 3-10(b) (depicting 6 panels), it can be observed that as the number of panels increases, the SW region becomes smaller for all values of φ, since more connectors are involved in resisting the vertical uplift load, resulting in a stronger and stiffer wall assembly.

For the case with no vertical load ($\tilde{q} = 0$), it can be observed that when the bi-directional behaviour of angle brackets is neglected ($\varphi = 0$), either CP or SW behaviour is attained for $\tilde{k}$ values greater than or lesser than 1, respectively, independent of the number of panels. However, when the vertical contribution of angle brackets is considered, the SW region is smaller for larger values of φ, and all three kinematic modes (CP, SW, and IN) are possible.

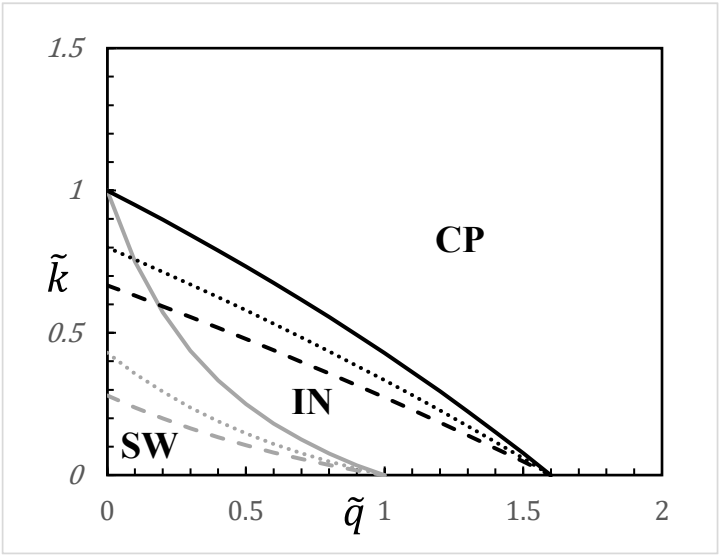

(a)

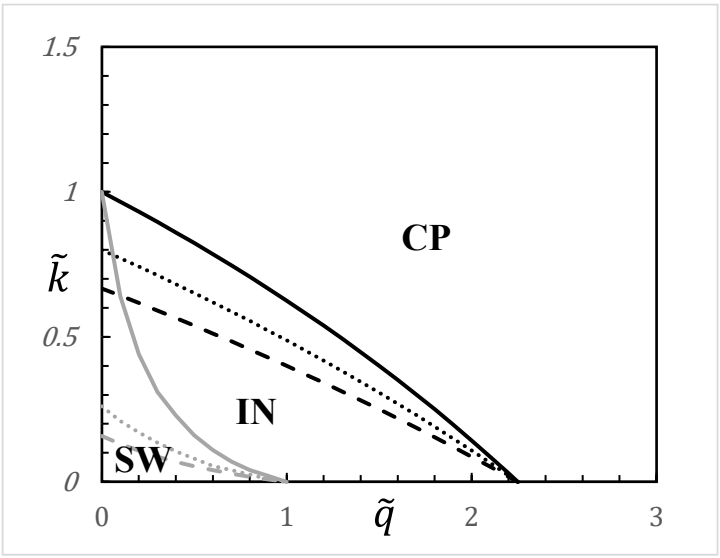

(b)

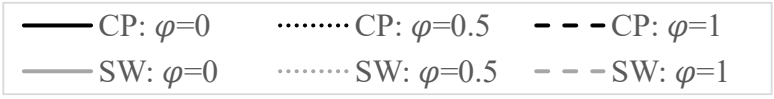

Figure 3-10: Kinematic consistency regions for a) $m = 4$; b) $m = 6$

By increasing the dimensionless vertical load, \widetilde{q}, the difference between the border lines for both CP and SW becomes smaller. This implies that the influence of angle bracket vertical (uplift) on overall wall behaviour is less significant when gravity load increases. It can be observed that at the SW limit, the border lines coincide at a value of $\tilde{q}$

equal to 1, irrespective of the number of panels (Figure 3-10), which means that for $\tilde{q} > 1$, the SW behaviour cannot be attained. For CP behaviour, the border lines coincide at a $\tilde{q}$ value that depends on the number of panels, the number of fasteners in the panel-to-panel connections and the geometry of the panels.

When $\tilde{k}$ exceeds a limit value, CP behaviour can be achieved regardless of the value of $\tilde{q}$ and the number of panels. This limit is equal to 1 ($\tilde{k} > 1$), for the case where the bi-directional effect of angle brackets is neglected. For the case where angle brackets with high vertical stiffness are considered ($\varphi = 1$) the limit value is obtained by equating the vertical uniform load, q, to zero based on the CP limit equation (Equation (3-19)), yielding a value of 0.67 ($\tilde{k} > 0.67$).

3.6.2. Sensitivity analysis

Sensitivity analyses are carried out to investigate the contribution of the vertical stiffness of the angle brackets, considering the developed elastic analytical expressions for values of $\tilde{k}$ between 0 and 1.5. This is done by varying the vertical stiffness of hold-down and maintaining the stiffness and number of fasteners in the panel-to-panel connections unchanged, while assuming only one angle bracket at the middle of each panel. The analysis is repeated for a range of angle brackets' stiffness ratios, φ, between 0.25 and 1. The results are compared to the reference case where the angle bracket's stiffness is neglected ($\varphi = 0$). The analyses are conducted for the number of panels equal to 4 and 8, and for a constant height and width of panels equal to 2.7 m and 1.4 m, respectively. Different $\tilde{q}$ values are considered (0, 1, 2 and 3.5), depending on the number of panels, in order to evaluate all possible kinematic modes (i.e., CP, SW and IN). The analyses were conducted by maintaining all parameters constant and varying one parameter. The parameters used in sensitivity analysis are summarized in Table 3-2.

Table 3-2: The values of parameters used in sensitivity analyses

Parameter	Value(s)/range
$\tilde{k}$	0 to1.5
$\tilde{q}$	0, 1, 2, 3.5
φ	0.25, 0.5, 0.75, 1
n_f	18
n_s	1
$k_f\ (KN/m)$	700
$k_{h,z}\ (KN/m)$	variable
$h\ (m)$	2.7
$b\ (m)$	1.4

The parameters studied include panel rotation (ϑ) and internal forces in hold-down in the vertical direction as well as fasteners in panel-to-panel connections ($T_{h,z}$ and $T_{f,j}$, respectively). In the CP region, the internal forces in the connectors are related linearly to the rotations, as concluded by considering Equations (3-12) and (3-14). For this reason, all the studied parameters are expected to have the same trends and are expressed as the same variable, x (i.e., ϑ, $T_{h,z}$ and $T_{f,j}$). On the contrary, in the SW region all three parameters are independent and therefore investigated separately. $\xi(x)$ expresses the ratio of the parameters studied (x) when the bi-directional effect of the angle brackets is neglected, $x_{\varphi=0}$, and considered, $x_{\varphi>0}$, as presented in Equation (3-70).

$$\xi(x) = \frac{x_{\varphi=0}}{x_{\varphi>0}} \tag{3-70}$$

Figure 3-11 presents the sensitivity analysis results for a 4 panel CLT shearwall with no uniform vertical load ($\tilde{q} = 0$), where all three possible behaviours can be achieved. The ratios of rotation, uplift forces in the hold-down and forces in the panel-to-panel connections are presented in Figure 3-11(a), Figure 3-11(b) and Figure 3-11(c), respectively.

The results of rotation and vertical forces in the hold-down show almost the same trend, where the highest effect is observed in the SW region, while in the CP region, the effect is relatively less significant. The internal forces in panel-to-panel connections are almost

unaffected by the vertical stiffness of the angle brackets in all regions, especially the SW region.

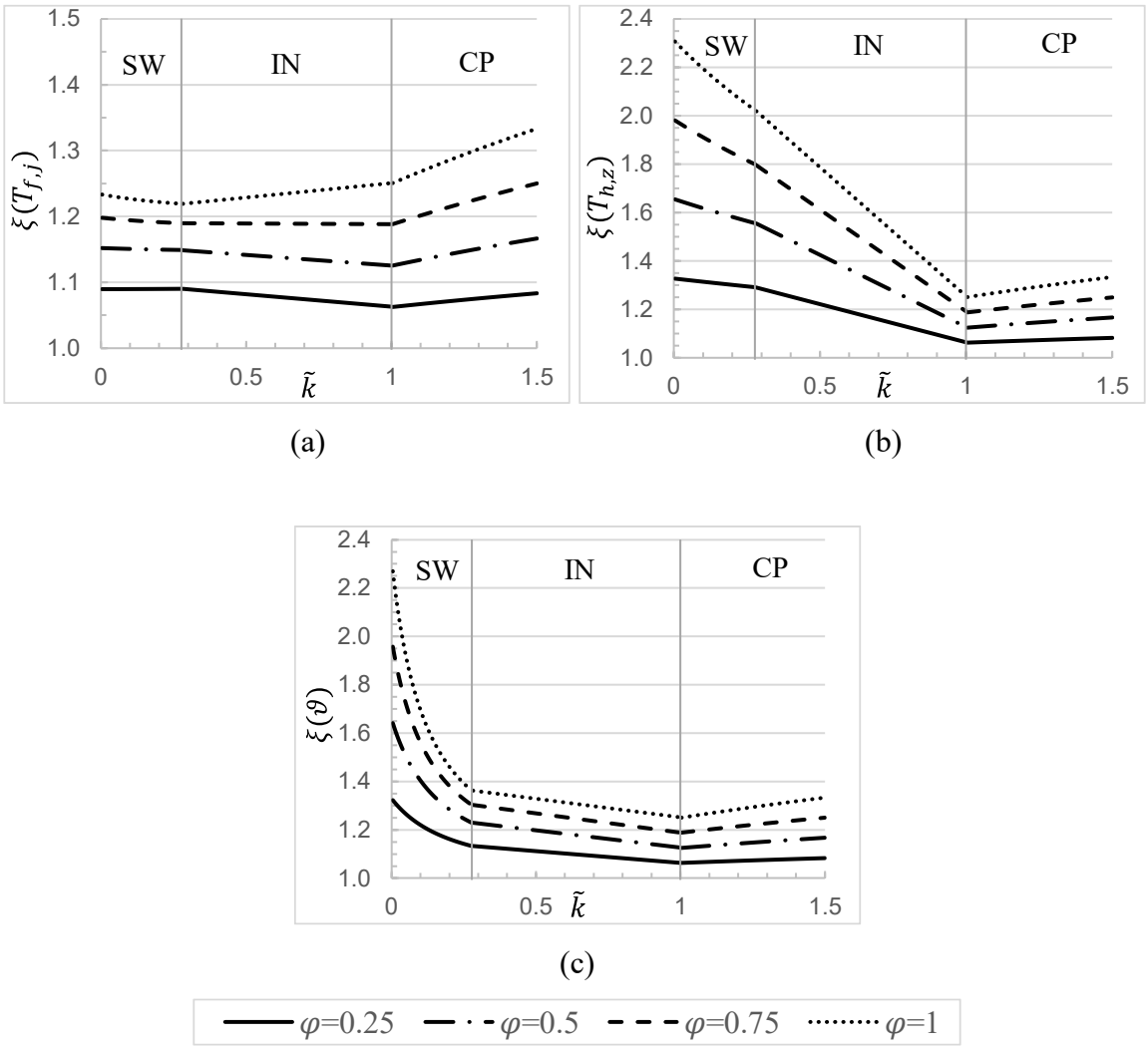

Figure 3-11: The result of sensitivity analysis for four-panel CLT shearwalls when $\tilde{q} = 0$: (a) internal forces in the panel-to-panel connections; (b) uplift forces in the hold-down; (c) angle of rotation

Figure 3-12 compares the results of the sensitivity analyses on the CP and SW behaviour for CLT shearwalls consisting of 4 and 8 panels. In order to maintain the CP behaviour, Figure 3-12(a), a value of $\tilde{q}$ was selected to be 2.0 and 3.5 for walls with 4 and 8 panels, respectively. For the SW behaviour, Figure 3-12(b), $\tilde{q}$ was set equal to 0 and the results are shown for the uplift forces in hold-down for which the most differences are observed. It can be observed that the effect of the number of panels seems insignificant in CP. On the

contrary, significant differences are observed in the SW when the number of panels is doubled.

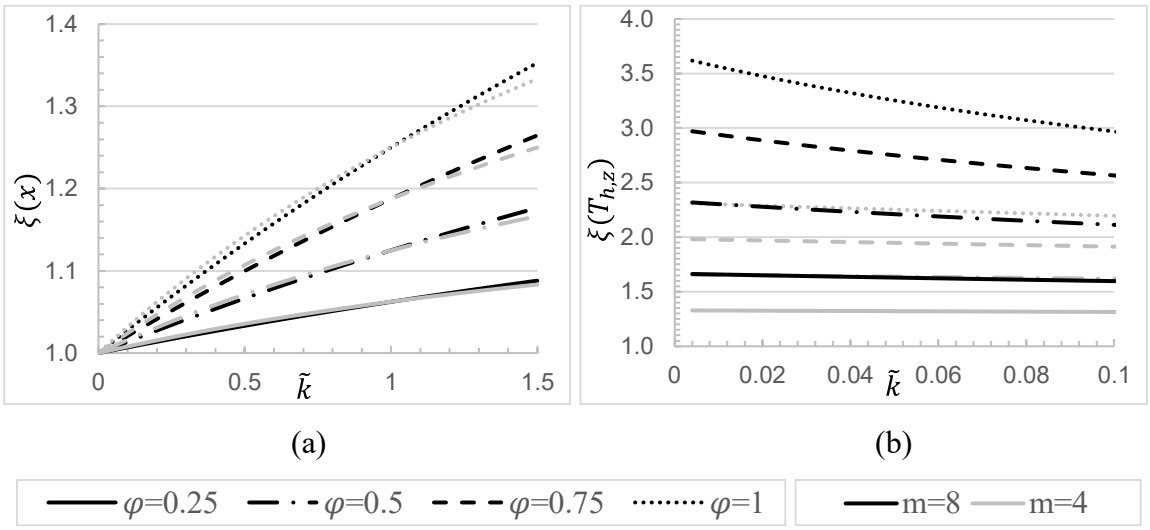

Figure 3-12: The result of sensitivity analysis for fourth and eight-panel CLT shearwalls: (a) CP; (b) SW

In order to measure the effect of multiple angle brackets in CP, a new variable, $\emptyset$, is defined, as shown in Equation (3-71). In this equation, α and φ can be obtained using Equations (3-2) and (3-4), respectively.

$$\emptyset = \alpha \cdot \varphi \tag{3-71}$$

The results of the sensitivity analyses of CP behaviour are summarized in Table 3-3. The analyses are conducted for values of $\tilde{k}$ equal to 0.5, 1 and 1.5, and values of $\tilde{q}$ equal to 0, 1, 2 and 3.5. To investigate the effect of multiple angle brackets, different values of $\emptyset$ between 0.125 and 1, are adopted. As seen in the table, varying $\tilde{k}$ seems to have a relatively small impact on the results. Comparing the differences between considering and neglecting the contribution of the angle brackets for different values of $\tilde{q}$, it can be observed that identical values are obtained. Table 3-3 shows that for $\emptyset$ values equal to 0.125 and 0.25, the greatest ratio observed is 1.17 and 1.33, respectively. This observation has a significant implication for the analysis and design of CLT shearwalls, and whether the bi-directional effect of angle brackets needs to be considered. Based on the results of this study, it can be concluded that the bi-directional contribution of the angle brackets may be neglected if

relatively flexible angle brackets are used ($\emptyset < 0.125$) in the CP behaviour. In those cases, a maximum difference of 17% or less is obtained. However, in the case of relatively stiff angle brackets or when multiple angle brackets with significant stiffness ($\emptyset = 1$) are used, it is observed that the bi-directional effect of the angle brackets is significant, in the range of 53 to 141%. Also, it should be noted that if SW behaviour is attained, considering the bi-directional effect of angle brackets is required since neglecting such an effect would lead to errors of more than 20%.

Table 3-3 The results of sensitivity analysis for CP behaviour

		$\tilde{q}=0$			$\tilde{q}=1$			$\tilde{q}=2$			$\tilde{q}=3.5$		
		$\tilde{k}$			$\tilde{k}$			$\tilde{k}$			$\tilde{k}$		
		0.5	1	1.5	0.5	1	1.5	0.5	1	1.5	0.5	1	1.5
Num. of panels	$\emptyset$	$\xi(x)$			$\xi(x)$			$\xi(x)$			$\xi(x)$		
4	0.125	N.A.	1.13	1.17	1.07	1.13	1.17	1.07	1.13	1.17	1.07	1.13	1.17
	0.25	N.A.	1.25	1.33	1.14	1.25	1.33	1.14	1.25	1.33	1.14	1.25	1.33
	0.375	N.A.	1.38	1.5	1.21	1.38	1.5	1.21	1.38	1.5	1.21	1.38	1.5
	0.5	N.A.	1.50	1.67	1.29	1.50	1.67	1.29	1.50	1.67	1.29	1.50	1.67
	0.75	N.A.	1.75	2.00	1.43	1.75	2.00	1.43	1.75	2.00	1.43	1.75	2.00
	1	N.A.	2.00	2.33	1.57	2.00	2.33	1.57	2.00	2.33	1.57	2.00	2.33
8	0.125	N.A.	1.13	1.18	N.A.	1.13	1.18	1.07	1.13	1.18	1.07	1.13	1.18
	0.25	N.A.	1.25	1.35	N.A.	1.25	1.35	1.13	1.25	1.35	1.13	1.25	1.35
	0.375	N.A.	1.38	1.53	N.A.	1.38	1.53	1.2	1.38	1.53	1.2	1.38	1.53
	0.5	N.A.	1.50	1.71	N.A.	1.5	1.71	1.27	1.50	1.71	1.27	1.50	1.71
	0.75	N.A.	1.75	2.06	N.A.	1.75	2.06	1.4	1.75	2.06	1.4	1.75	2.06
	1	N.A.	2.00	2.41	N.A.	2.00	2.41	1.53	2.00	2.41	1.53	2.00	2.41

3.7. Summary

Elastic analytical methods for multi-panel CLT shearwalls, including the bi-directional contribution of angle brackets and hold-downs, have been developed using minimum potential energy method. Expressions are developed in the elastic region to establish the CP and SW kinematic behaviours of the shearwall, and kinematic regions depicting areas where different kinematic modes govern the behaviour of the wall are also investigated. The inelastic expressions are provided for CP behaviour as initial elastic and ultimate inelastic behaviour.

The conclusions that can be drawn from the current section are:

- As expected, when the bi-directional effect of the angle brackets is considered in the analysis, especially for relatively stiff angle brackets in the vertical direction and a higher number of angle brackets, more panels are likely to maintain contact with the ground, resulting in less displacements and rotations. It was also observed that as the number of panels increases, the SW region becomes smaller for all values of angle bracket stiffness, since more connectors are involved in resisting the vertical uplift load.
- Results from the sensitivity analyses showed that the bi-directional contribution of the angle brackets may be neglected if relatively flexible angle brackets are used ($\emptyset < 0.125$), while ensuring CP behaviour. In those cases, a maximum difference of 17% or less is obtained. When SW behaviour is attained, considering the bi-directional effect of angle brackets is required, since neglecting such effect would lead to errors of at least 20%.

Chapter 4 - Elastic design and proposed capacity-based design

4.1. General

The concept of CD has been incorporated into structural design provisions to avoid brittle failure modes, especially seismic design, where energy dissipation is paramount. In this design approach, selected components are predetermined to behave as dissipative zones and the sequence of failure in the building elements is established to ensure that non-dissipative zones are capacity protected (e.g., Paulay & Priestly, 1992). The sequence of failure is determined by introducing over-strength factors, to provide capacity protection for non-ductile elements when the energy dissipative components reach a desired level of inelastic displacement. Although the CD philosophy has been the agreed upon principle to establish general design methodologies for seismic design, the applicability of such approach to timber buildings, especially those consisting of Cross Laminated Timber (CLT) shearwalls, has lacked analytical expressions that depend on the structural type (i.e., platform- or balloon framing) and failure mechanisms. Due to the brittle nature of wood, particularly in flexure, tension, and shear, the energy dissipation needs to occur through yielding of mechanical connectors. It is also important to select dissipative zones that ensure a global ductility and conform to the behavioural factor used to reduce elastic design forces.

As presented in Chapter 1, two types of Lateral Load Resistance Systems (LLRS) are usually considered in CLT buildings, namely monolithic shearwalls, which refer to single CLT panels, or multi-panel shearwalls, which consist of several wall segments connected together using panel-to-panel connections. Figure 4-1 reiterates the concept presented in Chapter 1 (Figure 1-2) for the purpose of CD discussion. In multi-panel shearwalls, the panel-to-panel connections can be designed to behave as semi-rigid connections, allowing slip, and hence potentially energy dissipation, to occur between the segments.

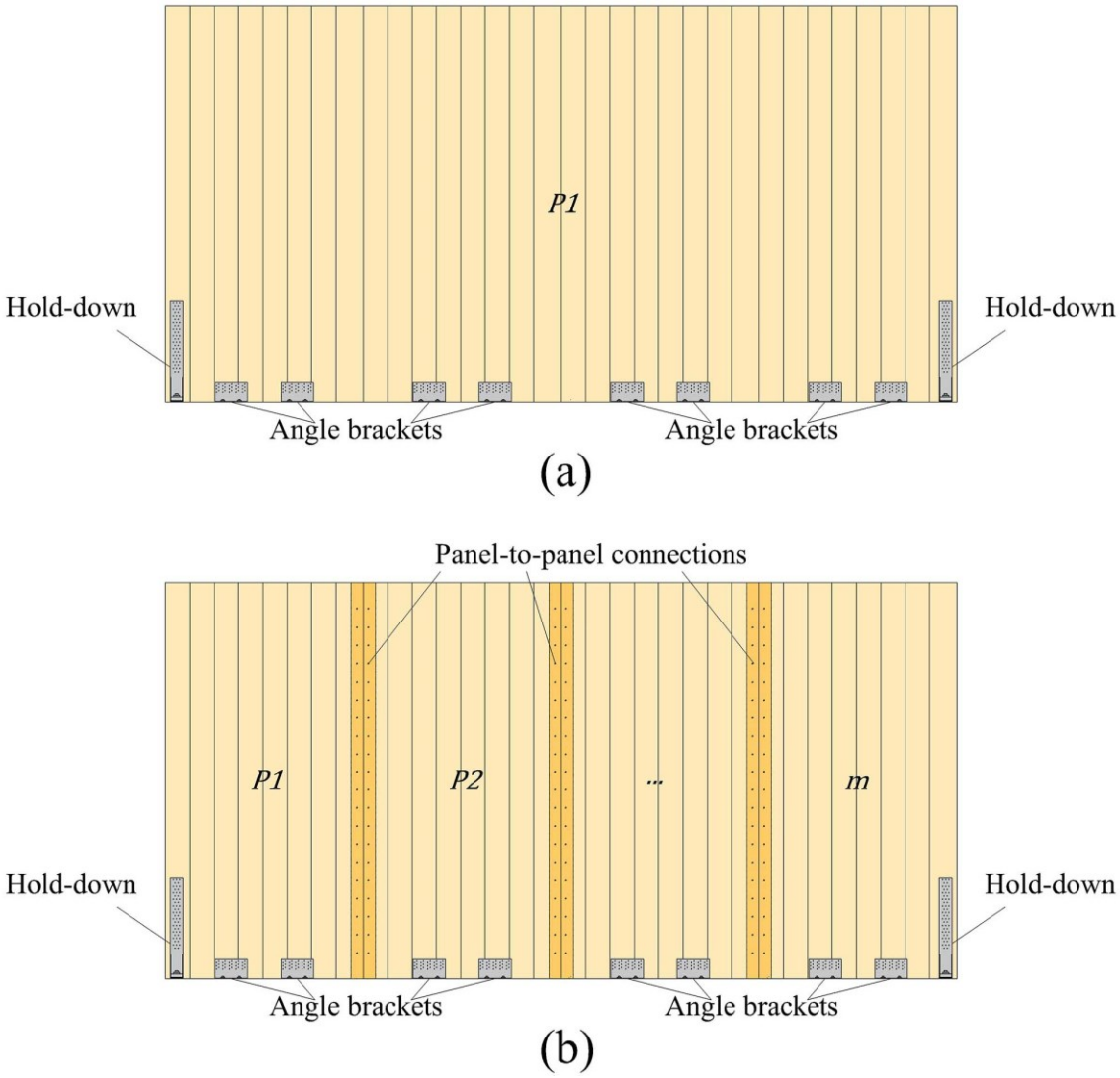

Figure 4-1: The configurations of CLT shearwalls: (a) Monolithic, (b) Multi-panel

Design provisions for platform-type CLT buildings with multi-panel shearwalls have been incorporated into established codes and standards, such as the Canadian timber design standard (CSA O86-19, 2019), where general design guidelines have been introduced. Multi-panel wall configurations are particularly desired in North America due to ease of transportation and the ability to optimize energy dissipation in panel-to-panel connections. Figure 4-1 also shows the layout of the hold-down connectors, which are typically placed at the ends of the shearwall or openings. In general, hold-downs are designed to resist the overturning moment, while the angle brackets, connecting the wall panels to the base, transfer the shear force.

The lack of analytical and design expressions in timber design standards has meant that only general guidelines are provided to establish the hierarchy of failure and ensure that energy dissipation occurs in predetermined components of the structure. To achieve seismic force reduction factors for CLT shearwalls according to the National Building Code of Canada (2022) , the panel-to-panel connections and angle brackets, only in the vertical direction (i.e., uplift), are defined as the dissipative zone and are required to contain moderately ductile connections. This is meant to ensure the rocking behaviour of CLT shearwalls as the predominant kinematic behaviour, while minimizing sliding.

The review of the available literature clearly reveals a gap in knowledge. This is particularly pertaining to the development of analytical expressions to ensure CD philosophy is achieved. Although an analytical CD approach for both single- and multi-panel CLT shearwalls has been proposed by Casagrande et al. (2019), the approach limits the contribution of angle brackets to that of shear, thereby excluding the vertical (uplift) component.

The methodology proposed in this section represents a generalized solution for multi-panel CLT shearwalls that covers important knowledge gaps found in previously developed analytical expressions while maintaining a format suitable for practical design purposes. As such, the current project aims at developing analytical expressions for the applicability of the CD philosophy for multi-panel CLT shearwalls used in multi-storey buildings with emphasis on including the bi-directional contribution of angle brackets. The focus is initially on developing a comprehensive elastic design approach for multi-panel CLT shearwalls with CP behaviour, to reduce sliding in the wall, optimize energy dissipation in the building, and conform to contemporary design standards (e.g., CSA O86-19, 2019).

Another unique contribution of the proposed design method is that it includes a CD procedure that addresses the hierarchy of yielding among different groups of dissipative zones. This is necessary since multiple joints (e.g., panel-to-panel connections and hold-downs) are assumed to contribute to the overall energy dissipation of the wall system.

4.2. Elastic design of multi-panel CLT shearwalls in CP behaviour

The proposed methodology for multi-panel CLT shearwalls applies to buildings with multiple levels. This is done by including the load transfer from upper storeys and considering the design bending moment, M_f, and shear, V_f, at each storey, obtained from the lateral loads applied along the height of a multi-storey shearwall. The general configuration of the multi-panel CLT shearwalls (Figure 4-2) is assumed to comprise of m panels, each with height and width equal to b and h, respectively. The cumulative uniform vertical load, at a given storey, includes the loads transferred from the storeys above and the self-weight of the CLT panels, denoted as q.

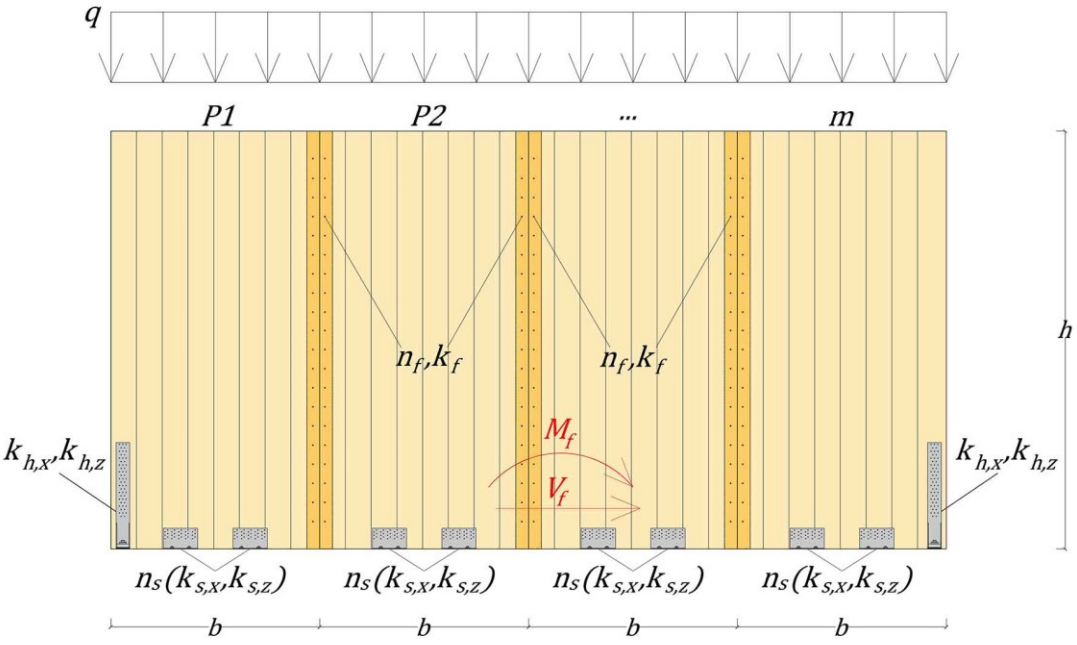

Figure 4-2: General configuration of multi-panel CLT shearwall model

The proposed design approach is based on the developed analytical expressions presented in Chapter 3, where further information on how some of the expressions were developed can be found, including internal forces in connections and yielding hierarchy development in CP behaviour. In the current chapter, this is done by developing equations expressed as a function of moment and base shear, rather than internal forces and displacements, which makes them particularly suitable for design.

Figure 4-3 provides the deformed shape in the CP behaviour of the multi-panel wall presented in Figure 4-2. It is assumed that the length of each panel is reduced by a factor ($\beta \leq 1$) that accounts for the compression zone. The connections are modelled consistent with Chapter 3 using elastic springs with their respective stiffness in the associated directions. The shear stiffness of the joints connecting two adjacent panels is incorporated into one spring element, equal to $n_f \cdot k_f$, where n_f is the number of connections and k_f is the stiffness of an individual connection in a panel-to-panel connection. The hold-down is assigned a vertical stiffness of k_{hz}, while the vertical and horizontal stiffnesses of each angle bracket are expressed as k_{sz} and k_{sx}. The strengths of the connections are denoted, r_f for the connections in the panel-to-panel connections, r_{hz} for the hold-down in the vertical direction, and r_{sz} and r_{sx} for each angle bracket in the vertical and horizontal directions, respectively. n_s denotes the number of angle brackets in each panel. It is noteworthy to mention that the horizontal contribution (i.e., shear) of hold-downs is neglected in this Chapter since such contribution was found to be negligible for conventional hold-downs, based on published experimental tests' results (e.g., Gavric et al., 2015). Also, considering such contribution leads to cumbersome expressions, which is not practical for design.

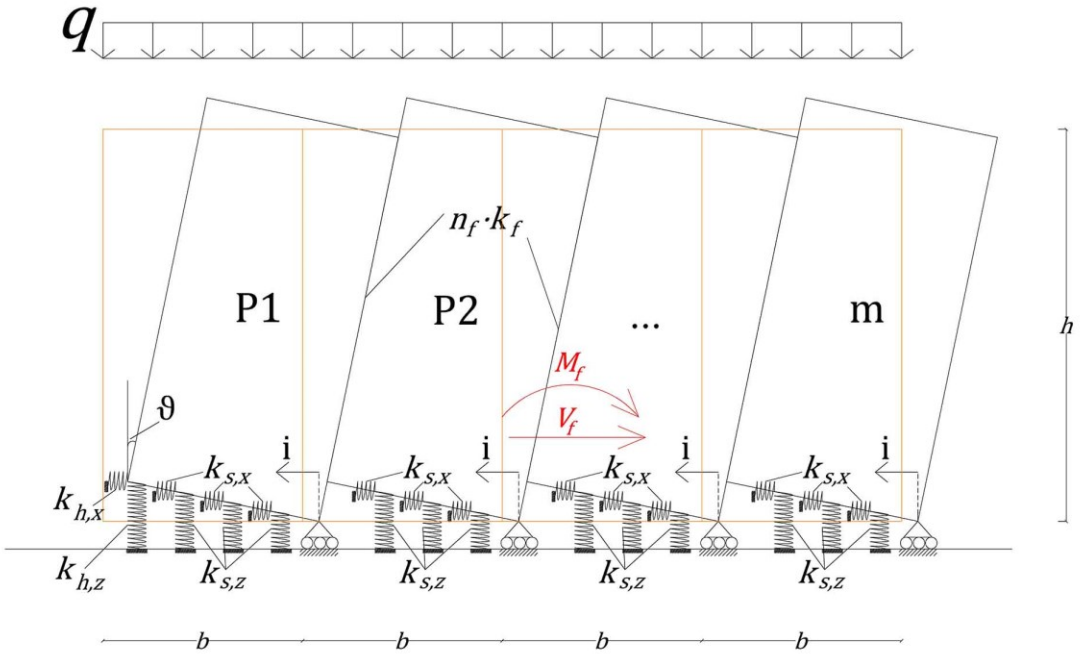

Figure 4-3: The CP lateral behaviour of a multi-panel CLT shearwalls

The proposed design method assumes that the internal bending moments and shear forces along the height of the multi-storey shearwall change proportionally to a change in the applied earthquake force, E_f, as demonstrated in Figure 4-4. Hold-down and panel-to-panel connections are characterized only by rocking behaviour, so their associated resistance expressions are based on bending moment alone. However, both bending moment and shear force need to be considered for angle bracket resistance, due to their bi-directional behaviour.

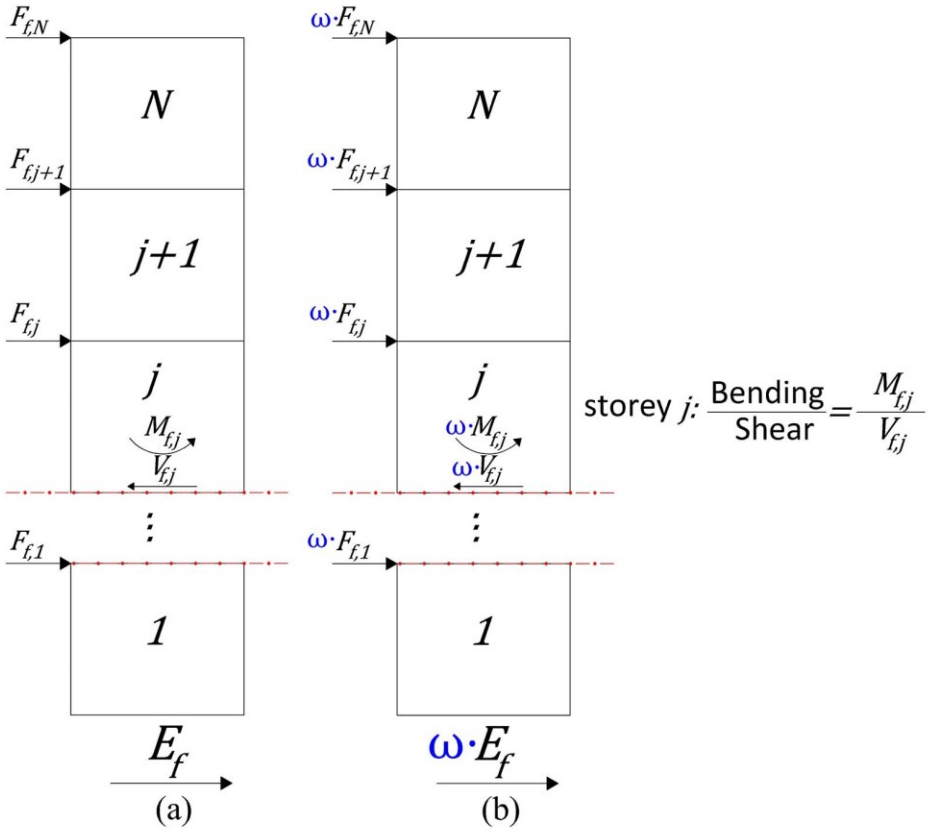

Figure 4-4: The proportional increase or decrease of lateral load, bending moment and shear force from (a) to (b)

As previously established in Chapter 3, two variables are defined in order to incorporate the contribution of the bi-directional angle brackets in the design procedure, namely the vertical stiffness ratio of the mechanical anchors, φ, which relates the vertical stiffness of one angle bracket to that of the hold-down, as shown in Equation (4-1), and parameter, α,

which accounts for the presence of multiple angle brackets in each panel, as outlined in Equation (4-2).

$$\varphi = \frac{k_{a,z}}{k_{h,z}} \tag{4-1}$$

$$\alpha = \sum_{i=1}^{n_a} \left[\frac{i}{(n_a + 1)} - (\beta - 1) \right]^2 \tag{4-2}$$

The dimensionless stiffness, $\tilde{k}$, which represents the ratio between the vertical stiffness of the hold-down and the shear stiffness of the panel-to-panel connections, is expressed in Equation (4-3), while the dimensionless moment ratio, $\widetilde{M}$, representing the ratio between the moment caused by the uniform vertical load and that caused by the lateral loads, M_f, is expressed in Equation (4-4).

$$\tilde{k} = \frac{k_{h,z}}{n_f \cdot k_f} \tag{4-3}$$

$$\widetilde{M} = \frac{q \cdot m^2 \cdot b^2}{2 \cdot M_f} \tag{4-4}$$

A CP behaviour is characterized by all panels remaining in contact with the ground, which can be ensured by satisfying Equation (4-5) and based on vertical equilibrium for the first panel, since the conditions for the other panels would automatically be satisfied in this case. It is noteworthy to mention that Equation (4-5) is expressed here in terms of bending moment rather than lateral force, as reported in Equation (3-19). The variable ρ_s represents the sum of the distances between each angle bracket and the center of rotation of each panel, normalized relative to the length of the panel, as expressed in Equation (4-6).

$$\tilde{k} \geq \frac{\beta \cdot \left\{ 1 - \frac{\widetilde{M} \cdot [4 \cdot m \cdot \beta - (m + 2 \cdot \beta)]}{m^2} \right\}}{(\beta + \varphi \cdot \rho_s) - \frac{\widetilde{M} \cdot [m \cdot (\beta + \varphi \cdot \rho_s) \cdot (2 \cdot \beta - 1) - 2 \cdot (\beta^2 + \alpha \cdot \varphi \cdot m)]}{m^2}} \tag{4-5}$$

$$\rho_s = \sum_{i=1}^{n_s} \left[\frac{i}{(n_s + 1)} - (\beta - 1) \right] \tag{4-6}$$

Based on the proposed methodology for elastic design, the shearwall strength is associated with either the panel-to-panel connections, hold-down, or the angle brackets reaching their respective yield strengths. As such, the bending moment strength of the shearwall

associated with the strength of each connection group is required to be greater than or equal to the effects of the applied load, represented by the design bending moment and shear.

The contribution of the connections' stiffness to the rocking behaviour k'_v, including the effect of hold-down, angle brackets, and panel-to-panel connections, can be calculated using Equation (4-7), obtained from Equation (3-6). The contribution of the stabilizing moment induced by the uniform vertical load, M_q, is presented in Equation (4-8).

$$k'_v = k_{h,z} \cdot [\beta^2 + \alpha \cdot \varphi \cdot m] + (m-1) \cdot \beta^2 \cdot n_f \cdot k_f \tag{4-7}$$

$$M_q = \frac{q \cdot m \cdot b^2 \cdot (2 \cdot \beta - 1)}{2} \tag{4-8}$$

As mentioned earlier, due to rocking behaviour, the resistance expressions for hold-down and panel-to-panel connections are based on bending moment alone. The expressions for bending moment strengths of the shearwall associated with the point of yielding of the panel-to-panel connections, $M_{r,f}^{el}$, and hold-down, $M_{r,h}^{el}$, are obtained by replacing the internal forces, reported in Equations (3-12) and (3-13), with the associated yield strengths, and the bending moment caused by the applied lateral load with the shearwall bending moment strength, as outlined in Equations (4-9) and (4-10), respectively.

$$M_{r,f}^{el} = r_f \cdot \frac{k'_v \cdot b}{\beta \cdot k_f} \geq M_f - M_q \tag{4-9}$$

$$M_{r,h}^{el} = r_{hz} \cdot \frac{k'_v \cdot b}{\beta \cdot k_{h,z}} \geq M_f - M_q \tag{4-10}$$

The bending moment and shear strength related to the point of yielding of the angle brackets when subjected to vertical uplift or shear force, $M_{r,s}^{el}$ and $V_{r,s}^{el}$, respectively, are expressed in Equations (4-11) and (4-12). These expressions are obtained by replacing the internal forces, reported in Equations (3-14) and (3-16), with the associated yield strengths.

$$M_{r,s}^{el} = \frac{k'_v \cdot r_{s,z} \cdot b}{\left[\frac{n_s}{n_s+1} - (\beta - 1)\right] \cdot \varphi \cdot k_{h,z}} \tag{4-11}$$

$$V_{r,s}^{el} = r_{sx} \cdot m \cdot n_s \tag{4-12}$$

The bi-directional behaviour of angle brackets needs to be considered, since they are subjected to both uplift due to bending moment and shear due to the base shear force. This interaction effect can be represented using the circular domain, and expressed in terms of shear and moment, as shown in Figure 3-8. The proposed expression for this circular domain is presented in Equation (4-13), which is consistent with that presented in European Technical Assessment ETA-06/0106 (2016), except that in the proposed method, they are expressed as a function of moment and base shear rather than forces and strengths.

$$\left(\frac{M_f - M_q}{M_{r,s}^{el}}\right)^2 + \left(\frac{V_f}{V_{r,s}^{el}}\right)^2 \leq 1 \tag{4-13}$$

It is noteworthy to mention that the requirement presented in Equation (4-13) is only derived for the angle brackets farthest away from the center of rotation in each panel, since they are expected to receive the highest uplift force due to the applied moment.

It should also be noted that the first term in Equation (4-13) can only be considered when the applied moment due to the lateral load is greater than the stabilizing effect from the uniform vertical load. As such, the requirement presented in Equation (4-14) needs to be satisfied. If this requirement is not met, the first term in Equation (4-13) should be set equal to zero and only the shear component needs to be considered.

$$M_f \geq M_q \tag{4-14}$$

4.3. Capacity-based design considerations for multi-panel CLT shearwalls

4.3.1. Background and proposed design concepts

The general philosophy of CD requires that the design strength of non-dissipative elements (e.g., CLT panels) is greater than or equal to that of dissipative elements through an over-strength factor, γ_{Rd}. This ensures that the non-dissipative elements remain elastic and are prevented from failure when the dissipative elements reach the 95th percentile of their maximum strength. Expressions for calculating the over-strength factor associated with non-dissipative elements in timber structures have been proposed in the literature, as presented in Equation (4-15) (Jorissen & Fragiacomo, 2011). In Equation (4-15), γ_{sc} represents the ratio between the 95th percentile, $R_{D,95^{th}}$, and 5th percentile, $R_{D,5^{th}}$, of the

dissipative elements' strengths, γ_{an} is the ratio between the 5th percentile of dissipative elements' strengths and the strength value obtained from analytical formulations, $R_{D,an}$, and γ_M is partial material factor.

$$\gamma_{Rd} = \frac{R_{D,95^{th}}}{R_{D,5^{th}}} \cdot \frac{R_{D,5^{th}}}{R_{D,an}} \cdot \gamma_M = \gamma_{sc} \cdot \gamma_{an} \cdot \gamma_M \quad (4\text{-}15)$$

Equation (4-16) presents the general concept for CD, where R_{ND} and R_D are the design strengths of the non-dissipative and dissipative elements, respectively. An alternative method to using the over-strength factor is requiring the non-dissipative elements to remain elastic when the dissipative elements reach the 95th percentile of their strength distribution, $R_{D,95^{th}}$, as expressed in the Canadian timber design standard, CSA O86-19 (2019).

$$R_{ND} \geq \gamma_{Rd} \cdot R_D = R_{D,95^{th}} \quad (4\text{-}16)$$

The design method proposed in this study is developed specifically to attain CP behaviour of multi-panel CLT shearwalls in both the elastic and plastic regions in order to promote a predominantly rocking behaviour and optimize the energy dissipation in the shearwall system. The basic premise of the proposed procedure is to promote a yield hierarchy that ensures CP behaviour is attained in the plastic region by yielding the panel-to-panel connections first, followed by yielding in the hold-down while ensuring that the angle brackets remain elastic. As such, the wall's strength is defined by the point at which the hold-down yields. It should be noted that although the angle brackets are not expected to yield, they still contribute to the strength of the shearwall. The yielding sequence of the connections is demonstrated in Figure 4-5, where the yielding commences in the panel-to-panel connections (a) followed by hold-down yielding (b).

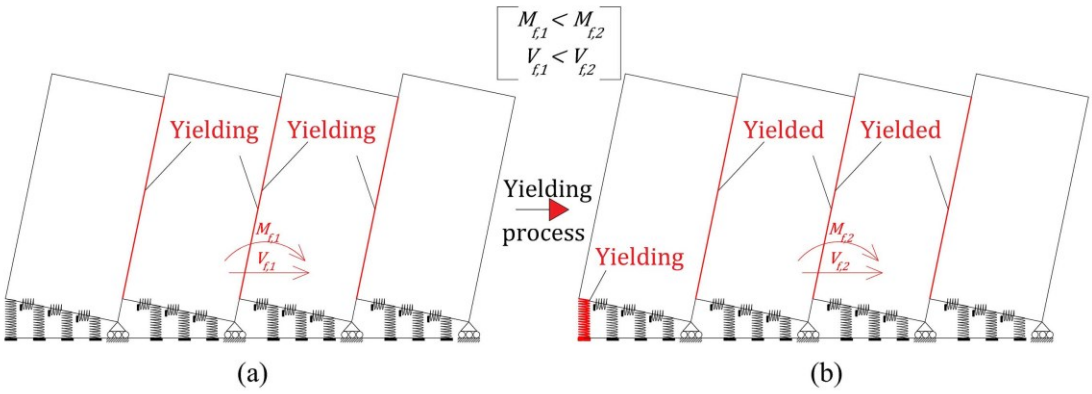

Figure 4-5: Developed yield hierarchy for the capacity-based design procedure: a) yielding in the panel-to-panel connections; b) yielding in the hold-down

To ensure this sequence of element yielding is achieved, a new category of elements with limited energy dissipative capabilities is introduced. As such, the structural elements comprising the shearwall are divided into four categories in terms of their ability to dissipate energy. These include: (1) primary dissipative elements, which are desired to yield prior to the yielding of any other element (e.g., panel-to-panel connections); (2) other dissipative elements (e.g., Hold-down), which are required to yield after the primary dissipative elements in category (1); (3) elements with limited energy dissipative capabilities (e.g., angle brackets), which are expected to remain elastic when the dissipative elements, category (1) and (2), yield; and (4) non-energy dissipative elements, which are required to remain elastic until the energy dissipative elements reach a desired level of inelastic displacement, since they are typically characterized by a brittle failure mode (e.g., CLT panels). A preferred sequence of yielding is presented for category (2) and (3), where yielding in the hold-down is ensured before that of the angle brackets. This is partially done because the proposed strength design procedure is limited by the yielding of the hold-down, but also to ensure that the sliding mechanism is minimized. Non-energy dissipative elements, category (4), are required to remain elastic throughout the entire behaviour. This approach yields three over-strength factors, as presented in Table 4-1, two of which ensure that the panel-to-panel connections yield prior to the yielding of the hold-down, $\gamma_{r,h}$, and that the angle brackets remain elastic when the hold-down yields, $\gamma_{r,s}$. The third over-strength factor, $\gamma_{r,ND}$, ensures that the CLT panels are capacity-protected and remain elastic when the wall reaches its maximum strength.

Table 4-1: Proposed framework for the over-strength factors

Category	Element	Behaviour	Over-strength factor	Percentile of dissipative element's strength
Primary Energy dissipative	Panel-to-panel connections	Yield	-	-
Other energy dissipative	Hold-down	Yield	$\gamma_{r,h}$	x^{th}
Limited energy dissipative	angle brackets	Elastic	$\gamma_{r,s}$	y^{th}
Non-energy dissipative	e.g., CLT panels	Elastic	$\gamma_{r,ND}$	95^{th}

Although developing specific values for the over-strength factors is dependent on the distribution in the behaviour of the connections selected, and is outside the scope of this study, a general concept is presented next to help evaluate such values. Regarding the over-strength factor associated with non-dissipative elements, such as CLT panels, a general expression involving the 95th percentile similar to that presented in Equation (4-15) could be adopted. Such stringent requirements may not be necessary for the protection of other dissipative elements, category (2), and limited energy dissipative elements, category (3), and therefore a generalized expression based on the x^{th} and y^{th} percentiles (assumed to be lesser than the 95^{th}), can be considered, as shown in Table 4-1, and discussed in detail in section 4.3.2. Examples of over-strength factors can be found in the literature (e.g., Fragiacomo et al., 2011; Sustersic et al., 2012; Izzi et al., 2016; Ottenhaus et al., 2018), however, more research is required in order to establish a complete characterization of the proposed procedure.

4.3.2. A capacity-based design proposal at the shearwall level

The proposed CD procedure is described in detail at the level of a single shearwall within a multi-storey building in this section (Section 4.3.2) and for the entire building comprised of LLRSs in Section 4.3.3. In general, the procedure comprises the following steps:

(1) Ensure CP behaviour, which is expressed as a function of stiffness, geometries, and forces in the elastic region, and yield levels of the connections in the plastic region. A prioritization of yielding in the panel-to-panel connections before the hold-down is ensured

at this point by means of over-strength factor $\gamma_{r,h}$ used for the hold-down design of the hold-down.

(2) Establish the shearwall strength at the point where the hold-down yields. This is thought to represent a reasonable balance between allowing the panel-to-panel connections to dissipate energy and preventing the angle brackets from yielding and initiating sliding behaviour. The latter is also ensured using over-strength factor $\gamma_{r,s}$ for the design of the angle brackets.

(3): Finally, the wall strength is modified by an over-strength factor, $\gamma_{r,ND}$, and used as a shear force to design the non-dissipative elements (e.g., CLT panels), thereby ensuring no brittle failure.

The first condition in the proposed approach is to satisfy Equation (4-5), in order to ensure that the wall exhibits CP behaviour in the elastic region. This entails that all panels remain in contact with the ground when the panel-to-panel connections yield. This can be ensured by replacing M_f with the associated bending moment strength when the panel-to-panel connections yield, $M_{r,f}^{el}$. The inelastic CP behaviour is attained when the panel-to-panel connections yield before the hold-down, which can be achieved by requiring that the bending moment strength related to the point of yielding of the panel-to-panel connections, $M_{r,f}^{el}$, is less than or equal to that associated with the hold-down, $M_{r,h}^{el}$, as shown in Equation (4-17). Simultaneously requiring the panel-to-panel connections to yield before the angle brackets is not necessary because a separate condition requiring the hold-down to yield before the angle brackets is presented later in Equation (4-22).

$$M_{r,f}^{el} \leq M_{r,h}^{el} \tag{4-17}$$

Where $M_{r,f}^{el}$ and $M_{r,h}^{el}$ can be obtained using Equations (4-9) and (4-10), respectively. The use of the elastic moment strength expression is justified since the panel-to-panel connections are on the verge of yielding and the hold-down connection has not yet yielded. As such, the wall is still in the elastic region.

The condition outlined in Equation (4-17) can be satisfied by considering the strengths associated with the hold-down and panel-to-panel connections, the dimensionless stiffness, $\tilde{k}$, and the over-strength factor, $\gamma_{r,h}$ (Casagrande et al., 2019).

$$r_{h,z} \geq \gamma_{r,h} \cdot n_f \cdot r_f \cdot \tilde{k} \tag{4-18}$$

Where $\gamma_{r,h}$ can be obtained using Equation (4-19), considering the x^{th} and 5^{th} percentile of panel-to-panel connections' strength distribution, $R_{f,x^{th}}$ and $R_{f,5^{th}}$, respectively, as well as the panel-to-panel connections' strength obtained from analytical models, $R_{f,an}$.

$$\gamma_{r,h} = \frac{R_{f,x^{th}}}{R_{f,5^{th}}} \cdot \frac{R_{f,5^{th}}}{R_{f,an}} \cdot \gamma_M \tag{4-19}$$

This requirement can also be written in conformance with the design approach outlined in the Canadian design standard (CSA O86-19, 2019), while considering $R_{f,x^{th}}$, as presented in Equation (4-20).

$$r_{h,z} \geq n_f \cdot R_{f,x^{th}} \cdot \tilde{k} \tag{4-20}$$

The moment strength of the shearwall associated with the yielding of both hold-down and panel-to-panel connections, $M_{r,h}^c$, can be obtained using Equation (4-21). This equation is derived by summing the bending moment strength associated with the yielding of the panel-to-panel connections, $M_{r,f}^{el}$, and the increase in bending moment required to attain yielding in the hold-down connection. This increase is obtained using Equation (4-10), while eliminating the contribution of the panel-to-panel connections to the total rocking stiffness of the connections, k_v', outlined in Equation (4-7).

$$\begin{aligned} M_{r,h}^c &= \frac{b \cdot (\beta^2 + \alpha \cdot \varphi \cdot m) \cdot \left(r_{h,z} - n_f \cdot r_f \cdot \tilde{k}\right)}{\beta} + M_{r,f}^{el} + M_q \\ &= b \cdot \left[r_{h,z} \cdot \left(\beta + \frac{\alpha \cdot \varphi \cdot m}{\beta}\right) + r_f \cdot n_f \cdot \beta \cdot (m-1) + \frac{q \cdot m \cdot b \cdot (2 \cdot \beta - 1)}{2} \right] \end{aligned} \tag{4-21}$$

In order to ensure that the angle brackets remain elastic when the hold-down reaches its yielding point, the interaction condition, outlined in Equation (4-13), can be rewritten as shown in Equation (4-22). The expression, $M_{r,f}^{el}/M_{r,s}^{el}$, represents the ratio of the applied

moments, at the point where the panel-to-panel connections start yielding, to the elastic bending moment resistance of the angle brackets. The expression, $\left[M_{r,h}^{c} - \left(M_{r,f}^{el} + M_q\right)\right]/M_{r,s}^{c}$, represents the ratio of the increase in bending moment strength of the shearwall between the yielding of the panel-to-panel connections and hold-down, and that of the shearwall associated with the yielding of the angle brackets, after the panel-to-panel connections have yielded, while the hold-down remains elastic, $M_{r,s}^{c}$. The latter is obtained by considering the contribution to rocking stiffness from the hold-down and angle brackets only, since the panel-to-panel connections have already yielded at this point, as shown in Equation (4-23). The second term in Equation (4-22), $C_h \cdot V_f/V_{r,s}^{c}$, represents the ratio of the shear force to the shear strength of the angle brackets. The shear force corresponds to the level where the hold-down yields. It can be obtained by multiplying the design shear force, V_f, by C_h, representing the ratio of the moment strength of the wall when hold-down yields, $M_{r,h}^{c}$, to the applied moment due to lateral load, M_f, as outlined in Equation (4-24). The shear strength of the angle brackets, $V_{r,s}^{c}$, is equal to the elastic shear strength, outlined in Equation (4-12). This is appropriate since no yielding has occurred in the angle brackets, and they are the only connections resisting horizontal load.

$$\left[\frac{M_{r,f}^{el}}{M_{r,s}^{el}} + \frac{M_{r,h}^{c} - \left(M_{r,f}^{el} + M_q\right)}{M_{r,s}^{c}}\right]^2 + \left(\frac{C_h \cdot V_f}{V_{r,s}^{c}}\right)^2 \leq 1 \tag{4-22}$$

$$M_{r,s}^{c} = \frac{(\beta^2 + \alpha \cdot \varphi \cdot m) \cdot r_{s,z} \cdot b}{\left[\frac{n_s}{n_s + 1} - (\beta - 1)\right] \cdot \varphi} \tag{4-23}$$

$$C_h = \frac{M_{r,h}^{c}}{M_f} \tag{4-24}$$

Where M_q, $M_{r,s}^{el}$, and $M_{r,h}^{c}$ can be obtained using Equations (4-8), (4-11), and (4-21), respectively.

The moment and shear expressions in Equation (4-22) were replaced by the expressions containing strengths related to the panel-to-panel connections, hold-down, and angle brackets, and simplified to obtain Equation (4-25). The over-strength factor related to the angle brackets, $\gamma_{r,s}$, is also incorporated in this Equation, while the y^{th} percentile of the hold-down's strength distribution, $R_{h,y^{th}}$, is presented in Equation (4-26), based on the Canadian timber design standard (CSA O86-19, 2019).

$$\left\{\frac{\left[\frac{n_s}{n_s+1}-(\beta-1)\right]\cdot\varphi\cdot\gamma_{r,s}\cdot r_{h,z}}{r_{sz}\cdot\beta}\right\}^2+\left(\frac{C_h\cdot V_f}{r_{s,x}\cdot m\cdot n_s}\right)^2<1 \tag{4-25}$$

$$\left\{\frac{\left[\frac{n_s}{n_s+1}-(\beta-1)\right]\cdot\varphi\cdot R_{h,y^{th}}}{r_{s,z}\cdot\beta}\right\}^2+\left(\frac{C_h\cdot V_f}{r_{s,x}\cdot m\cdot n_s}\right)^2<1 \tag{4-26}$$

Where $\gamma_{r,s}$ can be calculated using Equation (4-27), considering the y^{th} and 5^{th} percentile of the hold-down's strength distribution, $R_{h,y^{th}}$ and $R_{h,5^{th}}$, respectively, as well as the hold-down's strength obtained from analytical models, $R_{h,an}$.

$$\gamma_{r,s}=\frac{R_{h,y^{th}}}{R_{h,5^{th}}}\cdot\frac{R_{h,5^{th}}}{R_{h,an}}\cdot\gamma_M \tag{4-27}$$

The moment strength of the wall, $M_{r,w}$, is set to be equal to the bending moment strength related to the yielding of the hold-down after the yielding of the panel-to-panel connections, as outlined in Equation (4-21), and is required to be greater than or equal to the applied moment due to the lateral load, M_f, as shown in Equation (4-28).

$$M_{r,w}=M_{r,h}^{c}\geq M_f \tag{4-28}$$

The shear force applied to the wall at the point where the hold-down starts yielding, $V_{f,w}$, is obtained by the product of the design shear force, V_f, and C_h outlined in Equation (4-24), as shown in Equation (4-29).

$$V_{f,w}=C_h\cdot V_f=\left[r_{h,z}\cdot\left(\beta+\frac{\alpha\cdot\varphi\cdot m}{\beta}\right)+r_f\cdot n_f\cdot\beta\cdot(m-1)+\frac{q\cdot m\cdot b\cdot(2\cdot\beta-1)}{2}\right]\cdot\frac{b\cdot V_f}{M_f} \tag{4-29}$$

The over-strength factor related to the non-dissipative elements, $\gamma_{r,ND}$, can be obtained using Equation (4-30), considering the 95^{th} percentile of strength distribution for the panel-to-panel connections, $R_{f,95^{th}}$. The choice of relating the over-strength factor to panel-to-panel connections is due to the importance of the contribution of the panel-to-panel connections to energy dissipation and is consistent with that found in the Canadian timber design standard (CSA O86-19, 2019).

$$\gamma_{r,ND} = \frac{R_{f,95^{th}}}{R_{f,5^{th}}} \cdot \frac{R_{f,5^{th}}}{R_{c,an}} \cdot \gamma_M \tag{4-30}$$

In order to capacity-protect the CLT panel within the shearwall, the shear force, $V_{f,w}$, can be modified with the appropriate over-strength factor, $\gamma_{r,ND}$, and divided by the number of panels in the shearwall, m, to obtain the shear force acting on each panel, as shown in Equation (4-31). The shear strength of the CLT panels, $V_{r,CLT}$, needs to be greater than the shear force acting on them, $V_{f,CLT}$.

$$V_{f,CLT} = \frac{\gamma_{r,ND} \cdot V_{f,w}}{m} \leq V_{r,CLT} \tag{4-31}$$

Whereas the requirement in Equation (4-31) is applicable to CLT panels within each shearwall, a more general and less stringent requirement is presented in section 4.3.3 for all non-dissipative elements, such as floor-to-floor and floor-to-wall connections and connections between orthogonal walls, based on considerations for the entire building.

4.3.3. Capacity-based design considerations for multi-storey LLRS

The CD considerations outlined in section 4.3.2 are required to be satisfied for each shearwall at each level, including requirements for CP behaviour, Equation (4-5) and (4-18), and maintaining elastic behaviour in the angle brackets, Equation (4-25). Additional requirements to ensure that the behaviour of the building as a whole is adequate and reduce the probability of a soft storey mechanism are described next.

The over-capacity coefficient for each storey of the LLRS, $C_{sw,j}$, is defined as the ratio of the sum of the bending moment strengths of all shearwalls at the j^{th} storey oriented parallel to the seismic shear force direction, and the corresponding total seismic bending moment acting at the bottom of that storey, as presented in Equation (4-32). This ratio is required to be greater than or equal to unity, in order to ensure that the shearwalls at that storey have adequate capacity to resist the bending moment.

$$C_{sw,j} = \frac{\sum_{i=1}^{N} \left| M_{r,w,j}^{i} \right|}{\sum_{i=1}^{N} \left| M_{f,j}^{i} \right|} \geq 1 \tag{4-32}$$

Where $M_{r,w,j}^{i}$ is the bending moment strength of shearwall i at the j^{th} storey, which can be obtained using Equation (4-28), and $M_{f,j}^{i}$ is the associated bending moment due to the lateral load. N represents the number of shearwalls parallel to the applied load in storey j.

In order to ensure a uniform energy dissipation throughout the entire height of the building, the ratio between the over-capacity coefficient at storey j (for $j \geq 2$) and that at storey $j-1$ should be limited to a range, defined by values of ε_1 and ε_2, as outlined in Equation (4-33).

$$\varepsilon_1 \leq \frac{C_{sw,j}}{C_{sw,j-1}} \leq \varepsilon_2 \tag{4-33}$$

This approach is consistent, in principle, with that proposed in (Casagrande et al., 2019), where the ratio between maximum and minimum values of $C_{sw,j}$ is required to be less than a given value, suggested to be equal to 1.25. This approach also extends the requirement found in the Canadian design standard (CSA O86-19, 2019), which is limited to first and second storeys, to include all stories in the building. The range for ε provided in the CSA O86-19 (2019) is 0.9 to 1.2.

The behaviour of multi-storey LLRS comprised of CLT shearwalls can be considered as springs in series, represented by energy dissipative, $R_{D,j}$, and non-energy dissipative elements, $R_{ND,j}$, at storey j. The cumulative seismic effect at storey j (e.g., shear load or bending moment), $E_{f,j}$, is transferred through springs with different levels of energy dissipation, as shown in Figure 4-6(b), for a two-storey CLT shearwall system.

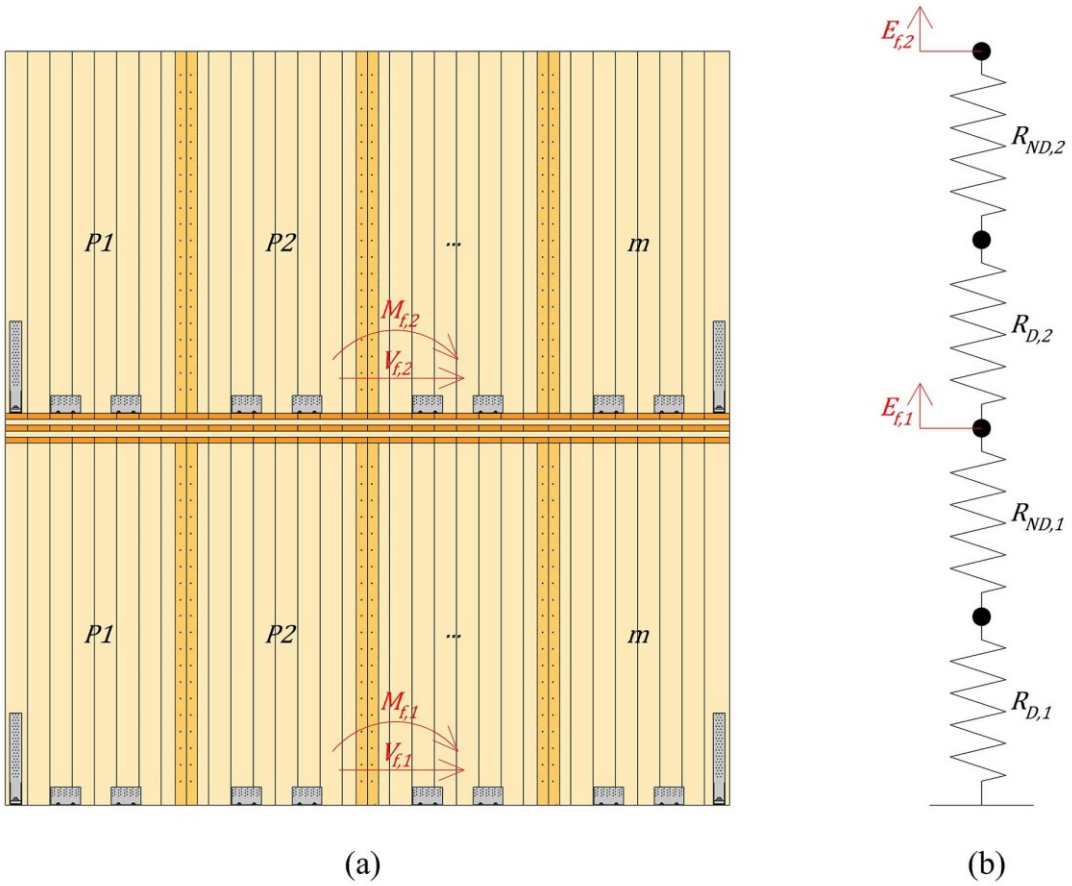

Figure 4-6: Isostatic behaviour of a two-storey CLT shearwalls: (a) Multi-storey CLT shearwalls; (b) Simulated format of multi-storey CLT shearwalls

The behaviour of any non-energy dissipative elements is related to the over-capacity coefficient of the weakest storey, $C_{sw,min} = min(C_{sw,j})$, as expressed in Equation (4-34).

$$E_{f,ND} = \gamma_{r,ND} \cdot C_{sw,min} \cdot E_f + E_g \leq E_{r,ND} \tag{4-34}$$

Where E_f and E_g are the actions due to seismic and gravity loads, respectively, and $E_{r,ND}$ is the strength of the non-dissipative element.

This generalization of the effect of seismic load is meant to be applicable to all non-dissipative elements, including CLT panels, floor-to-floor connections, floor-to-wall connections, etc. The logic of relating the design of non-dissipative elements to the smallest over-capacity coefficient in a structure is to avoid overly conservative designs. The proposed requirement is sufficient since for the multi-storey case, the overall building

capacity is related to failure in any storey. A value of $C_{sw,min}$ equal to 1.1 may be appropriate from a design perspective, since it is expected that the minimum over-capacity in a building would be close to unity.

4.4. Summary

This section presents a design approach addressing coupled-panel behaviour for multi-panel CLT shearwalls used in multi-storey buildings. Equations for shearwall strength associated with different connections are developed in terms of bending moment and shear. Analytical expressions, including design equations and requirements, are developed, with emphasis on including the bi-directional contribution of angle brackets. A capacity-based design procedure is proposed, promoting predominantly rocking behaviour and optimizing energy dissipation in the shearwall system. To achieve a desired yield sequence, a new category with limited energy dissipative capabilities is introduced, and expressions for the associated over-strength factors are defined. It was found that relating the over-strength factor associated with non-energy dissipative elements, such as CLT panels, to the 95^{th} percentile of the energy dissipative elements would be appropriate, whereas an approach using a lower percentile is proposed for other dissipative and limited energy dissipative elements.

Capacity-based design procedure at the building level is also proposed to achieve uniform energy dissipation along the height of the structure and to limit soft storey failure. This is done by requiring the ratios between over-capacity coefficients at adjacent storeys to be limited to a defined range.

Chapter 5 - Experimental tests on connections

5.1. General

As highlighted in previous chapters, connections used in CLT shearwalls are the main contributors to resisting lateral loads, as well as providing energy dissipation required when they are part of seismic design considerations. In the current study, a comprehensive experimental test program was conducted on three conventional connections used in CLT shearwalls, namely panel-to-panel, hold-down and angle bracket connections. The behaviour of the connections was examined under monotonic and cyclic loads, to investigate their performance in shearwall applications under wind and seismic loads, respectively. The mechanical properties of the connections will also be used as inputs to validate the proposed analytical expressions, as well as numerical models, presented in Chapter 7.

5.2. Joint description and test methods

Three types of conventional connections used in CLT shearwalls were tested as part of the current study, as summarized in Table 5-1. These connections were selected based on the available results provided in their technical approval documents and the preliminary numerical analyses conducted to evaluate their performance at shearwall-level, including seismic behaviour. The hold-down, WHT620 (*European Technical Approval ETA-11/0086*, 2018), consisted of a bracket attached to the base with one M20 bolt (EN 14592, 2022) and 20 mm washer, and fastened to the CLT panel with fifty-five or twenty-two nails, representing full or partial nailing, respectively. Angle brackets, TCN200 (*European Technical Assessment ETA 11/0496*, 2014), comprised of one bracket attached to the base with two M12 bolts (EN 14592, 2022) and fastened to the CLT panel with thirty or twenty nails, representing full or partial nailing, respectively. The purpose of using fully and partially nailed patterns for both hold-down and angle brackets was to evaluate the contribution of nails to the connections' performance and mechanical properties, including strength, stiffness, ductility, and ultimate failure. In only one test, an angle bracket was tested with a 12 mm thick washer under uplift load to observe the impact of using washers on the behaviour of the angel brackets. Panel-to-panel connections were used in spline-

joint connections, as presented in section 5.5, and consisted of hot galvanized spiral nails with a diameter of 3.4 mm, 3.4×63.5, or partially-threaded self-taping screws with the diameters of 6 mm, HBS 6×70, or 8 mm, HBS 8×80 (*European Technical Assessment ETA-11/0030*, 2019). Canadian Softwood Plywood (CSP) with thickness of $3/4$" and Douglas-Fir Plywood (DFP) with thickness of 1" were used for panel-to-panel spline, fastened with nails and screws, respectively.

Table 5-1: The components of tested connections

Connections	Fasteners
Hold-down WHT620	• 1 bolt | M20 × 100 • 1 washer $t = 20\ mm$ | WHTW70 • 55 or 22 nails | LBA 4 × 60
Angle brackets TCN200	• 2 bolts | M12 × 60 • 1 washer $t = 12\ mm$ | TCW200 • 30 or 20 nails | LBA 4 × 60
Panel-to-panel	• Spiral nail 3.4 × 63.5 mm 60 • Screw HBS 6 × 70 mm • Screw HBS 8 × 80 mm

Table 5-2 presents each test information, including load direction (uplift or shear), load type (monotonic or cyclic), nailing pattern for hold-down and angle brackets and type of the fasteners for panel-to-panel connections, and number of repeats for each test. Hold-down and angle brackets were tested separately in the vertical (uplift) and horizontal (shear) directions, and panel-to-panel connections were tested only in shear.

Table 5-2: Connection-level tests' information

Connections	Load direction	Load type	Nailing pattern/fasteners	Repeats
Hold-down WHT620	Uplift (tension)	Monotonic	Fully - 55 nails	3
			Partially - 22 nails	3
		Cyclic	Fully - 55 nails	3
			Partially - 22 nails	3
	Shear	Monotonic	Fully - 55 nails	3
Angle brackets TCN200	Uplift (tension)	Monotonic	Fully - 30 nails	2
			Partially - 20 nails	2
			Partially - 20 nails+washer	1
		Cyclic	Fully - 30 nails	3
			Partially- 20 nails	3
	Shear	Monotonic	Fully - 30 nails	3
			Partially - 20 nails	3
		Cyclic	Fully - 30 nails	3
			Partially - 20 nails	3
Panel-to-panel	Shear	Monotonic	Nail 3.4 × 63.5 mm	2
			HBS 6 × 70 mm	3
			HBS 8 × 80 mm	3
		Cyclic	Nail 3.4 × 63.5 mm	3
			HBS 6 × 70 mm	3
			HBS 8 × 80 mm	3

The CLT panels used in the experimental tests consisted of three 35 mm thick layers with a total thickness of 105 mm (35-35-35) while the boards had widths of 89 mm, as shown in Figure 5-1. Standard CLT panels, E1 stress grade, were used, based on ANSI/APA (2020). All CLT panels were maintained in a controlled climate condition, with temperature and relative humidity of 20 ± 2 ℃ and $65 \pm 5\%$, respectively, resulting in moisture content of $10 \pm 2\%$.

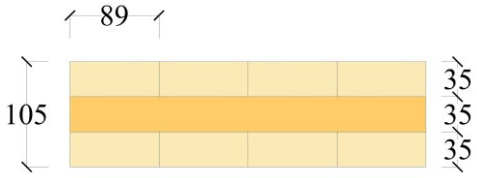

Figure 5-1:Three-layer CLT panels used in the experimental tests

Experimental tests were carried out using the MTS loading machine located in the Civil Engineering structural laboratory at the University of Ottawa. Four cable transducers with a maximum range of 150 mm were used to measure displacements. The purpose of using multiple of them was to improve the results' reliability. The location and measuring direction of each transducer are presented in the next sections concerning each type of test.

Appendix A.1 presents details related to test set-up attachments.

5.2.1. Load protocols

Monotonic and cyclic load protocols were used to investigate the behaviour of the connections. The main reason for this is to investigate whether the behaviour is significantly affected by the loading protocol, and also to develop representative connection force-displacement curves for wind (monotonic) and seismic (cyclic) considerations. The monotonic loading had constant loading rates, such as 3 mm/min for mechanical anchors (i.e., hold-down and angle brackets), and 4.5 mm/min for fasteners used as panel-to-panel connections, to maintain a consistent test duration. The cyclic testing protocol followed the ASTM E2126 (2019) cyclic displacement schedule, method B (see Figure 5-2), with a constant loading rate of 30 mm/min throughout the test in accordance with ISO 16670 (2003). The loading procedure consists of two primary groups of cycles: (1) five individual cycles with amplitudes of 1.25%, 2.5%, 5%, 7.5, and 10% of the ultimate displacement obtained from monotonic tests, Δ_m, and (2) sets of three cycles with amplitudes of 20%, 40%, 60%, 80%, 100%, and 120% of Δ_m.

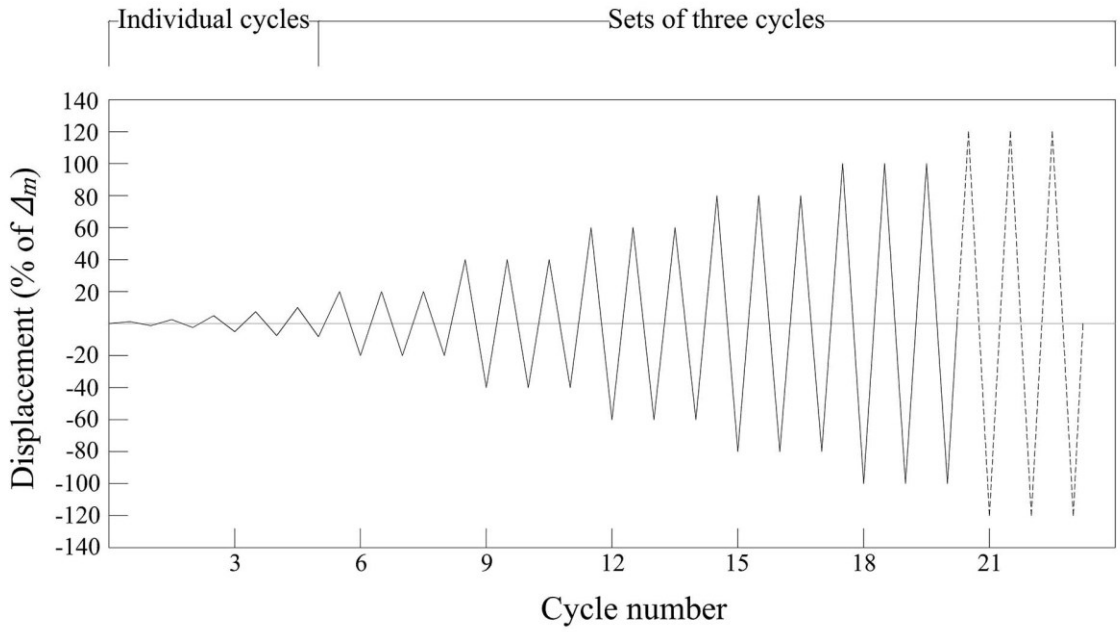

Figure 5-2: reversed cyclic load patterns, method B (ASTM E2126, 2019)

5.2.2. Data analysis

The results obtained from each test were processed to obtain the mechanical properties of the connections using two methods, namely the Energy Equivalent Elastic-Plastic (EEEP) and the tri-linear methods. The EEEP method refers to an elastic-perfectly plastic curve in which the enclosed areas by the EEEP curve and that enclosed by envelope curve from the origin to the ultimate displacement are equal, as defined in ASTM E2126 (2019) and shown in Figure 5-3. That can be ensured by equaling the area enclosed by the EEEP curve that are not inside the envelope curve ($A_1 + A_3$), and remaining area of the envelope curve that are not enclosed by the EEEP curve (A_2). The ultimate displacement of the EEEP curve, v_u, is defined as the displacement on the envelope curve corresponding to the 20% reduction in loads after reaching the maximum load, defined as ultimate load, F_u (i.e., $0.8 \times F_{max}$). $F_{y,EEEP}$ and $v_{y,EEEP}$ represent the yield load and displacement, respectively. Elastic stiffness, K_{EEEP}, is determined as the slope of the line connecting the origin and $0.4 \times F_{max}$. $v_{F_{max}}$ represents the displacement corresponding to the maximum load. The tri-linear simulation consists of three points; namely yield load (A), maximum load (B), and ultimate displacement (C), as shown in Figure 5-4. The yield point (A) represents the

intersection of two lines, that passing $0.1 \times F_{max}$ and $0.4 \times F_{max}$, C_1, and the tangent of the plastic portion of the envelope curve, C_2, as shown in Figure 5-4(a). The angle of the second line, C_2, can be defined as $\tan(C_2) = 1/6 \cdot \tan(C_1)$. The maximum load and corresponding displacement and ultimate displacement represent the same points as defined in the EEEP simulation, while ultimate load, F_u, is defined as the load on the envelope curve corresponding the ultimate displacement. $F_{y,trilinear}$ and $v_{y,trilinear}$ represent yield load and associated displacement respectively, as defined at point A. Elastic stiffness, $K_{trilinear}$, is determined as the slope of the line connecting the origin and point A. Ductility ratios based on EEEP and trilinear methods, D_{EEEP} and $D_{trilinear}$, can be obtained as the ratio of associated ultimate displacement to yield displacement, $v_u/v_{y,EEEP}$ and $v_{trilinear/v_u}$, respectively.

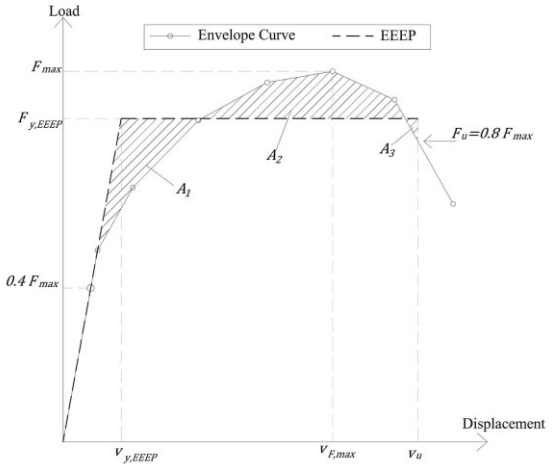

Figure 5-3: envelope load-displacement curve and its associated EEEP curve, based on ASTM E2126 (2019)

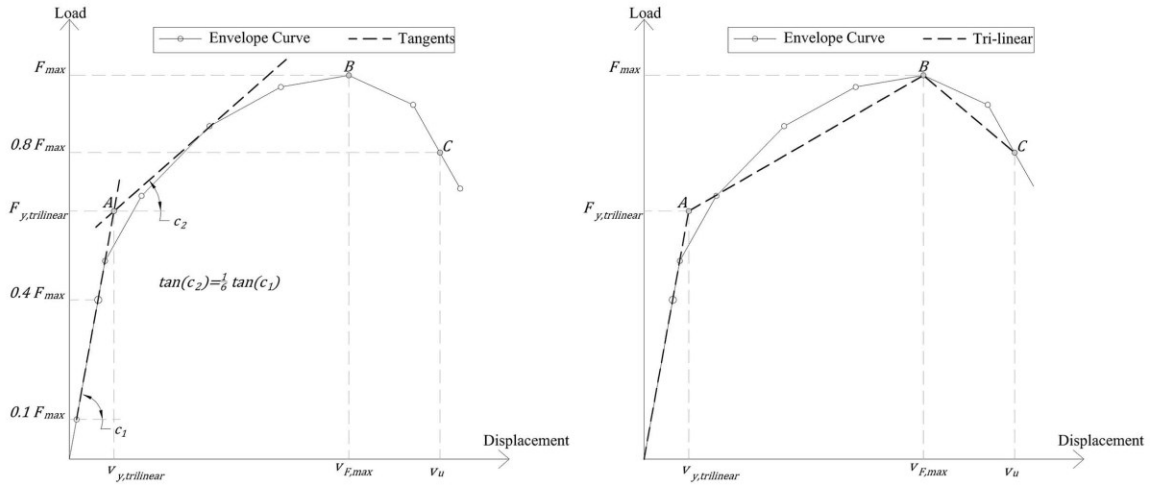

Figure 5-4: tri-linear simulation of an envelope curve, based on ON EN 12512 (2005): (a) find the yield point; (b) define the tri-linear curve

5.3. Hold-down

This section presents the experimental tests on hold-down connections, WHT620 (*European Technical Approval ETA-11/0086*, 2018), consisting of one high-strength M20 bolt and 20 mm thick washer to attach the hold-down to the base and threaded annular ring nails, LBA 4×60, with a nominal diameter of 4 mm and total length of 60 mm to attach the hold-down to the CLT panels, as depicted in Figure 5-5. Two nailing patterns, partially and fully nailed using 22 and 55 nails, respectively, were tested under monotonic and cyclic protocols in the vertical (uplift) direction, as presented in section 5.3.1, while only fully nailed pattern was used for hold-downs under monotonic protocol in the horizontal (shear) direction, as presented in section 5.3.2. The purpose of conducting shear tests on only fully nailed and under monotonic protocol was the inappropriate behaviour of hold-downs under such load in which nails had negligible effect on the resistance and deformability while rotation and local buckling in the bracket provided resistance. Section 5.3.3 provides an observations on the results obtained in sections 5.3.1 and 5.3.2.

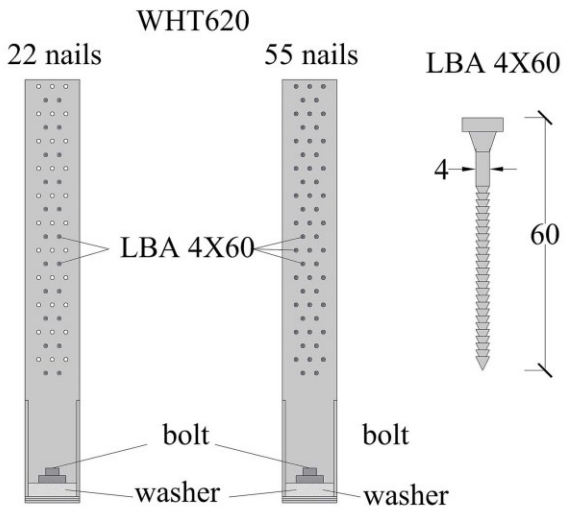

Figure 5-5: Hold-down connection WHT620

5.3.1. Tension load (uplift) tests

The hold-down connections were also tested under vertical tension (uplift) loading, as shown in Figure 5-11. Two notches were cut in the CLT panels to attach them to the top beam through threaded rods to facilitate the reversal of loading. Two transducers were attached to each face of CLT specimens to measure the vertical displacement relative to the base beam, representing uplift displacement.

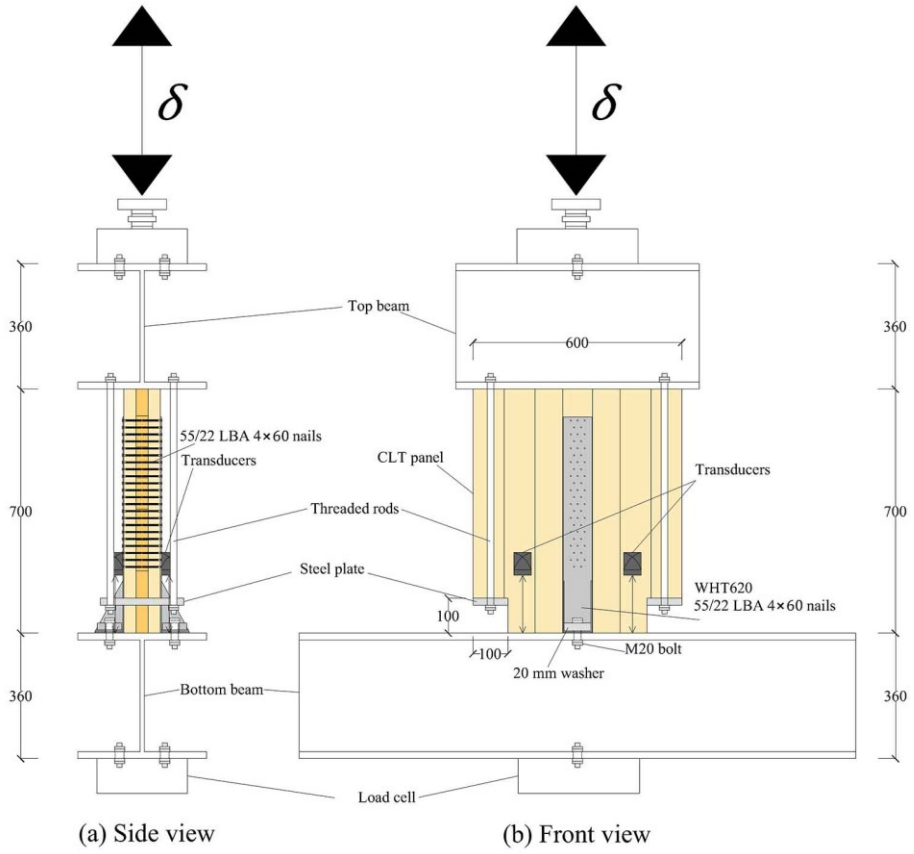

Figure 5-6: Test configuration of hold-down WHT620 subjected to uplift

Figure 5-7 and Figure 5-8 show typical load-displacement curves of fully and partially nailed hold-downs, respectively, subjected to monotonic and cyclic in the vertical (uplift) direction. The figures demonstrate very similar results of monotonic and cyclic loading patterns concerning the resistance, stiffness, and ultimate displacement. The low-cyclic fatigue effect was negligible.

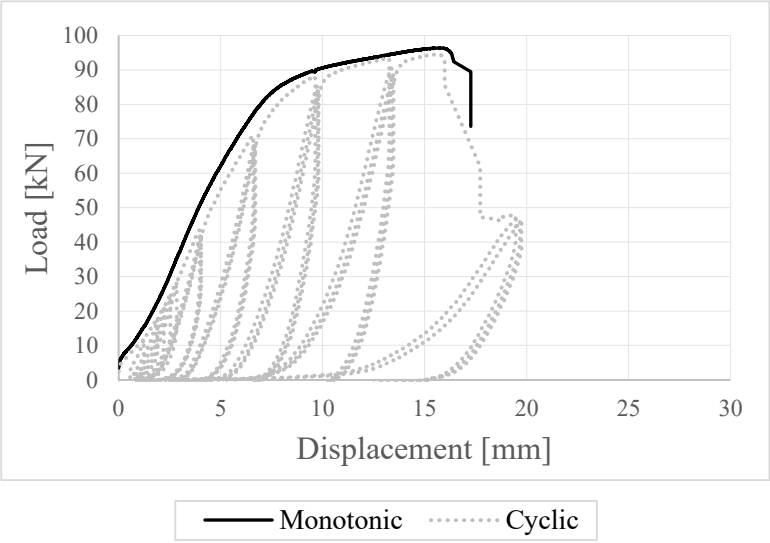

Figure 5-7: Typical load-displacement curves of fully nailed WHT620 hold-down connection under monotonic and cyclic uplift

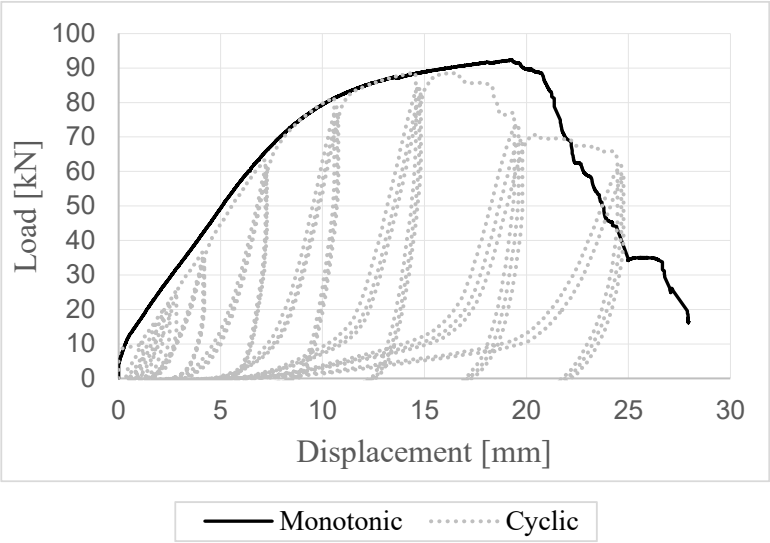

Figure 5-8: Typical load-displacement curves of partially nailed WHT620 hold-down connection under monotonic and cyclic uplift

Figure 5-9 and Figure 5-10 show representative pictures of the test specimens prior to and after the tests for fully and partially nailed hold-downs, respectively. The observed failure mechanisms were consistent in monotonic and cyclic tests, consisting of tensile failure in the vertical steel plate near the first row of nails for the fully nailed, as shown in Figure 5-9(b), while failure in nails due to head breakage combined with nail withdrawal and bending was observed for the partially nailed specimens, as shown in Figure 5-9(b).

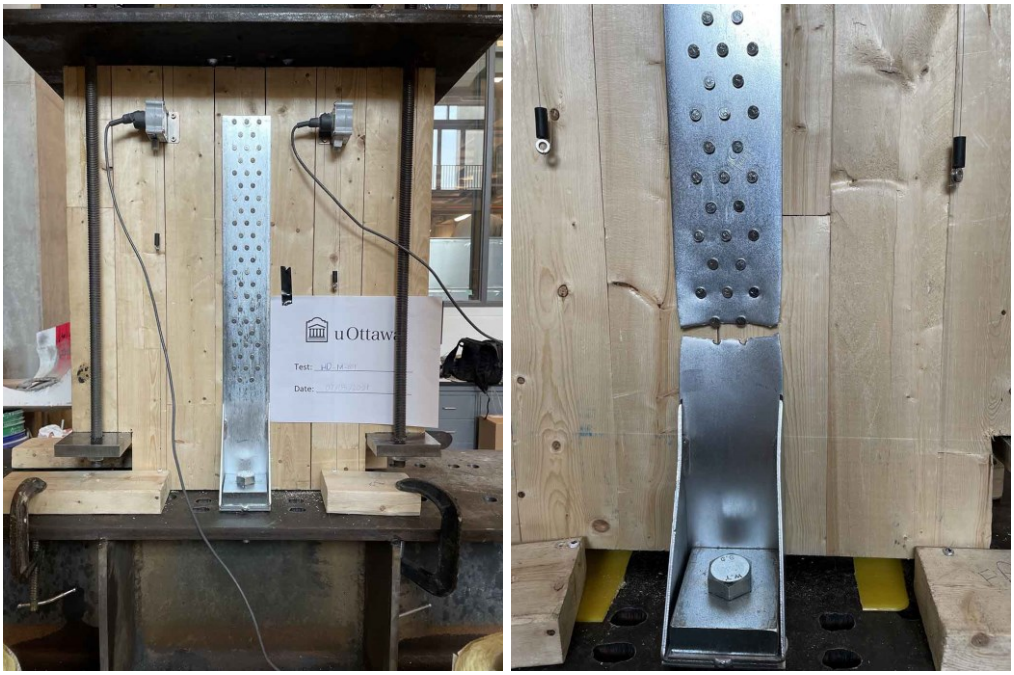

(a) (b)

Figure 5-9: Fully nailed hold-down under uplift: (a) prior to the test (b) after the test

(a) (b)

Figure 5-10: Partially nailed hold-down under uplift: (a) prior to the test (b) after the test

Table 5-3 and Table 5-4 present the mean and Coefficient of Variants (CoV) of the mechanical properties for fully and partially nailed hold-downs, respectively, obtained from three monotonic and three cyclic tests.

Table 5-3: Mean values and the associated CoV of mechanical properties of fully nailed WHS620 hold-down under monotonic and cyclic uplift

Method	Property	Unit	Monotonic		Cyclic	
			Mean	CoV (%)	Mean	CoV (%)
Maximum & ultimate	F_{max}	[kN]	93.4	4	90.9	3
	$v_{F,max}$	[mm]	14.1	15	13.4	2
	F_u	[kN]	73.9	2	73.0	3
	v_u	[mm]	17.2	7	16.9	2
EEEP	$F_{y,EEEP}$	[kN]	89.	3	85.1	4
	$v_{y,EEEP}$	[mm]	8.0	9	7.3	18
	$k_{e,EEEP}$	[kN/mm]	11.2	12	12.0	16
	D_{EEEP}	[-]	2.2	4	2.4	22
Trilinear	$F_{y,trilinear}$	[kN]	84.4	1	79.7	6
	$v_{y,trilinear}$	[mm]	7.6	12	6.8	21
	$k_{e,trilinear}$	[kN/mm]	11.2	11	12.0	18
	$D_{trilinear}$	[-]	2.3	5	2.6	26

Table 5-4: Mean values and the associated CoV of mechanical properties of partially nailed WHS620 hold-down under monotonic and cyclic uplift

Method	Property	Unit	Monotonic		Cyclic	
			Mean	CoV (%)	Mean	CoV (%)
Maximum & ultimate	F_{max}	[kN]	88.0	5	90.6	2
	$v_{F,max}$	[mm]	17.2	13	19.2	2
	F_u	[kN]	71.1	5	72.6	2
	v_u	[mm]	20.2	7	21.4	4
EEEP	$F_{y,EEEP}$	[kN]	81.4	5	83.1	1
	$v_{y,EEEP}$	[mm]	9.4	3	9.0	4
	$k_{e,EEEP}$	[kN/mm]	8.6	7	9.2	6
	D_{EEEP}	[-]	2.1	9	2.4	7
Trilinear	$F_{y,trilinear}$	[kN]	77.6	2	78.9	2
	$v_{y,trilinear}$	[mm]	9.0	5	8.6	6
	$k_{e,trilinear}$	[kN/mm]	8.6	8	9.2	4
	$D_{trilinear}$	[-]	2.2	12	2.5	9

Appendix A.2.1 and A.2.2 present the load-displacement curves and respective mechanical properties of tests conducted on WHT620 fully and partially nailed hold-downs under vertical (uplift) loads, respectively.

5.3.2. Shear load tests

Fully nailed hold-down connections, WHT620, were tested under monotonic displacement in shear, as shown in Figure 5-11. A T-shaped steel section was fastened to the top steel beam using 1” bolts. Two CLT specimens, each with two hold-downs on opposite faces, were positioned on each face of the T-shaped section. The hold-downs on the same face of each specimen were also attached together through the T-shaped section. The shear force was then transferred to the connections by moving the entire T-shaped assembly vertically. A 100 mm gap was adopted between the T-shaped section and the bottom steel beam to ensure sufficient space to move vertically. Two transducers were attached on each side of the T-shaped steel section to measure its vertical displacement relative to the base beam.

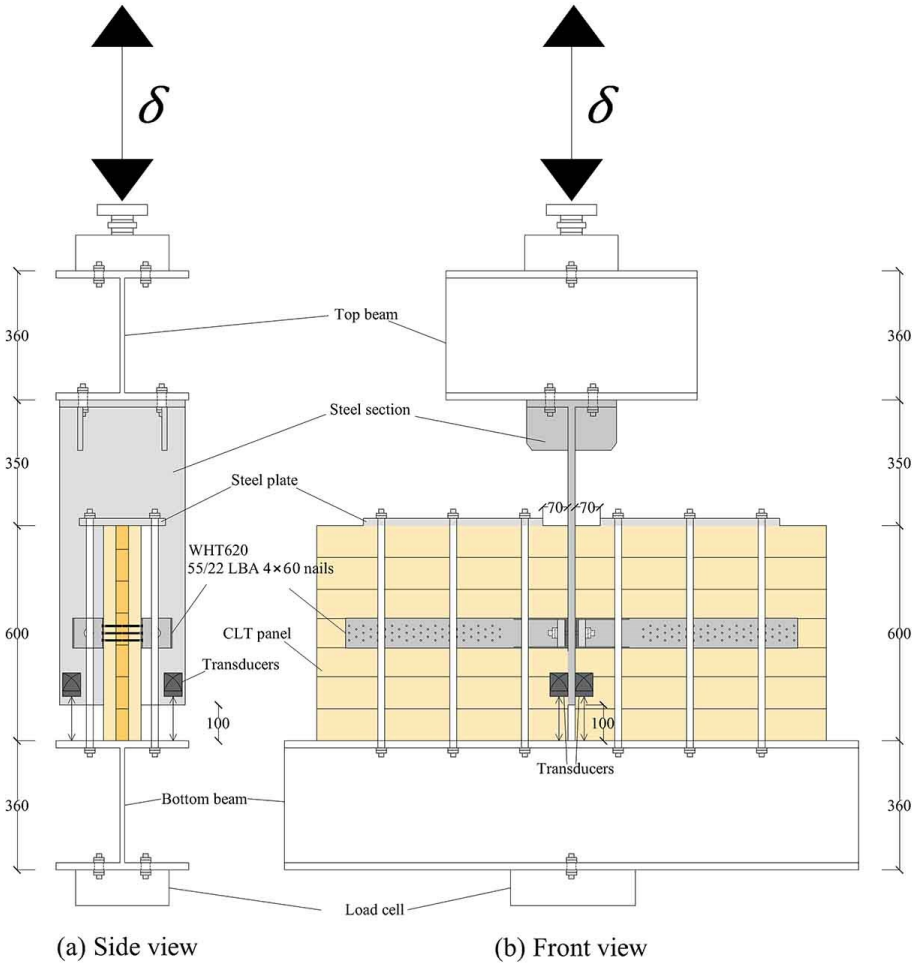

Figure 5-11: Test set-up of WHT620 hold-down connection subjected to shear

Figure 5-12 shows a typical load-displacement curve of a fully nailed hold-down subjected to monotonic shear. The curve highlights two linear parts representing high initial stiffness and a significant drop in stiffness and continuous linear behaviour until failure. The load resistance and failure were dominated by rotation and local buckling in the steel bracket, as shown in Figure 5-13(b).

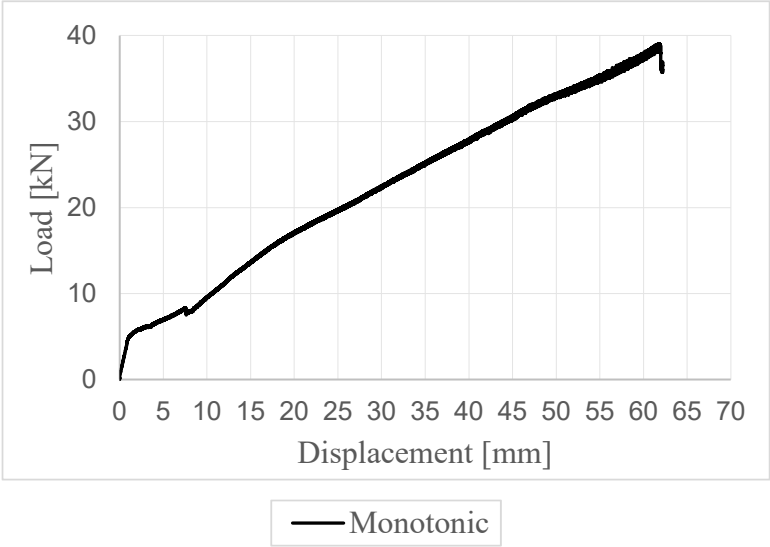

Figure 5-12: Typical load-displacement curve of fully nailed WHT620 hold-down connection under monotonic shear load

(a) (b)

Figure 5-13:Fully nailed hold-down under shear: (a) prior to test (b) after the test

Table 5-5 presents the mean and CoV of mechanical properties for fully nailed hold-downs, obtained from three monotonic tests in shear.

Table 5-5: Mean values and the associated CoV of mechanical properties of fully nailed WHS620 hold-down under monotonic shear

Method	Property	Unit	Monotonic	
			Mean	CoV (%)
Maximum & ultimate	F_{max}	[kN]	40.2	11
	$v_{F,max}$	[mm]	63.0	5
	F_u	[kN]	37.3	18
	v_u	[mm]	64.2	4
EEEP	$F_{y,EEEP}$	[kN]	33.7	15
	$v_{y,EEEP}$	[mm]	45.5	21
	$k_{e,EEEP}$	[kN/mm]	0.7	6
	D_{EEEP}	[-]	1.4	16
Trilinear	$F_{y,trilinear}$	[kN]	38.8	14
	$v_{y,trilinear}$	[mm]	53.2	20
	$k_{e,trilinear}$	[kN/mm]	0.9	34
	$D_{trilinear}$	[-]	0.9	84

Appendix A.2.3 presents the load-displacement curves and respective mechanical properties of tests conducted on WHT620 fully nailed hold-downs under horizontal (shear) loads.

5.3.3. Observation

The tested hold-down connections exhibited approximately the same mean values of resistances in the vertical (uplift) direction of around 90 kN, in both fully- and partially nailed configurations. The failure in fully nailed hold-down occurred in the bracket due to the high number of nails, whereas partially nailed hold-down failed in the nails as the bracket resistance was relatively higher. The similar magnitude of resistance despite different failure modes indicates that the partially nailed hold-down is close to failing and represents an optimized number of nails. The ultimate displacements in partially nailed hold-downs, 22.2 mm, were higher than those obtained for the fully nailed configuration, 17.2 mm. The stiffness for the hold-down with partial nailing was lower, around 9 kN/mm, than that obtained for the hold-down with fully nailed, 11.5 kN/mm for both monotonic

and cyclic protocols. This resulted in almost the same ductility ratio values, of around 2.2 under monotonic and 2.4 under cyclic loads.

Concerning fully nailed hold-downs under shear displacement, although the mean value of maximum load, F_{max}, was around 40 kN, the associated displacement with such load, $V_{F_{max}}$, was around 63 mm. This significant sliding displacement is impractical considering the contribution of angle brackets to resisting the shear load, as presented in section 5.4.2. The mean value of shear stiffness for fully nailed hold-downs was around 0.75-0.95 kN/mm, representing its negligible contribution to resisting sliding.

5.4. Angle bracket

This section presents experimental tests on angle bracket connections used to connect CLT panels to the base or floor below. The angle brackets, TCN200 (*European Technical Assessment ETA 11/0496*, 2014), included two M12 bolts to attach the bracket to the base and threaded annular ring nails, LBA 4×60, with a nominal diameter of 4 mm and total length of 60 mm to attach the bracket to the CLT panels, as depicted in Figure 5-14. Two nailing patterns, partial and fully nailed with 20 and 30 nails, respectively, were tested under monotonic and cyclic displacement in the vertical (uplift) and horizontal (shear) directions, as presented in sections 5.4.1 and 5.4.2, respectively. A washer with a thickness of 12 mm was used for only one test on a partially nailed angle bracket under monotonic vertical (uplift) displacement, to observe only the differences concerning failure and performance against those without a washer. Section 5.4.3 presents the observations on the results obtained in sections 5.4.1 and 5.4.2.

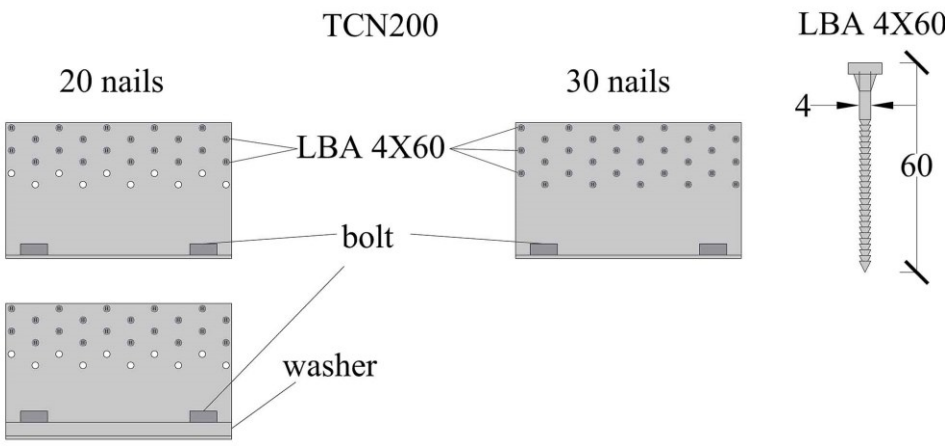

Figure 5-14: Angle bracket connection TCN200

Additional details related to test set-up attachments are presented in Appendix A.3.

5.4.1. Tension load (uplift) tests

The angle bracket connections were tested under tension (uplift) displacement, based on the test configuration shown in Figure 5-15. Two notches were cut in the CLT panels to connect them to the top beam through threaded rods to facilitate the reversal of loading. Two transducers were attached to each face of the CLT specimen to measure its vertical displacement relative to the base beam, representing uplift displacement.

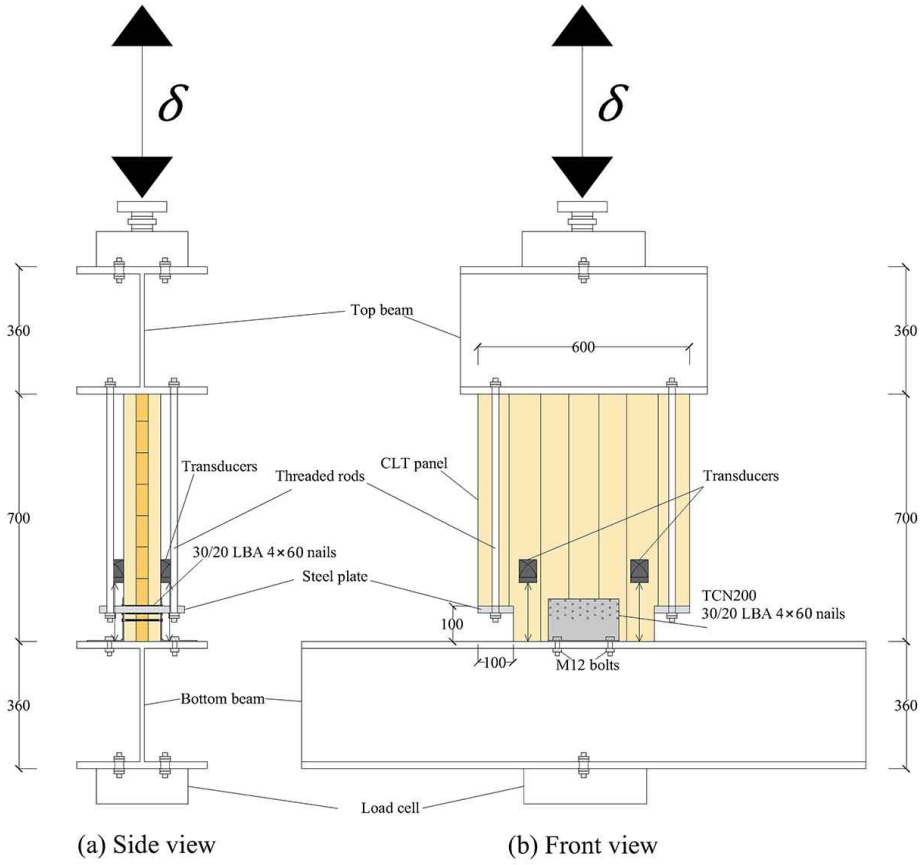

Figure 5-15: Test set-up of TCN200 angle bracket connection subjected to uplift

Figure 5-16 and Figure 5-17 show typical load-displacement curves for fully and partially nailed angle brackets without washers, respectively, subjected to monotonic and cyclic uplift displacement. Although the shapes of monotonic and cyclic curves are similar concerning initial stiffness, maximum force, and ultimate displacement, some discrepancies were observed in the plateau region, which can be attributed to the loosening of the bolts when the brackets yielded, and the specimen was under a reversed cycle.

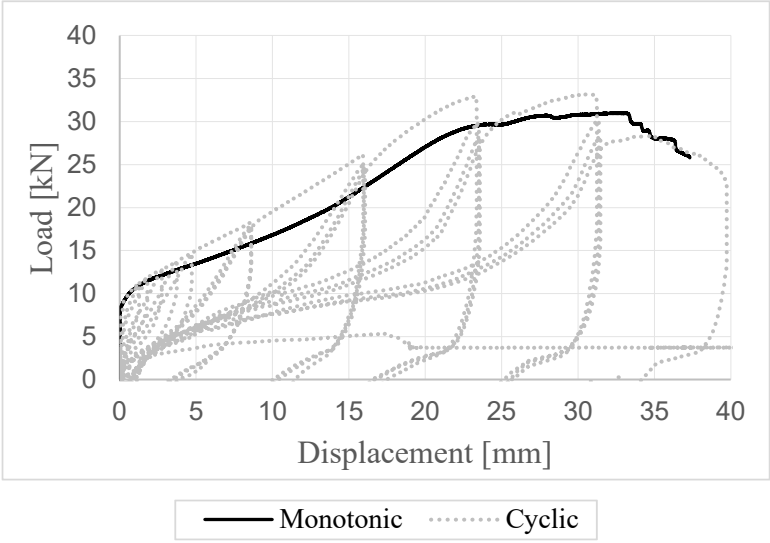

Figure 5-16: Typical load-displacement curves of fully nailed TCN200 angle bracket connection without washer under monotonic and cyclic uplift

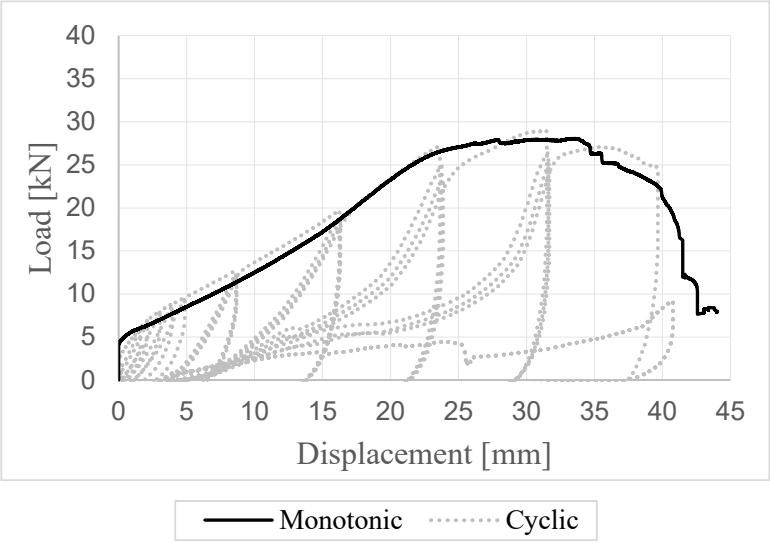

Figure 5-17: Typical load-displacement curves of partially nailed TCN200 angle bracket connection without washer under monotonic and cyclic uplift

Figure 5-18 shows the load-displacement curve of partially nailed angle brackets with washers subjected to monotonic uplift displacement.

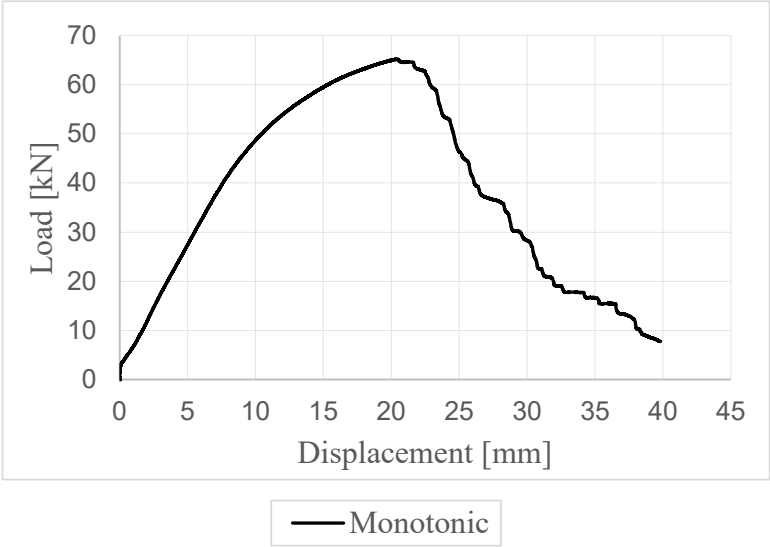

Figure 5-18: Typical load-displacement curves of partially nailed TCN200 angle bracket connection with washer under monotonic and cyclic uplift

Figure 5-19 and Figure 5-20 show the test specimens prior to and after the tests on fully and partially nailed angle brackets without washers, respectively. The observed failure mechanism was consistent for both nailing patterns consisting of plasticization in the steel bracket portion attached to the base, especially around the bolts. Figure 5-21 provides a similar comparison for partially nailed angle brackets with washers. The observed failure mechanism was nail bending combined with head breakage in the nails attaching the bracket to the CLT specimen.

(a) (b)

Figure 5-19: Fully nailed angle bracket without washer under uplift: (a) prior to the test (b) after the test

(a) (b)

Figure 5-20: Partially nailed angle bracket without wahser under uplift: (a) prior to the test (b) after the test

(a) (b)

Figure 5-21: Partially nailed angle bracket with washer under uplift: (a) prior to the test (b) after the test

Table 5-6 and Table 5-7 present the mean and CoV of the mechanical properties for fully and partially nailed angle brackets without washers, respectively, obtained from three monotonic and three cyclic tests. Table 5-8 presents the results from one monotonic test on a partially nailed angle bracket with washer.

Table 5-6: Mean values and the associated CoV of mechanical properties of fully nailed TCN200 angle bracket without wahser under monotonic and cyclic uplift

Method	Property	Unit	Monotonic		Cyclic	
			Mean	CoV (%)	Mean	CoV (%)
Maximum & ultimate	F_{max}	[kN]	31.1	1	33.6	4
	$v_{F,max}$	[mm]	30.7	11	31.6	1
	F_u	[kN]	25.9	1	27.4	4
	v_u	[mm]	37.5	1	37.8	5
EEEP	$F_{y,EEEP}$	[kN]	25.4	1	27.9	2
	$v_{y,EEEP}$	[mm]	6.8	18	6.5	29
	$k_{e,EEEP}$	[kN/mm]	4.4	18	4.4	38
	D_{EEEP}	[-]	5.4	23	6.2	31
Trilinear	$F_{y,trilinear}$	[kN]	20.1	9	19.1	31
	$v_{y,trilinear}$	[mm]	5.3	28	4.6	54
	$k_{e,trilinear}$	[kN/mm]	3.9	20	4.8	41
	$D_{trilinear}$	[-]	7.4	29	11.2	76

Table 5-7: Mean values and the associated CoV of mechanical properties of partially nailed TCN200 angle bracket without washer under monotonic and cyclic uplift

Method	Property	Unit	Monotonic		Cyclic	
			Mean	CoV (%)	Mean	CoV (%)
Maximum & ultimate	F_{max}	[kN]	28.6	3	29.4	2
	$v_{F,max}$	[mm]	33.1	2	31.6	1
	F_u	[kN]	22.9	3	23.5	2
	v_u	[mm]	40.6	3	38.3	1
EEEP	$F_{y,EEEP}$	[kN]	27.4	1	26.1	2
	$v_{y,EEEP}$	[mm]	23.9	4	17.5	3
	$k_{e,EEEP}$	[kN/mm]	1.4	5	1.4	3
	D_{EEEP}	[-]	1.7	8	2.2	3
Trilinear	$F_{y,trilinear}$	[kN]	27.6	3	26.4	2
	$v_{y,trilinear}$	[mm]	24.0	3	17.8	3
	$k_{e,trilinear}$	[kN/mm]	1.1	5	1.5	3
	$D_{trilinear}$	[-]	1.7	6	2.1	3

Table 5-8: Mechanical properties of partially nailed TCN200 angle bracket with washer under monotonic uplift

Method	Property	Unit	Monotonic
Maximum & ultimate	F_{max}	[kN]	65.2
	$v_{F,max}$	[mm]	20.5
	F_u	[kN]	52.2
	v_u	[mm]	24.3
EEEP	$F_{y,EEEP}$	[kN]	59.2
	$v_{y,EEEP}$	[mm]	11.2
	$k_{e,EEEP}$	[kN/mm]	5.5
	D_{EEEP}	[-]	2.2
Trilinear	$F_{y,trilinear}$	[kN]	56.8
	$v_{y,trilinear}$	[mm]	10.7
	$k_{e,trilinear}$	[kN/mm]	5.3
	$D_{trilinear}$	[-]	2.3

Appendix A.3.1 and A.3.2 present the load-displacement curves and respective mechanical properties of tests conducted on TCN200 fully and partially nailed angle brackets without washers under vertical (uplift) loads, respectively.

5.4.2. Shear load tests

The angle bracket connections were tested under shear loading in a test configuration shown in Figure 5-22. A T-shaped steel section was fastened to the top steel beam using 1" bolts. Two CLT specimens, each with two angle brackets on opposite faces, were positioned on each face of the T-shaped section. The angle brackets on the same face of each specimen were also attached together through the T-shaped section. The shear force was then transferred to the connections by moving the entire T-shaped assembly vertically. A 100 mm gap was adopted between the T-shaped section and the bottom steel beam to ensure sufficient space to move vertically. Two transducers were attached on each side of the T-shaped steel section to measure its vertical displacement relative to the base beam.

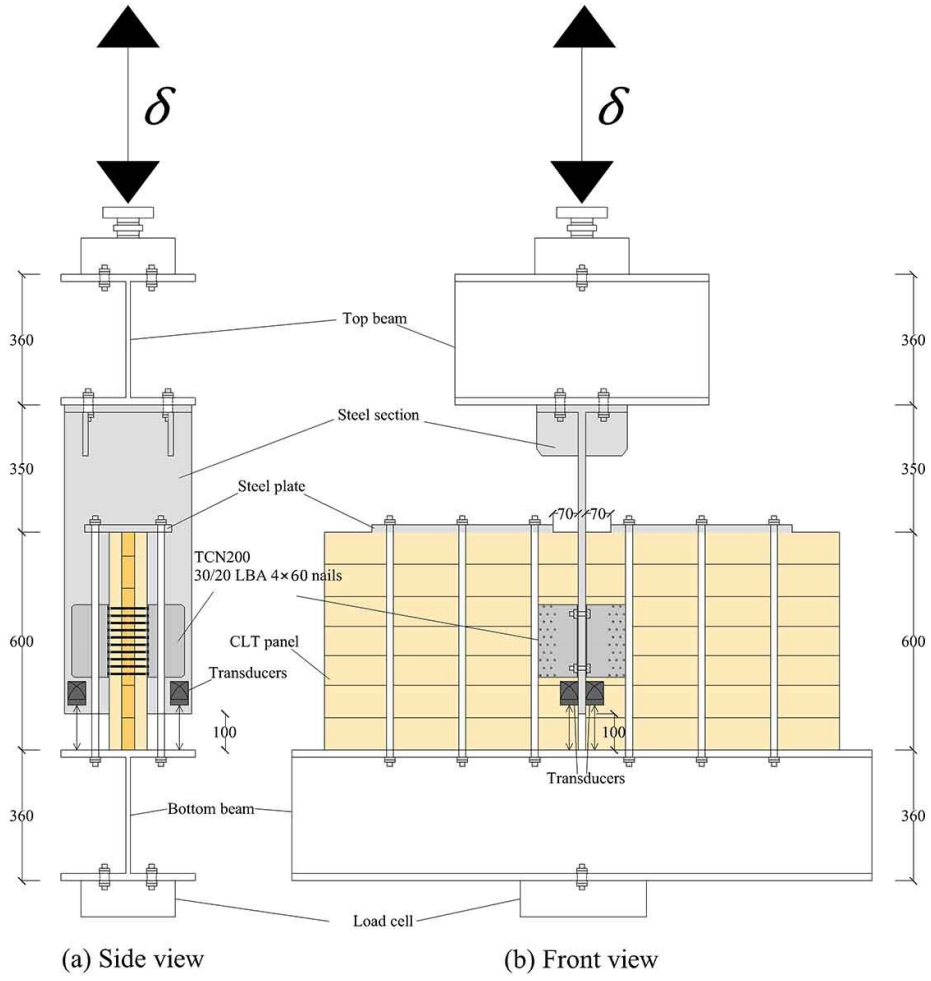

Figure 5-22: Test set-up of TCN200 angle bracket connection subjected to shear

Figure 5-23 and Figure 5-24 show typical load-displacement curves of fully and partially nailed angle brackets without washers, respectively, subjected to monotonic and reversed cyclic loading protocols. Figures show that monotonic and cyclic loading patterns produce similar results of resistance, stiffness, and ultimate displacement, and the low-cyclic fatigue effect is negligible.

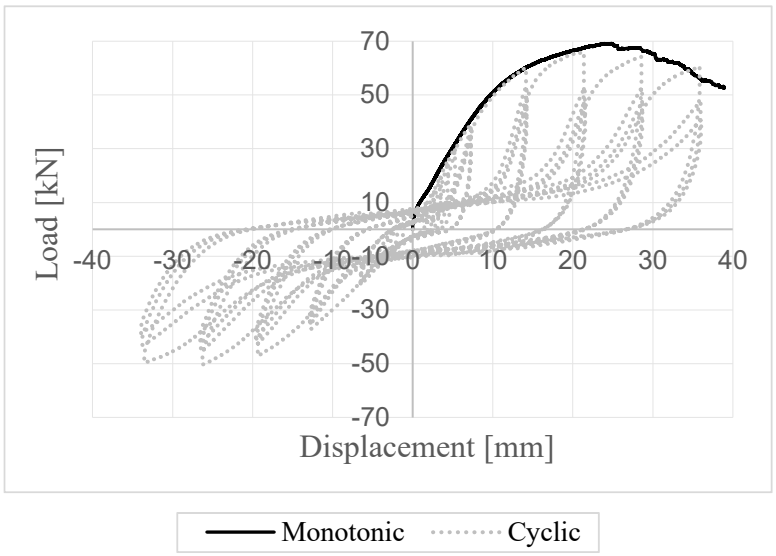

Figure 5-23: Typical load-displacement curves of fully nailed TCN200 angle bracket connection without washer under monotonic and cyclic shear

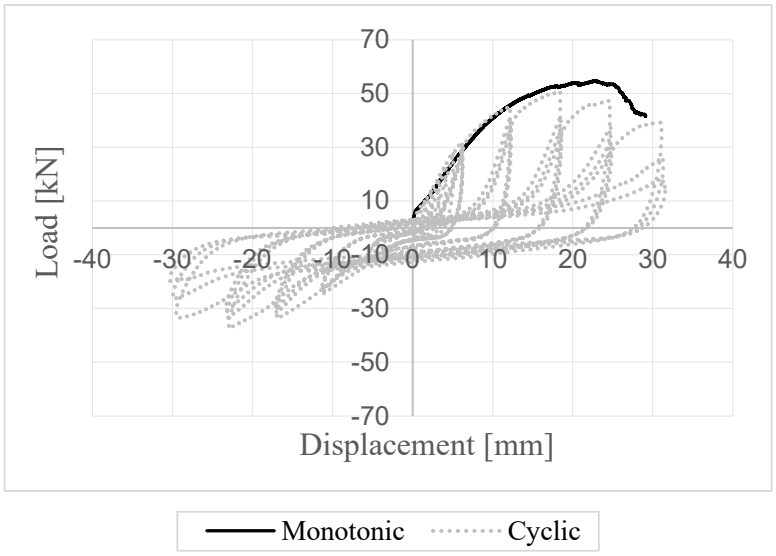

Figure 5-24: Typical load-displacement curves of partially nailed TCN200 angle bracket connection without washer under monotonic and cyclic shear

Figure 5-25 and Figure 5-26 show the test specimens before and after testing for fully and partially nailed angle bracket specimens without washers, respectively, obtained from three monotonic and three cyclic tests. The observed failure mechanism was consistent for both nailing patterns and consisted of yielding in the nails combined with crushing in wood.

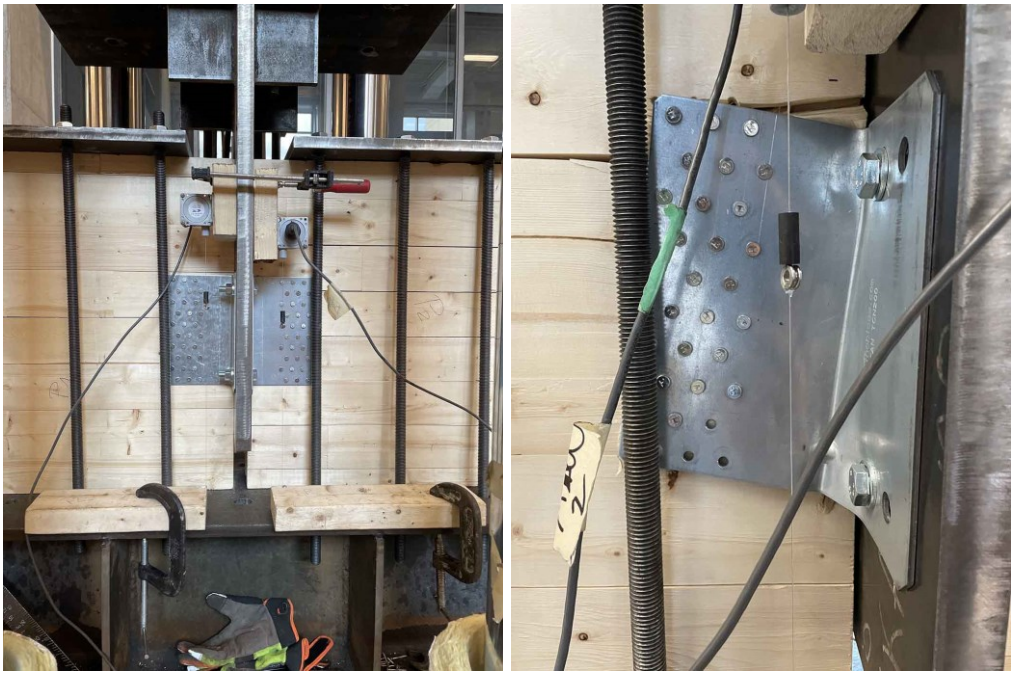

(a) (b)

Figure 5-25: Fully nailed angle bracket without washer under shear: (a) prior to the test (b) after the test

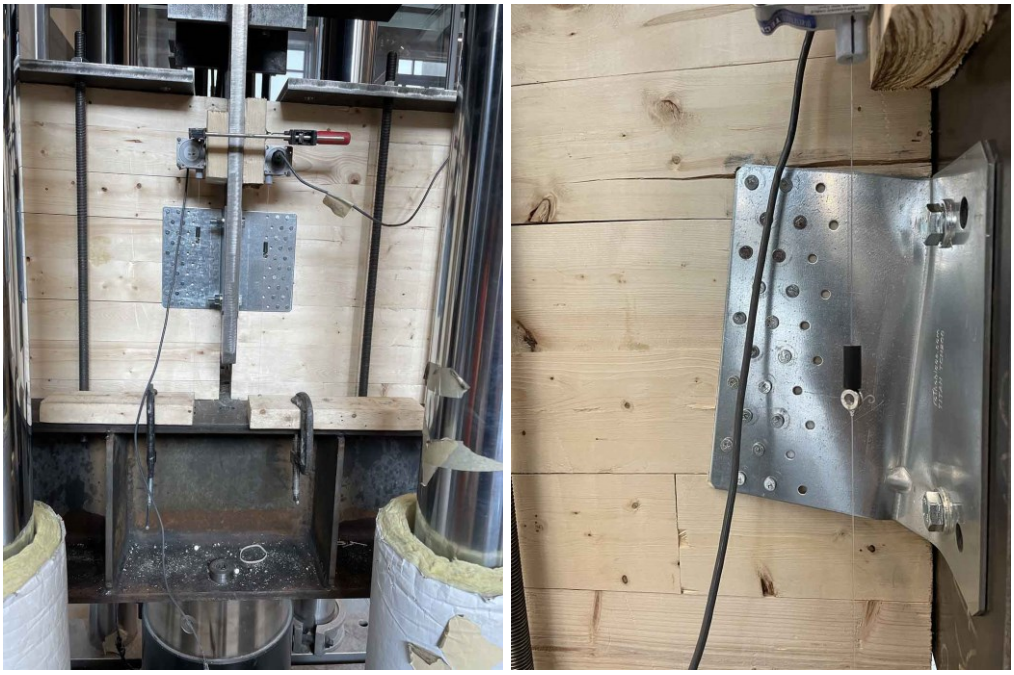

(a) (b)

Figure 5-26: Partially nailed angle bracket without washer under shear: (a) prior to the test (b) after the test

Table 5-6 and Table 5-7 present the mean and CoV of the mechanical properties for fully and partially nailed angle brackets without washer, respectively, obtained from three monotonic and three cyclic shear tests.

Table 5-9: Mean values and the associated CoV of mechanical properties of fully nailed TCN200 angle bracket without washer under monotonic and cyclic shear

Method	Property	Unit	Monotonic		Cyclic	
			Mean	CoV (%)	Mean	CoV (%)
Maximum & ultimate	F_{max}	[kN]	69.6	3	66.3	3
	$v_{F,max}$	[mm]	23.5	5	20.5	5
	F_u	[kN]	55.9	2	57.4	6
	v_u	[mm]	35.3	4	34.8	3
EEEP	$F_{y,EEEP}$	[kN]	63.1	2	62.2	4
	$v_{y,EEEP}$	[mm]	11.0	4	13.1	17
	$k_{e,EEEP}$	[kN/mm]	6.2	1	5.2	10
	D_{EEEP}	[-]	2.5	4	2.7	21
Trilinear	$F_{y,trilinear}$	[kN]	59.4	4	59.5	7
	$v_{y,trilinear}$	[mm]	10.4	5	12.6	21
	$k_{e,trilinear}$	[kN/mm]	5.7	3	4.8	17
	$D_{trilinear}$	[-]	3.4	9	2.9	26

Table 5-10: Mean values and the associated CoV of mechanical properties of partially nailed TCN200 angle bracket without washer under monotonic and cyclic shear

Method	Property	Unit	Monotonic		Cyclic	
			Mean	CoV (%)	Mean	CoV (%)
Maximum & ultimate	F_{max}	[kN]	50.5	8	50.7	3
	$v_{F,max}$	[mm]	22.0	15	20.5	17
	F_u	[kN]	40.4	7	41.2	5
	v_u	[mm]	30.9	11	30.2	2
EEEP	$F_{y,EEEP}$	[kN]	46.5	8	47.1	5
	$v_{y,EEEP}$	[mm]	10.8	13	12.5	35
	$k_{e,EEEP}$	[kN/mm]	4.7	11	4.0	33
	D_{EEEP}	[-]	2.5	5	2.6	35
Trilinear	$F_{y,trilinear}$	[kN]	44.9	7	45.2	10
	$v_{y,trilinear}$	[mm]	10.4	12	12.1	40
	$k_{e,trilinear}$	[kN/mm]	4.3	8	4.7	50
	$D_{trilinear}$	[-]	3.0	16	2.8	42

Appendix A.3.3 and A.3.4 present the load-displacement curves and respective mechanical properties of tests conducted on TCN200 fully and partially nailed angle brackets without washers under horizontal (shear) loads, respectively.

5.4.3. Observation

Fully- and partially nailed angle brackets without washers behaved similarly under uplift load, indicating that for the number of nails used in the current study the effect on their uplift load resistance is insignificant. This could be attributed to the weaker connection at the bracket attached to the base when a washer is not used (see Figure 5-19 and Figure 5-20). Using a washer helped avoid premature failure of the bracket, and the nails contributed to resisting the load (see Figure 5-21), resulting in more than double the resistance in partially nailed specimens. The results indicated a maximum load of around 30 kN in both nailing patterns without washer, while partially nailed angle bracket with washer showed a significantly higher maximum load of around 65 kN. The mean stiffness values for fully- and partially nailed angle brackets were around 4.4 and 1.3 kN/mm, respectively, while a value of around 5.4 kN/mm was obtained for partially nailed angle

bracket with washer, highlighting the contribution of nails to resisting the uplift load when using a washer. Ductility ratios was more than 5.5 for fully nailed brackets without washer, while those for partially nailed were around 1.7-2.2. The reason for significant differences between fully and partially nailed angle brackets ductility ratios can be attributed to the greater initial stiffness of fully nailed brackets and its impact on the definition of yield points. The ductility ratio for partially nailed brackets with washer displacement was around 2.2.

Concerning the shear load, nails contributed significantly to the resistance, as the maximum load obtained was around 66 and 50 kN for fully- and partially nailed, respectively, representing more than 30% difference. The mean stiffnesses for fully nailed brackets were around 6 and 5 kN/mm under monotonic and cyclic displacement respectively, and those of partially nailed were around 4.5 kN/mm, respectively. Ductility ratios appeared similar in both nailing patterns, around 2.5-3.5.

5.5. Panel-to-panel connections under shear

The spline panel-to-panel connections consisted of three CLT panels, plywood boards, and dowel-type fasteners, as illustrated in Figure 5-27(a). Notches were cut along the height of the panels on one edge for the side panels, P_1 and P_3, and on both edges for the middle panel, P_2. 1" DFP and $3/4$" CSP plywood were used along with screw and nail fasteners, respectively. Figure 5-27(b) shows the edge and middle spacing for each fastener. Monotonic and reversed cyclic tests under shear were conducted on three types of fasteners, including partially threaded screws HBS 6×70, HBS 8×80, and standard galvanized 3.4×63.5 spiral nails (see Figure 5-28).

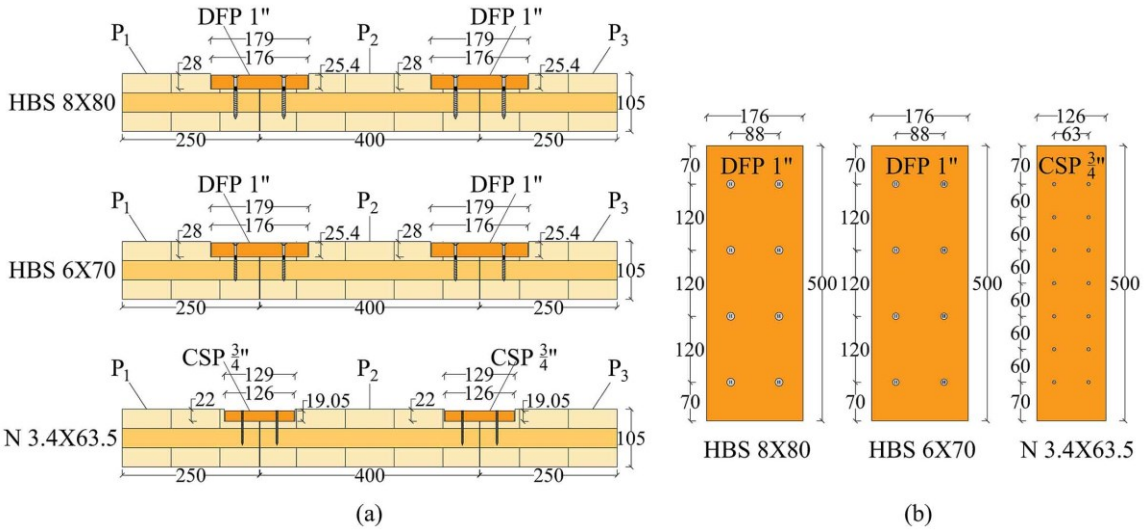

Figure 5-27: (a) top view of tested specimens; (b) spaces between fasteners and edge spacing in the plywood

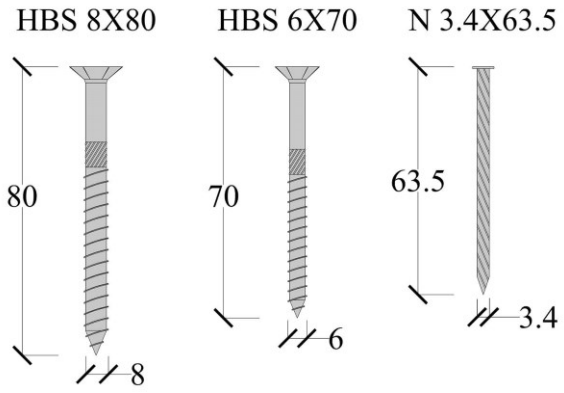

Figure 5-28: Fasteners used in panel-to-panel connections

Additional details related to test set-up attachments are presented in Appendix A.4.

Figure 5-29 illustrates the test set-up of panel-to-panel connections subjected to shear displacement. A gap between the middle panel and the base beam of 100 mm was provided to allow vertical displacement while the side panels were fixed to the base. Two transducers were attached to each face of the middle CLT specimen, P_2, to measure its vertical displacement relative to the base beam, representing shear displacement.

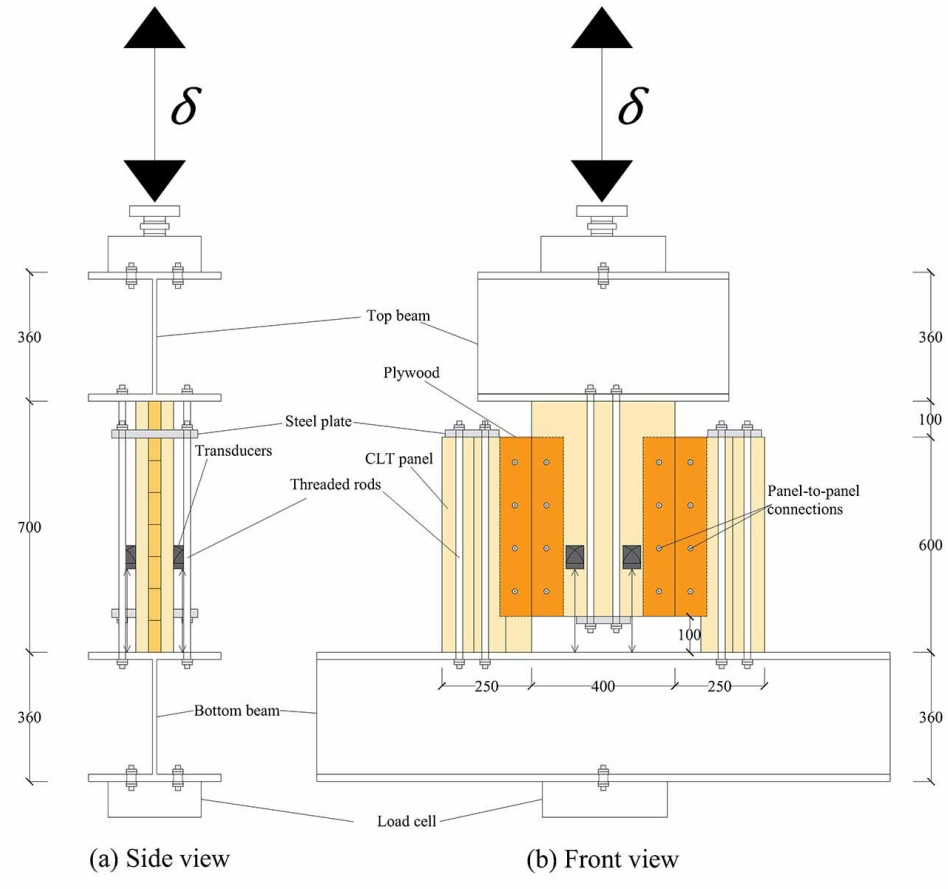

Figure 5-29: Test set-up of panel-to-panel connections subjected to shear

Figure 5-30 to Figure 5-33 show typical load-displacement curves for the HBS 8 × 80 mm, HBS 6 × 70 mm, and galvanized spiral 3.4 × 63.5 mm nail, respectively. Three monotonic and three cyclic tests were conducted for each fastener type. Low-cycle fatigue appeared to have a significant effect on panel-to-panel connections behaviour, represented as premature failure under cyclic load, especially for joints fastened with smaller diameter fasteners, such as nails and HBS 6 × 70 mm.

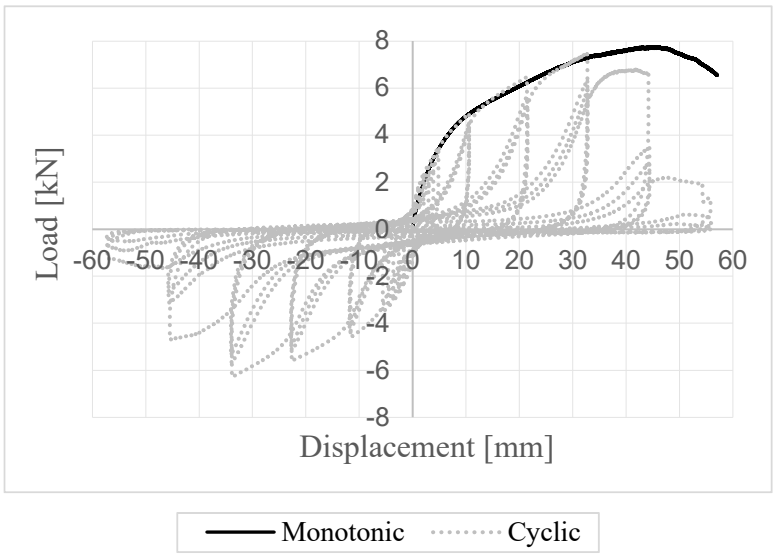

Figure 5-30: Typical load-displacement curves of HBS 8 × 80 mm fasteners used as panel-to-panel connections under monotonic and cyclic shear

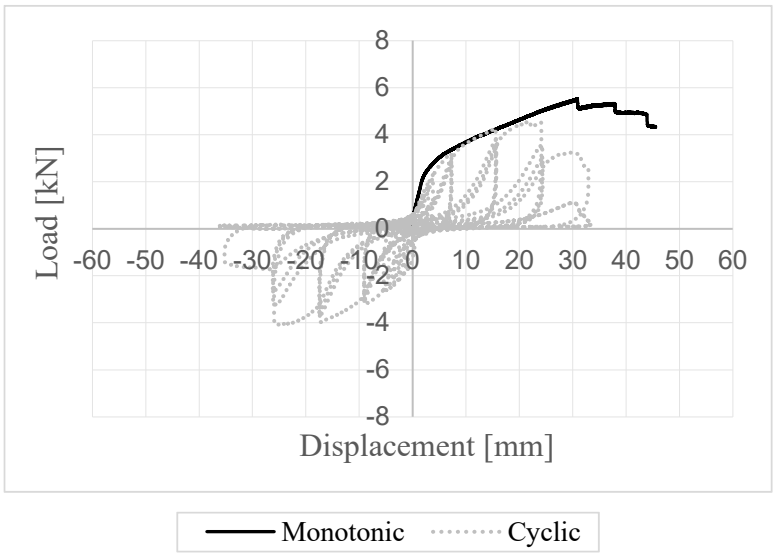

Figure 5-31: Typical load-displacement curves of HBS 6 × 70 mm fasteners used as panel-to-panel connections under monotonic and cyclic shear

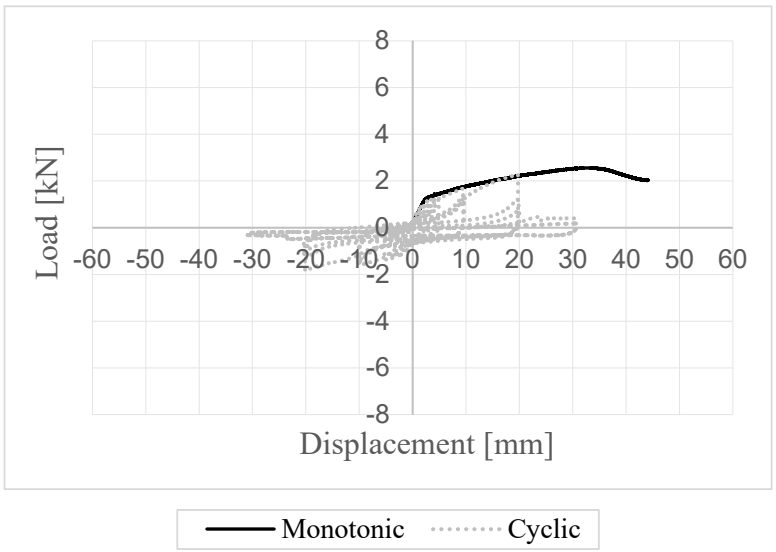

Figure 5-32: Typical load-displacement curves of galvanized spiral 3.4 × 63.5 mm nail fasteners used as panel-to-panel connections under monotonic and cyclic shear

Figure 5-33 to Figure 5-35 demonstrate the ultimate failure type for panel-to-panel connections. The failure mechanism was represented by a ductile failure mode, in which embedment crushing failure in the plywood and CLT combined with yielding in the fasteners and head pull-through in screws was observed.

(a) (b)

Figure 5-33: HBS 8 × 80 mm panel-to-panel connections under shear: (a) prior to the test (b) after the test

(a) (b)

Figure 5-34: HBS 6 × 70 mm panel-to-panel connections under shear: (a) prior to the test (b) after the test

(a) (b)

Figure 5-35: Galvanized spiral 3.4 × 63.5 mm nail panel-to-panel connections under shear: (a) prior to the test (b) after the test

Table 5-11 to Table 5-13 present the mean and CoV obtained from shear tests on panel-to-panel connections, obtained from three monotonic and three cyclic tests for each type of fastener.

Table 5-11: Mean values and the associated CoV of mechanical properties of HBS 8 × 80 panel-to-panel connections under monotonic and cyclic shear

Method	Property	Unit	Monotonic		Cyclic	
			Mean	CoV (%)	Mean	CoV (%)
Maximum & ultimate	F_{max}	[kN]	7.5	3	7.4	3
	$v_{F,max}$	[mm]	43.2	6	39.9	16
	F_u	[kN]	6.5	3	5.9	3
	v_u	[mm]	55.7	3	46.5	10
EEEP	$F_{y,EEEP}$	[kN]	6.4	4	6.3	2
	$v_{y,EEEP}$	[mm]	10.2	5	8.0	24
	$k_{e,EEEP}$	[kN/mm]	0.6	9	0.7	21
	D_{EEEP}	[-]	5.5	7	6.0	21
Trilinear	$F_{y,trilinear}$	[kN]	4.5	2	4.4	3
	$v_{y,trilinear}$	[mm]	6.9	7	5.4	25
	$k_{e,trilinear}$	[kN/mm]	0.7	8	0.8	23
	$D_{trilinear}$	[-]	8.1	9	8.9	22

Table 5-12: Mean values and the associated CoV of mechanical properties for HBS 6 × 70 panel-to-panel connections under monotonic and cyclic shear

Method	Property	Unit	Monotonic		Cyclic	
			Mean	CoV (%)	Mean	CoV (%)
Maximum & ultimate	F_{max}	[kN]	5.6	5	4.5	2
	$v_{F,max}$	[mm]	29.5	5	19.1	23
	F_u	[kN]	4.5	5	3.6	2
	v_u	[mm]	42.9	11	25.1	7
EEEP	$F_{y,EEEP}$	[kN]	4.8	4	3.4	15
	$v_{y,EEEP}$	[mm]	5.0	19	5.4	15
	$k_{e,EEEP}$	[kN/mm]	1.0	25	0.6	5
	D_{EEEP}	[-]	8.9	27	4.8	21
Trilinear	$F_{y,trilinear}$	[kN]	3.1	6	3.7	11
	$v_{y,trilinear}$	[mm]	3.0	29	5.8	13
	$k_{e,trilinear}$	[kN/mm]	1.1	27	0.6	4
	$D_{trilinear}$	[-]	15.1	39	4.4	14.4

Table 5-13: Mean values and the associated CoV of mechanical properties for galvanized spiral 3.4 × 63.5 nail panel-to-panel connections under monotonic and cyclic shear

Method	Property	Unit	Monotonic		Cyclic	
			Mean	CoV (%)	Mean	CoV (%)
Maximum & ultimate	F_{max}	[kN]	2.8	1	2.2	5
	$v_{F,max}$	[mm]	34.9	8	19.5	1
	F_u	[kN]	2.1	1	1.8	7
	v_u	[mm]	48.3	15	24.4	19
EEEP	$F_{y,EEEP}$	[kN]	2.1	1	1.8	13
	$v_{y,EEEP}$	[mm]	4.3	1	7.3	71
	$k_{e,EEEP}$	[kN/mm]	0.5	1	0.3	59
	D_{EEEP}	[-]	11.3	16	4.2	47
Trilinear	$F_{y,trilinear}$	[kN]	1.2	8	1.5	34
	$v_{y,trilinear}$	[mm]	2.3	5	6.6	89
	$k_{e,trilinear}$	[kN/mm]	0.5	3	0.3	59
	$D_{trilinear}$	[-]	21.3	20	5.9	70

Appendix A.4.1, A.4.2, and A.4.3 present the load-displacement curves and respective mechanical properties of tests conducted on panel-to-panel connections consisting of HBS 6×70, HBS 8×80, and standard galvanized 3.4×63.5 spiral nails under horizontal (shear) loads, respectively.

5.5.1. Observation

Panel-to-panel connections attached through different fasteners behaved relatively ductile under monotonic shear load. The mean values of ductility ratio using EEEP, D_{EEEP}, under such load for galvanized spiral 3.4×63.5 mm nails, HBS 6×70 mm, and HBS 8×80 mm were around 11.3, 8.9, and 5.5, respectively. It can be observed that using small diameter fasteners, such as nails, led to around double the ductility under monotonic load when compared to fasteners with larger diameter and length, such as HBS 8×80.

Contrarily, larger fasteners, such as HBS 8×80 mm, behaved relatively ductile under reversed cyclic shear load, while those with smaller diameters failed prematurely before reaching the maximum monotonic load and associated displacement. The mean values of ductility ratio using EEEP, D_{EEEP}, under such load for 3.4×63.5 mm nails, HBS 6×70 mm, and HBS 8×80 mm screws were around 4.2, 4.7, and 6.0, respectively. This implies that smaller dimension fasteners are more prone to low-cycle fatigue than larger ones, as further represented by comparing the cyclic with monotonic curves, depicted in Figure 5-30 to Figure 5-32. The ultimate displacement of nail fasteners under reversed cyclic load represented failure at around 50% displacement of that observed under monotonic loading, and around 60% and 83% for the HBS 6×70 mm and 8×80 mm fasteners, respectively.

The results highlighted the mean values of maximum load for HBS 8×80 mm, HBS 6×70 mm, and galvanized spiral 3.4×63.5 mm nail, of around 7.5 kN, 5.6 kN, and 2.5 kN, respectively, under monotonic displacement, and 7.4 kN, 4.5 kN, and 2.2 kN, respectively, under cyclic displacement. The mean values of stiffness based on EEEP method for HBS 8×80 mm, HBS 6×70 mm, and galvanized spiral 3.4×63.5 mm nail, were obtained around 0.6, 1.0, and 0.5 kN/mm, respectively, under monotonic displacement, and around 0.7, 0.6, and 0.3 kN/mm, respectively, under cyclic

displacement. That highlights low-cycle fatigue affects more severely the resistance and stiffness of smaller fasteners, such 3.4×63.5 mm nails.

The low-cycle fatigue in small fasteners requires considerable attention when such fasteners are used as panel-to-panel connections in CLT shearwalls in a seismic region since the ductility in those systems stems primarily from such fasteners. That is also emphasized in the CD proposal in Chapter 4, in which panel-to-panel connections are designed as primary dissipative connections that provide sufficient seismic energy dissipation in CLT shearwalls.

5.6. Summary

This chapter presents experimental tests conducted on various conventional connections used in CLT shearwalls, such as hold-down, angle brackets, and panel-to-panel connections. Fully and partially nailed hold-down and angle brackets were tested to evaluate the effect of nail number on their performance. Tests were also conducted on three types of fasteners used in spline panel-to-panel connections to investigate the impact of the type and size of the fasteners on their behaviour.

This section draws the following conclusions:

- The tested hold-down connections, WHT620, resisted similar uplift loads in both fully- and partially nailed applications. The failure in the fully nailed configuration occurred in the bracket due to the higher number of nails leading to their strong connections, while partially nailed hold-down failed in the nails. Similar values for ductility ratios, around 2.2, were obtained for both nailing patterns due to the greater ultimate displacements and lower stiffnesses of partially nailed than fully nailed.
- Fully nailed hold-down under shear displacement exhibited rotation in the lower part of the bracket. Although the maximum load was reasonably high, around 40 kN, the stiffness was very low representing its negligible contribution to resisting sliding on CLT shearwalls.
- Angle brackets tested without washer under uplift failed in the section attached to the base by bolts. The bracket exhibited bending and bolt withdrawal, which

rendered the number of nails connecting the bracket to the CLT panel inconsequential. Using a washer avoided brittle and premature failure of the bracket and resulted in the nails contributing more significantly to resisting the load. This resulted in more than double the maximum resistance with the washer than without it.

- The shear resistance and stiffness of angle brackets were greater for fully nailed than partially nailed brackets due to the contribution of nails to resisting the load. However, the ductility ratios appeared similar in both nailing patterns.
- Panel-to-panel connections attached using different fasteners behaved relatively ductile under monotonic shear load, particularly the smaller fasteners (i.e., nails). While larger fasteners, such as HBS 8×80, behaved relatively ductile under reversed cyclic shear load, smaller diameter nail fasteners failed prematurely prior to reaching the maximum monotonic load and associated displacement. This is attributed to the smaller dimension fasteners being more prone to low-cyclic fatigue than larger ones. The fatigue in small fasteners requires considerable attention when such fasteners are used as panel-to-panel connections in CLT shearwalls in a seismic region since the ductility in those systems stems significantly from such fasteners.

Chapter 6 - Experimental tests on CLT shearwalls

6.1. General

This chapter investigates the behaviour of multi-panel CLT shearwalls by conducting monotonic shearwall-level experimental tests on different configurations while varying the number of panels, connection type and configuration, and gravity load. The goal of this part of the experimental campaign is to investigate the performance of multi-panel CLT shearwalls with regards to their kinematic modes, resistance, and lateral displacement. The obtained results are then utilized in chapter 7 to validate the developed analytical (in Chapter 3) and proposed design approaches (in Chapter 4).

6.2. Test Configurations

The same type of CLT panels used in the connection-level tests (Section 5.2), which consisted of 3-ply 105 mm thick (35-35-35), were utilized in the full scale shearwall tests. As presented in Table 6-1, a total of twelve shearwalls were investigated. Five walls were tested without angle brackets ($n_s = 0$), walls #1-#5, in which sliding was prevented, and seven walls included angle brackets ($n_s \neq 0$), in which sliding was resisted by angle brackets. The main purpose of this investigation was to study the contribution of angle brackets to the rocking and shear resistance of walls. Test ID and configuration represent the test sequence number (#1-#12) and CLT panels and their connections [(a)-(h)]. In five test configurations, a gravity load, q, was applied to the top face of each panel, representing an equivalent uniformly distributed gravity load of 5.22 kN/m. Variables b and h are the length and height of each panel, while B is the total length of the wall ($b \cdot m$), n_h represents the number of hold-downs on the uplift side of the shearwall, m is the number of panels, and n_F is the number of panel-to-panel connections. The tested configurations were selected based on preliminary numerical models to achieve either CP or SW kinematic modes.

Table 6-1: Shearwall-level tests information

Test ID-configuration	q (KN/m)	$b \times h$ (m)	B (m)	n_h	m	n_s	n_F	Expected mode
#1-(a)	0	1.22x2.44	3.66	2	3	0	9	CP
#2-(a)	5.22	1.22x2.44	3.66	2	3	0	9	CP
#3-(b)	0	1.22x2.44	3.66	1	3	0	35	SW
#4-(b)	5.22	1.22x2.44	3.66	1	3	0	35	SW
#5-(c)	5.22	1.22x2.44	3.66	1	3	0	26	SW
#6-(d)	0	1.22x2.44	3.66	2	3	2	9	CP
#7-(d)	5.22	1.22x2.44	3.66	2	3	2	9	CP
#8-(e)	0	1.22x2.44	3.66	0	3	2	9	CP
#9-(f)	0	1.22x2.44	3.66	1	3	2	35	SW
#10-(f)	5.22	1.22x2.44	3.66	1	3	2	35	SW
#11-(g)	0	1.22x2.44	2.44	2	2	2	9	CP
#12-(h)	0	0.61x2.44	2.44	2	4	1	9	CP

Figure 6-1 presents the test configurations, including the size of the panels and the connections used. For configurations (a)-(c), a cut was introduced to the bottom wall corner about which rotation occurs, to prevent sliding since no angle brackets were used (walls #1-#5). Configurations (d)-(h) consisted of fully nailed angle brackets without washers and with hold-downs (walls #6-#7 and #9-#12), while Configuration (e) was tested with angle brackets only and without hold-downs. The specifications of the connections used in each configuration are depicted in Figure 6-1 with numbers 1-5 and presented in Table 6-2.

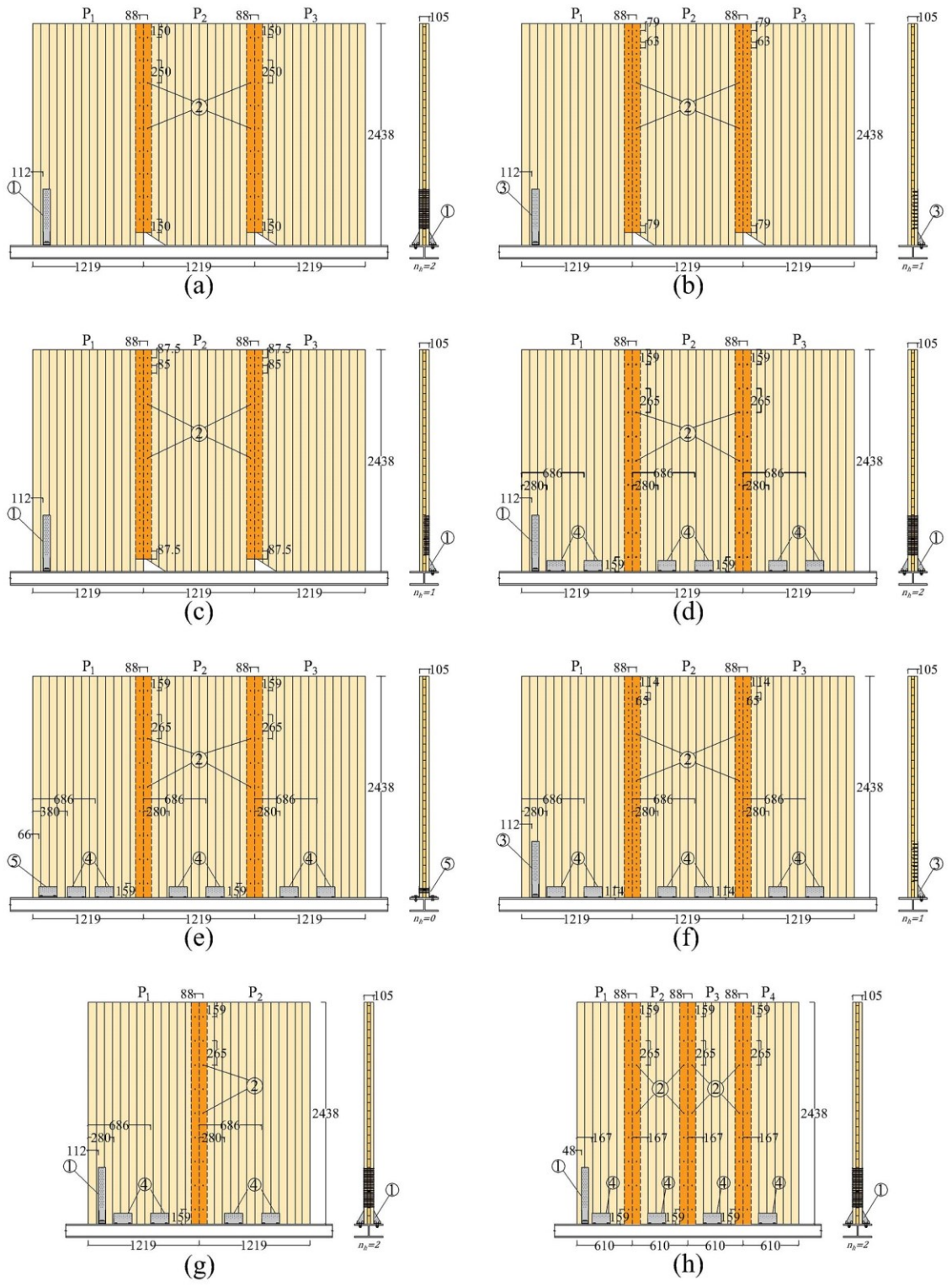

Figure 6-1: Shearwall level experimental test configurations

Table 6-2: Connections used in shearwall-level tests

Connection ID	Specification
(1)	• Hold-down WHT620 • 1 bolt | M20 × 100 • 1 washer $t = 20\ mm$ | WHTW70 • 55 nails | LBA 4 × 60 mm
(2)	• Panel-to-panel connection • Screw HBS 6 × 70 mm
(3)	• Hold-down WHT620 • 1 bolt | M20 × 100 • 1 washer $t = 20\ mm$ | WHTW70 • 22 nails | LBA 4 × 60 mm
(4)	• Angle bracket | TCN200 • 2 bolts | M12 × 60 • 30 nails | LBA 6 × 40 mm
(5)	• Angle bracket | TCN200 • 2 bolts | M12 × 60 • 1 washer $t = 12\ mm$ | TCW200 • 30 nails | LBA 6 × 40 mm

6.3. Test set-up

Figure 6-2 presents the test set-up for walls without angle brackets (i.e., walls #1-#5), where sliding was prevented through steel angle supports at the bottom of the wall. Two cuts were made in the second and third panels, P_2 and P_3, to accommodate the sliding supports at the center of rotation of the panels. The sliding support was removed and replaced by angle brackets along the length of the wall for walls #6-#12. In order to transfer the horizontal load, a steel plate was attached at the top and centre of each panel by means of twenty-six HBS 6×70 mm screws, and an E-shaped steel plate was attached to the actuator and two steel channels, C5@9, with the length of 4060 mm. A threaded rod was used to attach the top steel plates on each face of each panel to the two channels.

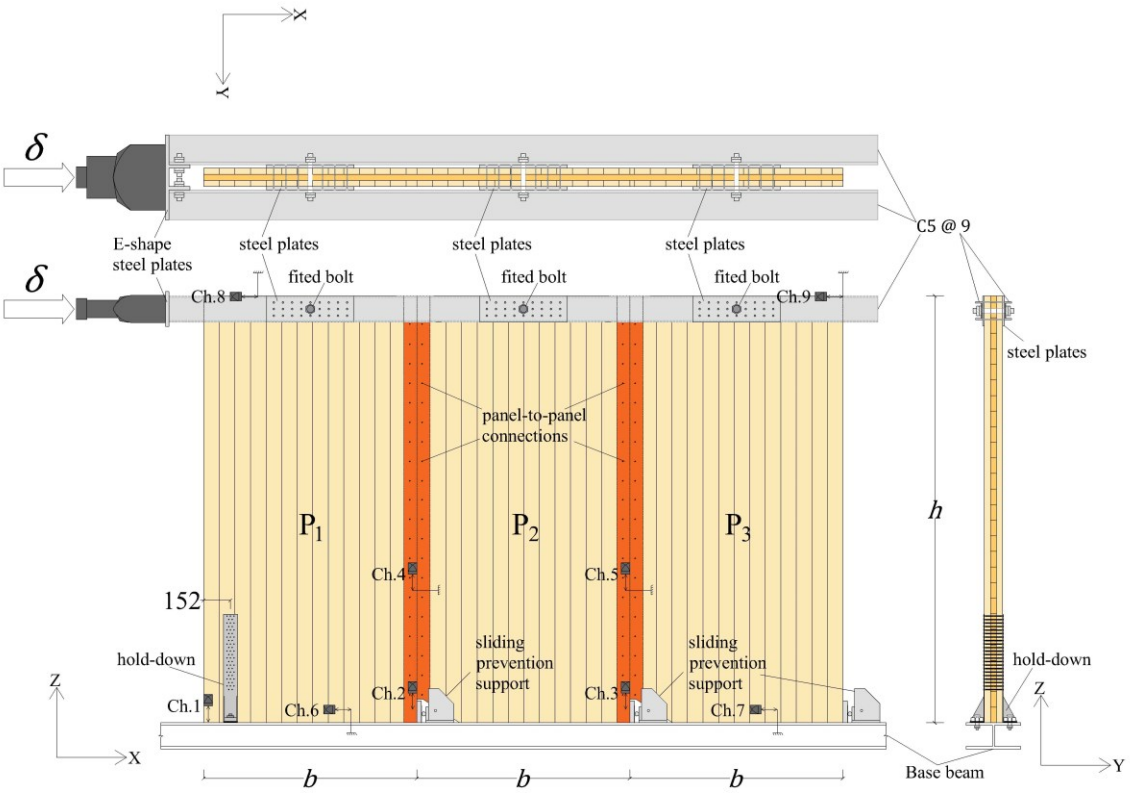

Figure 6-2: Set-up of CLT shearwall-level tests without angle brackets

This mechanism was meant to transfer equal displacement to each panel simulating diaphragm behaviour at the top of the wall and was provided using fitted connections between steel plates at the top edges of each panel (Figure 6-3) and two channels on each face of the shearwall (Figure 6-4). The fitted connections were ensured by using steel nuts the same size as the holes in steel plates and channels and connecting them with threaded rods.

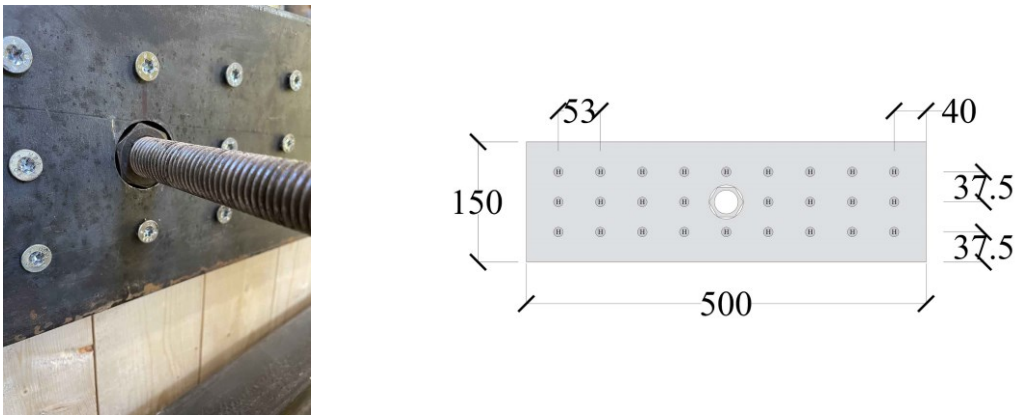

Figure 6-3: fitted connection between steel plates and treaded rods

Figure 6-4: fitted connection between steel channels and treaded rods

To avoid contact between threaded rods and CLT panels, panel holes were drilled with larger diameters than steel plates and channels (around 38 mm).

Lateral supports were provided at two points on each face of the test shearwalls, using the support system shown in Figure 6-5. The support frame consisted of steel I-section columns and hollow section beams and was placed at each face of the wall to avoid out of plane lateral displacement or buckling. Figure 6-6 shows a close-up view of the contact between the steel lateral support and CLT panels.

Figure 6-7 illustrates the gravity load system in CLT shearwall tests. One hollow steel section (H_1) with a length of 1016 mm was attached to the top of each panel through eight HBS 6×70 screws. Another hollow steel section (H_2) was attached to H_1 using steel angles and one bolt, and was oriented orthogonally to the wall length. Two concrete blocks with a total mass of 600 kg were then hung from section H_2.

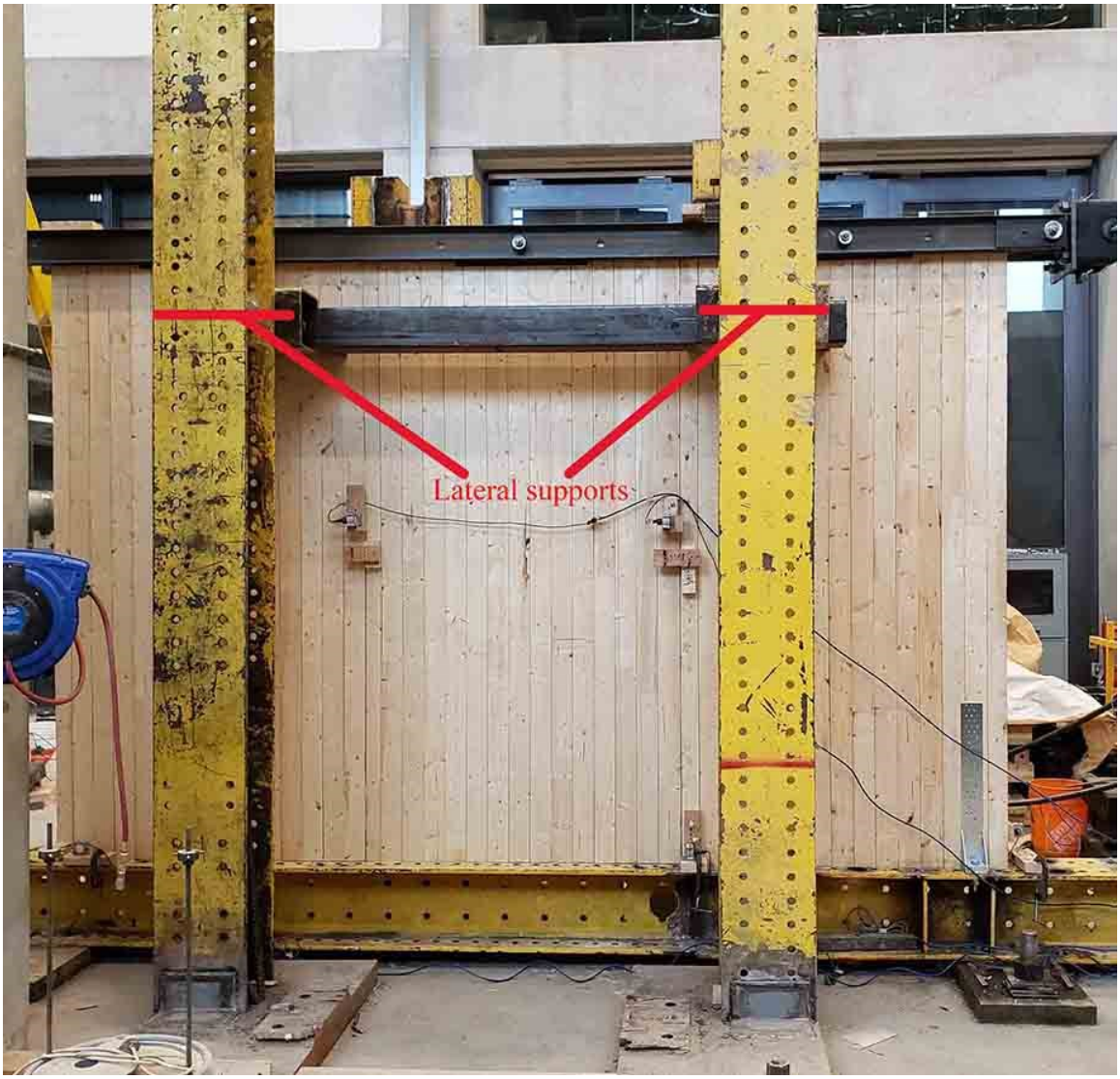

Figure 6-5: Lateral supports used in CLT shearwall tests

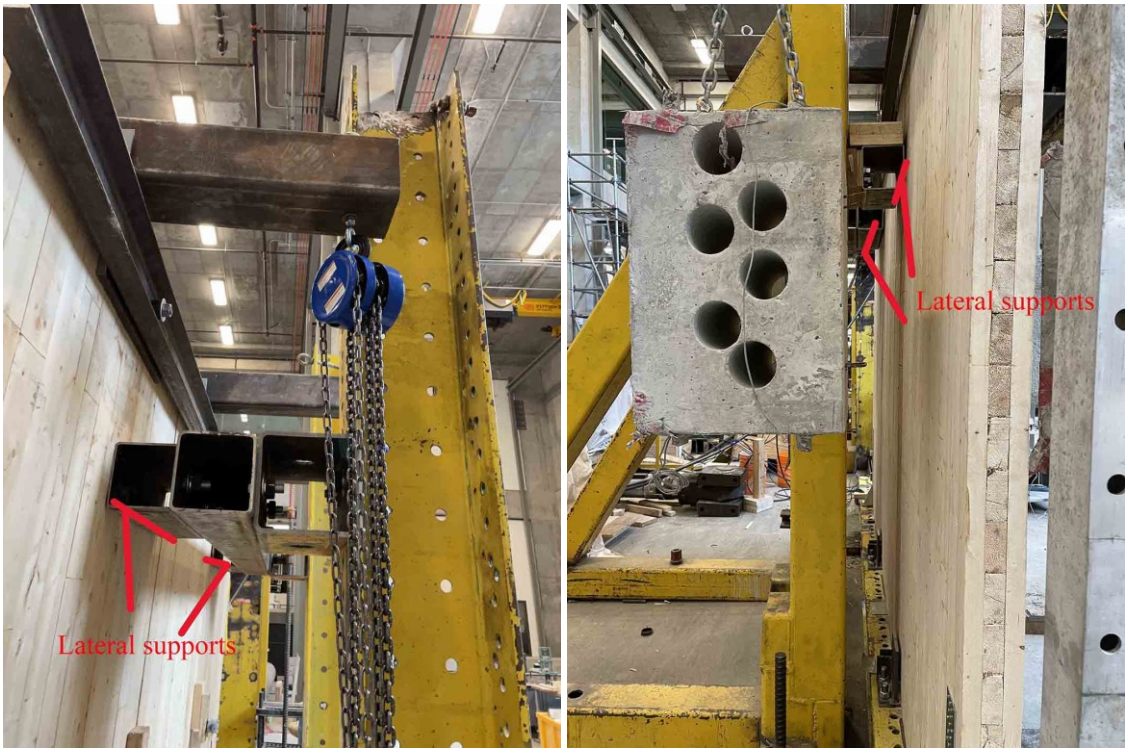

Figure 6-6: Lateral supports used at each face of shearwalls

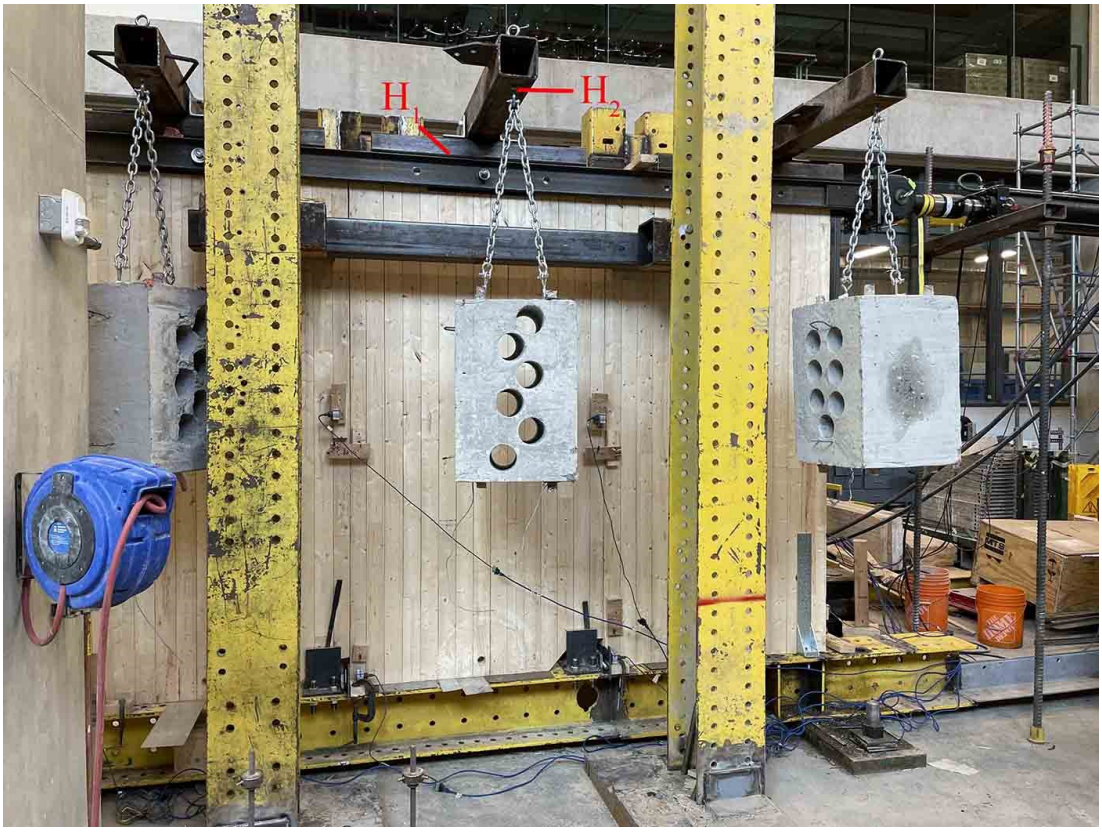

Figure 6-7: Gravity load system in CLT shearwall tests

The horizontal displacement at the top of the shearwall was applied through two steel channels on each face of the shearwall using an MTS hydraulic actuator (201.35A) with a maximum compression capacity of 365 kN. The displacement rate at the top of the walls was selected to be 6 mm/min to achieve consistent displacement rates in the shearwall-level tests as those in the connection tests. All CLT panels were also kept in consistent temperature and relative humidity conditions of 20 ± 2 ℃ and $65 \pm 5\%$, respectively, achieving an equilibrium moisture content in the specimens at around $10 \pm 2\%$.

Nine cable transducers were utilized in all tests to measure the respective displacements, shown as channel number (Ch.x), as shown in Figure 6-2. Table 6-3 presents the position and direction of each channel. Ch.1 was used to measure the vertical (uplift) displacement in the first panel, representing the uplift in the hold-down. Ch.2 and Ch.3 were used to measure the vertical displacement in the center of rotation of the first and second panel, respectively, indicating whether these panels maintain contact with the ground. Ch.4 and Ch.5 were used to measure the vertical displacement at the center of rotation of the first panel relative to the uplift side of the second panel and the vertical displacement at the center of rotation of the second panel relative to the uplift side of the third panel, respectively. Ch.6 and Ch.7 measured horizontal (sliding) displacements at the bottom of the first and third panels, respectively, and Ch.8 and Ch.9 measured the respective horizontal displacements of the first and third panels at their top. Channels δ and F represent the horizontal displacement of the actuator and associated load, respectively.

Table 6-3: Channels list and their representation

Channel	Position	Direction/component
1	Uplift side of the first panel	Vertical/displacement
2	Center of rotation of the first panel	Vertical/displacement
3	Center of rotation of the second panel	Vertical/displacement
4	Panel 1 and panel 2	Relative vertical/displacement
5	Panel 2 and panel 3	Relative vertical/displacement
6	Bottom of panel 1	Horizontal/displacement
7	Bottom of panel 3	Horizontal/displacement
8	Top of panel 1	Horizontal/displacement
9	Top of panel 3	Horizontal/displacement
$\boldsymbol{\delta}$	Actuator	Horizontal/displacement
$\boldsymbol{F}$	Actuator	Horizontal/load

More details on the test set-up can be found in Appendix B.

6.4. Shearwall test results

This section discusses the results obtained from shearwall tests, presented in Table 6-1. Figure 6-8 illustrates the lateral load versus wall top displacement curves and presents the curve obtained from the experimental campaign, as well as the idealized bi-linear and tri-linear curves, as described in section 5.2.2. It can be noted that the general shape of the curves with and without gravity loads appeared to be similar for the same configurations (e.g., comparisons between walls #1 and #2 and walls #3 and #4), however, adding gravity load is observed to have resulted in greater yield and maximum resistances. It can also be observed that walls with SW behaviour (i.e., walls #3-#5 and #9-#10) had greater stiffness but lower ultimate displacement and ductility than walls with CP behaviour. This can be attributed to the number of panel-to-panel connections. For example, wall #5 was relatively more flexible and ductile than other walls with SW behaviour due to the use of fewer panel-to-panel connections and fully nailed hold-downs. Wall #8 which consisted of fully nailed angle brackets with washers used to resist the uplift force instead of hold-downs exhibited a larger plateau after yielding when compared to shearwall #6. Walls #11 and #12 with the same total length, but different numbers of panels (i.e., two vs. four) showed that using more panels led to lower resistance and stiffness but significantly larger ultimate displacement.

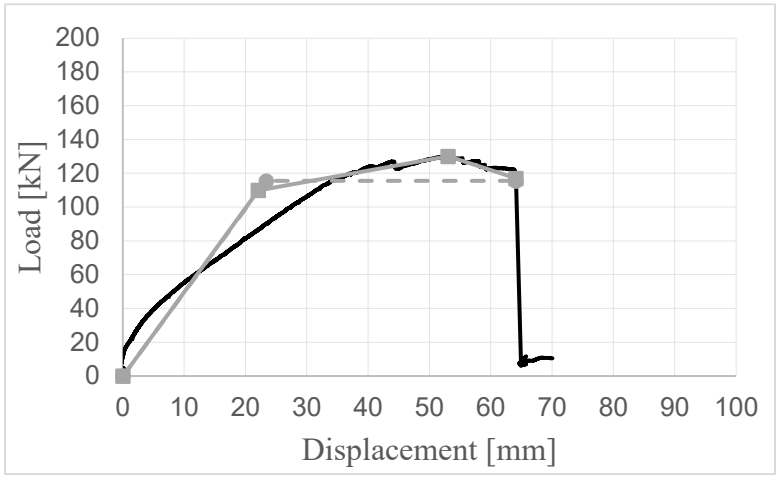

wall #1

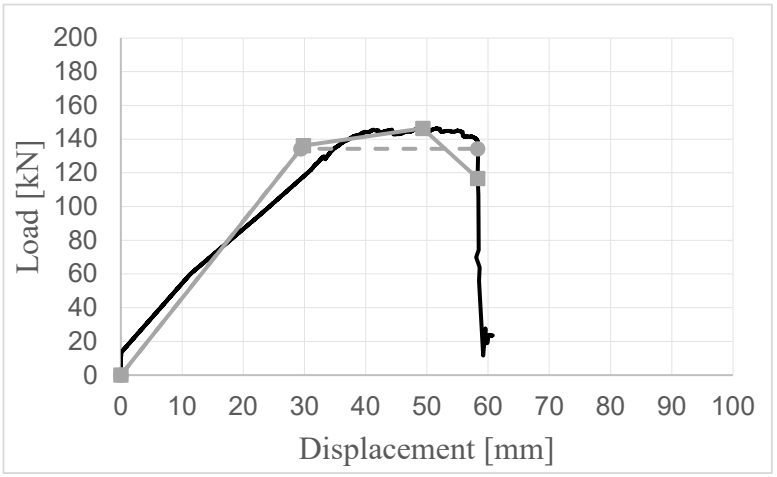

wall #2

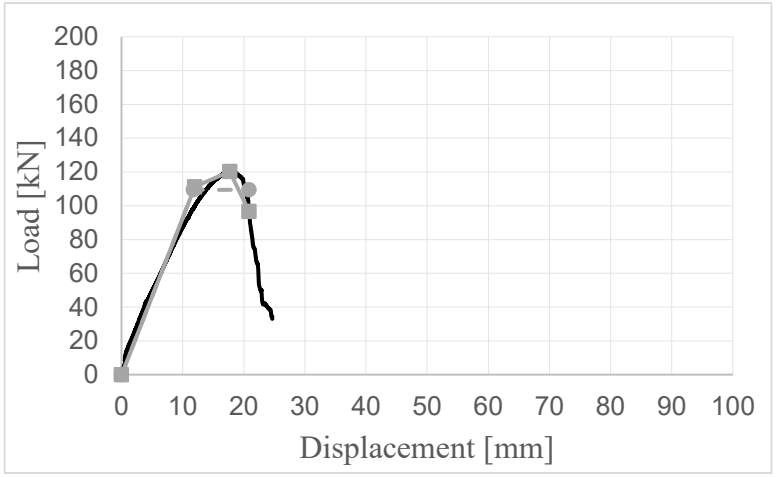

wall #3

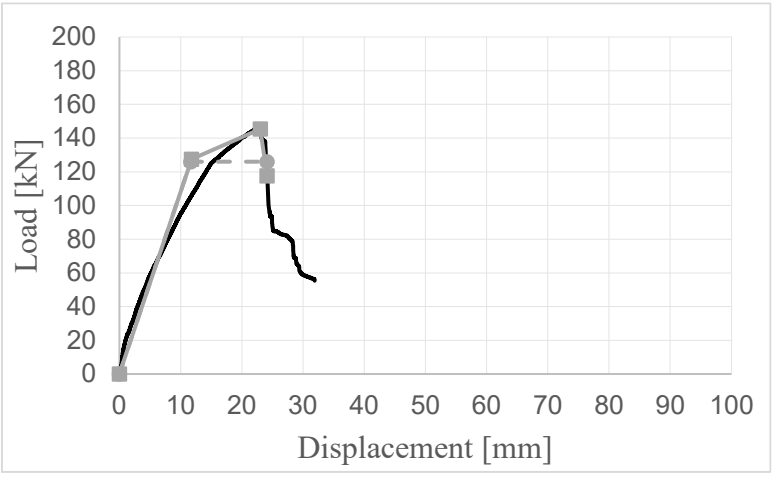

wall #4

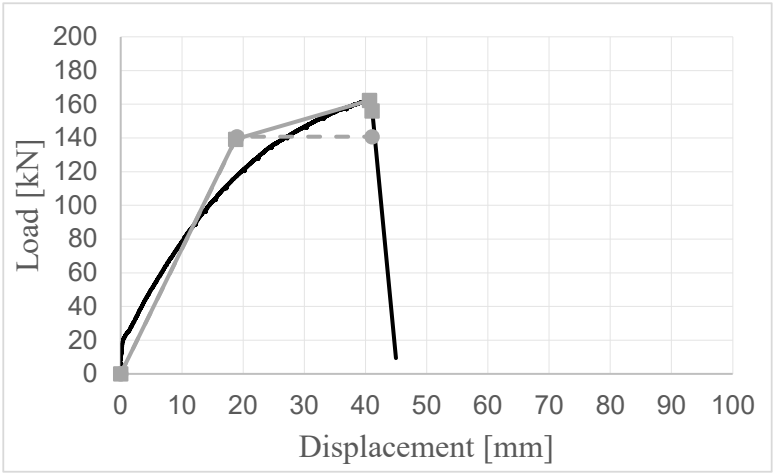

wall #5

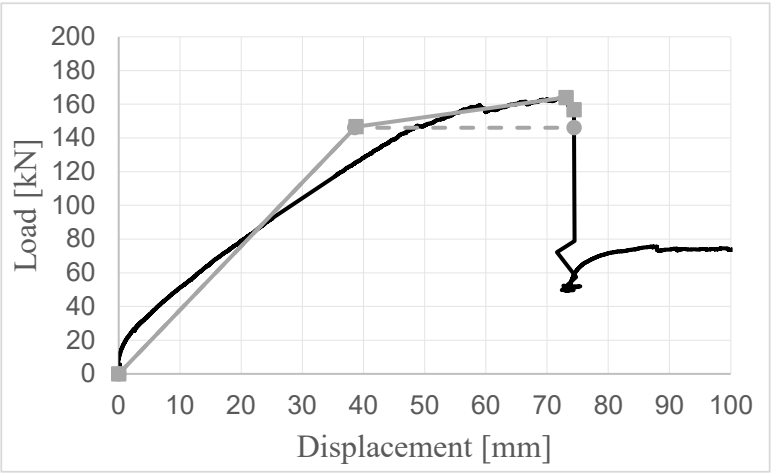

wall #6

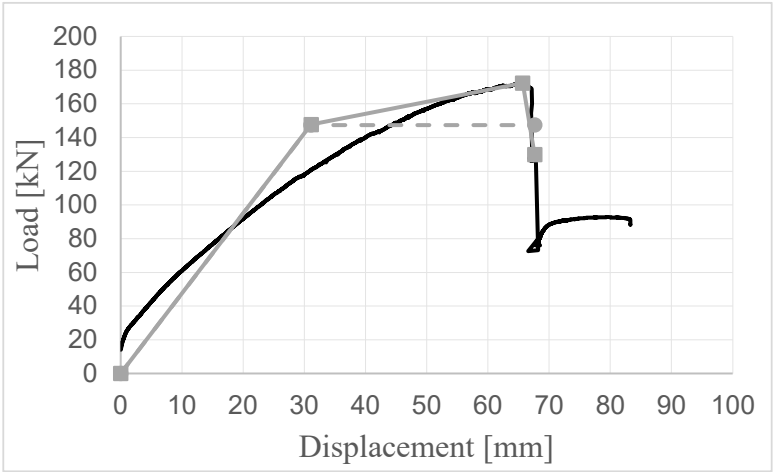

wall #7

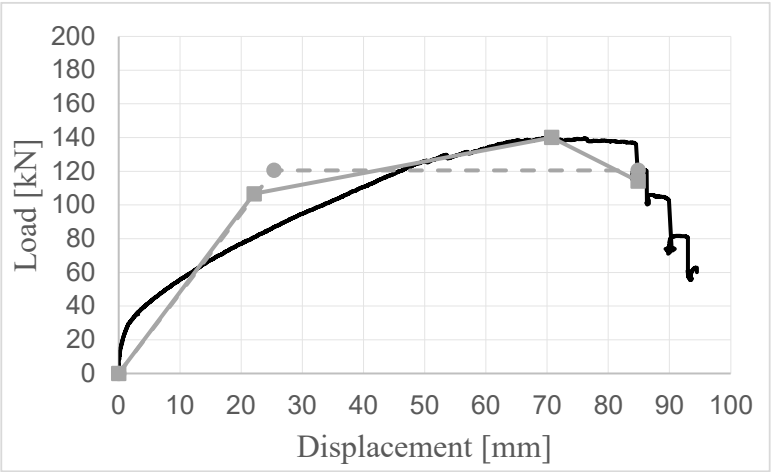

wall #8

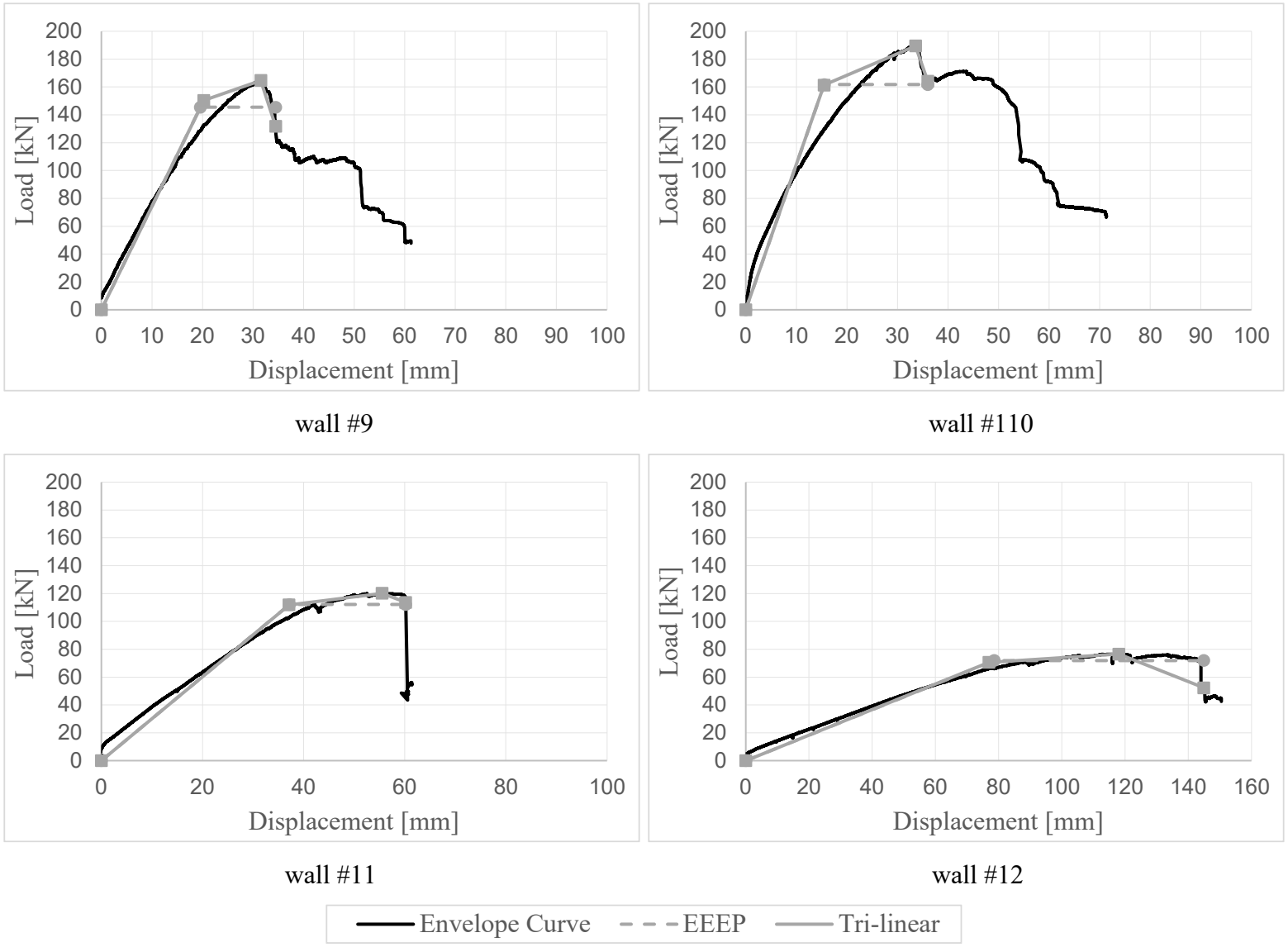

Figure 6-8: Load-displacement curves of shearwall tests

6.4.1. Observed kinematic modes

It is very important to note that the kinematic modes observed from the full scale shearwall tests were consistent with those predicted based on the preliminary numerical models. For walls #1-#2, #6-#8, and #11-#12 CP mode was achieved, in which individual centers of rotation for each panel were observed throughout the tests, while SW mode was attained for walls #3-#5 and #9-#10 in which the first and second panels were lifted, and only one center of rotation appeared in panel 3 (Figure 6-9). The observed behaviour was also consistent with the assumption about the activation load, where for example for all walls with SW behaviour the panels initially remained in contact with the ground until the stabilizing effect of gravity load was overcome, and the entire wall rotated. Initially, all walls with SW exhibited CP behaviour, but as the lateral load increased, they exhibited SW behaviour. It is also noteworthy to mention that wall #5 took longer to detach from the ground, compared to other walls with SW (e.g., #3 and #4), due to the relatively more flexible panel-to-panel connections.

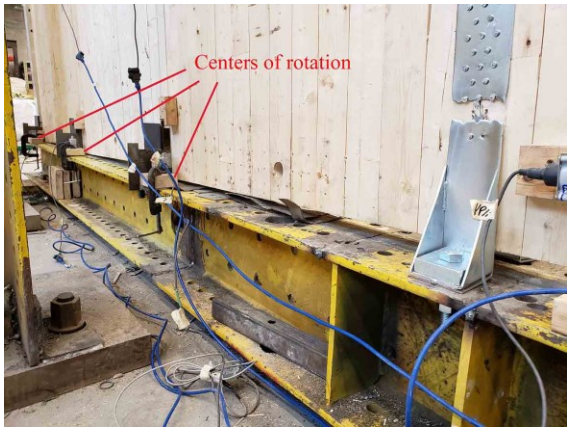

wall #1

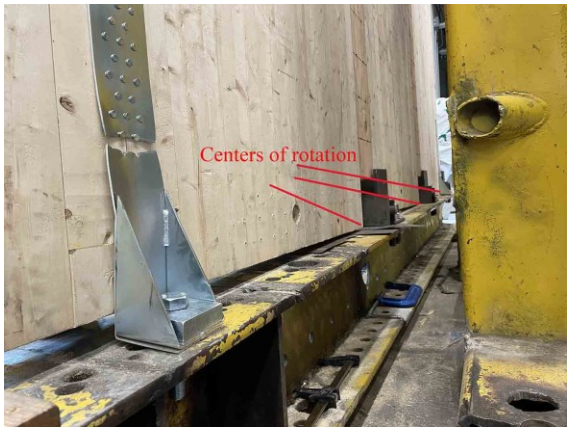

wall #2

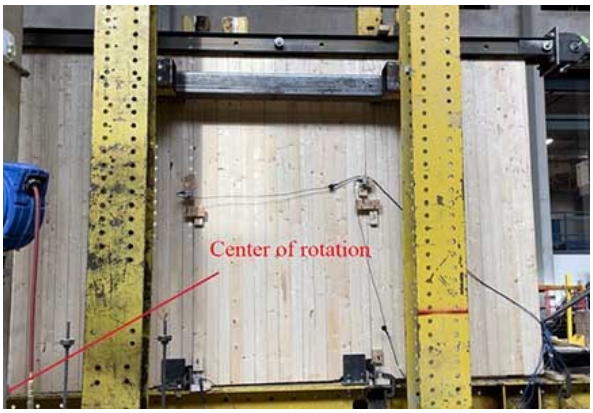

wall #3

wall #4

wall #5

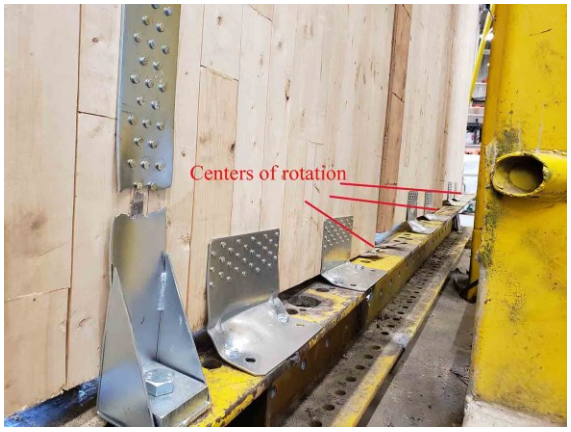

wall #6

wall #7

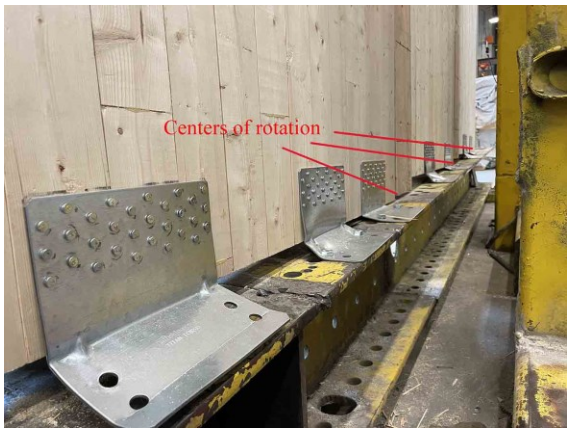

wall #8

wall #9

wall #10

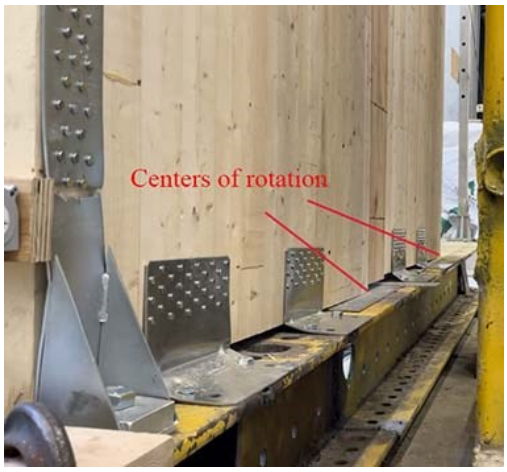

wall #11

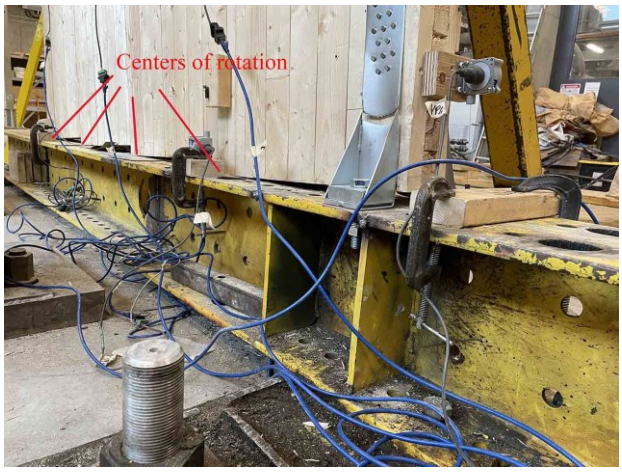

wall #12

Figure 6-9: Kinematic mode after failure for shearwall tests

6.4.2. Observed ultimate failures

Figure 6-10-Figure 6-21 present representative pictures of the tested walls before and after failure. The observed ultimate failure mechanisms occurred in hold-down connections, which can be attributed to the lower ultimate displacement of hold-downs than panel-to-panel connections. It was observed that walls with fully nailed hold-downs (i.e., walls #1, #2, #5, #6, #7, #11, and #12) experienced uplift failure, similar to that presented in Section 5.3.1, consisting of tensile failure in the vertical steel plate near the first row of nails. The walls with partially nailed hold-downs (i.e., walls #3, #4, #9, and #10) also observed uplift

failures, similar to that described in Section 5.3.1, where in the nail fasteners failed due to the head breakage combined with nail withdrawal and bending. For wall #8, as fully nailed angle brackets were replaced with hold-downs, failure occurred in the angle brackets due to the bolts' breakage, as shown in Figure 6-17.

(a) (b)

Figure 6-10: Shearwall test #1: (a) before failure (b) after failure

(a) (b)

Figure 6-11: Shearwall test #2: (a) before failure (b) after failure

(a) (b)

Figure 6-12: Shearwall test #3: (a) before failure (b) after failure

(a) (b)

Figure 6-13: Shearwall test #4: (a) before failure (b) after failure

(a) (b)

Figure 6-14: Shearwall test #5: (a) before failure (b) after failure

(a) (b)

Figure 6-15: Shearwall test #6: (a) before failure (b) after failure

(a) (b)

Figure 6-16: Shearwall test #7: (a) before failure (b) after failure

(a) (b)

(c)

Figure 6-17: Shearwall test #8: (a) before failure (b) after failure (c) failure in bolts

(a) (b)

Figure 6-18: Shearwall test #9: (a) before failure (b) after failure

(a) (b)

Figure 6-19: Shearwall test #10: (a) before failure (b) after failure

(a) (b)

Figure 6-20: Shearwall test #11: (a) before failure (b) after failure

(a) (b)

Figure 6-21: Shearwall test #12: (a) before failure (b) after failure

6.4.3. Investigation of uplift and slip in the panels

Figure 6-22 illustrates the curves of the lateral load as a function of the uplift displacement of the first panel (Uplift), and relative slips between panels one and two (Slip 1), two and three (Slip 2), as well as three and four for wall #12 (Slip 3). Additionally, two vertical lines were plotted associated with the average yield displacements of the hold-downs and panel-to-panel connections, based on the results obtained from connection-level tests presented in Chapter 5 while the values for the hold-downs were modified based on their distance from the edge of the first panel. The three curves, representing uplift and slip, for walls with CP behaviour appear consistent, confirming that equal displacements were transferred to each panel, leading to them experiencing the same rotation. This result validates the test-up method, designed to simulate diaphragm behaviour at the top of the shearwall. As expected, the uplift displacement was higher than the relative slips for walls with SW behaviour since the centers of rotation in the first and second panels detached from the ground, resulting in lower relative slips. It can be seen that wall #5 experienced more relative slips than other walls with SW (i.e., #3, #4, #9, and #10) which can again be attributed to the more flexible panel-to-panel connections.

It can be observed that the panel-to-panel connections yielded before hold-downs for walls with CP mode (e.g., walls #1 and #2), while for walls with SW mode (e.g., walls #3 and #4) the panel-to-panel connections remained elastic throughout the tests and the hold-down yielded and failed. For wall #5 with SW mode, the hold-down started yielding before the panel-to-panel connections, followed by panel-to-panel connections yielding prior to the ultimate failure of the hold-down. In addition, walls #9 and #10 with SW behaviour experienced yielding in their panel-to-panel connections near walls' maximum resistance, as well as ultimate failures in the hold-down.

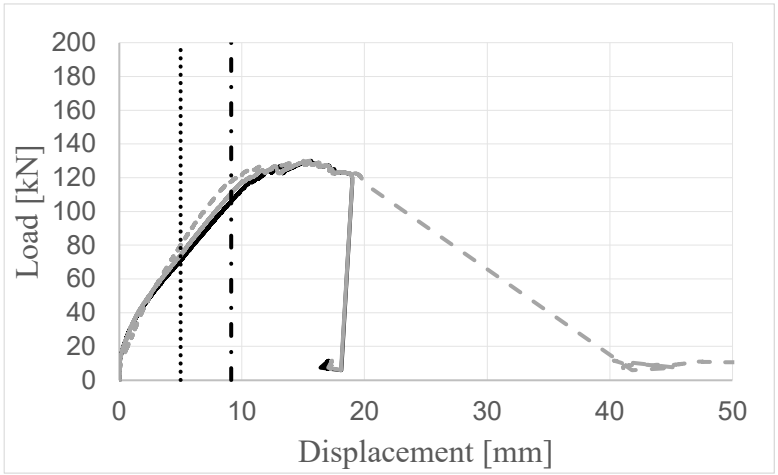

wall #1

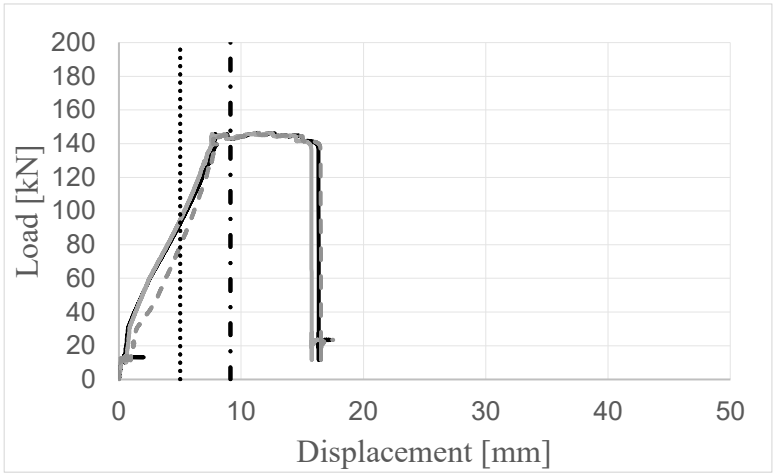

wall #2

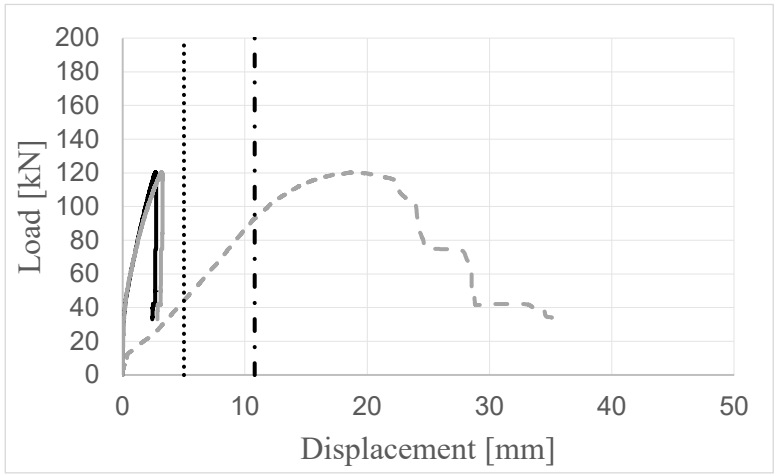

wall #3

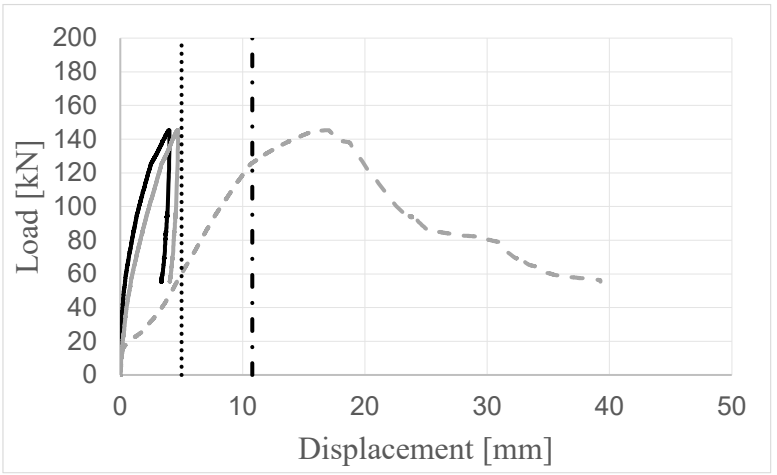

wall #4

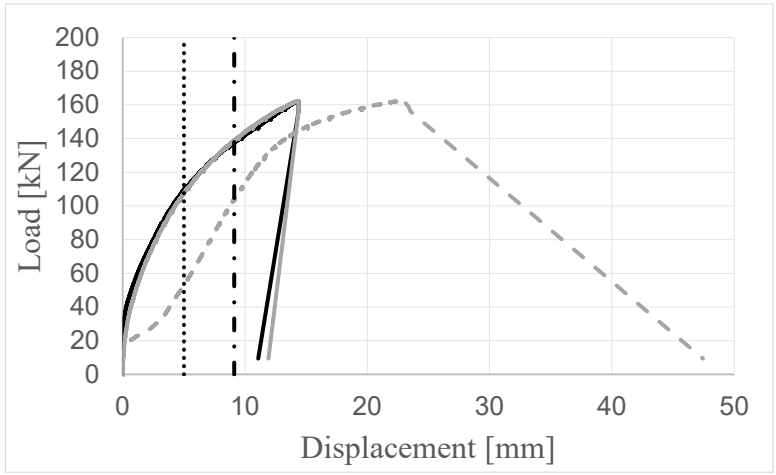

wall #5

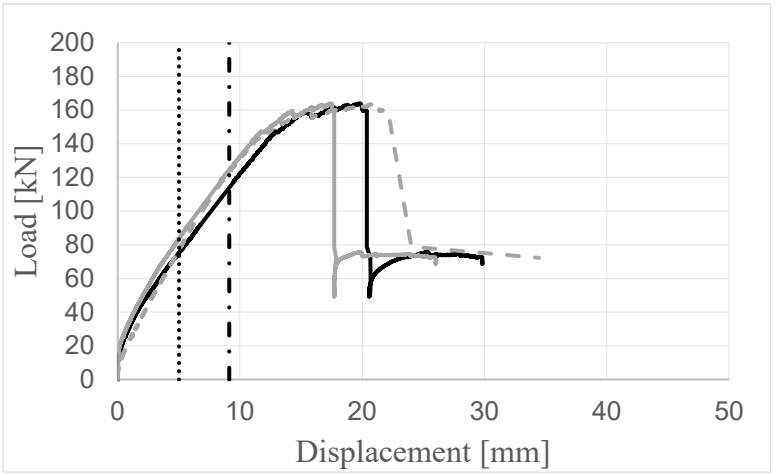

wall #6

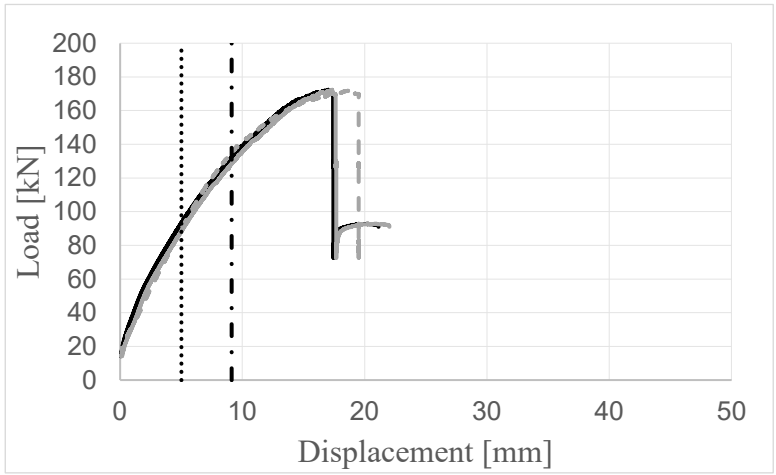

wall #7

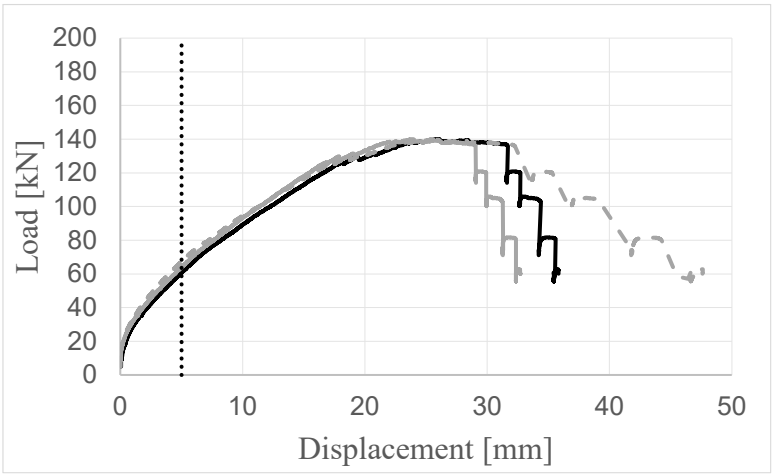

wall #8

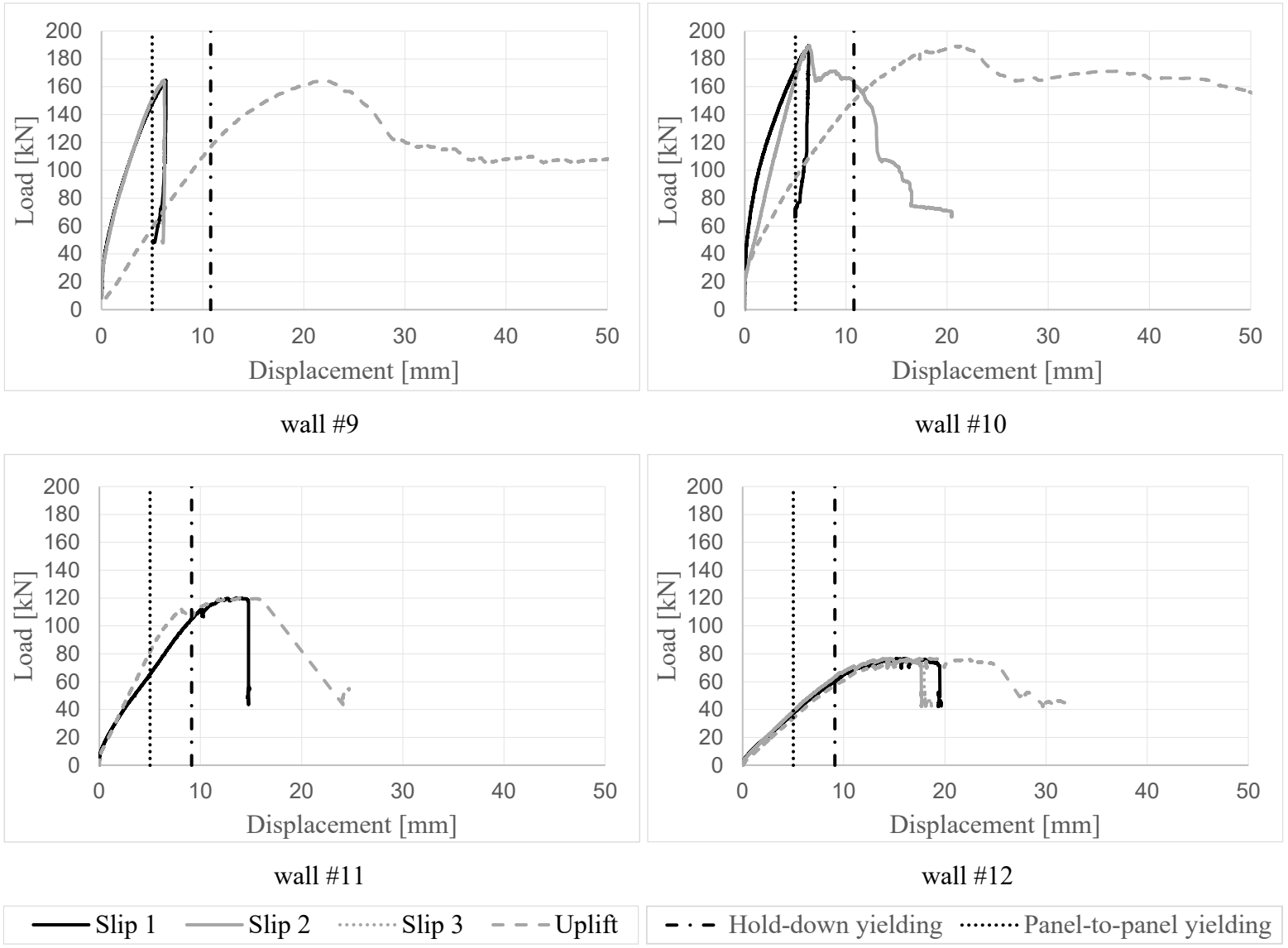

Figure 6-22: Lateral load vs the vertical displacement in the uplift side of the first panel, slip 1, and slip 2, for shearwall tests

A different way of representing the kinematic behaviour in the walls is illustrated in where the uplift displacement of the three panels is shown Figure 6-23. It can be observed that the uplift displacement at the center of rotation of each panel for walls with CP behaviour was equal to zero up to failure, while incremental panel uplift, depending on their distance from the wall centre of rotation is observed in walls with SW behaviour (walls #3-#5, and #9-#10). These results emphasize once again that the obtained kinematic modes matched well with those expected based on the preliminary numerical models.

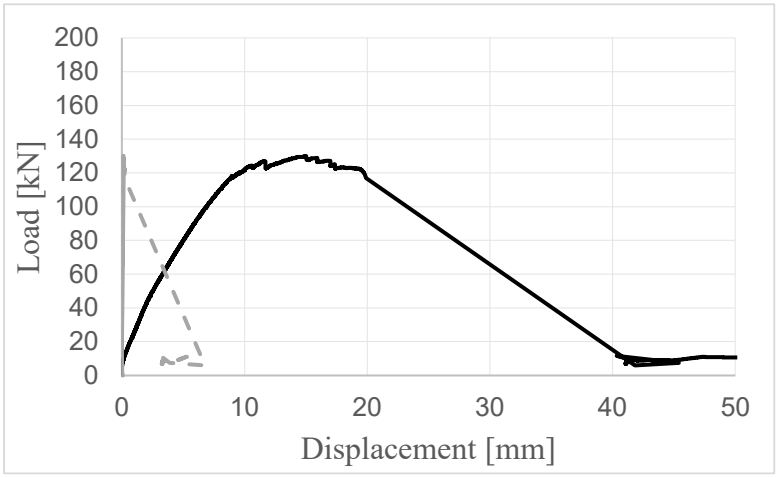

wall #1

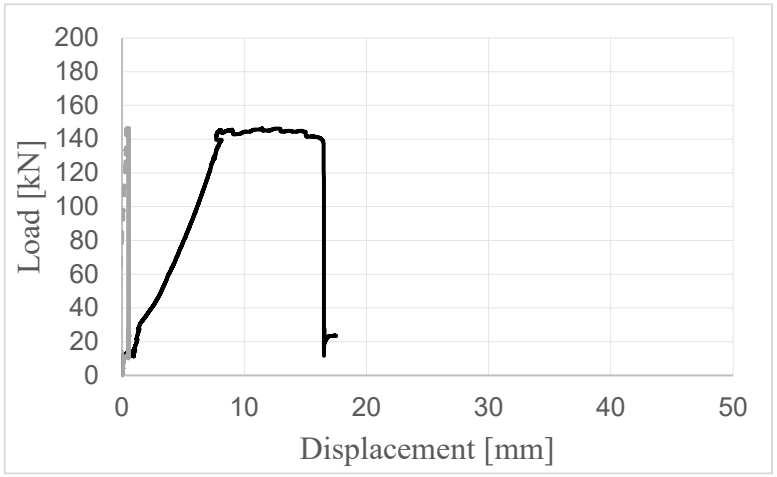

wall #2

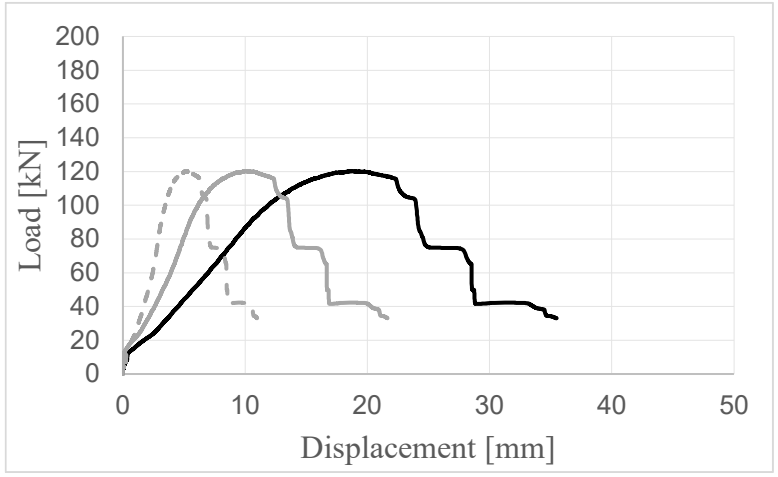

wall #3

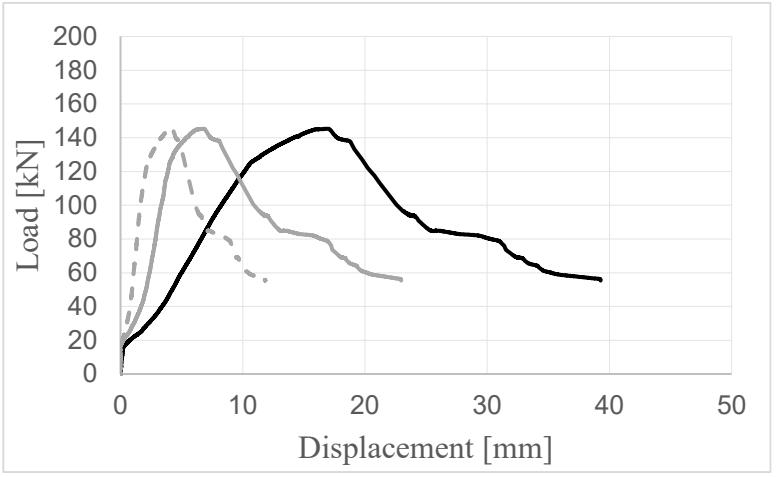

wall #4

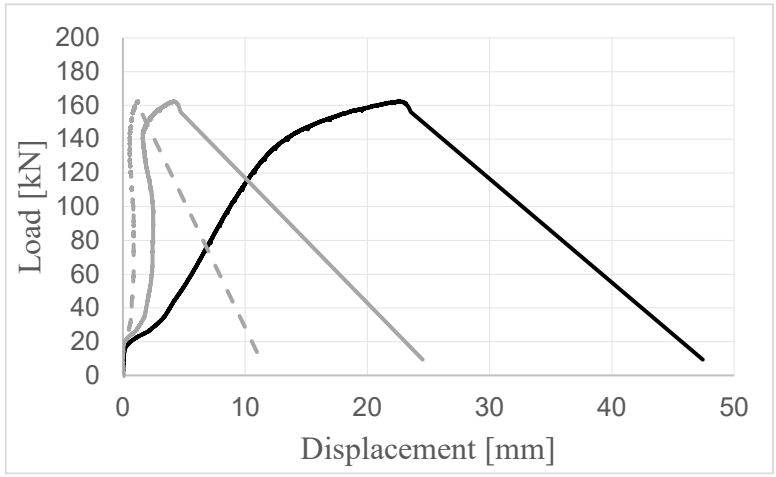

wall #5

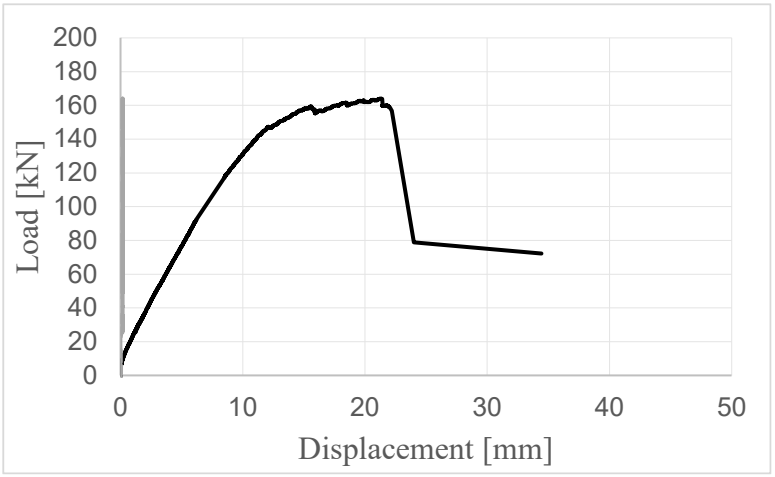

wall #6

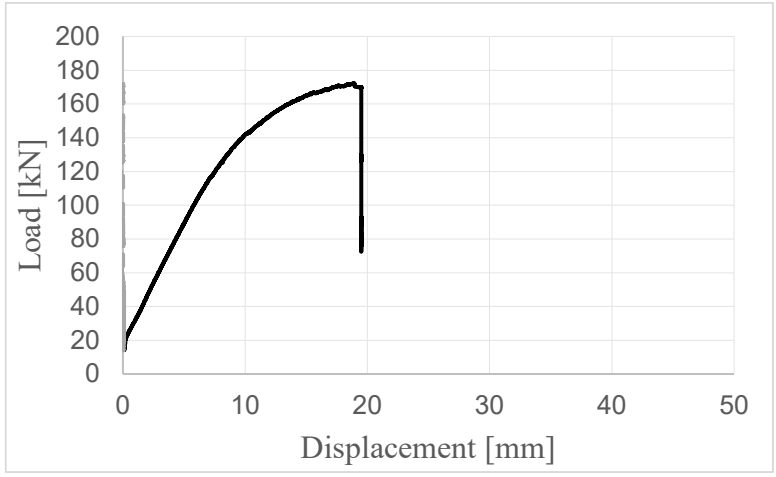

wall #7

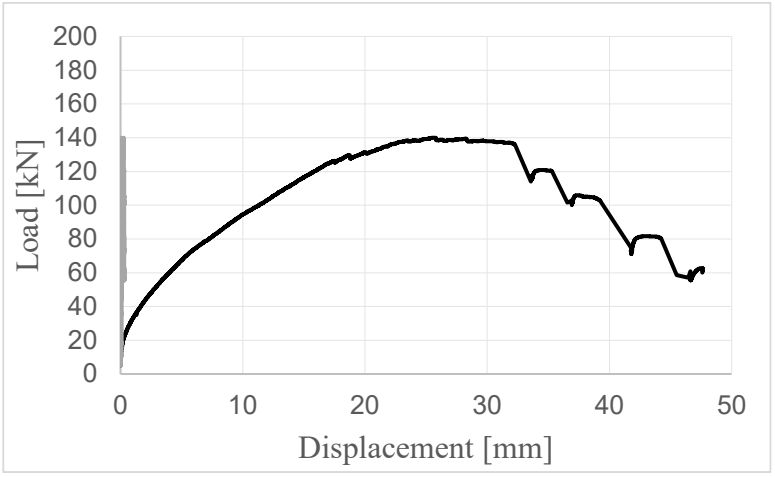

wall #8

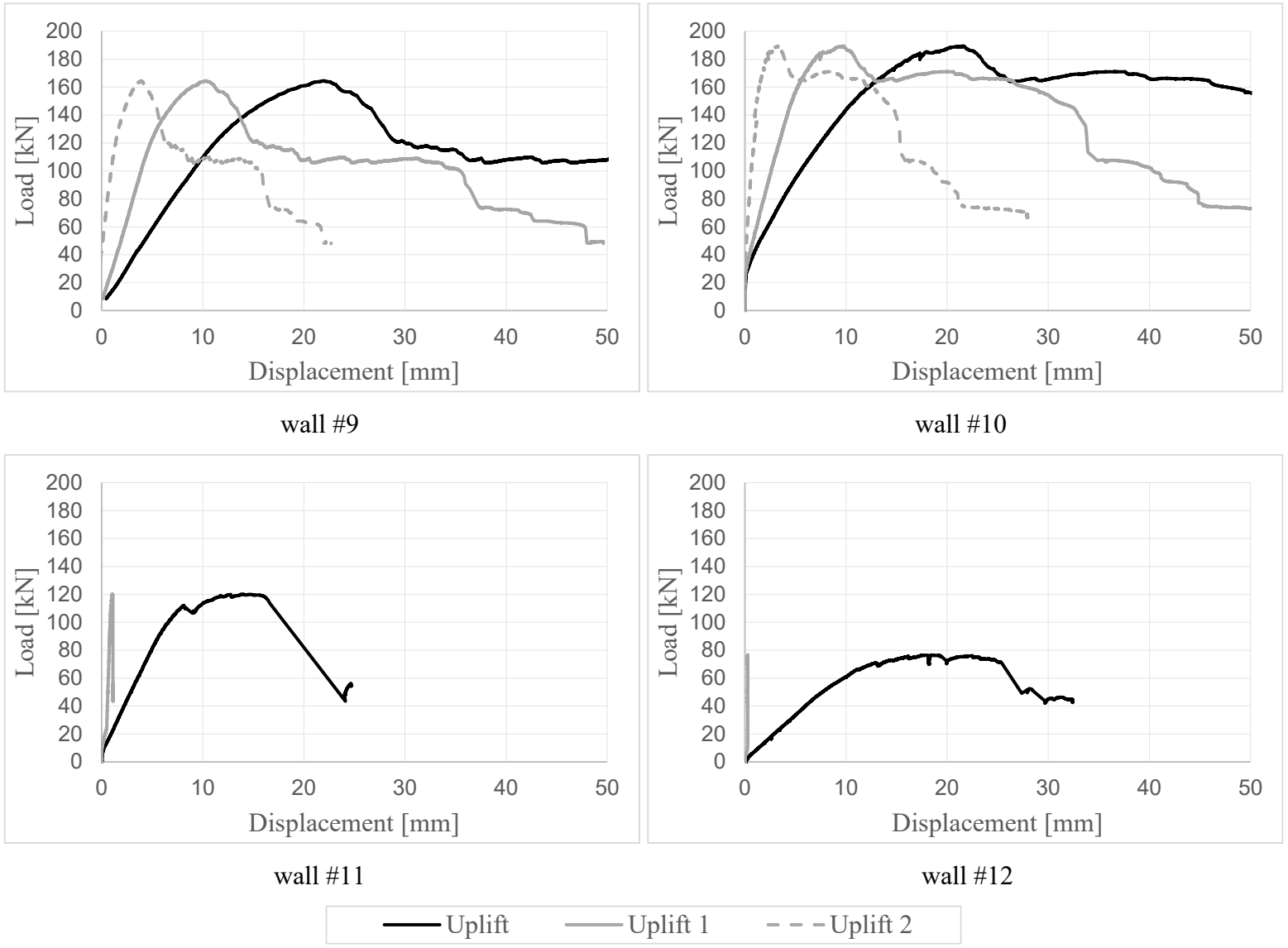

Figure 6-23: Lateral load vs the vertical displacement in the uplift side of the first panel (Uplift) and center of rotations of first (Uplift 1) and second (Uplift 2), for shearwall tests

6.4.4. Investigation of the results

Table 6-4 and Table 6-5 summarize the mechanical properties of shearwall tests without and with angle brackets, respectively, including maximum force and its respective displacement, ultimate displacement, and the properties obtained from EEEP and trilinear simulations, as defined in section 5.2.2. The results show that gravity load increased the resistance of the shearwall in both CP and SW behaviour, while its impact on other properties such as stiffness and ductility seemed insignificant. Ductility ratios in CP behaviour were in the range of 2.0-2.9 while this range was around 1.7-2.3 for SW behaviour. For wall #8, for which hold-downs were replaced with angle brackets with washers, a ductility ratio more than 3.3 was achieved. The stiffnesses obtained in walls with SW behaviour were almost double those with CP behaviour due to the increase in panel-to-panel connections. Additionally, walls with CP behaviour experienced significantly greater ultimate displacement around 58-70 mm, compared to walls with SW behaviour with ultimate displacement around 21-24 mm for walls #3 and #4, around 35 for walls #9 and #10, and around 41 mm for wall #5. Using four narrow CLT panels (wall #12) resulted in significantly lower resistance, around 76 kN, compared to the wall with the same total length with two panels (wall #11) with a resistance of around 120 kN. Also, the stiffness of wall #11 was more than triple that of wall #12. The results also highlighted that wall #12 had a slightly higher ductility ratio than wall #11 even though it showed a significant high value of ultimate displacement, which can be attributed to its very low stiffness.

For walls with angle brackets, higher resistance was observed. For example, in CP, resistance was around 164 kN for wall #6, while it was around 130 kN for wall #1 with the same configuration without angle brackets. That showed around a 26% increase in resistance. In SW, the difference among walls #3 and #9 was around 37%, showing more contribution of angle brackets in such kinematic mode.

Table 6-4: Mechanical properties of shearwall-level tests without angle brackets under monotonic load

Parameter	Unit	CP		SW		
		#1	#2	#3	#4	#5
F_{max}	[kN]	130.07	146.36	120.25	145.31	162.26
$v_{F,max}$	[mm]	53.04	49.32	17.71	23.00	40.66
v_u	[kN]	64.10	58.30	20.84	24.13	41.09
$F_{y,EEEP}$	[mm]	115.46	134.27	109.49	125.98	140.69
$v_{y,EEEP}$	[mm]	23.36	29.38	11.76	11.65	19.00
$k_{e,EEEP}$	[kN/mm]	4.94	4.57	9.31	10.81	7.40
$D_{m,EEEP}$	[-]	2.74	1.98	1.77	2.07	2.16
$F_{y,trilinear}$	[kN]	109.87	136.10	111.29	127.46	139.17
$v_{y,trilinear}$	[mm]	22.09	29.82	11.96	11.79	18.77
$k_{e,trilinear}$	[kN/mm]	4.97	4.56	9.30	10.81	7.41
$D_{m,trilinear}$	[-]	2.90	1.95	1.74	2.05	2.19

Table 6-5: Mechanical properties of group B shearwall-level tests under monotonic load

Parameter	Unit	CP			SW		CP	
		#6	#7	#8	#9	#10	#11	#12
F_{max}	[kN]	163.96	172.34	140.06	164.65	189.46	120.14	76.53
$v_{F,max}$	[mm]	73.08	65.67	70.76	31.54	33.58	55.53	118.02
v_u	[kN]	74.40	67.64	84.89	34.47	36.02	60.19	144.93
$F_{y,EEEP}$	[mm]	146.07	147.44	120.55	145.45	161.75	112.13	71.93
$v_{y,EEEP}$	[mm]	38.57	31.06	25.39	19.57	15.52	37.23	78.58
$k_{e,EEEP}$	[kN/mm]	3.79	4.75	4.75	7.43	10.42	3.01	0.92
$D_{m,EEEP}$	[-]	1.93	2.18	3.34	1.76	2.32	1.62	1.84
$F_{y,trilinear}$	[kN]	146.69	147.68	106.67	150.36	161.30	111.82	70.55
$v_{y,trilinear}$	[mm]	38.75	31.12	22.12	20.28	15.47	37.12	76.94
$k_{e,trilinear}$	[kN/mm]	3.79	4.75	4.82	7.41	10.42	3.01	0.92
$D_{m,trilinear}$	[-]	1.92	2.17	3.84	1.70	2.33	1.62	1.88

6.5. Observations and summary

This section summarizes the observations from experimental tests conducted on twelve multi-panel CLT shearwalls presented in sections 6.4.

The key points are:

- The expected kinematic modes based on preliminary numerical models were achieved consistently for all walls emphasizing the accuracy of the developed expressions in predicting kinematic modes. Individual centers of rotation for each panel were achieved for CP, while only one center of rotation in the last CLT panel was observed for SW behaviour. The kinematic modes were checked by plotting the curves of lateral load versus the uplift displacement in the centers of rotation of each panel, except the last panel which was always in contact with the ground.
- The ultimate failure modes occurred constantly in the hold-downs, which was consistent with them having lower ultimate displacement than panel-to-panel connections and angle brackets. Fully nailed hold-downs failed as tensile failure in the vertical steel plate near the first row of nails, while partially nailed hold-down failed in nails due to the head breakage combined with nail withdrawal and bending. Only in shearwall #8, in which hold-downs were replaced with fully nailed angle brackets with washers, failure occurred in the bolts used to connect those brackets to the base.
- Walls with CP behaviour exhibited relatively more ductility due to the engagement of panel-to-panel connections.
- Panel-to-panel connections yielded prior to hold-downs in the walls with CP behaviour, while they remained elastic throughout the tests with SW behaviour. An exception to this is wall #5, where the panel-to-panel joints yielded after the hold-down due to the use of relatively fewer connections. However, the ultimate failure occurred in the hold-down. In addition, walls #9 and #10 with SW behaviour experienced yielding in their panel-to-panel connections in close proximity to walls' maximum force, as well as ultimate failures in the hold-down.
- Gravity loads improved the lateral resistance of the walls while having no significant effect on stiffness and ductility.
- Stiffness was greater in walls in SW mode due to the greater number of panel-to-panel connections.
- As a result of angle brackets resisting uplift forces, walls with angle brackets experienced higher resistance than those without.

- Using relatively narrow panels while maintaining wall length resulted in significantly lower resistance and stiffness while slightly higher ductility.

Chapter 7 - Mathematical accuracy and validation of the analytical and design expressions

7.1. General

This chapter presents the verification of analytical expressions and CD procedure to show their mathematical accuracy using numerical models using SAP2000 software (CSI, 2018). A case study of a two-storey building consisting of multi-panel CLT shearwalls is presented to demonstrate the applicability of CD equations to multi-storey applications. Finally, the experimental tests results presented in Chapter 6 were compared and discussed against numerical models and analytical equations. This was done to validate the developed analytical expressions.

7.2. Numerical models: general information

Figure 7-1 illustrates the numerical model configuration used in this chapter. The CLT panels were modelled by shell elements of 61×61 mm. The mesh size was determined by the mesh sensitivity analysis presented in Appendix B.2. The CLT panels were defined as rigid to verify the analytical expressions and CD procedures developed, which is consistent with the assumptions made during the development process and CSA O86 commentary. For validation against experimental results, orthotropic material properties were used. The required properties were obtained from (ANSI/APA, 2020) for E1 CLT grade, including E_0, E_{90}, and G_0, and were equal to 11700, 300, and 731 MPa, respectively. The effective moduli, utilized to define orthotropic material properties, $E_{eff,1}$ (along the horizontal direction), $E_{eff,2}$ (along the vertical direction), and G_{eff}, are obtained using Equations (7-1)-(7-4), based on work by Brandner et al. (2017).

$$E_{eff,1} = \frac{E_0 \cdot t_{90} + E_{90} \cdot t_0}{t_{CLT}} = \frac{11700 \cdot 35 + 300 \cdot 70}{105} = 4100\ MPa \tag{7-1}$$

$$E_{eff,2} = \frac{E_0 \cdot t_0 + E_{90} \cdot t_{90}}{t_{CLT}} = \frac{11700 \cdot 70 + 300 \cdot 35}{105} = 7900\ MPa \tag{7-2}$$

$$\alpha = 0.53 \cdot \left(\frac{t_{mean}}{w}\right)^{-0.79} = 0.53 \cdot \left(\frac{35}{89}\right)^{-0.79} = 1.11 \tag{7-3}$$

$$G_{eff} = \frac{G_0}{1 + 6 \cdot \alpha \cdot \left(\frac{t_{mean}}{w}\right)^2} = \frac{731}{1 + 6 \cdot 1.11 \cdot \left(\frac{35}{89}\right)^2} = 361.1\ MPa \quad (7\text{-}4)$$

Where t_0 and t_{90} are the total thicknesses of the longitudinal (vertical) and transverse (horizontal) layers, equal to 70 and 35 mm, respectively, t_{CLT} is the total thickness of the panel, equal to 105 mm, and w is the width of the laminations, equal to 89 mm.

The connections were modelled using multi-linear link elements representative of either: (1) the envelope curves obtained from experimental tests on connections presented in Chapter 5 to validate the models against experimental tests, or (2) the bi-linear elastic-perfectly-plastic simulations of the envelope curves to verify the mathematical accuracy of the developed analytical procedures. The mechanical anchors were modelled assuming that the hold-down is only active in uplift due to its negligible contribution to shear, as presented in section 5.3.2, while the angle brackets were considered in both uplift and shear. To simulate the contact bearing between the CLT panels and the foundation or floor below, rigid gap elements in compression with zero tension stiffness, were utilized. A vertical gravity load was considered in the analysis and assumed to be uniformly applied on top of each panel. A concentrated lateral load was applied to a rigid bar attached to the CLT panel, as shown in Figure 7-1 to simulate the lateral loads. To investigate different cases with different moment to shear ratios for CD verification, different heights of the bar (L_r) were used, as described in section 7.3.2. Diaphragm constraints were applied at the top and bottom of the panels according to the assumptions made in the analytical developments and experimental tests.

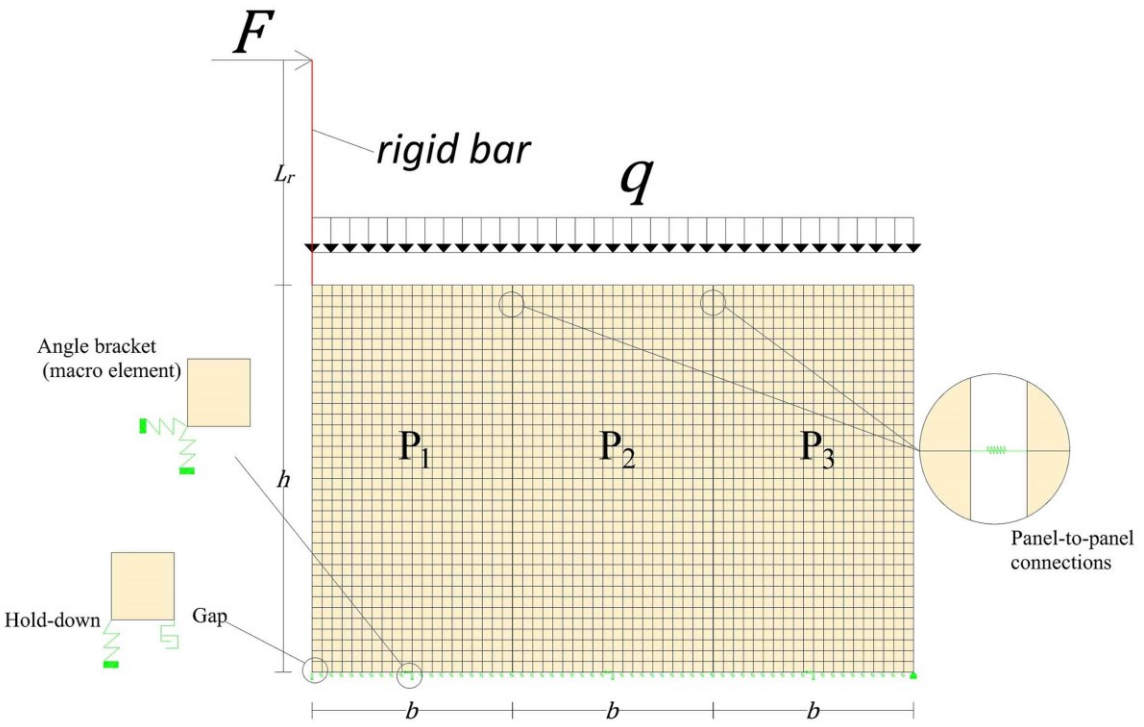

Figure 7-1: Numerical model of a three-panel CLT shearwall in SAP2000

The mechanical properties of connections in this chapter were the same as those used in the experimental tests presented in Chapter 5. Figure 7-2 and Figure 7-3 illustrate the average load-displacement envelope curves of fully- and partially nailed WHT620 hold-downs under uplift loading and HBS 6×70 mm fasteners used as panel-to-panel connections under shear loading, respectively. In order to facilitate the incorporation of the interaction between shear and uplift based on the circular domain for bi-directional angle brackets, it was necessary to utilize elastic-perfectly-plastic simulations as shown in Figure 7-4 and Figure 7-5. The behaviour was obtained from the average envelope curves of fully nailed TCN200 angle brackets with and without washers, respectively. Due to the fact that no connection-level tests were performed on fully nailed angle brackets with washers in this thesis, their mechanical properties under uplift were obtained from linear interpolation, using the results from the test conducted on partially nailed angle brackets with washers, presented in Table 5-8, and experimental tests conducted by Casagrande et al. (2016) of fully nailed brackets with a number of nails exceeding those used in the full-scale tests of the current study. The mechanical properties of angle brackets with washers under shear

were considered equal to those without washers since the behaviour and failure were dominated by the nails.

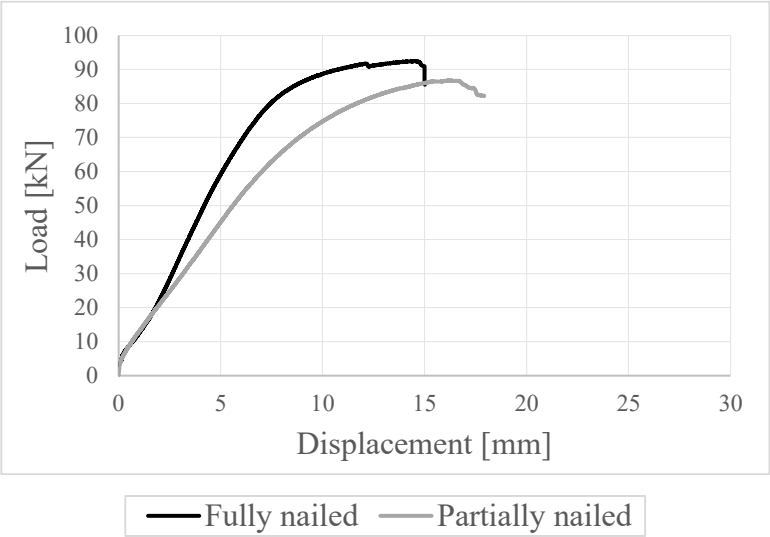

Figure 7-2: The average load-displacement envelope curves of fully- and partially nailed WHT620 hold-down connections under monotonic uplift

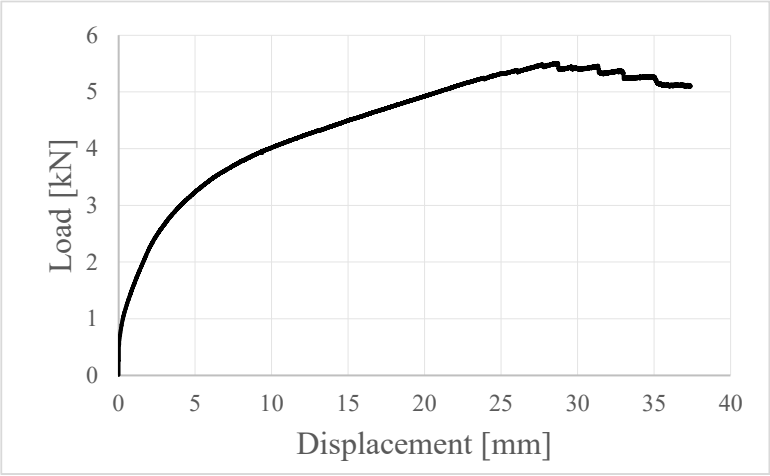

Figure 7-3: The average load-displacement envelope curve of HBS 6 × 70 mm fasteners used as panel-to-panel connection under monotonic shear

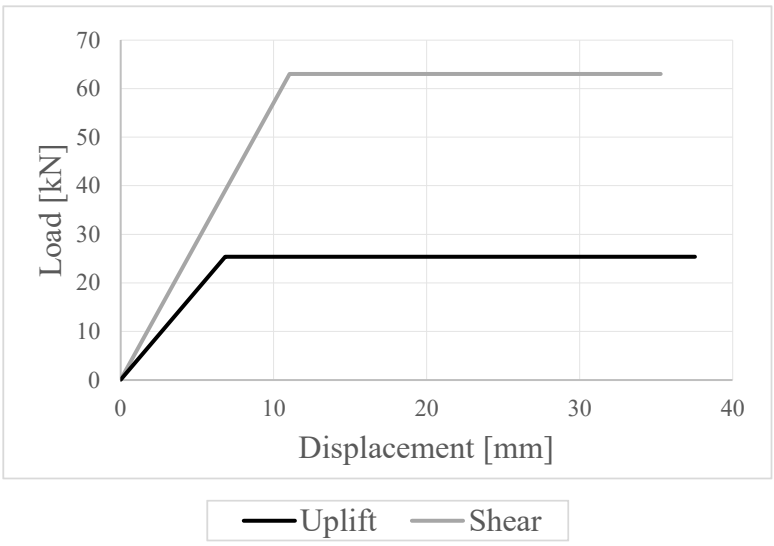

Figure 7-4: The average bi-linear load-displacement curves of TCN200 angle bracket connections without washer under monotonic uplift and shear

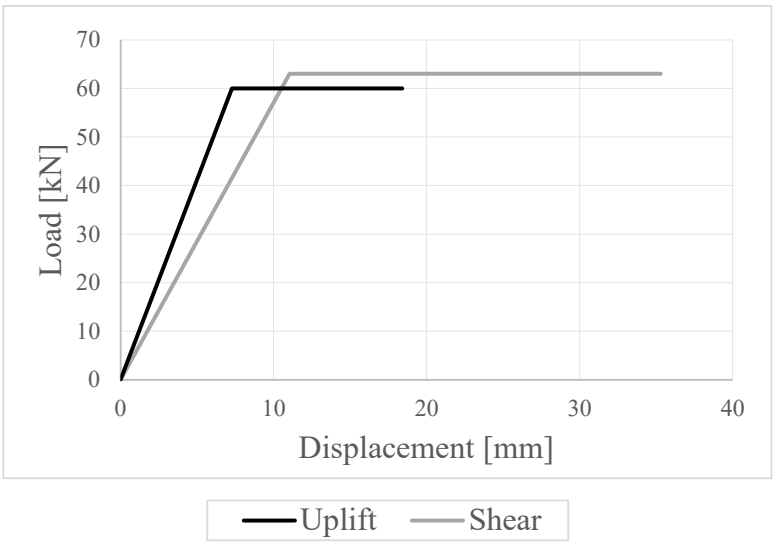

Figure 7-5: The average bi-linear load-displacement curves of TCN200 angle bracket connections with washers under monotonic uplift and shear

Table 7-1: Elastic-perfectly-plastic properties of connections used in numerical models

Connection	Type	Load type	k	r_y	d_y	d_u
			[kN/mm]	[kN]	[mm]	[mm]
Hold-down	Fully nailed	Tension (uplift)	11.16	89.21	7.99	17.19
	Partially nailed	Tension (uplift)	8.61	81.37	9.45	20.18
Angle brackets	Fully nailed	Tension (uplift)	3.72	25.39	6.83	37.53
		Shear (sliding)	5.71	63.06	11.04	35.30
	Fully nailed (with washer)	Tension (uplift)	8.25	60.00	7.27	18.40
		Shear (sliding)	5.71	63.06	11.04	35.30
Panel-to-panel	Screw (6 mm)	Shear	0.95	4.76	5.01	42.95

The interaction between shear and uplift for angle brackets was simulated through a macro element representing the circular domain (D'Arenzo, Casagrande, et al., 2021b). An L-shaped rigid bar was used to simulate the bi-directional properties of each angle bracket, as shown in Figure 7-6. The horizontal part of the bar with a length of 10 mm (L_h) was attached to the wall while moment and torsion releases were applied in order to only transfer horizontal and vertical shear loads. The vertical part with the length of 10 mm (L_v) was attached to the elastic springs and was assigned the uplift and shear stiffness of angle brackets. The M_2-M_3 plastic hinges were defined at the end of the vertical part (close to the elastic springs) in order to incorporate the nonlinearity of the links. The properties of the plastic hinges were defined according to Equations (7-5)-(7-8), and include the yield bending moments, $M_{y,x}$ and $M_{y,z}$, and ultimate rotations, $\theta_{u,x}$ and $\theta_{u,z}$, in the horizontal shear (with subscript x) and vertical uplift (with subscript z) directions, respectively.

$$M_{y,x} = r_{s,x} \cdot L_H \tag{7-5}$$

$$M_{y,z} = r_{s,z} \cdot L_V \tag{7-6}$$

$$\theta_{u,x} = \frac{d_{u,sx} - d_{y,sx}}{L_H} \quad (7\text{-}7)$$

$$\theta_{u,z} = \frac{d_{u,sz} - d_{y,sz}}{L_V} \quad (7\text{-}8)$$

Where, $r_{s,z}$ and $r_{s,x}$ are the strengths of the connection in the vertical and horizontal directions, respectively, considering elastic-perfectly-plastic behaviour, and $d_{u,sz}$, $d_{y,sz}$, $d_{u,sx}$, and $d_{y,sx}$ are the ultimate and yield displacements of angle brackets in the vertical and horizontal directions, respectively.

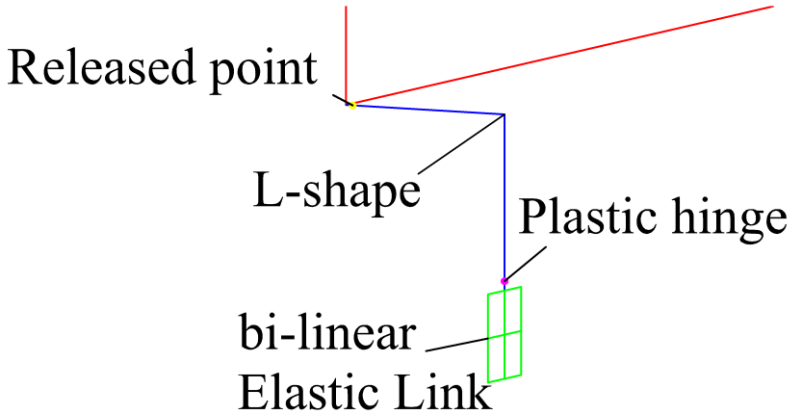

Figure 7-6: Macro element for interaction effect of shear and uplift

It is noteworthy to mention that angle brackets were consistently modelled using bi-linear elastic-perfectly-plastic behaviour in both the mathematical verification and validation sections, since implementing envelope curves in macro elements is not feasible. Using Equations (7-5)-(7-8), the calculated values of yield bending moments and ultimate rotations are summarized in Table 7-2 to define the plastic hinges in the macro elements for the bi-directional properties of angle brackets.

Table 7-2: Yield bending moments and ultimate rotations in the horizontal and vertical directions used in macro element models for fully nailed TCN200 angle brackets

Property-Equation	Unit	Without washer	With washer
$M_{y,x}$-(7-5)	[kN·mm]	630.60	630.60
$M_{y,z}$-(7-6)	[kN·mm]	253.90	545.39
$\theta_{u,x}$-(7-7)	[rad]	2.43	2.43
$\theta_{u,z}$-(7-8)	[rad]	3.07	1.61

7.3. Verification and case study

In this section, examples of single-storey multi-panel CLT shearwalls using the modelling approach and defined properties presented in section 7.2 are presented to demonstrate the mathematical correctness of the developed analytical expressions, presented in Chapter 3, as well as to show the applicability of the proposed CD procedure, presented in Chapter 4. Furthermore, a case study for a two-storey building composed of three-panel and two-panel CLT shearwalls is presented to demonstrate the applicability of the CD expressions for the multi-storey buildings.

7.3.1. Verification of the analytical expressions

To demonstrate the accuracy of the proposed analytical expressions for elastic CP and SW kinematic modes, four examples are presented. The walls with elastic CP (Examples 1 and 2) were also used to verify the developed inelastic CP procedure, presented in section 0, by implementing the plasticity of the connections. Table 7-3 provides the model properties used in verification. Each model was composed of three CLT panels ($m = 3$), each measuring 1.22 and 2.44 metres in width and height, respectively. The total length of the walls, B, is 3.66 m ($B = b \cdot m$). Fully and partially nailed hold-downs were used for walls with CP and SW behaviours, respectively, along with fully nailed angle brackets without washers and HBS 6x70 mm for panel-to-panel connections for all walls. The connections' mechanical properties were determined according to Table 7-1. The compression zone was neglected (i.e., $\beta = 1$) for simplification. The lateral load was applied at the top left corner of the wall ($L_r = 0$).

Table 7-3: Models Properties used in the analytical verification

Ex.	q (kN/m)	F (kN)	$b \times h$ (m)	B (m)	n_h	m	n_s	n_F	Kinematic mode
1	0	100	1.22x2.44	3.66	2	3	1	9	CP
2	15	150	1.22x2.44	3.66	2	3	1	9	CP
3	0	100	1.22x2.44	3.66	1	3	1	40	SW
4	5	150	1.22x2.44	3.66	1	3	1	40	SW

The results from the numerical (SAP) and analytical (Ana.) models are summarized and compared in Table 7-4. Parameters considered in the comparison include: total lateral displacements ($\Delta_{r,s}$), sliding displacement ($\Delta_{r,s}$), rotation angles (ϑ), and internal forces in connectors, $T_{h,Z}$, $T_{f,j}$, and $T_{s,z,i,j}$, representing the vertical uplift force in the hold-down, shear force in panel-to-panel connections, and vertical uplift force in the angle brackets, respectively. The error (ξ) in all cases was less than 0.4%, which is acceptable.

To verify the analytical expressions against the numerical models in the inelastic range, the two examples with CP behaviour (i.e., examples 1 and 2) were considered while using double fully nailed angle brackets without washers along the length of each panel (i.e., $n_s = 2$ and angle bracket stiffness and strength were doubled) and single fully nailed hold-down ($n_h = 1$). The results obtained from the inelastic analysis are shown in Figure 7-7. As can be seen, the analytical solution matches that obtained from the numerical model almost perfectly. This comparison emphasizes the adequacy of the proposed model in the inelastic region. The associated lateral forces and displacements also matched the developed method. In both cases, the numerical models matched different connection yield points (P_i) as defined in Chapter 3, and the failure occurred in the hold-down after the last angle brackets away from the centers of rotation yielded (P_3) and before other angle brackets yielded (P_4). Thus, yield point P_4 was not reached in either example.

Table 7-4: verification results for elastic multi-panel CLT shearwalls

Examples		**1**			**2**			**3**			**4**	
Sap/Ana.	**SAP**	**Ana.**	$\xi(\%)$	**SAP**	**Ana.**	$\xi(\%)$	**SAP**	**Ana.**	$\xi(\%)$	**SAP**	**Ana.**	$\xi(\%)$
$\Delta_{r,s}$ (mm)	15.32	15.31	0.1%	21.68	21.67	0.0%	11.96	11.96	0.0%	17.44	17.44	0.0%
Δ_s (mm)	5.84	5.84	0.0%	8.76	8.76	0.0%	5.84	5.84	0.0%	8.76	8.76	0.0%
ϑ $(mrad)$	3.88	3.88	0.0%	5.29	5.29	0.0%	2.51	2.50	0.4%	3.56	3.56	0.0%
$T_{h,z}$ (KN)	105.67	105.75	0.1%	143.99	144.12	0.1%	48.16	48.16	0.0%	65.89	65.87	0.0%
$T_{f,1}$ (KN)	4.51	4.50	0.2%	6.15	6.13	0.3%	1.58	1.58	0.0%	2.31	2.31	0.0%
$T_{f,2}$ (KN)	4.50	4.50	0.0%	6.13	6.13	0.0%	1.83	1.83	0.0%	2.79	2.79	0.0%
$T_{s,z,1,1}$ (KN)	8.79	8.81	0.2%	11.98	12.01	0.2%	15.11	15.11	0.0%	20.38	20.39	0.0%
$T_{s,z,1,2}$ (KN)	8.82	8.81	0.1%	12.02	12.01	0.1%	9.91	9.92	0.1%	13.26	13.28	0.2%
$T_{s,z,1,3}$ (KN)	8.80	8.81	0.1%	11.99	12.01	0.2%	5.67	5.69	0.4%	8.04	8.07	0.4%

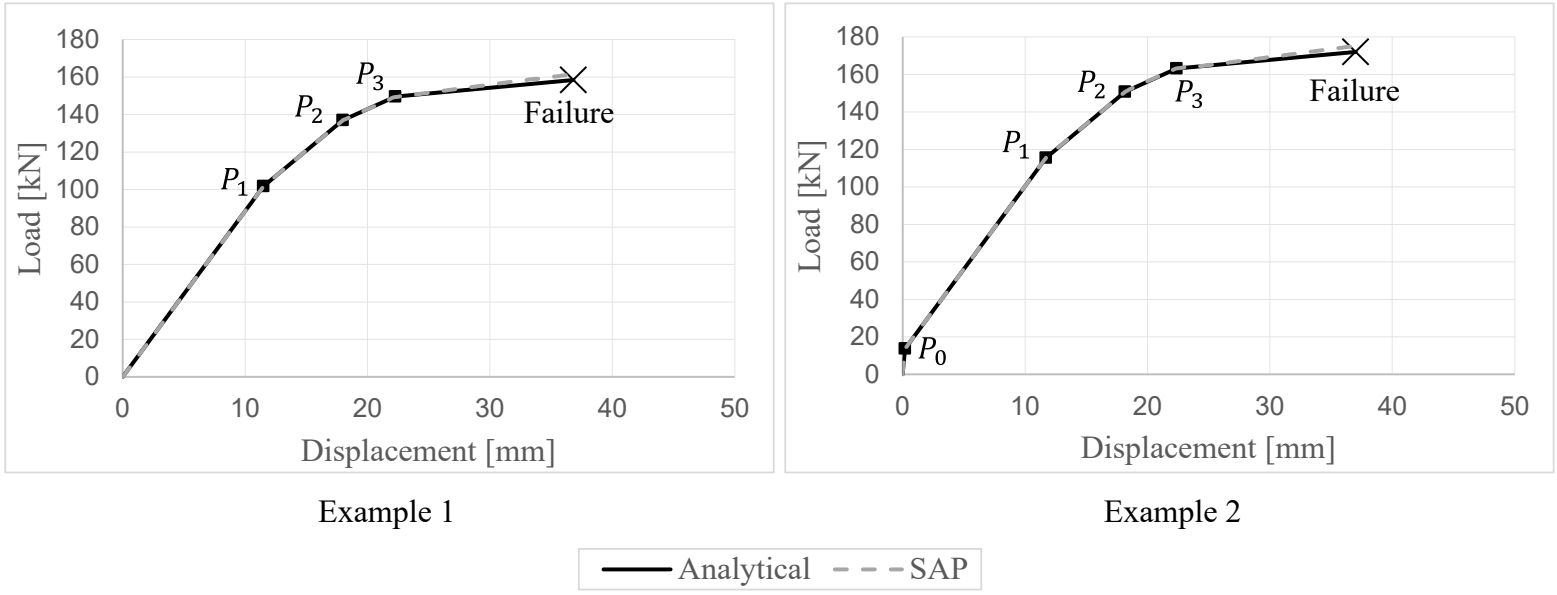

Figure 7-7: The load-displacement curves of inelastic examples

7.3.2. Capacity-based design verification

This section provides a numerical verification of the equations developed in the proposed CD procedure at the shearwall level, presented in section 4.3.2. Numerical verification was carried out to demonstrate that when the proposed requirements were met, the desired hierarchy of yielding at shearwall level was achieved. In particular, the design equations pertaining to the shearwall strength were verified using numerical models.

Numerical models were carried out based on the approach presented in section 7.2 while different heights of the rigid bar (L_r) were selected to simulate different levels of bending moment and shear force at the bottom of the shearwalls. The compression zone was neglected (i.e., $\beta = 1$) for simplification, and all over-strength factors were set equal to unity, due to the deterministic nature of the examples used in these comparisons. The model properties are presented in Table 7-5. The comparison was done on different models, where gravity loads, number of panels, and number of connections were varied. It should be noted that although the connection types were kept constant in the models (e.g., $k_{h,z}$ and r_f), different behaviours were achieved by, for example, considering the relative behaviour between the panel-to-panel connections and hold-down (e.g., changing n_f), or by varying the number of angle brackets (e.g., changing n_s). Single fully nailed hold-down and double angle brackets without washers were used along with HBS 6x70 mm for panel-to-panel connections in all examples. The connections' mechanical properties were determined according to Table 7-1.

Table 7-5: Models Properties used in the CD verification

Ex.	q (KN/m)	M_f $(kN \cdot m)$	V_f (kN)	$b \times h$ (m)	B (m)	L_r (m)	n_h	m	n_s	n_F
1	10	120	40	1.22x2.44	2.44	0.56	1	2	1	7
2	10	150	50	1.22x2.44	3.66	0.56	1	3	2	9
3	15	400	100	1.22x2.44	3.66	1.56	1	3	1	12
4	15	400	100	1.22x2.44	4.88	1.56	1	4	2	12

Pushover analyses were conducted on the four models outlined in Table 7-5, and the results were compared with those obtained from the proposed analytical models, as illustrated in Figure 7-8.

Prior to examining the force-displacement curves in Figure 7-8, an important verification was made regarding the applicability of the proposed conditions to the CD approach in the numerical and proposed analytical models. This included a check that CP behaviour was achieved in both elastic and plastic regions in accordance with Equations (4-5) and (4-20), respectively, and that the angle brackets remained elastic when the ultimate wall strength was attained (i.e., hold-down yielding), as presented in Equation (4-25).

As can be seen in Figure 7-8, three important points were identified, including P_0, which represents the activation point where the wall started rotating and the stabilizing effect from the uniform vertical load was overcome, and P_1 and P_2 representing the yielding points of panel-to-panel connections and hold-down, respectively. It should be noted that the analyses continued past the shearwall strength, $V_{f,w}$, occurring at point P_2, since the angle brackets still contributed to the behaviour of the wall. It was observed in all investigated cases that the yielding in the panel-to-panel connections (P_1) occurred prior to the yielding in the hold-down (P_2), which indicated that when the conditions in the proposed procedure were met, the desired behaviour was ensured. Also, when the applied shear force at P_2, $V_{f,w}$, was calculated based on the proposed methodology, presented in Equation (4-29), it correctly coincided with the yielding of the hold-down, (P_2), obtained from the numerical models.

The results of the bending moment strength, $M_{r,w}$, and the corresponding applied shear force, $V_{f,w}$, obtained from the numerical and proposed CD approach, are presented in Table 7-6. It can be observed that the difference between the results, ξ, does not exceed 0.3%. This further emphasizes the accuracy of the proposed model.

Table 7-6: The results of numerical and design approaches for capacity-based design

Method	Properties	Unit	Ex.			
			1	2	3	4
Numerical	$M_{r,w}$	$kN \cdot m$	245.31	504.93	402.68	722.72
	$V_{f,w}$	kN	81.77	168.31	100.67	180.68
CD	$M_{r,w}$	$kN \cdot m$	244.89	504.09	402.48	720.42
	$V_{f,w}$	kN	81.63	168.03	100.62	180.1
-	ξ	%	0.2%	0.2%	0.0%	0.3%

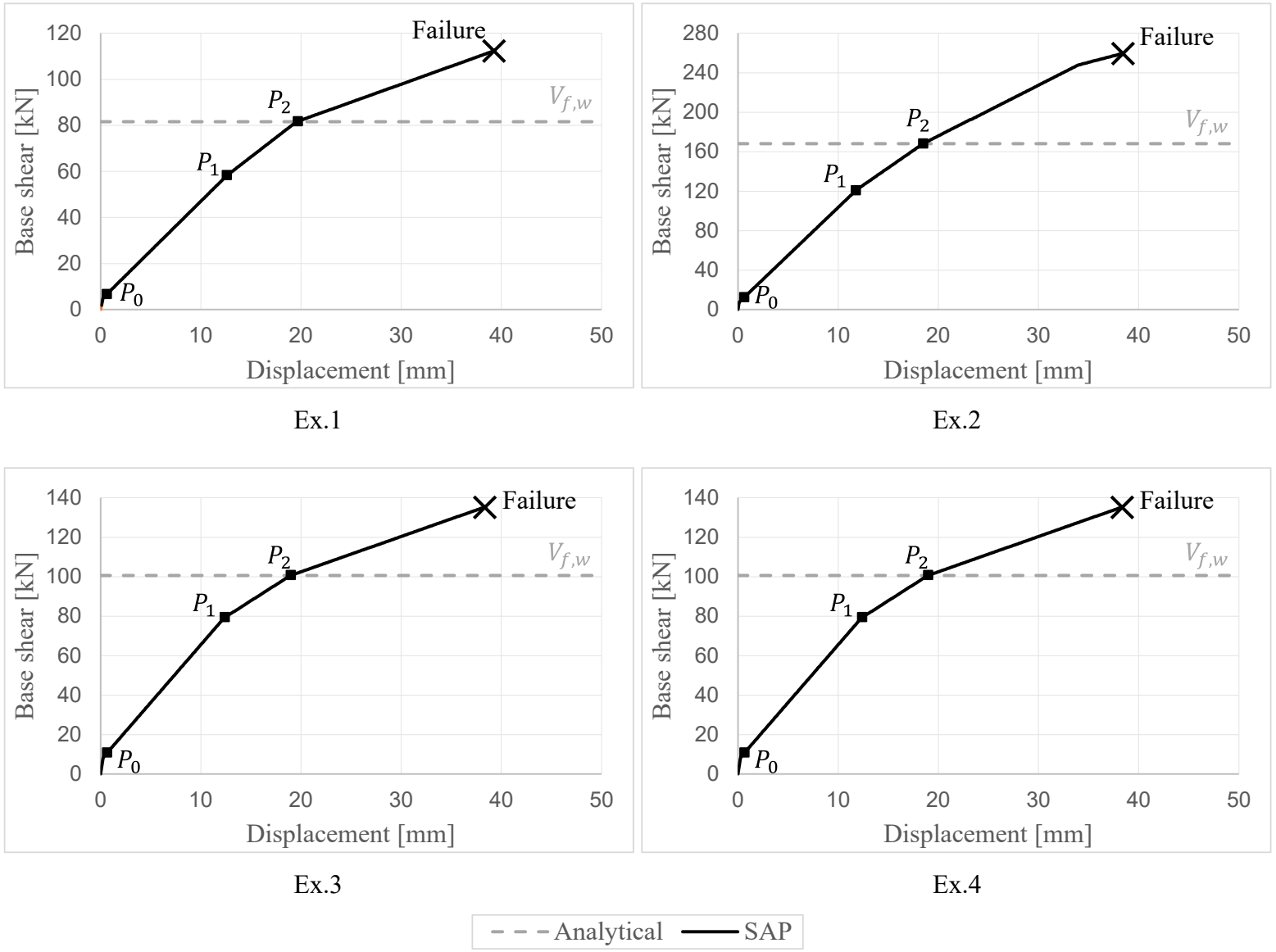

Figure 7-8: The base shear-displacement curves of CD wall examples

7.3.3. Case study: two-storey multi-panel CLT shearwall

In order to demonstrate the applicability of the proposed CD procedure, a case study for a two-storey building composed of three-panel and two-panel CLT shearwalls is presented (Figure 7-9). The mechanical properties of the connections were selected based on the values provided in section 7.2 and are summarized in Table 7-7. Fully nailed hold-downs and angle brackets with washers were used along with HBS 6x70 mm for panel-to-panel connections in all examples. The connections' mechanical properties were determined according to Table 7-1. For panel-to-panel connections, fifteen and ten connections were used for storeys 1 and 2, respectively. Double hold-downs located on each side of the wall were considered in storey 1, while a single hold-down connection was considered for storey 2 (Figure 7-9). Each panel was assumed to have a single angle bracket. A uniform vertical load, q, equal to 15 and 10 kN/m was applied to storeys 1 and 2, respectively. The value of the overstrength factor for the non-dissipative elements ($\gamma_{r,ND}$) was assumed equal to 1.6, which was obtained based on the 95th percentile of strength capacity of typical panel-to-panel connections, as reported in Gavric et al. (2015). As mentioned previously in Chapter 4, since no values regarding the precentiles of dissipative elements' strengths had been reported in the literature for the purpose of designing other dissipative and limited-dissipative elements' strengths, approximate values of overstrength factors for hold-down ($\gamma_{r,h}$) and angle brakcets ($\gamma_{r,a}$) equal to 1.1 and 1.2, respectively, were assumed. It should be noted that the values for the overstrength factors may differ depending on design procedures to obtain factor resistances. It is therefore not the magnitude of the overstrength factors that is emphasized in this context but rather the general procedure to determine the forces on non-dissipative and other-dissipative components. The factor incorporating the compression zone effect, β, was set equal to 0.95 (10% reduction in length), obtained from experimental test results on CLT shearwalls carried out by D'Arenzo et al. (2021).

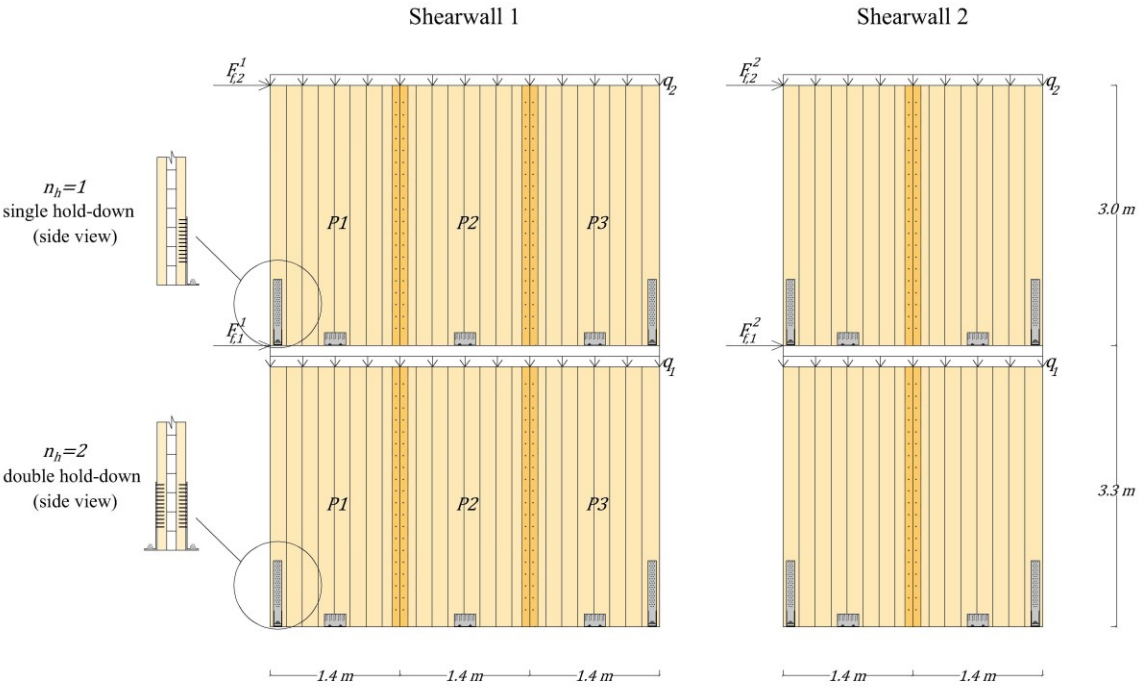

Figure 7-9: The CLT shearwalls model's views of the case of study for a multi-storey building

Table 7-7: Models Properties used in the case study

Parameters	Unit	Storey	Shearwall	
		j	$i=1$	$i=2$
q_j^i	kN/m	1	20	
		2	5	
m_j^i	-	1	3	2
		2		
$b_j^i \times h_j^i$	$m \times m$	1	1.4x3.3	
		2	1.4x3.0	
B_j^i	m	1	4.2	2.8
		2		
$n_{h,j}^i$	-	1	2	
		2	1	
$n_{f,j}^i$	-	1	15	
		2	10	
$n_{s,j}^i$	-	1	1	
		2	1	

Table 7-8 presents all the inputs and calculated output variables with references to the relevant equations. The factored lateral load acting on shearwall i at storey j, $F_{f,j}^i$, and the associated factored bending moments and shear forces, $M_{f,j}^i$ and $V_{f,j}^i$, respectively, are

presented in Table 7-9. The bending moment resistance, $M_{r,j}^{i}$, was calculated using Equation (4-28) and is summarized in Table 7-9. The over-capacity coefficient, $C_{sw,j}^{i}$, was determined for each storey using Equation (4-32). To ensure the soft-storey mechanism is avoided, it is required to satisfy Equation (4-33), as shown in Equation (7-9).

$$\varepsilon_1 \leq \frac{C_{sw,j}^{i}}{C_{sw,j-1}^{i}} \leq \varepsilon_2 \xrightarrow{j=2} 0.9 < \frac{1.76}{1.49} = 1.18 < 1.2 \checkmark \tag{7-9}$$

To ensure the applicability of the CD approach, three requirements need to be satisfied. The first requirement entails ensuring CP elastic behaviour for each shearwall i (refer to Equation (4-9)), as shown in Equations (7-10) and (7-11), for storeys $j = 1$ and $j = 2$, respectively. The values in Equations (7-10) and (7-11) were obtained from Table 7-8 and Table 7-9.

$$\begin{aligned} &\tilde{k}_j^i = 1.17 > 0.69\ (j = 1, i = 1)\ \& \\ &\tilde{k}_j^i = 1.17 > 0.71\ (j = 1, i = 2)\ \checkmark \end{aligned} \tag{7-10}$$

$$\begin{aligned} &\tilde{k}_j^i = 2.35 > 0.52\ (j = 2, i = 1)\ \& \\ &\tilde{k}_j^i = 2.35 > 0.56\ (j = 2, i = 2)\ \checkmark \end{aligned} \tag{7-11}$$

The second requirement ensures the yielding of the panel-to-panel connections prior to other connections (refer to Equation (4-18)), as outlined in Equation (7-12) and (7-13), for storeys $j = 1$ and $j = 2$, respectively.

$$\begin{aligned} &r_{h,z,j}^{i} = 178.42\ kN > 123.02\ kN\ (j = 1, i = 1)\ \& \\ &r_{h,z,j}^{i} = 178.42\ kN > 123.02\ kN\ (j = 1, i = 2)\ \checkmark \end{aligned} \tag{7-12}$$

$$\begin{aligned} &r_{h,z,j}^{i} = 89.21\ kN > 61.51\ kN\ (j = 2, i = 1)\ \& \\ &r_{h,z,j}^{i} = 89.21\ kN > 61.51\ kN\ (j = 2, i = 2)\ \checkmark \end{aligned} \tag{7-13}$$

The final requirement is to ensure that the yielding of panel-to-panel connections and hold-down (dissipative elements) occurs prior to yielding of the angle brackets (limited-dissipation), as summarized in Table 7-9 (3^{rd} check, Equation (4-25)). It is noted that all design checks were satisfied.

Table 7-8: Input parameters and calculated parameters used for CBD for shearwall i $(i = 1,2)$ and storey j $(j = 1,2)$

Parameters	Unit	Storey	Shearwall		Eq.
		j	$i = 1$	$i = 2$	
$k^i_{h,z,j}$	kN/m	1	22320		-
		2	11160		
$k^i_{s,x,j}$	kN/m	1	5710		-
		2			
$k^i_{s,z,j}$	kN/m	1	8250		-
		2			
$k^i_{f,j}$	kN/m	1	950		-
		2			
$r^i_{h,z,j}$	kN	1	178.42		-
		2	89.21		
$r^i_{a,x,j}$	kN	1	63.06		-
		2			
$r^i_{a,z,j}$	kN	1	60.00		-
		2			
φ^i_j	-	1	0.37		(4-1)
		2	0.74		
α^i_j	-	1	0.20		(4-2)
		2			
$\widetilde{k}^i_j$	-	1	1.17		(4-3)
		2	2.35		
$\widetilde{M}^i_j$		1	0.32	0.20	(4-4)
		2	0.44	0.26	
ρ^i_j	-	1	0.45		(4-6)
		2			
$k'^{,i}_{v,j}$	kN/m	1	59455	40635	(4-7)
		2	23661	17703	
$M^i_{q,j}$	$kN \cdot m$	1	39.7	26.5	(4-8)
		2	26.5	17.64	
$M^{el,i}_{r,f,j}$	$kN \cdot m$	1	487.7	326.5	(4-9)
		2	201.2	148.4	
$M^{el,i}_{r,h,j}$	$kN \cdot m$	1	740.1	505.1	(4-10)
		2	305.2	226.2	
$M^{el,i}_{r,s,j}$	$kN \cdot m$	1	1099.8	751.7	(4-11)
		2	437.7	327.5	
$V^{el,i}_{r,s,j}$	$kN \cdot m$	1	189.2	126.1	(4-12)
		2			

Table 7-9: Factored lateral load, shear force and bending moment used in the case of study for shearwall i ($i = 1,2$) and storey j ($j = 1,2$)

Parameters	Unit	Storey	Shearwall		Eq.
		j	$i = 1$	$i = 2$	
$F_{f,j}^{i}$	kN	1	20	15	-
		2	50	40	
$V_{f,j}^{i}$	kN	1	70	55	-
		2	50	40	
$M_{f,j}^{i}$	$kN \cdot m$	1	381.0	301.5	-
		2	150.0	120.0	
$M_{r,j}^{i}$	$kN \cdot m$	1	589.3	429.8	(4-28)
		2	267.5	207.3	
$C_{sw,j}^{i}$		1	1.49		(4-32)
		2	1.76		
1^{st} check	-	1	0.69	0.71	(4-5)
		2	0.52	0.56	
2^{nd} check	-	1	123.02		(4-18)
		2	61.51		
3^{rd} check	-	1	0.91	0.97	(4-25)
		2	0.81	0.88	

In order to design the CLT panels, characterized as non-dissipative elements, Equation (4-34) was used to calculate the factored shear force acting on each panel at shearwall 1 and 2, respectively, as shown in Equation (7-14) and (7-15). The minimum over-capacity coefficient was calculated as $C_{sw,min} = min(1.49,1.76) = 1.49$, and the factored action applied to each panel, E_f, was obtained as $V_{f,j}^{i}/m$, which represents the maximum value for shearwall 1 ($70/3 = 35\ kN$), and for shearwall 2 ($55/2 = 27.5\ kN$).

$$E_{f,w}^{1} = \gamma_{r,ND} \cdot C_{sw,min} \cdot E_f + E_g = 1.6 \cdot 1.49 \cdot 35 + 0 = 83.44\ kN \leq E_{r,ND} \quad (7\text{-}14)$$

$$E_{f,w}^{2} = \gamma_{r,ND} \cdot C_{sw,min} \cdot E_f + E_g = 1.6 \cdot 1.49 \cdot 27.5 + 0 = 65.56\ kN \leq E_{r,ND} \quad (7\text{-}15)$$

The shear resistance of the CLT panels, $E_{r,w}$, must be greater than the factored actions, $E_{f,w} = 83.44\ kN$, to avoid brittle failure.

7.4. Validation against experimental tests: General

This section presents the validation of the analytical expressions presented in Chapter 3 as well as in the literature (Nolet et al. 2019) against the results derived from experimental tests on multi-panel CLT shearwalls presented in Chapter 6. The information for each wall can be found in Table 6-1. The aim here is to demonstrate that the developed equations are capable of accurately predicting the kinematic mode and the behaviour of walls. Moreover, the results obtained from the experimental tests were compared to those obtained from the numerical models considering the modifications necessary to account for experimental test conditions, including the positions of the lateral load actuator, hold-down, and angle brackets in the shearwall. Hence, the connections were positioned according to the configurations shown in Figure 6-1, and a concentrated lateral load was applied to the wall at the top, as per the loading actuator position in the experimental tests, 75 mm below the wall's edge. Uniformly distributed gravity loads, q, of 1.45 and 6.67 kN/m were applied on top of the wall for walls without and with gravity loads, respectively, to account for the weight of the panels, test setup attachments, and superimposed gravity loads.

Consistent with the defined groups in Chapter 6, validation was conducted for walls without (walls #1-#5) and with (walls #6-12) angle brackets, presented in Chapter 6. The walls without angle brackets were analyzed using the expressions proposed by Nolet et al. (2019), while preventing sliding at the center of rotation of each panel, and the walls with angle brackets were analyzed according to the developed expressions presented in Chapter 3. Modifications to the equations were employed in accordance with experimental tests and numerical models.

The CLT panels were modelled according to the orthotropic properties presented in section 7.2. Since the analytical expressions were developed assuming the rigid behaviour of the CLT panels, shear and bending deformations of panels, Δ_{sh} and Δ_b, respectively, were added to account for the flexibility in the panels. As previously established in Chapter 3, shear and bending deformations can be determined using Equations (7-16) and (7-17), respectively.

$$\Delta_b = \frac{F \cdot h^3}{3 \cdot EI_{eff}} \tag{7-16}$$

$$\Delta_{sh}=\frac{F\cdot h}{G_{eff}\cdot t_{CLT}\cdot m\cdot b} \quad (7\text{-}17)$$

Where F is the lateral load and G_{eff} is equal to $361.1\ MPa$, as previously calculated using Equation (7-4).

The values for EI_{eff} for CLT panels composed of three panels (walls #1-#10) and two panels (wall #11) with an actual width of 1219.2 mm can be calculated using Equations (7-18) and (7-19), while using Equation (7-20) for wall #12 with four panels with a width of 609.6 mm.

$$EI_{eff}=m\cdot\left(E_0\cdot t_0\cdot\frac{b^3}{12}+E_{90}\cdot t_{90}\cdot\frac{b^3}{12}\right)=3.76\cdot10^{14}\ N\cdot mm^2 \quad (7\text{-}18)$$

$$EI_{eff}=m\cdot\left(E_0\cdot t_0\cdot\frac{b^3}{12}+E_{90}\cdot t_{90}\cdot\frac{b^3}{12}\right)=2.51\cdot10^{14}\ N\cdot mm^2 \quad (7\text{-}19)$$

$$EI_{eff}=m\cdot\left(E_0\cdot t_0\cdot\frac{b^3}{12}+E_{90}\cdot t_{90}\cdot\frac{b^3}{12}\right)=6.26\cdot10^{13}\ N\cdot mm^2 \quad (7\text{-}20)$$

Nolet et al. (2019) presented analytical procedures to predict the rocking behaviour of three-panel CLT shearwalls for CP and SW kinematic modes, as illustrated in Figure 7-10. Table 7-10 summarizes the expressions required in the analytical procedures for each point defined in Figure 7-10. The expressions for CP were updated by factors τ_1 and τ_2 to account for the real position of the hold-down and the loading actuator in experimental tests. These variables represent the ratio of the distance between the center of rotation of the first panel and the hold-down to the length of each panel (b) and the ratio of the distance between the bottom of the wall and the position of the lateral load to the height of the wall. The analytical equations are calculated using elastic-perfectly-plastic mechanical properties for connections, as summarized in Table 7-1. In the SW expressions provided in Table 7-10, $F_{sw,i}$ and $\Delta_{sw,i}$ are the lateral load and rocking displacements, at point i, for $i=2:4$. Table 7-11 and Table 7-12 summarize the values for each analytical point in CP and SW examples, respectively, including force and rocking, shear, and bending displacements. Additionally, the total displacement is tabulated, presenting the sum of all contributions (i.e., rocking, shear, and bending deformations).

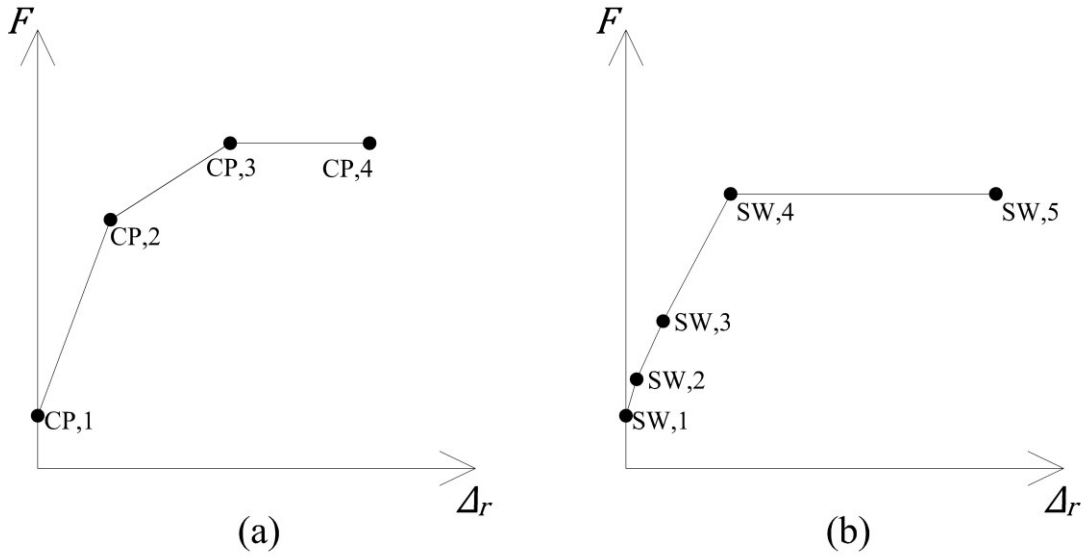

Figure 7-10: analytical curves developed by Nolet et al. (2019)Nolet et al. (2019): (a) for CP; (b) for SW

Table 7-10: analytical expressions developed by Nolet et al. (2019) for CP and SW behaiours

Point	F	Δ_r
CP,1	$\frac{q \cdot m \cdot b^2}{2 \cdot h \cdot \tau_2}$	0
CP,2	$\frac{[{\tau_1}^2 \cdot k_h + (m-1) \cdot n_c \cdot k_c]\, b}{k_c \cdot \tau_2} + \frac{q \cdot m \cdot b^2}{2 \cdot h \cdot \tau_2}$	$d_{y,c} \cdot \frac{h}{b}$
CP,3	$\frac{b}{h \cdot \tau_2} \cdot \left[\tau_1 \cdot r_h + r_c \cdot (m-1) \cdot n_c + \frac{q \cdot m \cdot b}{2}\right]$	$\frac{d_{y,h}}{\tau_1} \cdot \frac{h}{b}$
CP,4	$\frac{b}{h \cdot \tau_2} \cdot \left[\tau_1 \cdot r_h + r_c \cdot (m-1) \cdot n_c + \frac{q \cdot m \cdot b}{2}\right]$	$min\left(d_{u,c}, \frac{d_{u,h}}{\tau_1}\right) \cdot \frac{h}{b}$
SW,1	$\frac{q \cdot m \cdot b^2}{2 \cdot h \cdot \tau_2}$	0
SW,2	$\frac{q \cdot m^2 \cdot b^2}{2 \cdot h} \cdot \frac{k_h \cdot \left(\frac{3 \cdot m - 2}{m^2}\right) + \left(\frac{2 - m}{m^2}\right)}{n_c \cdot k_c - k_h}$	$\left(F_{SW,2} - \frac{q \cdot m \cdot b^2}{2 \cdot h}\right) \frac{h^2}{b^2 \cdot [k_h + (m-1) \cdot n_c \cdot k_c]}$
SW,3	$\frac{q \cdot m^2 \cdot b^2}{2 \cdot h} \cdot \frac{k_h \cdot \left(\frac{m + 6}{m^2}\right) + \left(\frac{5 \cdot m - 6}{m^2}\right)}{n_c \cdot k_c - k_h}$	$\left(F_{SW,3} - \frac{q \cdot m \cdot b^2}{2 \cdot h}\right) \frac{h^2 \cdot [k_h + n_c \cdot k_c]}{b^2 \cdot [(m+2) \cdot k_h + (m-2) \cdot n_c \cdot k_c] \cdot n_c \cdot k_c}$
SW,4	$\frac{1}{h} \cdot \left[r_h \cdot m \cdot b + \frac{q \cdot m^2 \cdot b^2}{2}\right]$	$\left\{\frac{F_{sw,4} \cdot h^2}{b^2} - \left[\frac{\left(\frac{1}{k_h} + \frac{m-1}{n_c \cdot k_c}\right)^{-1}}{k_h} \cdot \frac{q \cdot m^2}{2 \cdot h}\right]\right\} \cdot \frac{1}{m^2 \cdot \left(\frac{1}{k_h} + \frac{m-1}{n_c \cdot k_c}\right)^{-1}}$
SW,5	$\frac{1}{h} \cdot \left[r_h \cdot m \cdot b + \frac{q \cdot m^2 \cdot b^2}{2}\right]$	$\Delta_{r,SW,4} + \left[\frac{h}{m \cdot b} \cdot (d_{u,h} - d_{y,h})\right]$

Table 7-11: Analytical values for walls with CP behaviour: group A

Wall	**#1**					**#2**				
Parameter	F	Δ_r	Δ_{sh}	Δ_b	Δ_{total}	F	Δ_r	Δ_{sh}	Δ_b	Δ_{total}
Unit	kN	mm	mm	mm	mm	kN	mm	mm	mm	mm
CP,1	1.4	0.0	0.0	0.0	0.0	6.3	0.0	0.1	0.1	0.2
CP,2	87.7	9.5	1.5	1.1	12.2	92.6	9.5	1.6	1.2	12.3
CP,3	126.3	18.3	2.2	1.6	22.1	131.2	18.3	2.3	1.7	22.3
CP,4	126.3	39.3	2.2	1.6	43.1	131.2	39.3	2.3	1.7	43.3

Table 7-12: Analytical values for walls with SW behaviour: group A

Wall	**#3**					**#4**					**#5**				
Parameter	F	Δ_r	Δ_{sh}	Δ_b	Δ_{total}	F	Δ_r	Δ_{sh}	Δ_b	Δ_{total}	F	Δ_r	Δ_{sh}	Δ_b	Δ_{total}
Unit	kN	mm	mm	mm	mm	kN	mm	mm	mm	mm	kN	mm	mm	mm	mm
SW,1	1.4	0.0	0.0	0.0	0.0	6.3	0.0	0.1	0.1	0.2	6.3	0.0	0.1	0.1	0.2
SW,2	4.0	0.1	0.1	0.0	0.2	18.2	0.6	0.3	0.2	1.2	23.4	1.1	0.4	0.3	1.8
SW,3	6.6	0.3	0.1	0.0	0.4	30.2	1.4	0.5	0.4	2.3	45.8	2.7	0.8	0.6	4.0
SW,4	126.0	9.5	2.2	0.2	11.9	140.4	9.9	2.5	1.8	14.1	156.9	10.9	2.8	2.0	15.7
SW,5	126.0	16.7	2.2	0.2	19.1	140.4	17.0	2.5	1.8	21.3	156.9	29.1	2.8	2.0	33.9

The analytical procedures presented in Chapter 3 were used for the seven tested walls (i.e., walls #6-#12), where angle brackets were used in the length of each panel, and as such the bi-directional contribution of angle brackets was included. The stiffness and strength of the hold-down and angle brackets, as well as the height of the wall were updated to account for the real position of the connections and the loading actuator in experimental tests. The analytical equations were calculated using elastic-perfectly-plastic mechanical properties for connections, as summarized in Table 7-1. For walls with SW, only elastic results were provided as no inelastic expressions were developed for SW behaviour considering the bi-directional contribution of angle brackets.

7.5. Validation against experimental tests: results and discussion

7.5.1. Experimental vs numerical

The observed kinematic modes were consistent between experimental and numerical results. Figure 7-11 shows the load-displacement curves obtained from experimental and numerical results. As can be observed, the numerical models utilizing envelope curves of connections derived from experimental tests presented in Chapter 5 led to a reasonable match for all walls. It was found that the numerical models agreed with experimental envelope curves for different load levels in the elastic and plastic regions.

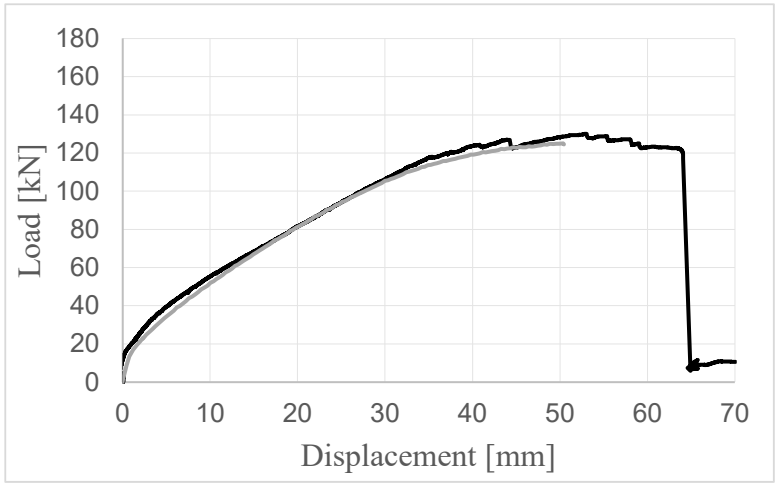

wall #1

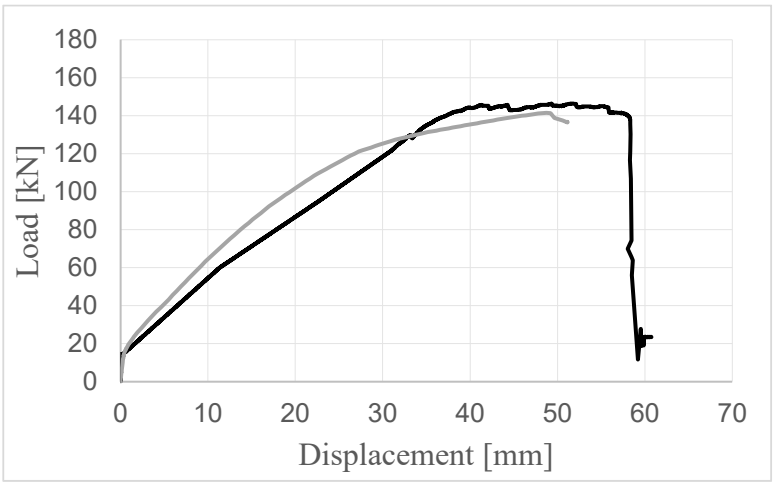

wall #2

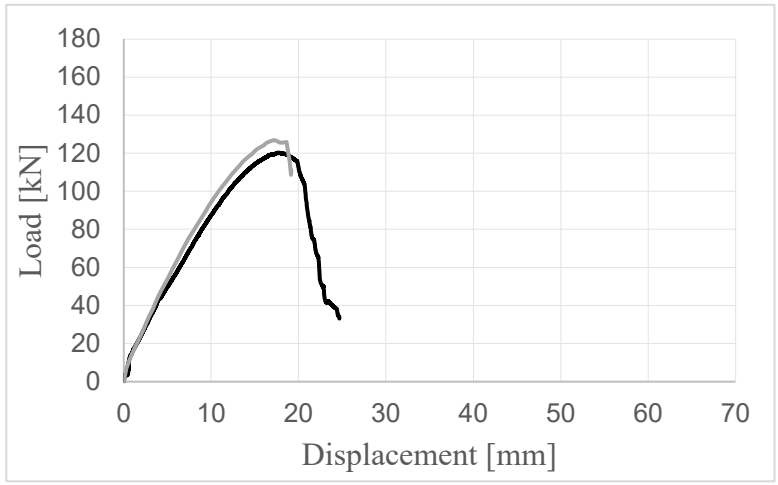

wall #3

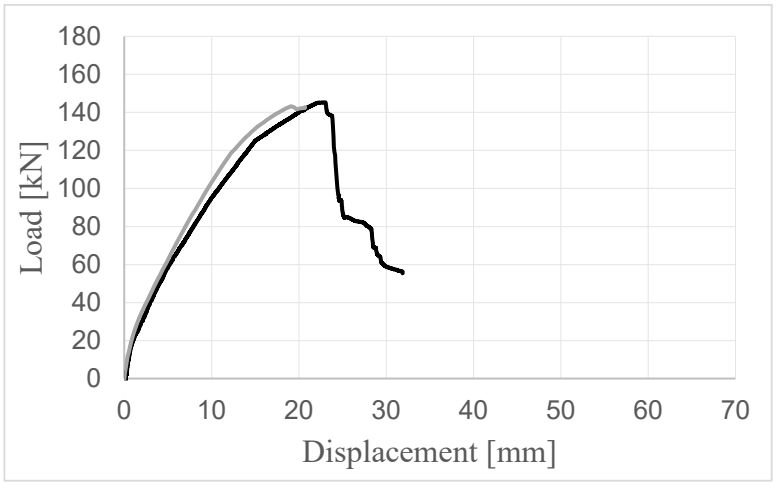

wall #4

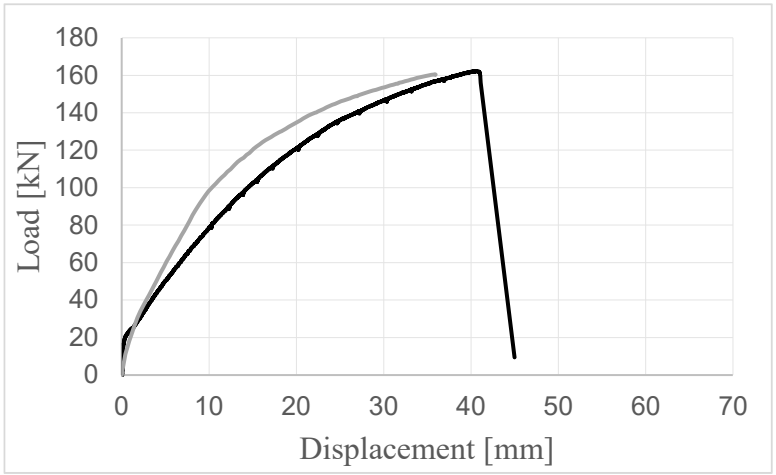

wall #5

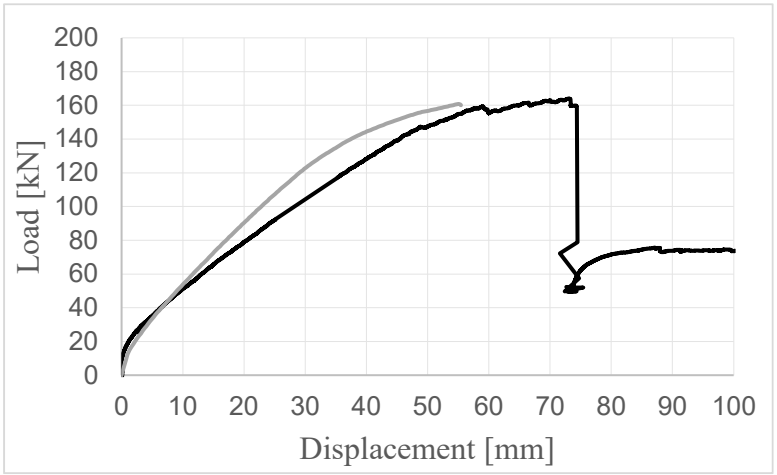

wall #6

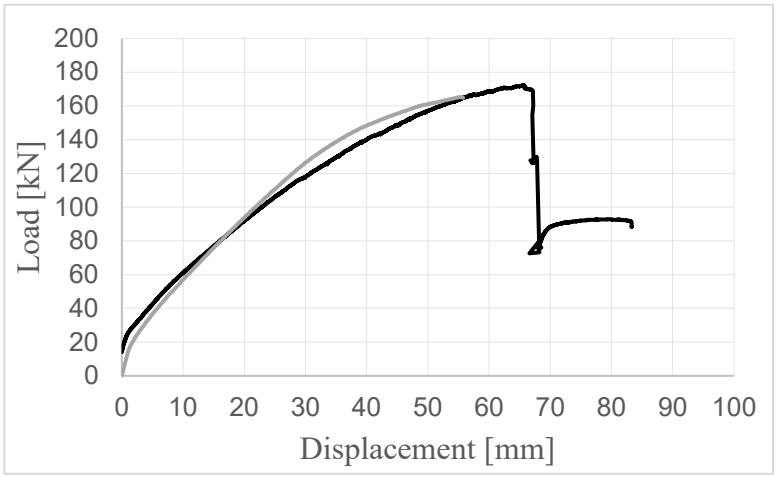

wall #7

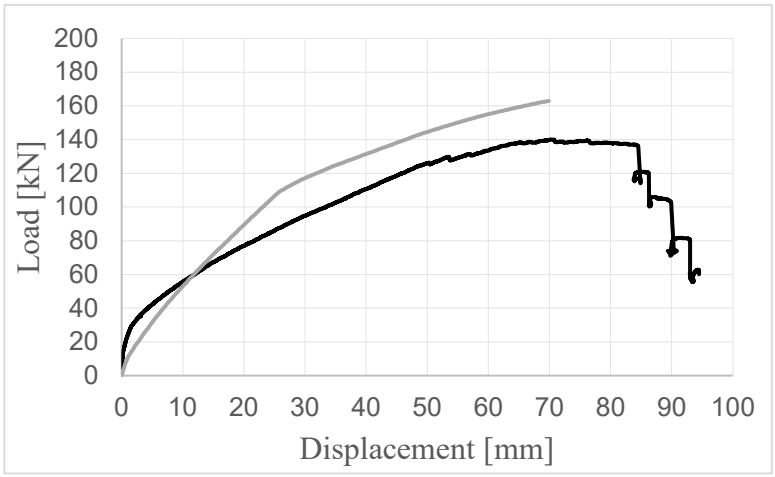

wall #8

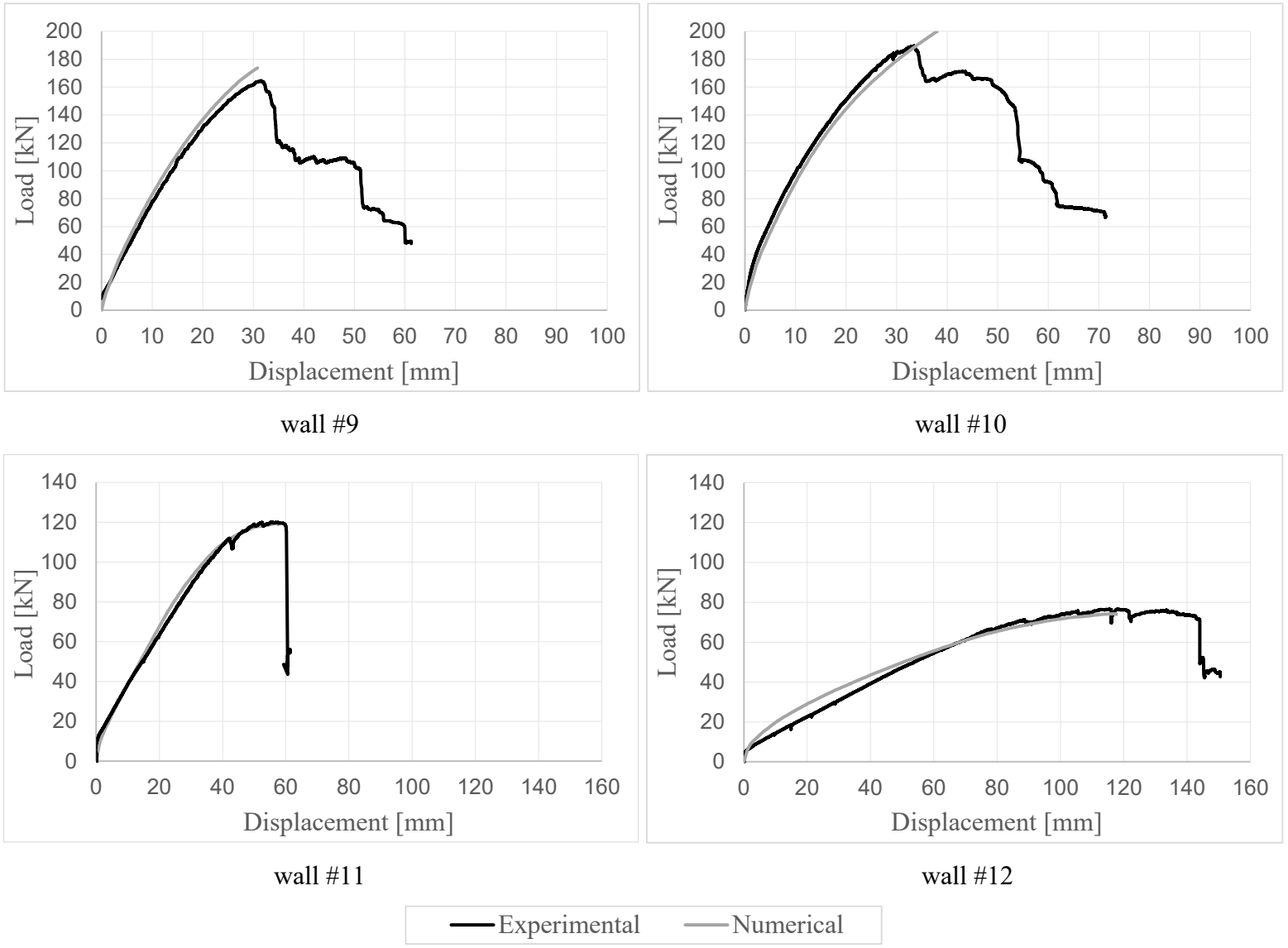

Figure 7-11: Experimental and numerical curves of the shearwalls presented in Chapter 6

Table 7-13 summarizes the key parameters obtained from each method, including the percentage difference between experimental test and numerical model results denoted as $\xi_{T/N}$. The last three rows indicate the maximum, minimum, and mean values of $\xi_{T/N}$. The results showed that the maximum and yield forces, F_{max} and $F_{y,EEEP}$, respectively, matched reasonably well with a difference in the range of 0.4%-15.1%. The associated displacements with the maximum and yield forces, $V_{F_{max}}$ and $V_{y,EEEP}$, respectively, showed slightly higher discrepancies in the ranges of 0.7%-28.1% and 0.1%-42.8%, with mean differences of 8.7% and 17.3%, respectively. As for the elastic stiffness, k_{EEEP}, the differences were in the range of 1.0% and 20.3%, except for wall #5 where the difference was 33.7%, which could be attributed to its unique behaviour, near the interface between SW and IN kinematic modes. A discrepancy of 4.7%-29.3% was observed in the ultimate displacement, $v_{u,EEEP}$.

Table 7-13: results obtained from experimental tests and numerical models

Wall-mode	Content	F_{max} [kN]	$v_{F_{max}}$ [mm]	$F_{y,EEEP}$ [mm]	$v_{y,EEEP}$ [mm]	k_{EEEP} [kN/mm]	$v_{u,EEEP}$ [mm]	D_{EEEP} [-]
#1-CP	**Test**	130.1	53.0	115.5	23.4	4.9	64.1	2.7
	Numerical	125.0	50.4	110.1	24.0	4.2	50.5	2.1
	$\xi_{T/N}$	4.0%	5.1%	4.8%	2.7%	16.2%	23.7%	26.3%
#2-CP	**Test**	146.4	49.3	134.3	29.4	4.6	58.3	2.0
	Numerical	141.4	48.7	126.5	21.4	5.4	51.2	2.4
	$\xi_{T/N}$	3.5%	1.3%	6.0%	31.7%	16.6%	13.0%	19.1%
#3-SW	**Test**	120.3	17.7	109.5	11.8	9.3	20.8	1.8
	Numerical	127.0	17.2	114.2	10.9	10.5	19.1	1.8
	$\xi_{T/N}$	5.4%	3.0%	4.2%	7.5%	11.7%	8.5%	1.1%
#4-SW	**Test**	145.3	23.0	126.0	11.7	10.8	24.1	2.1
	Numerical	143.2	19.1	126.6	11.0	10.7	19.8	1.8
	$\xi_{T/N}$	1.5%	18.5%	0.5%	6.1%	1.0%	19.7%	13.6%
#5-SW	**Test**	162.3	40.7	140.7	19.0	7.4	41.1	2.2
	Numerical	160.5	35.8	138.6	12.6	10.4	35.8	2.8
	$\xi_{T/N}$	1.1%	12.7%	1.5%	40.5%	33.7%	13.8%	27.2%
#6-CP	**Test**	164.0	73.1	146.1	38.6	3.8	74.4	1.9
	Numerical	160.8	55.1	142.3	30.8	4.2	55.4	1.8
	$\xi_{T/N}$	1.9%	28.1%	2.6%	22.4%	10.3%	29.3%	7.0%
#7-CP	**Test**	172.3	65.7	147.4	31.1	4.8	67.6	2.2
	Numerical	165.3	55.4	146.8	31.1	4.5	55.8	1.8
	$\xi_{T/N}$	4.2%	17.0%	0.4%	0.1%	5.4%	19.2%	19.4%
#8-CP	**Test**	140.1	70.8	120.6	25.4	4.8	84.9	3.3
	Numerical	163.0	69.9	139.5	30.0	4.4	69.9	2.3
	$\xi_{T/N}$	15.1%	1.2%	14.6%	16.6%	7.7%	19.4%	35.6%
#9-SW	**Test**	164.7	31.5	145.5	19.6	7.4	34.5	1.8
	Numerical	173.8	30.8	147.9	18.2	7.8	30.8	1.7
	$\xi_{T/N}$	5.4%	2.4%	1.7%	7.3%	4.9%	11.2%	3.9%
#10-SW	**Test**	189.5	33.6	161.8	15.5	10.4	36.0	2.3
	Numerical	199.9	38.0	166.0	18.3	8.5	38.0	2.1
	$\xi_{T/N}$	5.4%	12.3%	2.6%	16.4%	20.3%	5.3%	11.1%
#11-CP	**Test**	120.1	55.5	112.1	37.2	3.0	60.2	1.6
	Numerical	119.4	56.9	109.4	32.6	3.1	57.4	1.8
	$\xi_{T/N}$	0.6%	2.4%	2.5%	13.3%	2.9%	4.7%	8.3%
#12-CP	**Test**	76.5	118.0	71.9	78.6	0.9	144.9	1.8
	Numerical	74.2	117.2	63.2	50.9	1.1	117.7	2.3
	$\xi_{T/N}$	3.1%	0.7%	12.9%	42.8%	17.8%	20.7%	22.8%
$\xi_{T/N}$	**Maximum**	15.1%	28.1%	14.6%	42.8%	33.7%	29.3%	35.6%
	Minimum	0.6%	0.7%	0.4%	0.1%	1.0%	4.7%	1.1%
	Mean	4.3%	8.7%	4.5%	17.3%	12.4%	15.7%	16.3%

7.5.2. Experimental vs analytical

Figure 7-12 illustrates the load-displacement curves obtained from experimental tests and their corresponding EEEP simulations, as well as the results derived from analytical expressions, such as maximum force and initial stiffness. In particular, the match between the models and test results concerning initial stiffness for walls dominated by SW behaviour (walls #3-#5 and #9-#10) exhibited a close match due to the fact that the behaviour was generally dominated by hold-down mechanical properties. For walls with CP behaviour (i.e., #1-#2, #6-#8, and #11-#12), both the hold-down and panel-to-panel connections contributed to the wall's performance, and therefore, some discrepancy was observed between the experimental and analytical results, particularly in the stiffness, for which the assumption of elastic-perfectly plastic properties is expected to play a significant role. Moreover, the maximum forces determined by both methods matched reasonably well, with the analytical values being lower than the experimental ones in most cases, except for walls #3 and #9, where the analytical values were slightly higher. Concerning the yield hierarchy achieved in each example, consistency was observed among all models. For walls with CP, the panel-to-panel connections yielded before the hold-downs, while for walls with SW, the hold-downs yielded before the panel-to-panel connections. Also, it was observed that angle brackets yielded after other connections had yielded, following the proposed CD requirement. Thus, the analytical requirements to generate the yield hierarchy necessary for CD were correct.

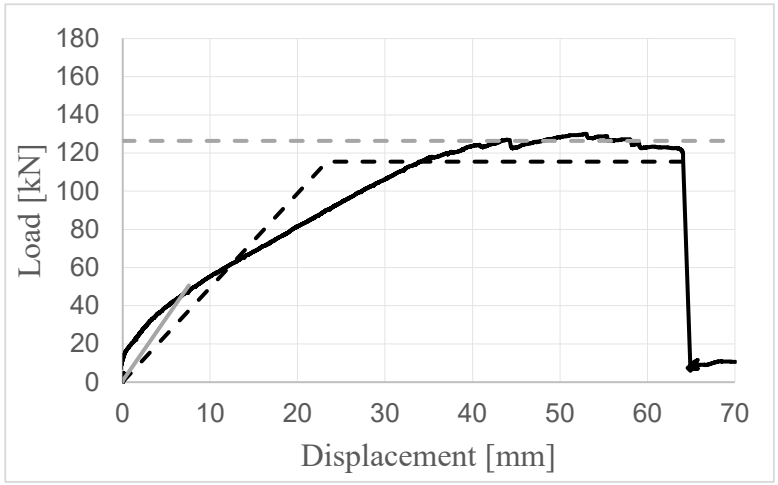

wall #1

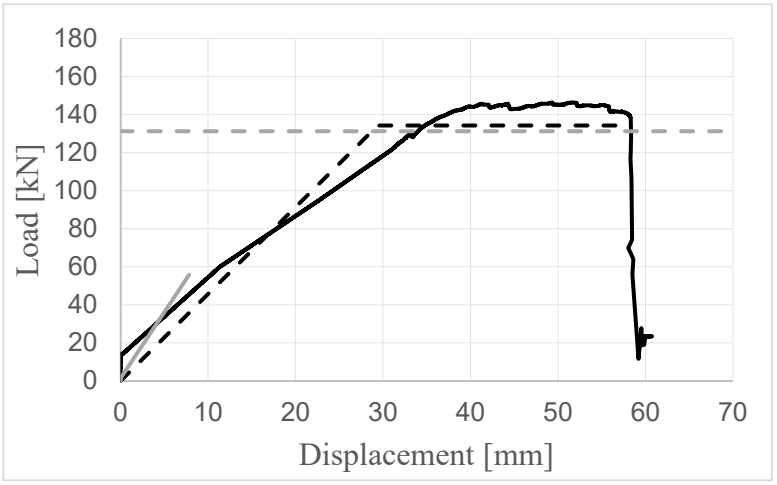

wall #2

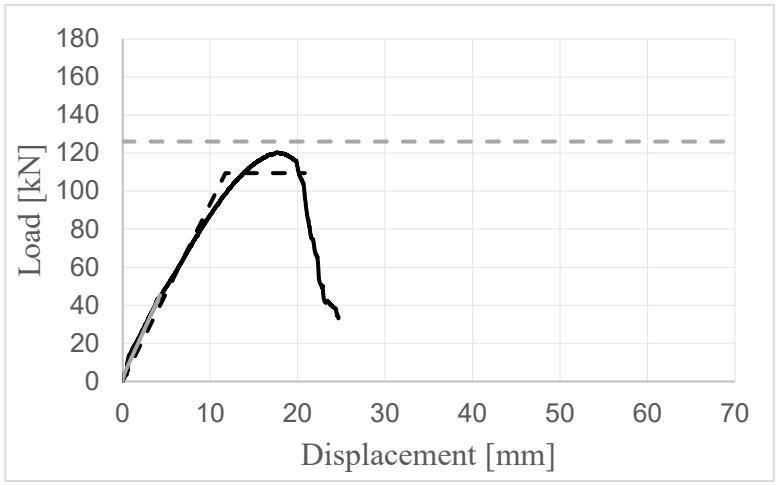

wall #3

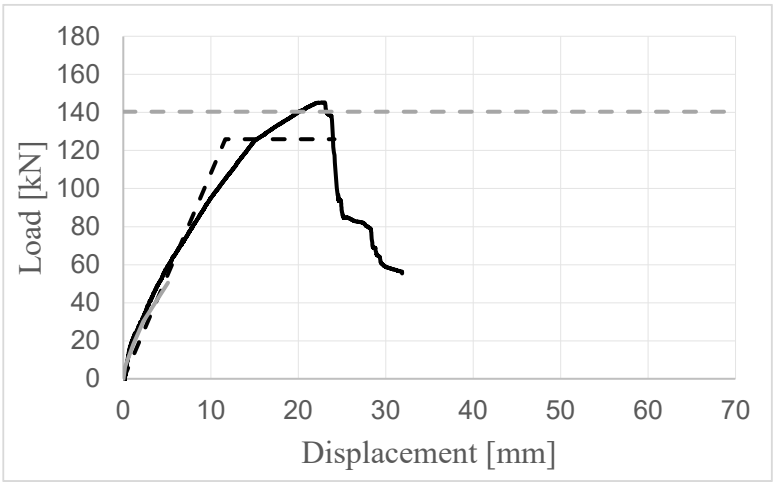

wall #4

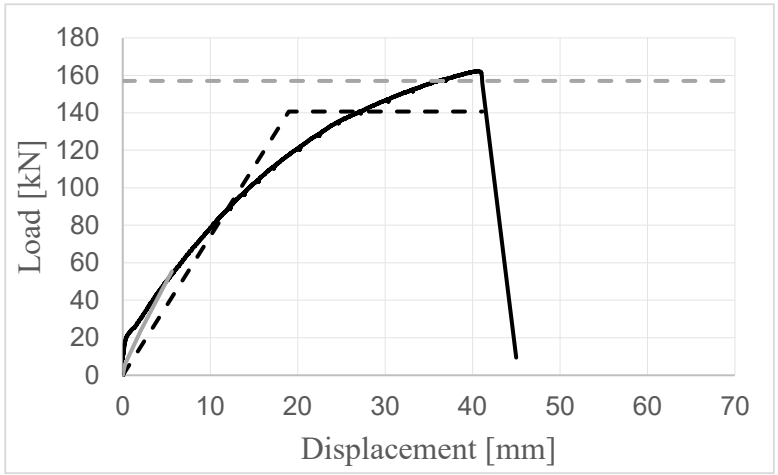

wall #5

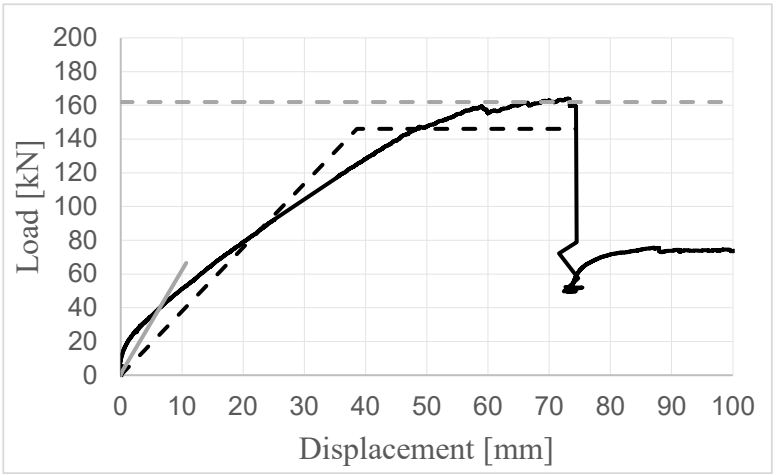

wall #6

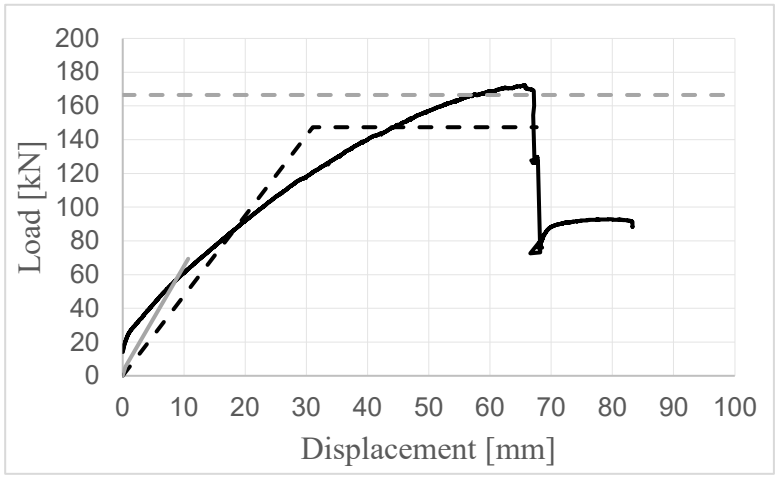

wall #7

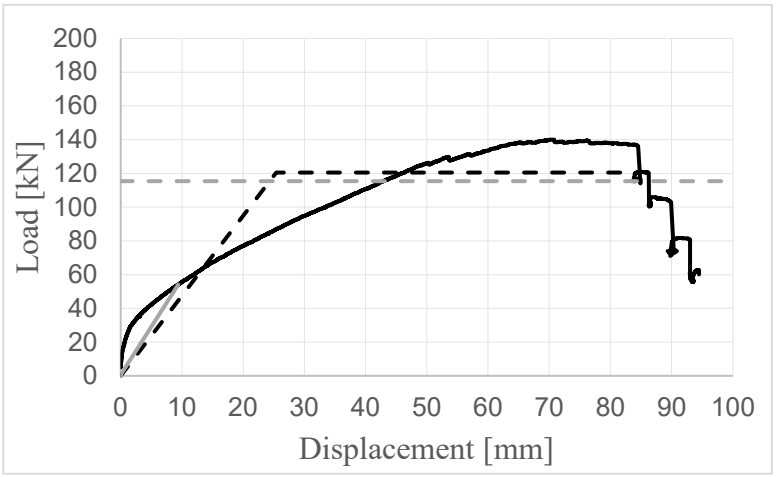

wall #8

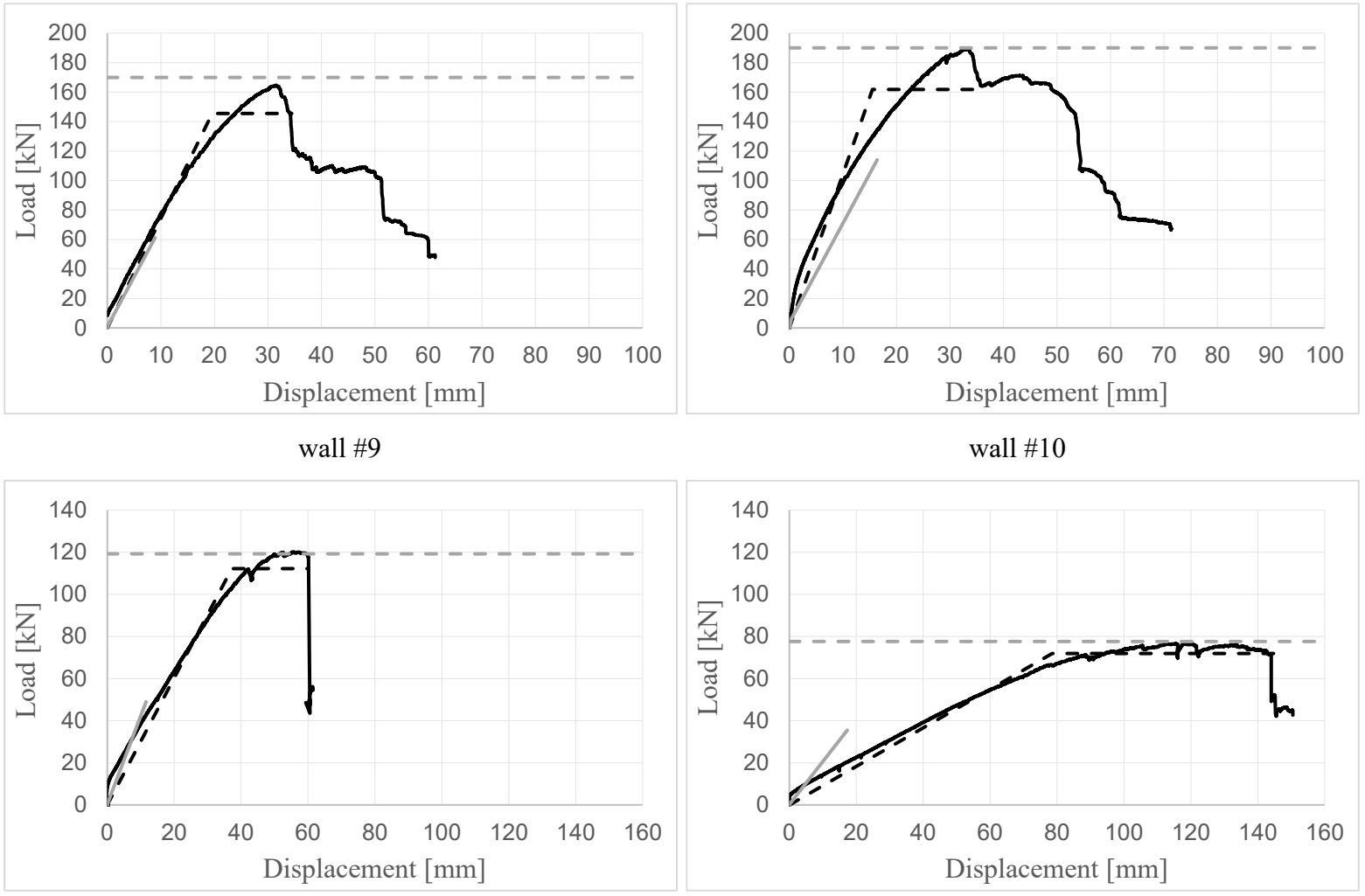

Figure 7-12: Experimental and analytical results of the shearwalls presented in Chapter 6

As shown in Table 7-14, the maximum force, F_{max}, and initial stiffness, k_e, obtained from each method are summarized, along with the percentage difference between experimental results and numerical results, denoted as $\xi_{T/N}$. In this section, initial stiffness is defined as the elastic stiffness obtained from EEEP simulation for experimental results, as well as the elastic stiffness calculated from analytical results before yielding the connections. The maximum force, F_{max}, matched reasonably well, with a difference in the range of 1%-11%. However, wall #8 showed a difference of 19%, which may be related to the interpolation made for simulating the mechanical properties of fully nailed angle brackets with washers discussed in section 7.2. For the elastic stiffness, k_{EEEP}, greater differences were observed especially for walls with CP behaviour, ranging from 8%-46% and 10%-40% for walls with and without angle brackets, respectively. An exceptionally high discrepancy of 76% was found in wall #12, which may be due to the use of four panels, resulting in more panel-to-panel engagements. Stiffness is notoriously difficult to estimate due to the non-linear nature of the behaviour of wood shearwalls even at low displacement levels. The discrepancy could also be attributed to using the EEEP idealization curve for panel-to-panel connections. It can be observed that a significantly better fit was obtained for these walls in the numerical model owing to using the real connection curves obtained from the joint-level tests.

Table 7-14: results obtained from experimental tests and analytical models

Wall-mode	Content	F_{max} [kN]	k_e [kN/mm]	$\xi_{T/A}$ [F_{max}]	$\xi_{T/A}$ [k_e]
#1-CP	**Test**	130.1	4.9	3%	30%
	Numerical	126.3	6.6		
#2-CP	**Test**	146.4	4.6	11%	40%
	Numerical	131.2	6.9		
#3-SW	**Test**	120.3	9.3	5%	10%
	Numerical	126.0	10.3		
#4-SW	**Test**	145.3	10.8	4%	17%
	Numerical	140.3	9.1		
#5-SW	**Test**	162.3	7.4	3%	26%
	Numerical	156.9	9.6		
#6-CP	**Test**	164.0	3.8	1%	46%
	Numerical	161.9	6.1		
#7-CP	**Test**	165.5	4.8	1%	25%
	Numerical	166.6	6.2		
#8-CP	**Test**	140.1	4.8	19%	17%
	Numerical	115.4	5.7		
#9-SW	**Test**	164.7	7.4	-	8%
	Numerical	-	6.8		
#10-SW	**Test**	189.5	10.4	-	43%
	Numerical	-	6.7		
#11-CP	**Test**	120.1	3.0	1%	31%
	Numerical	119.2	4.1		
#12-CP	**Test**	76.5	0.9	1%	76%
	Numerical	77.6	2.0		

7.6. Summary

This section presents the verification of the developed expressions in Chapter 3 against numerical models to demonstrate their mathematical accuracy in both elastic and inelastic ranges. In addition, the CD expressions developed in Chapter 4 were verified, and their applicability to multi-storey shearwalls was illustrated by introducing a case study. Validation against the experimental tests presented in Chapter 6 was conducted for the analytical expressions developed by Nolet et al. (2019), in which the contribution of angle brackets was neglected, and those developed in Chapter 3, in which the contribution of angle brackets was included.

This section contains the following observations:

- The elastic analytical expressions were verified in CP and SW kinematic ranges against four examples created based on the connections tested in Chapter 5. The error in all cases was less than 0.4%, which is acceptable, and the behaviour was deemed accurately predicted.

  The results obtained from inelastic analyses show that the analytical solution matched that obtained from the numerical models almost perfectly, including the general shape of the results, developed yield points, and stiffnesses.
- CD approach was verified against numerical models, indicating that the yield hierarchy and the applied shear force matched perfectly when the hold-down yielded. Additionally, the applicability of the approach to multi-storey buildings was proved by conducting a case study for a two-storey shearwall and using the mechanical properties for connections obtained from Chapter 5.
- A reasonable match was found in terms of the general behaviour and the shape of the curves for all walls when the numerical models were compared with the experimental results. The discrepancy in terms of the maximum and yield forces was within an acceptable range while slightly higher differences were observed for the displacements corresponding to these forces.
- The results from the analytical model showed that the maximum lateral force could be predicted with acceptable accuracy, while for the initial elastic stiffness, k_e, greater differences were observed, especially for CP models. This discrepancy could be attributed to using the EEEP idealization curve for panel-to-panel connections. It could be observed that a significantly better fit was obtained for these walls in the numerical model owing to using the real connection curve obtained from the joint-level tests.
- Consistency was observed among all models concerning the yield hierarchy achieved. For walls with CP behaviour, the panel-to-panel connections yielded before the hold-downs, and for walls with SW, the hold-downs yielded before the panel-to-panel connections. The angle brackets yielded after the hold-downs in both CP and SW models. Predicting the yield hierarchy correctly proved that meeting the proposed CD requirements was needed to achieve CP behaviour and adequate energy dissipation.

Chapter 8 - Conclusions and recommendations

8.1. General

This study examines the behaviour of multi-panel CLT shearwalls subjected to lateral loads. This study developed an analytical approach to predict general behaviour, including wall strength and deflection based on the mechanical properties of the connections. This chapter summarizes the primary findings of the study and propose future research directions.

8.2. Conclusions

The current study draws the following conclusions:

- An analytical method for CLT shearwalls consisting of multiple panels has been developed based on the principle of minimum potential energy. Expressions for CP and SW behaviour were provided in the elastic region, while inelastic for CP behaviour based on initial CP elastic and ultimate CP plastic behaviour was derived.
- As expected, the walls were more likely to remain in CP behaviour when angle brackets behaved bi-directionally, particularly with relatively stiff angle brackets in the vertical direction and/or a greater number of angle brackets. This resulted in less rocking displacement and more lateral resistance of the wall.
- According to the sensitivity analysis, the bi-directional contribution of angle brackets may be neglected if relatively flexible angle brackets are used, while maintaining CP behaviour. For SW behaviour, angle brackets need to include bi-directional behaviour since ignoring this effect would lead to relatively significant errors.
- Design expressions for the shearwall strength associated with different connections were developed in terms of bending moment and shear with emphasis on including the bi-directional contribution of angle brackets. A capacity-based design procedure, which promotes predominantly rocking behaviour and optimizes energy dissipation in the shearwall system, was proposed.
- To ensure adequate energy dissipation in the shearwall, a yield hierarchy was provided among the various connections. It is necessary to define different

resistance percentiles for panel-to-panel connections to ensure the intended yield hierarchy and to prevent failure in the non-dissipative elements. At the building level, a capacity-based design procedure was also proposed to achieve uniform energy dissipation along the height of the structure. To accomplish this, it is necessary to limit the ratios between over-capacity coefficients on adjacent floors to a defined range.

- Different conventional connections used in CLT shearwalls were tested under monotonic and cyclic loading, including hold-down, angle brackets, and panel-to-panel connections. The performance and mechanical properties of each connection type were evaluated, and comparisons between various configurations were discussed.
- The elastic and inelastic analytical expressions were verified in both major kinematic ranges, CP and SW, against various numerical models, and the behaviour was deemed accurately predicted. Additionally, a capacity-based approach was verified against numerical models, indicating that the proposed requirements matched with high accuracy. A case study of a two-storey building composed of multi-panel CLT shearwalls was also presented to show the applicability of the developed CD expressions to multi-storey applications.
- Full-scale experimental tests were conducted on CLT shearwalls with connection types and configurations similar to those tested at the component level. All walls exhibited the expected kinematic modes based on preliminary numerical models, emphasizing the accuracy of the developed expressions. Comparing the results with analytical and numerical models showed that satisfying the developed expressions provided high accuracy in predicting the behaviour of multi-panel CLT walls. Despite a reasonable match for the SW behaviour, some discrepancy was observed for the CP behaviour since both hold-down and panel-to-panel connections were engaged in the behaviour. Using the EEEP idealization curve for panel-to-panel connections was identified as one source of discrepancy.
- Consistency was achieved for all models when the yield hierarchy was evaluated. For walls with CP behaviour, the panel-to-panel connections yielded before the hold-downs, and for walls with SW, the hold-downs yielded before the panel-to-

panel connections. In all cases, the angle brackets yielded after both hold-downs and panel to panel joints. It was also shown that satisfying the proposed capacity-based requirements was needed to achieve the desired behaviour involving high energy dissipation.

8.3. Recommendations for future studies

Following are recommendations for future studies based on the observations and results obtained from the current study:

- In light of the complexity of SW behaviour equations and the difficulty in obtaining closed form solutions when the bi-directional contribution of angle brackets is included, it is recommended that sensitivity and parametric studies be conducted to develop simplified equations with acceptable accuracy.
- It is recommended that experimental tests and numerical modeling be undertaken of walls subjected to cyclic loads to further investigate the CD requirements. In these studies, the main aim would be to obtain optimal and realistic values of overstrength factors by investigating different connections and wall configurations.
- Related to the previous recommendation, an extensive experimental campaign on conventional panel-to-panel connections is suggested. These tests would include all possible generic panel-to-panel connection types to establish appropriate values for overstrength factors at different percentiles. These values could then be incorporated into the Canadian design standard as an alternative to the more rigorous capacity-based design approach.
- It is recommended to conduct a study focusing on developing hold-down connections with high energy-dissipative capabilities and higher ultimate displacement. Such connection is expected to provide an increase in the general energy dissipation of the wall assembly and enhanced deformation capacity.
- It is important to study floors' contribution, including the connections between them and shearwalls. That effect might be developed as analytical expressions and added to the developed expressions provided in the current study. Experimental investigations on CLT shearwalls with floors could be used to investigate this contribution in-depth and validate the newly derived expressions.

- Experimental and numerical models could be used to investigate analytical expressions for multi-storey applications. By comparing the results obtained from these methods with those developed in this study, important discussions could be initiated.

References

A. Ceccotti, & M. Follesa. (2006). Seismic Behaviour of Multi-Storey XLam Buildings. *International Workshop on "Earthquake Engineering on Timber Structures*, 81–95.

ANSI/APA. (2020). ANSI/APA PRG 320:2019 Standard for Performance-Rated Cross-Laminated Timber. *APA- The Engineered Wood Association*.

ASTM E2126. (2019). *Standard test methods for cyclic (reversed) load test for shear resistance of vertical elements of the lateral force resisting systems for buildings*.

Blomgren, H.-E., Pei, S., Jin, Z., Powers, J., Dolan, J. D., van de Lindt, J. W., Barbosa, A. R., & Huang, D. (2019). Full-Scale Shake Table Testing of Cross-Laminated Timber Rocking Shear Walls with Replaceable Components. *Journal of Structural Engineering*, *145*(10). https://doi.org/10.1061/(ASCE)ST.1943-541X.0002388

Brandner, R., Dietsch, P., Dröscher, J., Schulte-Wrede, M., Kreuzinger, H., & Sieder, M. (2017a). Cross laminated timber (CLT) diaphragms under shear: Test configuration, properties and design. *Construction and Building Materials*, *147*, 312–327. https://doi.org/10.1016/j.conbuildmat.2017.04.153

Brandner, R., Dietsch, P., Dröscher, J., Schulte-Wrede, M., Kreuzinger, H., & Sieder, M. (2017b). Cross laminated timber (CLT) diaphragms under shear: Test configuration, properties and design. *Construction and Building Materials*, *147*, 312–327. https://doi.org/10.1016/j.conbuildmat.2017.04.153

Canadian Commission on Building and Fire Codes. (2022). *National Building Code of Canada* (2020th ed.). National Research Council of Canada.

Casagrande, D., Doudak, G., Mauro, L., & Polastri, A. (2018). Analytical Approach to Establishing the Elastic Behavior of Multipanel CLT Shear Walls Subjected to Lateral Loads. *Journal of Structural Engineering*, *144*(2), 04017193. https://doi.org/10.1061/(ASCE)ST.1943-541X.0001948

Casagrande, D., Doudak, G., & Polastri, A. (2019). A proposal for the capacity-design at wall- and building-level in light-frame and cross-laminated timber buildings. *Bulletin*

of Earthquake Engineering, *17*(6), 3139–3167. https://doi.org/10.1007/s10518-019-00578-4

Casagrande, D., Fanti, R., Doudak, G., & Polastri, A. (2021). Experimental and numerical study on the mechanical behaviour of CLT shearwalls with openings. *Construction and Building Materials*, *298*, 123858. https://doi.org/10.1016/j.conbuildmat.2021.123858

Casagrande, D., Polastri, A., Sartori, T., Loss, C., & Chiodega, M. (2016). Experimental campaign for the mechanical characterization of connection systems in the seismic design of timber buildings. *World Conference on Timber Engineering (WCTE)*.

Casagrande, D., Rossi, S., Sartori, T., & Tomasi, R. (2016). Proposal of an analytical procedure and a simplified numerical model for elastic response of single-storey timber shear-walls. *Construction and Building Materials*, *102*, 1101–1112. https://doi.org/10.1016/j.conbuildmat.2014.12.114

Casagrande, D., Rossi, S., Tomasi, R., & Mischi, G. (2016). A predictive analytical model for the elasto-plastic behaviour of a light timber-frame shear-wall. *Construction and Building Materials*, *102*, 1113–1126. https://doi.org/10.1016/j.conbuildmat.2015.06.025

Ceccotti, A., Sandhaas, C., Okabe, M., Yasumura, M., Minowa, C., & Kawai, N. (2013). SOFIE project - 3D shaking table test on a seven-storey full-scale cross-laminated timber building. *Earthquake Engineering & Structural Dynamics*, *42*(13), 2003–2021. https://doi.org/10.1002/eqe.2309

CSA O86-19. (2019). *Engineering design in wood. CSAO86:19*. CSA Group.

CSI. (2018). *SAP2000 Integrated Software for Structural Analysis and Design* (No. 18). Computers and Structures Inc.

D'Arenzo, G., Casagrande, D., Polastri, A., Fossetti, M., Fragiacomo, M., & Seim, W. (2021a). CLT Shear Walls Anchored with Shear-Tension Angle Brackets: Experimental Tests and Finite-Element Modeling. *Journal of Structural Engineering*,

147(7), (ASCE)ST.1943-541X.0003008. https://doi.org/10.1061/(ASCE)ST.1943-541X.0003008

D'Arenzo, G., Casagrande, D., Polastri, A., Fossetti, M., Fragiacomo, M., & Seim, W. (2021b). CLT Shear Walls Anchored with Shear-Tension Angle Brackets: Experimental Tests and Finite-Element Modeling. *Journal of Structural Engineering*, *147*(7). https://doi.org/10.1061/(ASCE)ST.1943-541X.0003008

D'Arenzo, G., Rinaldin, G., Fossetti, M., & Fragiacomo, M. (2019). An innovative shear-tension angle bracket for Cross-Laminated Timber structures: Experimental tests and numerical modelling. *Engineering Structures*, *197*, 109434. https://doi.org/10.1016/j.engstruct.2019.109434

D'Arenzo, G., Schwendner, S., & Seim, W. (2021). The effect of the floor-to-wall interaction on the rocking stiffness of segmented CLT shear-walls. *Engineering Structures*, *249*, 113219. https://doi.org/10.1016/j.engstruct.2021.113219

Dires, S., & Tannert, T. (2022). Performance of coupled CLT shear walls with internal perforated steel plates as vertical joints and hold-downs. *Construction and Building Materials*, *346*, 128389. https://doi.org/10.1016/j.conbuildmat.2022.128389

EN 1995-1-1:2004/A2. (2013). *Eurocode 5: Design of timber structures*. CEN: European Committee for Standardization.

EN 1998-1. (2014). *Eurocode 8: Design of Structures for Earthquake Resistance*. European Committee for Standardization.

EN 12512. (2005). *Timber structures - Test methods - Cyclic testing of joints made with mechanical fasteners*.

EN 14592. (2022). *Timber structures Dowel type fasteners: Requirements*. European Committee for Standardization (CEN).

European Technical Approval ETA-11/0086. (2018). European Organization for Technical approval.

European Technical Assessment ETA 11/0496. (2014).

European technical assessment ETA-06/0106. (2016).

European Technical Assessment ETA-11/0030. (2019). European Organization for Technical approval.

Flatscher, G., Bratulic, K., & Schickhofer, G. (2015). Experimental tests on cross-laminated timber joints and walls. *Proceedings of the Institution of Civil Engineers - Structures and Buildings*, *168*(11), 868–877. https://doi.org/10.1680/stbu.13.00085

Flatscher, G., & Schickhofer, G. (2015). Shaking-table test of a cross-laminated timber structure. *Proceedings of the Institution of Civil Engineers - Structures and Buildings*, *168*(11), 878–888. https://doi.org/10.1680/stbu.13.00086

Flatscher, G., & Schickhofer, G. (2016). Displacement-based determination of laterally loaded Cross Laminated Timber (CLT) wall systems. *In: INTER - International Network on Timber Engineering Research [INTER/49-12-1]*.

Follesa, M., Fragiacomo, M., Casagrande, D., Tomasi, R., Piazza, M., Vassallo, D., Canetti, D., & Rossi, S. (2018). The new provisions for the seismic design of timber buildings in Europe. *Engineering Structures*, *168*, 736–747. https://doi.org/10.1016/j.engstruct.2018.04.090

Follesa, M., Fragiacomo, M., Vassallo, D., Piazza, M., Tomasi, R., Casagrande, D., & Rossi, S. (2015). A proposal for a new background document of Chapter 8 of Eurocode 8. *2nd. International Network on Timber Engeneering - INTER*.

Fragiacomo, M., Dujic, B., & Sustersic, I. (2011). Elastic and ductile design of multi-storey crosslam massive wooden buildings under seismic actions. *Engineering Structures*, *33*(11), 3043–3053. https://doi.org/10.1016/j.engstruct.2011.05.020

Fragiacomo, M., Follesa, M., Casagrande, D., & Piazza, M. (2019). The revision of the timber chapter of the Eurocode 8. *In Proc., 5th Int. Conf. on Structural Health Assessment of Timber Structures*.

Gavric, I., Fragiacomo, M., & Ceccotti, A. (2013). Capacity seismic design of x-lam wall systems based on connection mechanical properties. *International Council for Research and Innovation in Building and Construction, CIB-W18/46-15-2*.

Gavric, I., Fragiacomo, M., & Ceccotti, A. (2015a). Cyclic behavior of typical screwed connections for cross-laminated (CLT) structures. *European Journal of Wood and Wood Products*, *73*(2), 179–191. https://doi.org/10.1007/s00107-014-0877-6

Gavric, I., Fragiacomo, M., & Ceccotti, A. (2015b). Cyclic behaviour of typical metal connectors for cross-laminated (CLT) structures. *Materials and Structures*, *48*(6), 1841–1857. https://doi.org/10.1617/s11527-014-0278-7

Gavric, I., Fragiacomo, M., & Ceccotti, A. (2015c). Cyclic Behavior of CLT Wall Systems: Experimental Tests and Analytical Prediction Models. *Journal of Structural Engineering*, *141*(11), 04015034. https://doi.org/10.1061/(ASCE)ST.1943-541X.0001246

Hashemi, A., Zarnani, P., Masoudnia, R., & Quenneville, P. (2017). Seismic resistant rocking coupled walls with innovative Resilient Slip Friction (RSF) joints. *Journal of Constructional Steel Research*, *129*, 215–226. https://doi.org/10.1016/j.jcsr.2016.11.016

Himes, A., & Busby, G. (2020). Wood buildings as a climate solution. *Developments in the Built Environment*, *4*, 100030. https://doi.org/10.1016/j.dibe.2020.100030

Hossain, A., Danzig, I., & Tannert, T. (2016). Cross-Laminated Timber Shear Connections with Double-Angled Self-Tapping Screw Assemblies. *Journal of Structural Engineering*, *142*(11). https://doi.org/10.1061/(ASCE)ST.1943-541X.0001572

Hossain, A., Popovski, M., & Tannert, T. (2019). Group Effects for Shear Connections with Self-Tapping Screws in CLT. *Journal of Structural Engineering*, *145*(8). https://doi.org/10.1061/(ASCE)ST.1943-541X.0002357

Hristovski, V., Dujic, B., Stojmanovska, M., & Mircevska, V. (2013). Full-Scale Shaking-Table Tests of XLam Panel Systems and Numerical Verification: Specimen 1. *Journal of Structural Engineering*, *139*(11), 2010–2018. https://doi.org/10.1061/(ASCE)ST.1943-541X.0000754

Hristovski, V., Mircevska, V., Dujic, B., & Garevski, M. (2018). Comparative dynamic investigation of cross-laminated wooden panel systems: Shaking-table tests and

analysis. *Advances in Structural Engineering*, *21*(10), 1421–1436. https://doi.org/10.1177/1369433217749766

ISO 16670. (2003). *Timber structures - Joints made with mechanical fasteners - Quasi-static reversed cyclic test method*.

Izzi, M., Flatscher, G., Fragiacomo, M., & Schickhofer, G. (2016). Experimental investigations and design provisions of steel-to-timber joints with annular-ringed shank nails for Cross-Laminated Timber structures. *Construction and Building Materials*, *122*, 446–457. https://doi.org/10.1016/j.conbuildmat.2016.06.072

Izzi, M., Polastri, A., & Fragiacomo, M. (2018). Modelling the mechanical behaviour of typical wall-to-floor connection systems for cross-laminated timber structures. *Engineering Structures*, *162*, 270–282. https://doi.org/10.1016/j.engstruct.2018.02.045

Jorissen, A., & Fragiacomo, M. (2011). General notes on ductility in timber structures. *Engineering Structures*, *33*(11), 2987–2997. https://doi.org/10.1016/j.engstruct.2011.07.024

Liu, J., & Lam, F. (2018). Experimental test of coupling effect on CLT angle bracket connections. *Engineering Structures*, *171*, 862–873. https://doi.org/10.1016/j.engstruct.2018.05.013

Liu, J., & Lam, F. (2019). Experimental test of coupling effect on CLT hold-down connections. *Engineering Structures*, *178*, 586–602. https://doi.org/10.1016/j.engstruct.2018.10.063

Liu, J., Lam, F., Foschi, R. O., & Li, M. (2020). Modeling the Coupling Effect of CLT Connections under Biaxial Loading. *Journal of Structural Engineering*, *146*(4). https://doi.org/10.1061/(ASCE)ST.1943-541X.0002589

Loo, W. Y., Kun, C., Quenneville, P., & Chouw, N. (2014). Experimental testing of a rocking timber shear wall with slip-friction connectors. *Earthquake Engineering & Structural Dynamics*, *43*(11), 1621–1639. https://doi.org/10.1002/eqe.2413

Loo, W. Y., Quenneville, P., & Chouw, N. (2014). A new type of symmetric slip-friction connector. *Journal of Constructional Steel Research*, *94*, 11–22. https://doi.org/10.1016/j.jcsr.2013.11.005

Lukacs, I., Björnfot, A., & Tomasi, R. (2019). Strength and stiffness of cross-laminated timber (CLT) shear walls: State-of-the-art of analytical approaches. *Engineering Structures*, *178*, 136–147. https://doi.org/10.1016/j.engstruct.2018.05.126

M. P. Lauriola, & C. Sandhaas. (2006). Quasi-Static and Pseudo-Dynamic Tests on XLAM Walls and Buildings. *International Workshop on "Earthquake Engineering on Timber Structures*, 119–133.

Moroder, D., Smith, T., Dunbar, A., Pampanin, S., & Buchanan, A. (2018). Seismic testing of post-tensioned Pres-Lam core walls using cross laminated timber. *Engineering Structures*, *167*, 639–654. https://doi.org/10.1016/j.engstruct.2018.02.075

Myllyviita, T., Soimakallio, S., Judl, J., & Seppälä, J. (2021). Wood substitution potential in greenhouse gas emission reduction–review on current state and application of displacement factors. *Forest Ecosystems*, *8*(1), 42. https://doi.org/10.1186/s40663-021-00326-8

NDS. (2018). *National Design Specification (NDS) for Wood Construction*. American Wood Council.

Nolet, V., Casagrande, D., & Doudak, G. (2019). Multipanel CLT shearwalls: an analytical methodology to predict the elastic-plastic behaviour. *Engineering Structures*, *179*, 640–654. https://doi.org/10.1016/j.engstruct.2018.11.017

Ottenhaus, L.-M., Li, M., Smith, T., & Quenneville, P. (2018). Overstrength of dowelled CLT connections under monotonic and cyclic loading. *Bulletin of Earthquake Engineering*, *16*(2), 753–773. https://doi.org/10.1007/s10518-017-0221-8

Paulay, T., & Priestly, M. J. N. (1992). *Seismic Design of Reinforced Concrete and Masonry Buildings*. John Wiley & Sons, Inc. https://doi.org/10.1002/9780470172841

Polastri, A., Giongo, I., Angeli, A., & Brandner, R. (2018). Mechanical characterization of a pre-fabricated connection system for cross laminated timber structures in seismic

regions. *Engineering Structures*, *167*, 705–715. https://doi.org/10.1016/j.engstruct.2017.12.022

Popovski, M., & Gavric, I. (2016). Performance of a 2-Story CLT House Subjected to Lateral Loads. *Journal of Structural Engineering*, *142*(4). https://doi.org/10.1061/(ASCE)ST.1943-541X.0001315

Popovski, M., Schneider, J., & Schweinsteiger, M. (2010). LATERAL LOAD RESISTANCE OF CROSS-LAMINATED WOOD PANELS. *World Conference on Timber Engineering (WCTE)*.

Pozza, L., Ferracuti, B., Massari, M., & Savoia, M. (2018). Axial – Shear interaction on CLT hold-down connections – Experimental investigation. *Engineering Structures*, *160*, 95–110. https://doi.org/10.1016/j.engstruct.2018.01.021

Pozza, L., Saetta, A., Savoia, M., & Talledo, D. (2017). Coupled axial-shear numerical model for CLT connections. *Construction and Building Materials*, *150*, 568–582. https://doi.org/10.1016/j.conbuildmat.2017.05.141

Pozza, L., Saetta, A., Savoia, M., & Talledo, D. (2018). Angle bracket connections for CLT structures: Experimental characterization and numerical modelling. *Construction and Building Materials*, *191*, 95–113. https://doi.org/10.1016/j.conbuildmat.2018.09.112

Sarti, F., Palermo, A., & Pampanin, S. (2016). Quasi-Static Cyclic Testing of Two-Thirds Scale Unbonded Posttensioned Rocking Dissipative Timber Walls. *Journal of Structural Engineering*, *142*(4). https://doi.org/10.1061/(ASCE)ST.1943-541X.0001291

Schneider, J., Tannert, T., Tesfamariam, S., & Stiemer, S. F. (2018). Experimental assessment of a novel steel tube connector in cross-laminated timber. *Engineering Structures*, *177*, 283–290. https://doi.org/10.1016/j.engstruct.2018.09.058

Shahnewaz, M., Tannert, T., & Popovski, M. (2017). Capacity-based design for cross-laminated timber buildings. *In: Structures Congress*, 400–410.

Sustersic, I., Fragiacomo, M., & Dujic, B. (2012). Influence of the connection behaviour on the seismic resistance of multi-storey crosslam buildings. *In Vol. 2 of Proc., World*

Conf. on Timber Engineering. Architecture and Engineering Case Studies WCTE, 402–410.

Tomasi, R., & Smith, I. (2015). Experimental Characterization of Monotonic and Cyclic Loading Responses of CLT Panel-To-Foundation Angle Bracket Connections. *Journal of Materials in Civil Engineering*, *27*(6). https://doi.org/10.1061/(ASCE)MT.1943-5533.0001144

Wood design manual- commentary CSA O86-19 (9th ed., Vol. 2). (2020). Canadian Wood Council (CWC).

Wrzesniak, D., Rodgers, G. W., Fragiacomo, M., & Chase, J. G. (2016). Experimental testing of damage-resistant rocking glulam walls with lead extrusion dampers. *Construction and Building Materials*, *102*, 1145–1153. https://doi.org/10.1016/j.conbuildmat.2015.09.011

Yasumura, M., Kobayashi, K., Okabe, M., Miyake, T., & Matsumoto, K. (2016). Full-Scale Tests and Numerical Analysis of Low-Rise CLT Structures under Lateral Loading. *Journal of Structural Engineering*, *142*(4). https://doi.org/10.1061/(ASCE)ST.1943-541X.0001348

Appendix A - Details of Connection results

A.1. Test set-ups

In this section, the details of test-ups for connection level, outlined in Chapter 5, are presented. Figure A-1 to Figure A-5 illustrate the test set-ups for hold-down under uplift and shear, angle brackets under uplift and shear, and panel-to-panel connections, respectively.

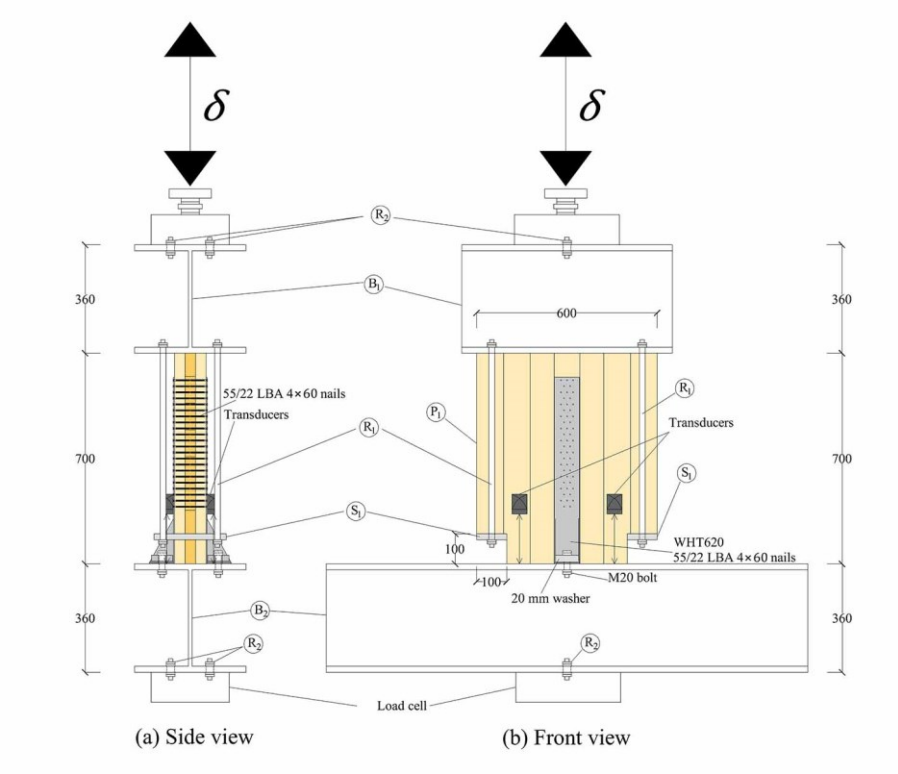

Figure A-1: Test configuration of hold-down WHT620 subjected to uplift

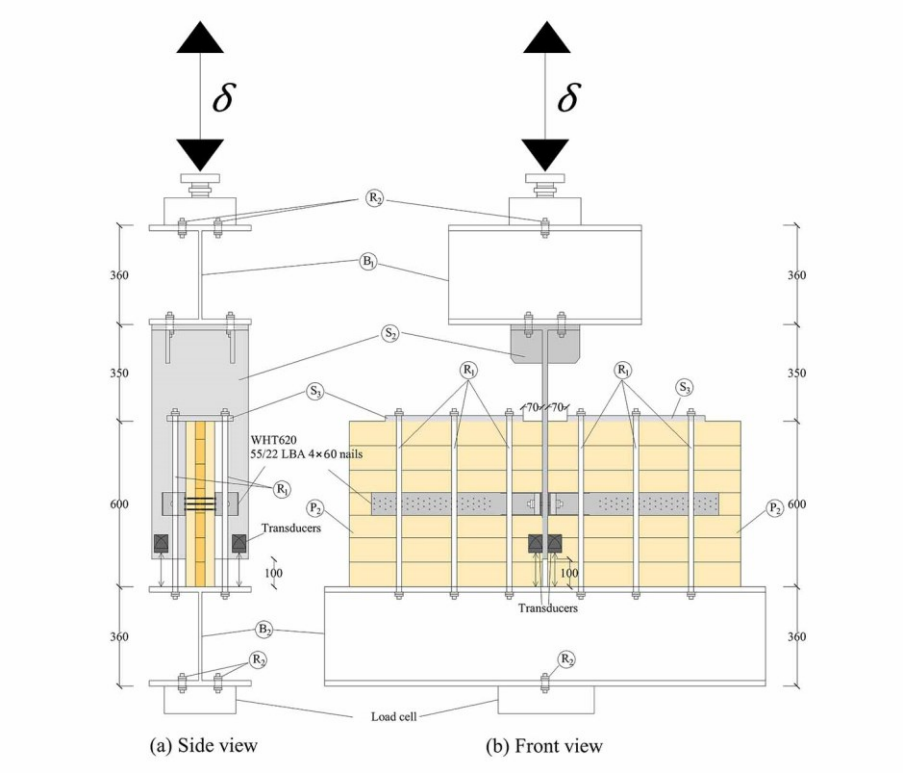

Figure A-2: Test set-up of WHT620 hold-down connection subjected to shear

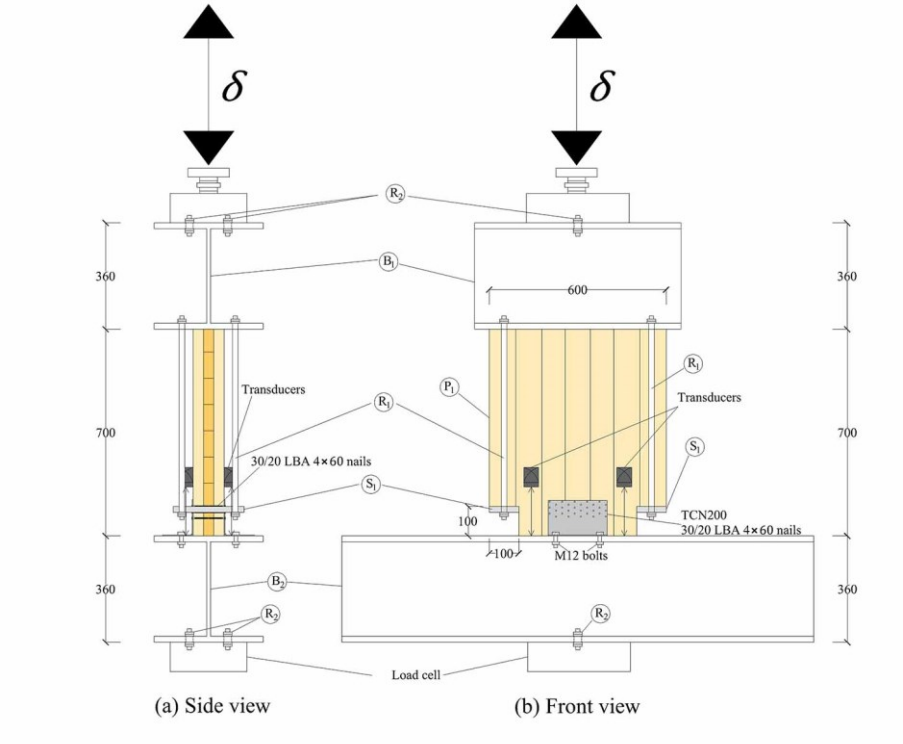

Figure A-3: Test set-up of TCN200 angle bracket connection subjected to uplift

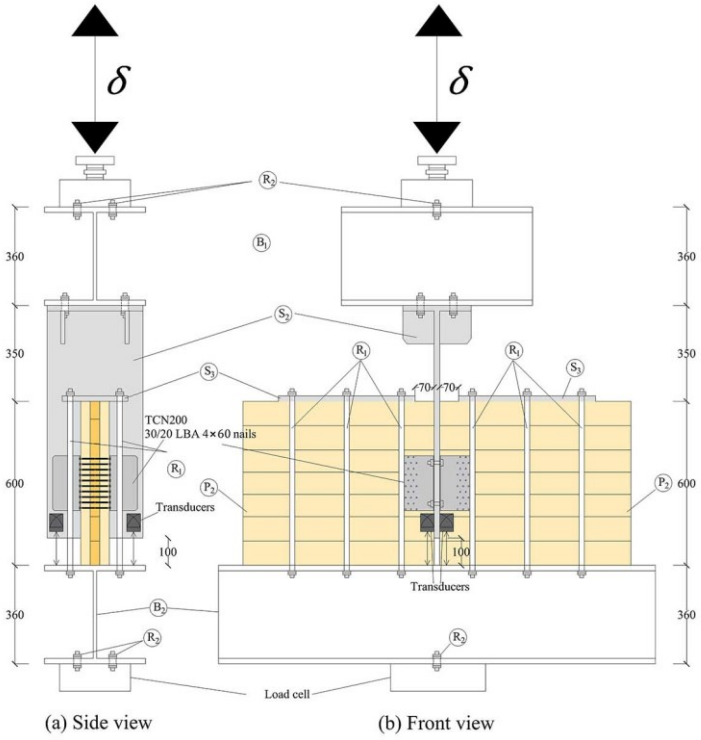

Figure A-4: Test set-up of TCN200 angle bracket connection subjected to shear

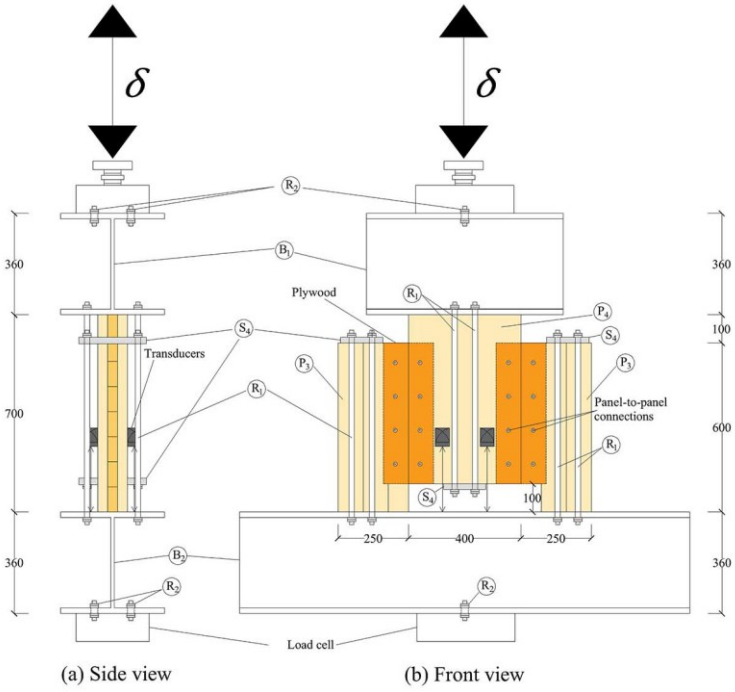

Figure A-5: Test set-up of panel-to-panel connections subjected to shear

In the figures, the components used are named as follows:

- P_1 to P_4: CLT panel specimens, as shown in Figure A-6.
- B_1 and B_2: H steel section top and bottom beams, respectively, as shown in Figure A-7.
- S_1 to S_4: Steel plates and sections, as shown in Figure A-8.
- R_1 to R_2: Steel threaded rods, as shown in Figure A-9.

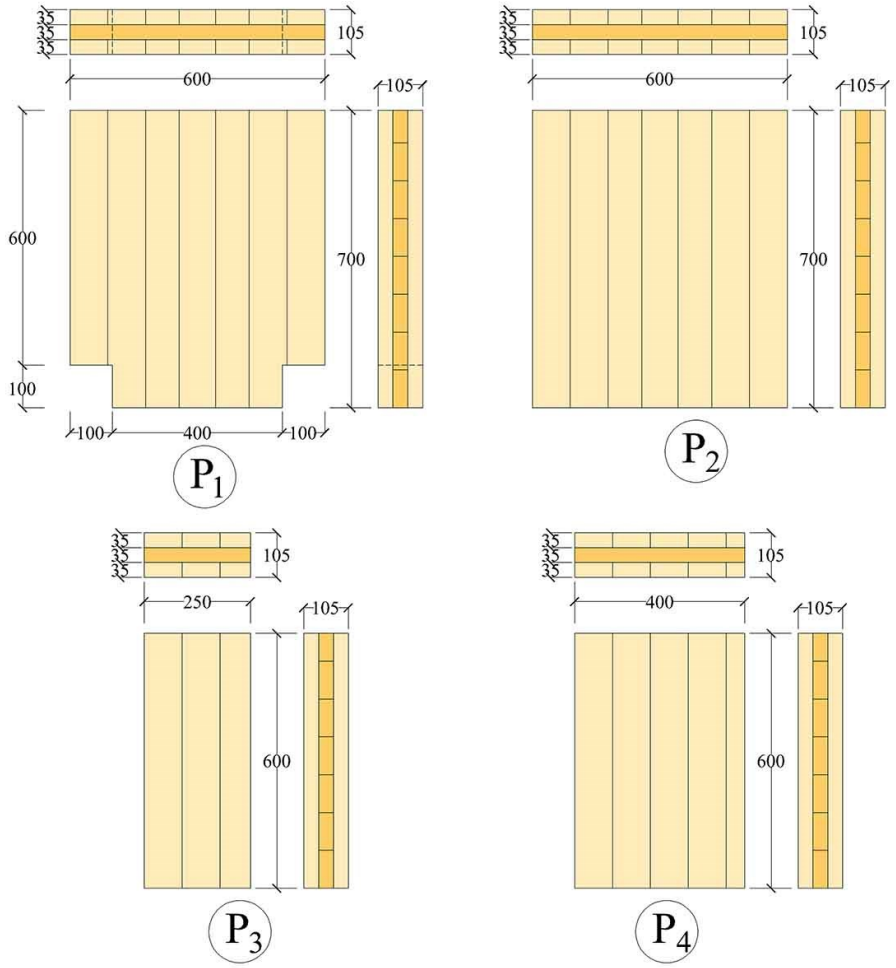

Figure A-6: CLT specimens used in connection-level test set-ups

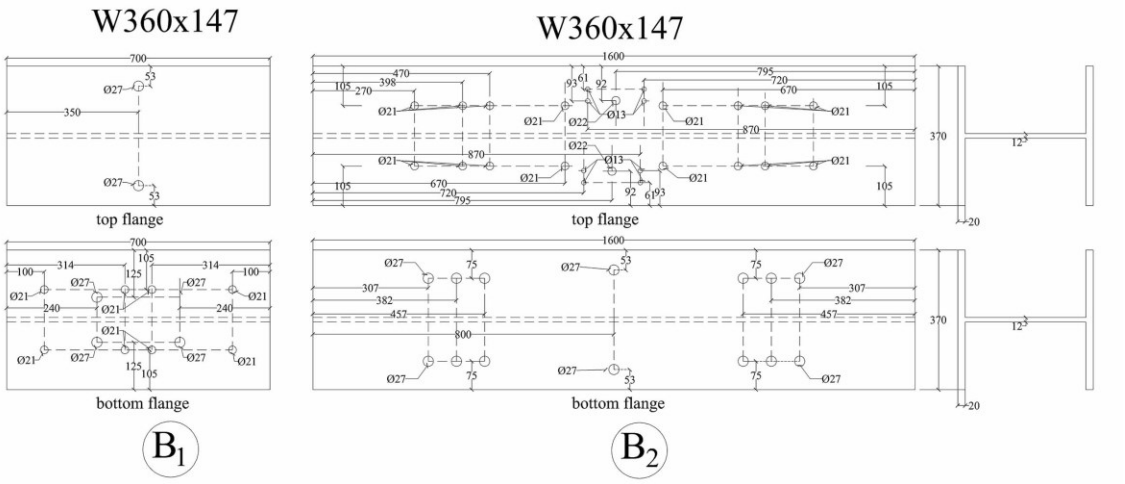

Figure A-7: H steel sections used in connection-level test set-ups

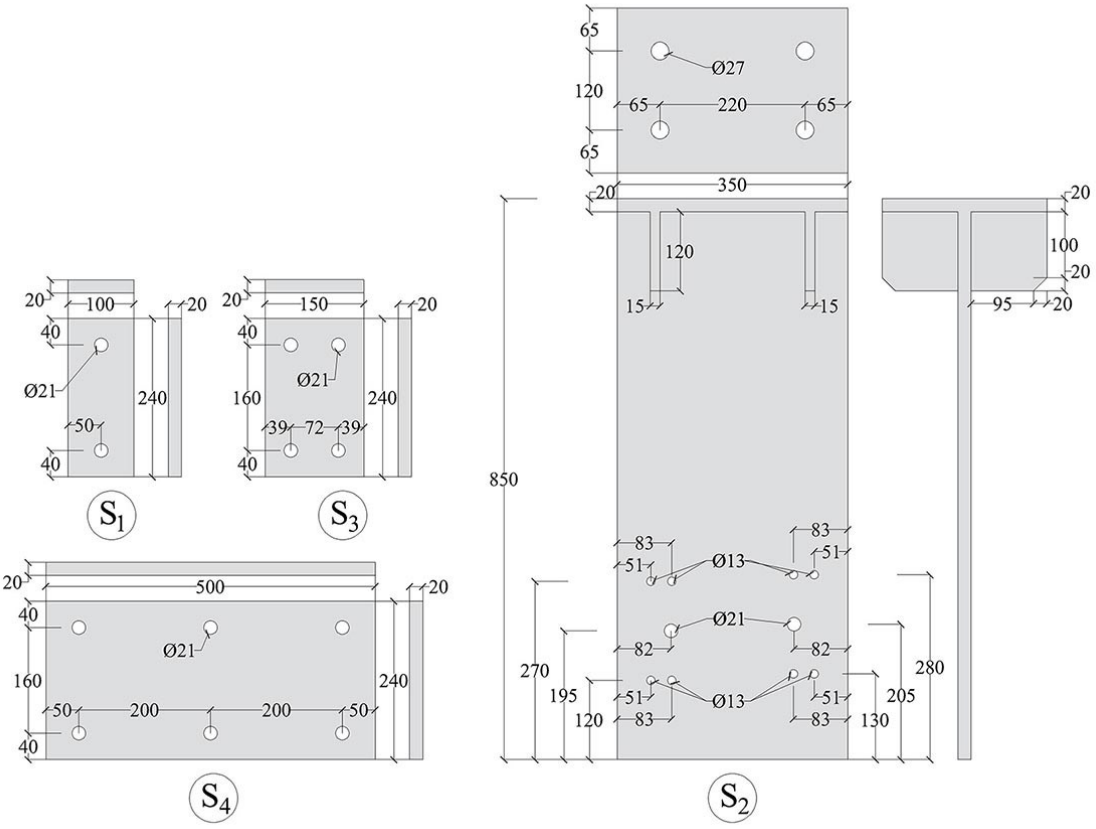

Figure A-8: Steel plates and sections used in connection-level test set-ups

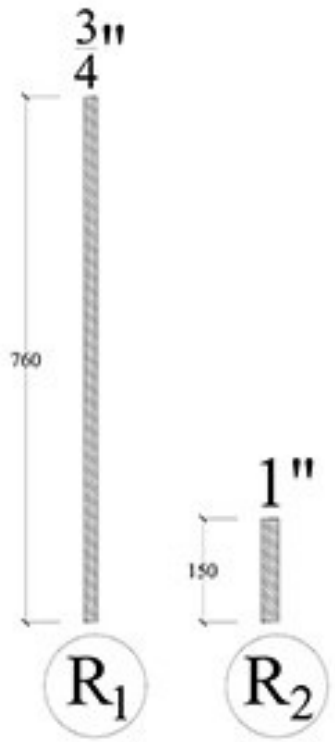

Figure A-9: Steel threaded rods used in connection-level test set-ups

The nomenclature for the test specimens follows the logic outlined in Table A-1, where "X_1" refers to the connection's type, "X_2" indicates the nailing pattern for hold-down and angle brackets and fastener's diameter for panel-to-panel connections, "Y_1" refers to loading type, "Y_2" indicates load protocol, and "Z" refers to test repeat number. As an example, a specimen with a title of A-P-S-C-2 indicates the second test on a partially nailed angle bracket connection under cyclic shear displacement.

Table A-1: Test information of the hold-down tests under vertical tension force

Letter	Description	Variable
X_1	Connection's type	Hold-down: H Angle bracket: A Panel-to-panel connection: P
X_2	Nailing pattern or fastener diameter	Partially nailed hold-down or angle bracket: P Fully nailed hold-down or angle bracket: F panel-to-panel connection's diameter in mm (3.4, 6 or 8)
Y_1	Load type	Tension: T Shear: S
Y_2	Load protocol	Monotonic: M Cyclic: C
Z	Test's number	E.g., test number 3: 3

A.2. Hold-down

A.2.1. Fully nailed under uplift

A.2.1.1 Monotonic

Table A-2: Mechanical properties of fully nailed WHT620 hold-down under monotonic uplift

Parameter	Unit	H-F-T-M-1	H-F-T-M-2	H-F-T-M-3	Mean	CoV
F_{max}	[kN]	96.37	94.49	89.46	93.44	3.82
$v_{F,max}$	[mm]	15.75	14.88	11.82	14.15	14.58
v_u	[kN]	17.27	15.98	18.32	17.19	6.83
$F_{y,EEEP}$	[mm]	91.84	89.82	85.98	89.21	3.33
$v_{y,EEEP}$	[mm]	7.71	7.43	8.82	7.99	9.15
$k_{e,EEEP}$	[kN/mm]	11.91	12.08	9.75	11.25	11.53
$D_{m,EEEP}$	[-]	2.24	2.15	2.08	2.16	3.73
$F_{y,trilinear}$	[kN]	85.34	83.69	84.05	84.36	1.03
$v_{y,trilinear}$	[mm]	7.31	6.92	8.61	7.61	11.62
$k_{e,trilinear}$	[kN/mm]	11.68	12.09	9.76	11.18	11.12
$D_{m,trilinear}$	[-]	2.36	2.31	2.13	2.27	5.42

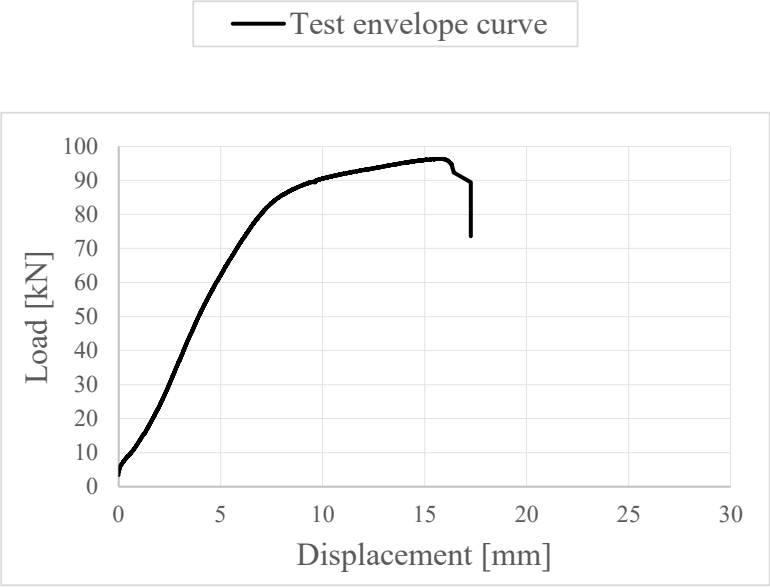

Figure A-10: load-displacement curve of test H-F-T-M-1

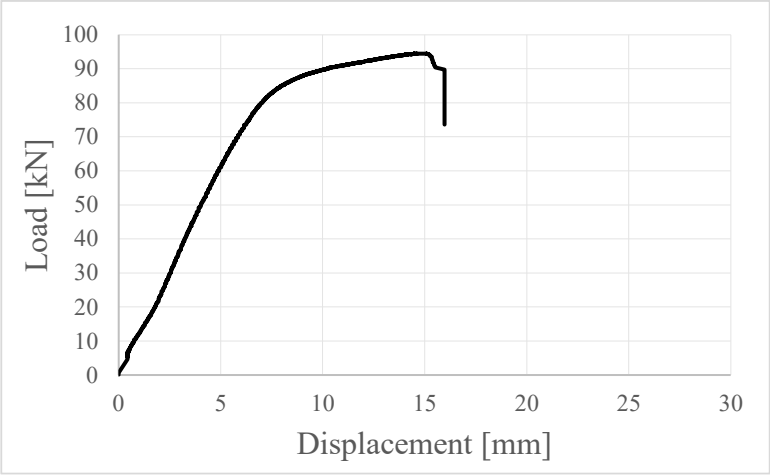

Figure A-11: load-displacement curve of test H-F-T-M-2

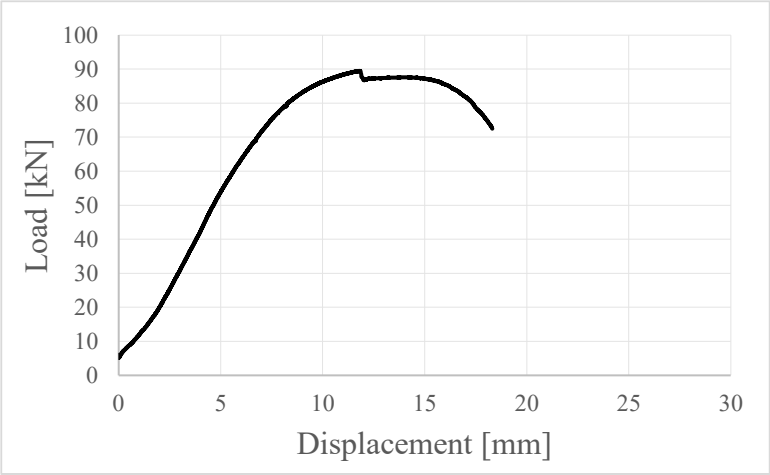

Figure A-12: load-displacement curve of test H-F-T-M-3

A.2.1.2 Cyclic

Table A-3: Mechanical properties of fully nailed WHT620 hold-down under cyclic uplift

Parameter	Unit	H-F-T-C-1	H-F-T-C-2	H-F-T-C-3	Mean	CoV
F_{max}	[kN]	89.78	89.44	93.47	90.90	2.46
$v_{F,max}$	[mm]	13.76	13.32	13.28	13.45	1.99
v_u	[kN]	17.26	16.67	16.86	16.93	1.76
$F_{y,EEEP}$	[mm]	82.36	84.45	88.56	85.12	3.71
$v_{y,EEEP}$	[mm]	5.72	8.02	8.07	7.27	18.47
$k_{e,EEEP}$	[kN/mm]	14.20	10.60	11.17	11.99	16.16
$D_{c,EEEP}$	[-]	3.02	2.08	2.09	2.39	22.49
$F_{y,trilinear}$	[kN]	74.12	80.60	84.28	79.67	6.46
$v_{y,trilinear}$	[mm]	5.14	7.66	7.69	6.83	21.41
$k_{e,trilinear}$	[kN/mm]	14.42	10.53	10.96	11.97	17.82
$D_{c,trilinear}$	[-]	3.36	2.18	2.19	2.58	26.27
ΔF_{1-3}	[%]	4.34	4.68	4.60	4.54	3.89
$v_{eq,1}$	[%]	7.92	7.52	6.55	7.33	9.62
$v_{eq,3}$	[%]	3.58	3.52	2.81	3.30	13.03

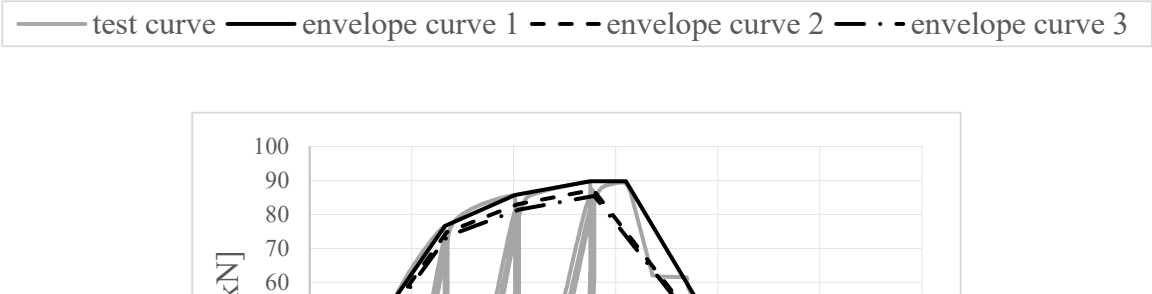

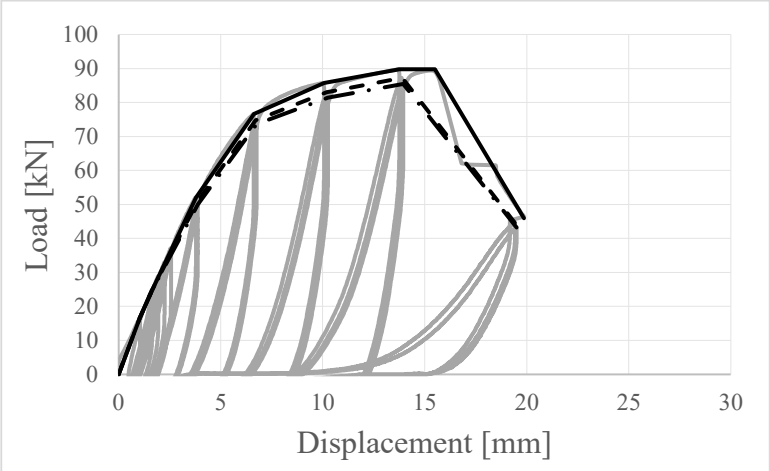

Figure A-13: load-displacement curve of test H-F-T-C-1

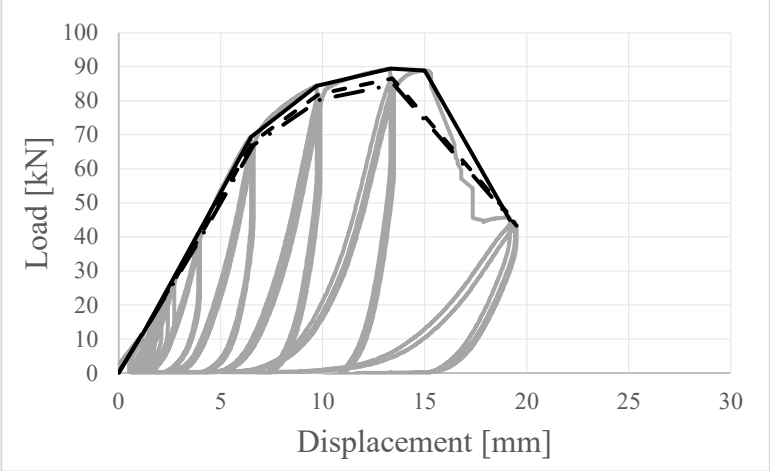

Figure A-14: load-displacement curve of test H-F-T-C-2

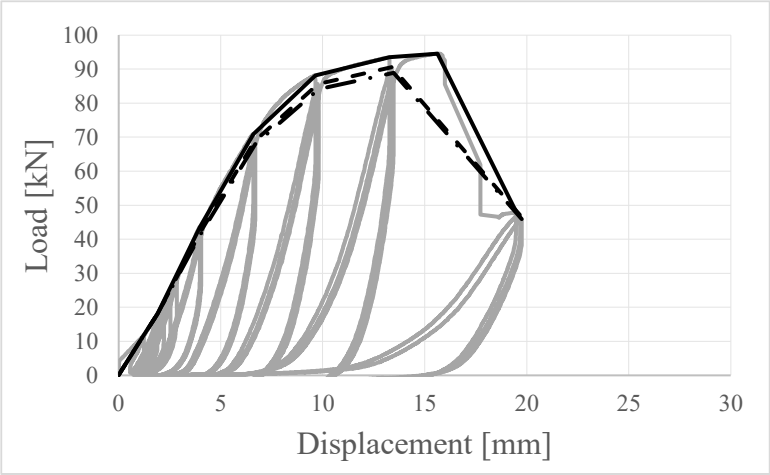

Figure A-15: load-displacement curve of test H-F-T-C-3

A.2.2. Partially nailed under uplift

A.2.2.1 Monotonic

Table A-4: Mechanical properties of partially nailed WHT620 hold-down under monotonic uplift

Parameter	Unit	H-P-T-M-1	H-P-T-M-2	H-P-T-M-3	Mean	CoV
F_{max}	[kN]	92.31	83.92	87.76	88.00	4.77
$v_{F,max}$	[mm]	19.29	14.91	17.46	17.22	12.77
v_u	[kN]	21.70	19.61	19.23	20.18	6.59
$F_{y,EEEP}$	[mm]	85.82	78.01	80.29	81.37	4.94
$v_{y,EEEP}$	[mm]	9.16	9.45	9.76	9.45	3.13
$k_{e,EEEP}$	[kN/mm]	9.36	8.26	8.23	8.62	7.50
$D_{m,EEEP}$	[-]	2.37	2.08	1.97	2.14	9.61
$F_{y,trilinear}$	[kN]	79.50	76.00	77.25	77.59	2.28
$v_{y,trilinear}$	[mm]	8.43	9.19	9.37	9.00	5.55
$k_{e,trilinear}$	[kN/mm]	9.43	8.27	8.24	8.65	7.84
$D_{m,trilinear}$	[-]	2.57	2.13	2.05	2.25	12.46

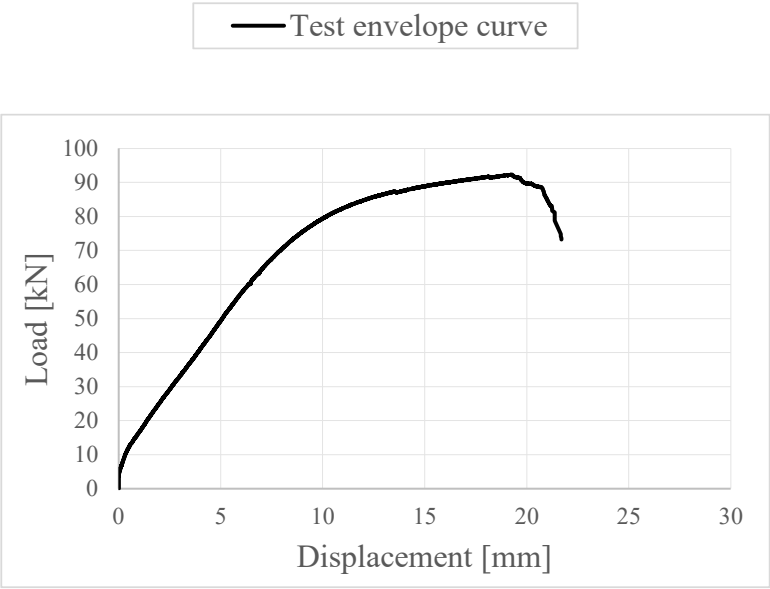

Figure A-16: load-displacement curve of test H-P-T-M-1

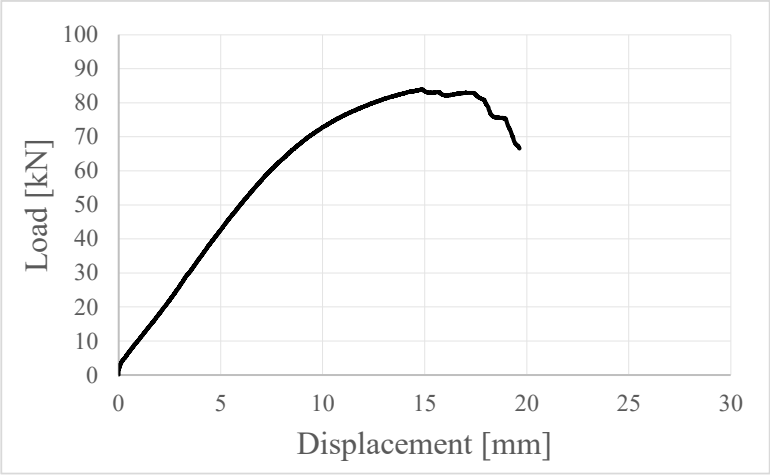

Figure A-17: load-displacement curve of test H-P-T-M-2

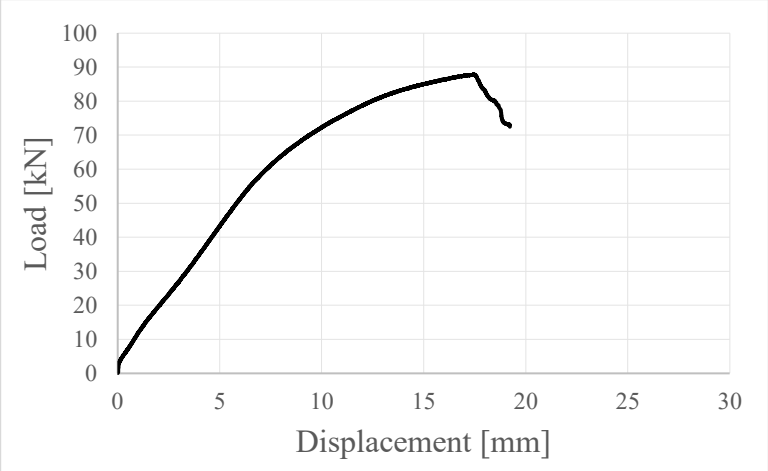

Figure A-18: load-displacement curve of test H-P-T-M-3

A.2.2.2 Cyclic

Table A-5: Mechanical properties of partially nailed WHT620 hold-down under cyclic uplift

Parameter	Unit	H-P-T-C-1	H-P-T-C-2	H-P-T-C-3	Mean	CoV
F_{max}	[kN]	91.59	88.58	91.51	90.56	1.89
$v_{F,max}$	[mm]	18.71	19.41	19.45	19.17	2.11
v_u	[kN]	21.89	20.41	21.95	21.41	4.06
$F_{y,EEEP}$	[mm]	83.57	82.23	83.55	83.12	0.92
$v_{y,EEEP}$	[mm]	8.68	9.31	9.01	9.00	3.52
$k_{e,EEEP}$	[kN/mm]	9.77	8.76	9.08	9.20	5.62
$D_{c,EEEP}$	[-]	2.52	2.19	2.44	2.38	7.17
$F_{y,trilinear}$	[kN]	77.18	79.71	79.81	78.90	1.89
$v_{y,trilinear}$	[mm]	8.02	9.02	8.60	8.55	5.87
$k_{e,trilinear}$	[kN/mm]	9.62	8.83	9.28	9.24	4.26
$D_{c,trilinear}$	[-]	2.73	2.26	2.55	2.51	9.35
ΔF_{1-3}	[%]	7.08	19.11	8.99	11.73	55.09
$v_{eq,1}$	[%]	6.53	6.81	5.36	6.24	12.32
$v_{eq,3}$	[%]	3.66	3.32	2.58	3.19	17.30

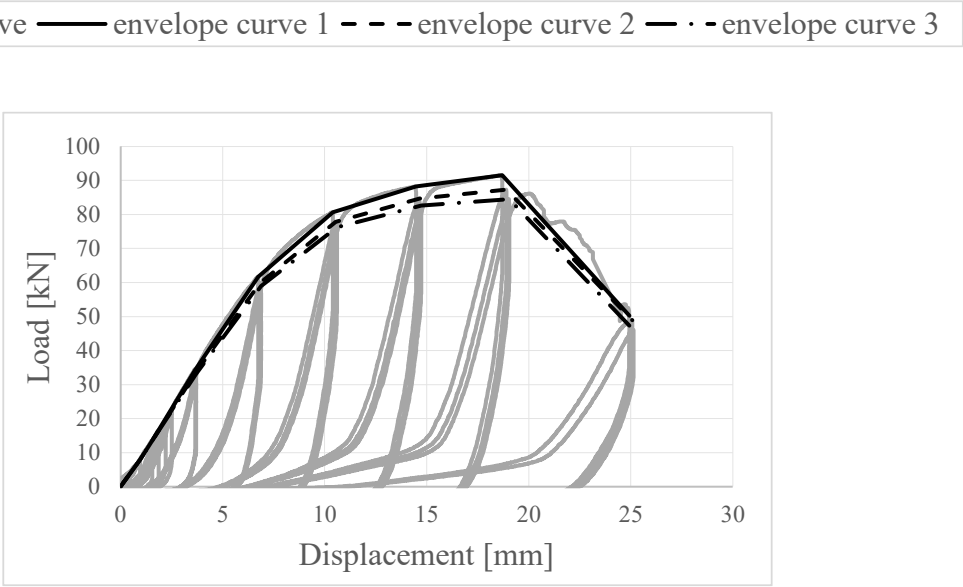

Figure A-19: load-displacement curve of test H-P-T-C-1

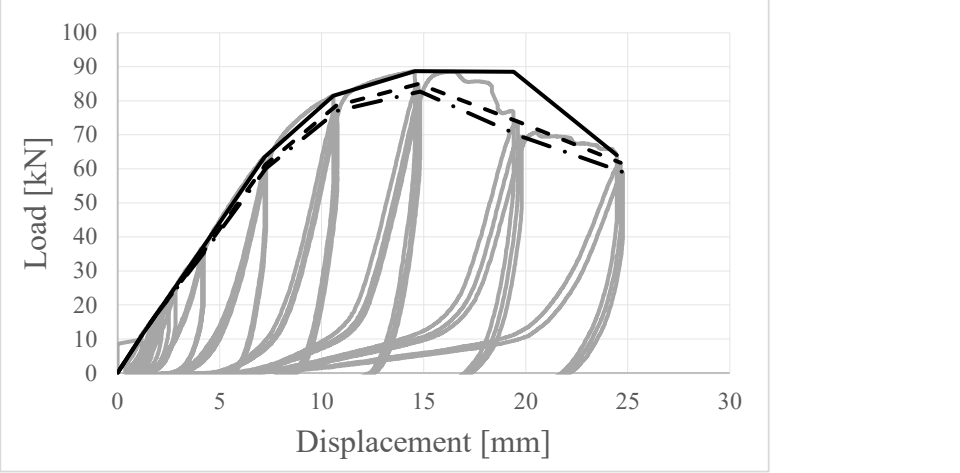

Figure A-20: load-displacement curve of test H-P-T-C-2

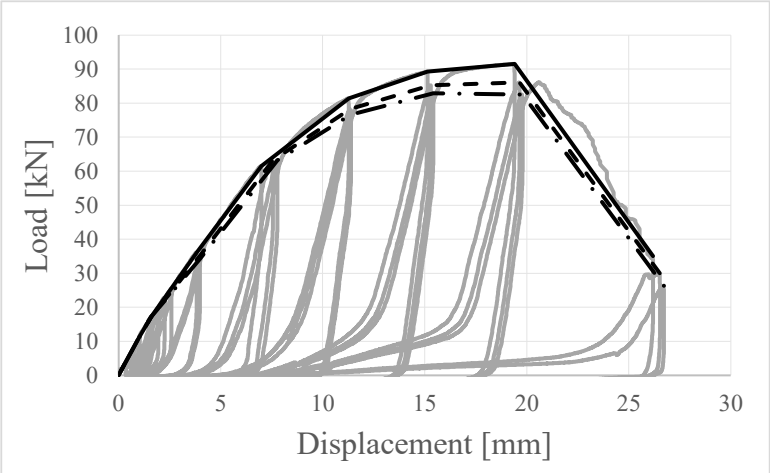

Figure A-21: load-displacement curve of test H-P-T-C-3

A.2.3. Fully nailed under shear

A.2.3.1 Monotonic

Table A-6: Mechanical properties of fully nailed WHT620 hold-down under monotonic shear

Parameter	Unit	H-F-S-M-1	H-F-S-M-2	H-F-S-M-3	Mean	CoV
F_{max}	[kN]	39.03	36.32	45.31	40.22	11.48
$v_{F,max}$	[mm]	61.83	60.47	66.67	62.99	5.18
v_u	[kN]	62.21	63.64	66.70	64.19	3.57
$F_{y,EEEP}$	[mm]	31.50	30.08	39.40	33.66	14.92
$v_{y,EEEP}$	[mm]	40.49	39.32	56.79	45.53	21.45
$k_{e,EEEP}$	[kN/mm]	0.78	0.77	0.69	0.75	6.09
$D_{m,EEEP}$	[-]	1.54	1.62	1.17	1.44	16.38
$F_{y,trilinear}$	[kN]	37.26	34.22	44.91	38.80	14.19
$v_{y,trilinear}$	[mm]	48.77	45.38	65.59	53.25	20.32
$k_{e,trilinear}$	[kN/mm]	0.76	0.75	1.31	0.94	33.73
$D_{m,trilinear}$	[-]	1.28	1.40	0.03	0.90	84.45

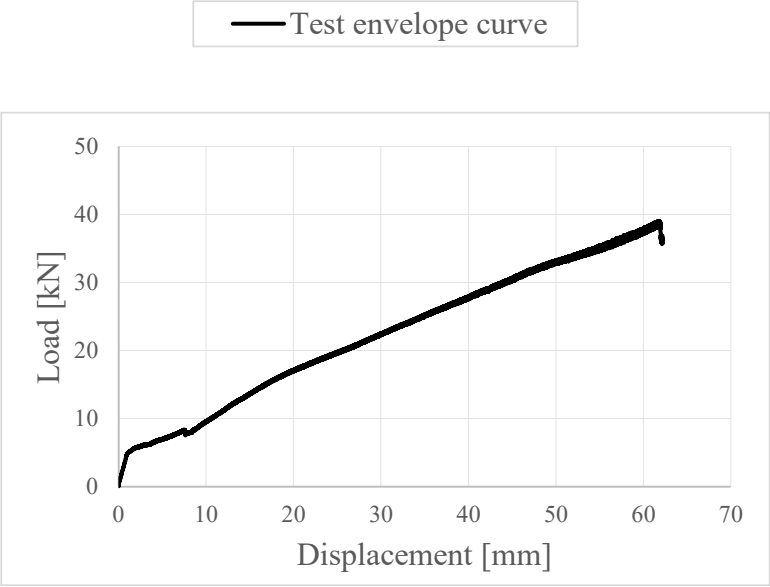

Figure A-22: load-displacement curve of test H-F-S-M-1

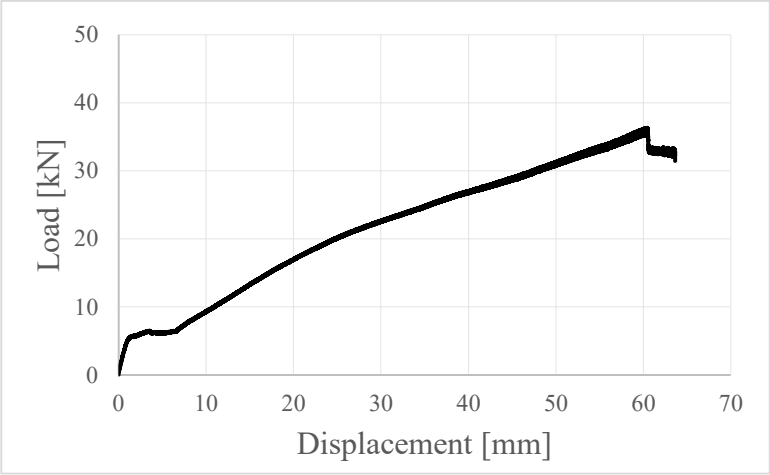

Figure A-23: load-displacement curve of test H-F-S-M-2

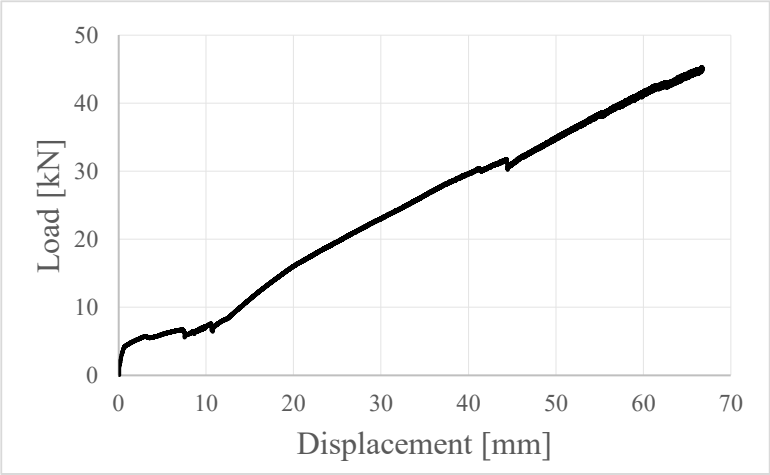

Figure A-24: load-displacement curve of test H-F-S-M-3

A.3. Angle bracket

A.3.1. Fully nailed under uplift

A.3.1.1 Monotonic

Table A-7: Mechanical properties of fully nailed TCN200 angle bracket under monotonic uplift

Parameter	Unit	A-F-T-M-1	A-F-T-M-2	Mean	CoV
F_{max}	[kN]	31.01	31.28	31.14	0.62
$v_{F,max}$	[mm]	33.14	28.28	30.71	11.20
v_u	[kN]	37.31	37.75	37.53	0.82
$F_{y,EEEP}$	[mm]	25.35	25.43	25.39	0.22
$v_{y,EEEP}$	[mm]	7.69	5.97	6.83	17.83
$k_{e,EEEP}$	[kN/mm]	3.86	4.98	4.42	17.99
$D_{m,EEEP}$	[-]	2.39	2.38	2.38	0.44
$F_{y,trilinear}$	[kN]	21.33	18.89	20.11	8.58
$v_{y,trilinear}$	[mm]	6.30	4.22	5.26	27.99
$k_{e,trilinear}$	[kN/mm]	3.38	4.48	3.93	19.65
$D_{m,trilinear}$	[-]	5.92	8.94	7.43	28.78

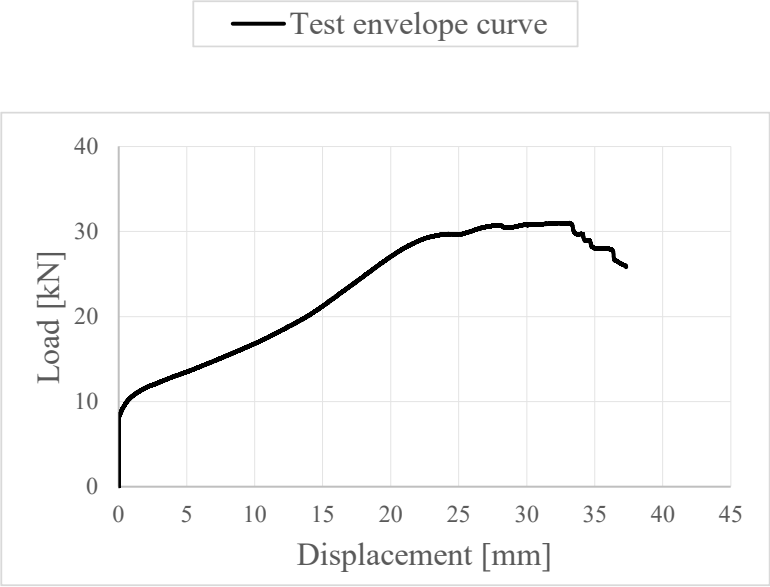

Figure A-25: load-displacement curve of test A-F-T-M-1

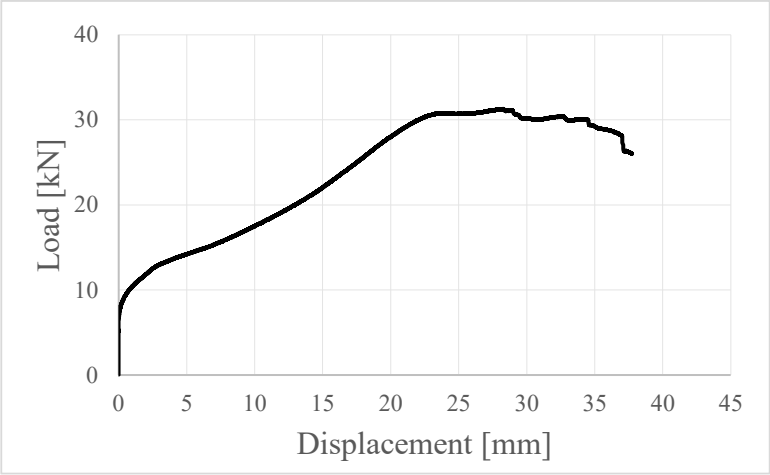

Figure A-26: load-displacement curve of test A-F-T-M-2

A.3.1.2 Cyclic

Table A-8: Mechanical properties of fully nailed TCN200 under cyclic uplift

Parameter	Unit	A-F-T-C-1	A-F-T-C-2	A-F-T-C-3	Mean	CoV
F_{max}	[kN]	32.71	32.97	35.15	33.61	3.99
$v_{F,max}$	[mm]	31.87	31.54	31.24	31.55	0.99
v_u	[kN]	39.81	37.04	36.57	37.81	4.63
$F_{y,EEEP}$	[mm]	27.59	27.44	28.59	27.87	2.25
$v_{y,EEEP}$	[mm]	7.54	7.54	4.32	6.46	28.79
$k_{e,EEEP}$	[kN/mm]	3.42	3.38	6.29	4.37	38.21
$D_{c,EEEP}$	[-]	5.28	4.91	8.47	6.22	31.46
$F_{y,trilinear}$	[kN]	22.40	22.57	12.37	19.11	30.57
$v_{y,trilinear}$	[mm]	6.02	6.10	1.74	4.62	54.06
$k_{e,trilinear}$	[kN/mm]	3.72	3.70	7.12	4.85	40.65
$D_{c,trilinear}$	[-]	6.61	6.07	21.06	11.25	75.59
ΔF_{1-3}	[%]	4.35	4.14	4.83	4.44	8.01
$v_{eq,1}$	[%]	10.24	10.99	11.20	10.81	4.65
$v_{eq,3}$	[%]	8.75	7.79	7.57	8.04	7.83

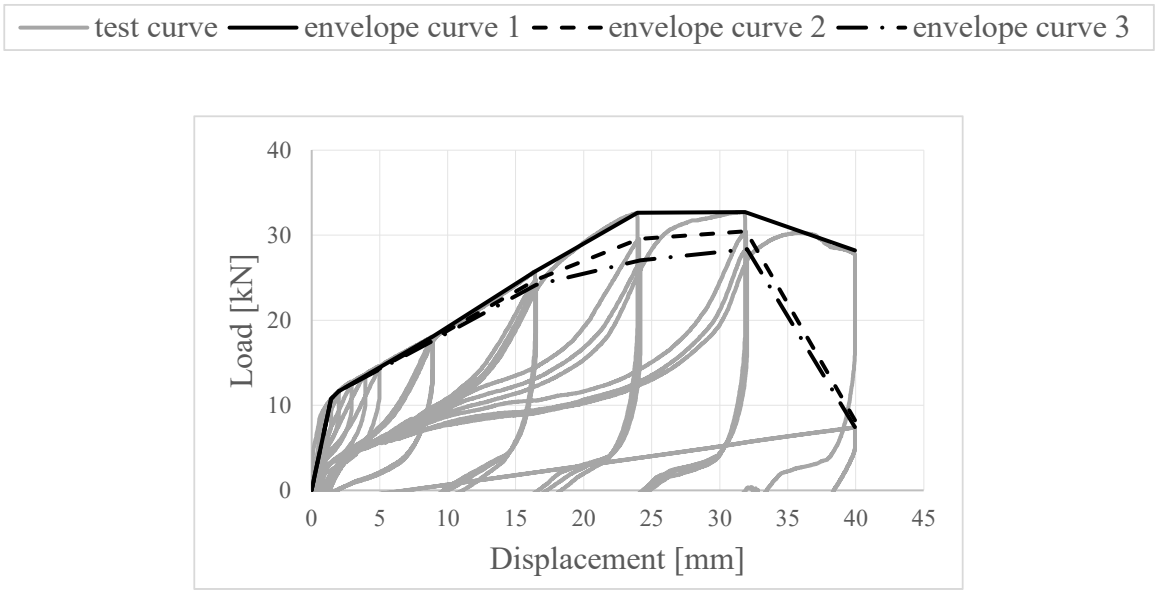

Figure A-27: load-displacement curve of test A-F-T-C-1

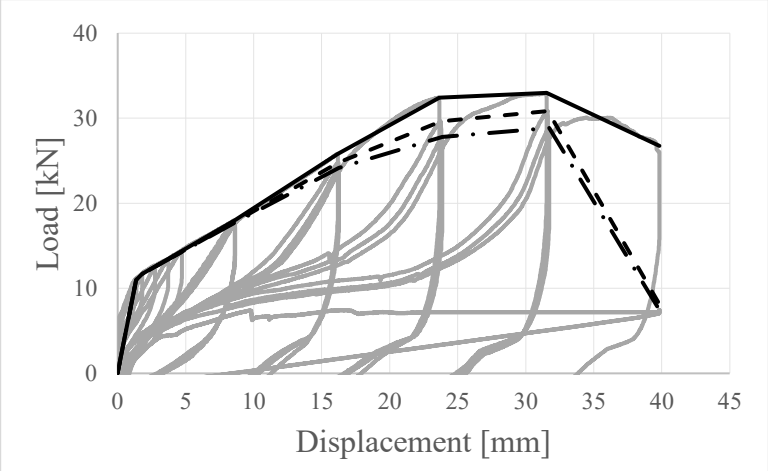

Figure A-28: load-displacement curve of test A-F-T-C-2

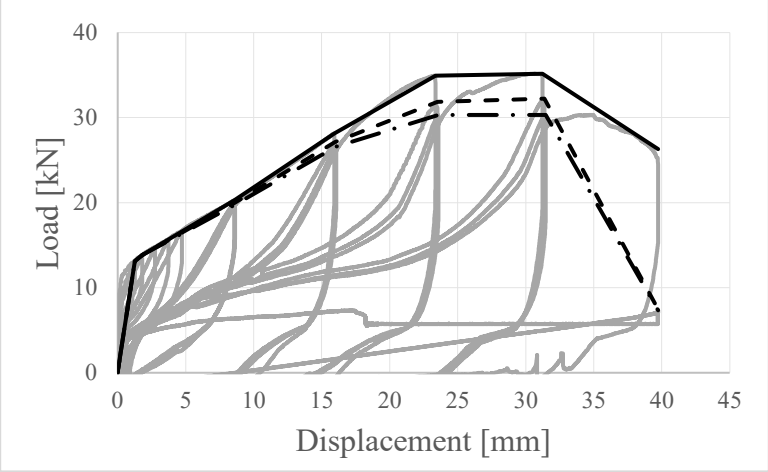

Figure A-29: load-displacement curve of test A-F-T-C-3

A.3.2. Partially nailed under uplift

A.3.2.1 Monotonic

Table A-9: Mechanical properties of partially nailed TCN200 angle bracket under monotonic uplift

Parameter	Unit	A-P-T-M-1	A-P-T-M-2	Mean	CoV
F_{max}	[kN]	28.05	29.13	28.59	2.66
$v_{F,max}$	[mm]	33.55	32.56	33.06	2.13
v_u	[kN]	39.71	41.51	40.61	3.13
$F_{y,EEEP}$	[mm]	27.19	27.57	27.38	0.97
$v_{y,EEEP}$	[mm]	24.60	23.12	23.86	4.38
$k_{e,EEEP}$	[kN/mm]	1.32	1.42	1.37	5.13
$D_{m,EEEP}$	[-]	2.90	2.82	2.86	1.89
$F_{y,trilinear}$	[kN]	27.04	28.08	27.56	2.66
$v_{y,trilinear}$	[mm]	24.45	23.60	24.02	2.50
$k_{e,trilinear}$	[kN/mm]	1.11	1.19	1.15	5.15
$D_{m,trilinear}$	[-]	1.62	1.76	1.69	5.63

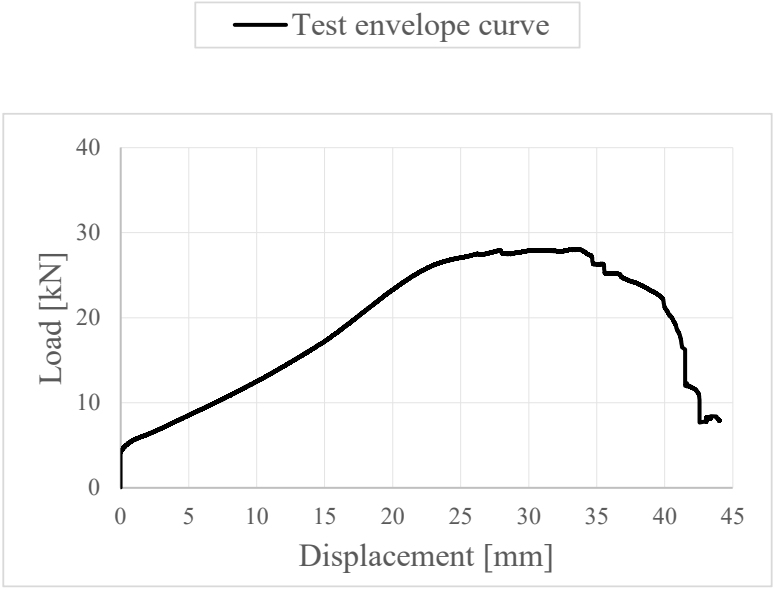

Figure A-30: load-displacement curve of test A-P-T-M-1

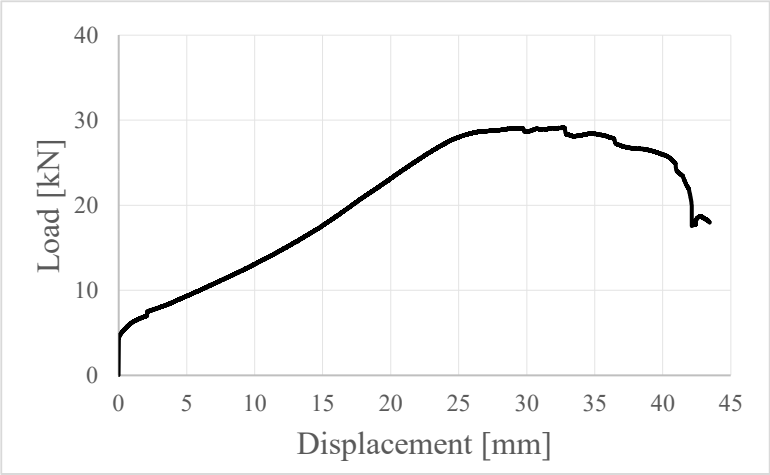

Figure A-31: load-displacement curve of test A-P-T-M-2

A.3.2.2 Cyclic

Table A-10: Mechanical properties of partially nailed TCN200 under cyclic uplift load

Parameter	Unit	A-P-T-C-1	A-P-T-C-2	A-P-T-C-3	Mean	CoV
F_{max}	[kN]	29.39	28.93	29.91	29.41	1.67
$v_{F,max}$	[mm]	31.85	31.49	31.55	31.63	0.62
v_u	[kN]	38.00	38.83	38.11	38.31	1.18
$F_{y,EEEP}$	[mm]	25.97	25.71	26.49	26.06	1.53
$v_{y,EEEP}$	[mm]	16.85	17.76	17.93	17.51	3.32
$k_{e,EEEP}$	[kN/mm]	1.43	1.34	1.37	1.38	3.25
$D_{c,EEEP}$	[-]	2.26	2.19	2.13	2.19	2.97
$F_{y,trilinear}$	[kN]	26.43	26.01	26.90	26.44	1.68
$v_{y,trilinear}$	[mm]	17.17	17.97	18.23	17.79	3.10
$k_{e,trilinear}$	[kN/mm]	1.54	1.45	1.48	1.49	3.17
$D_{c,trilinear}$	[-]	2.21	2.16	2.09	2.15	2.84
ΔF_{1-3}	[%]	3.92	3.84	3.51	3.75	5.85
$v_{eq,1}$	[%]	11.02	10.82	10.85	10.90	0.99
$v_{eq,3}$	[%]	9.20	7.55	9.02	8.59	10.51

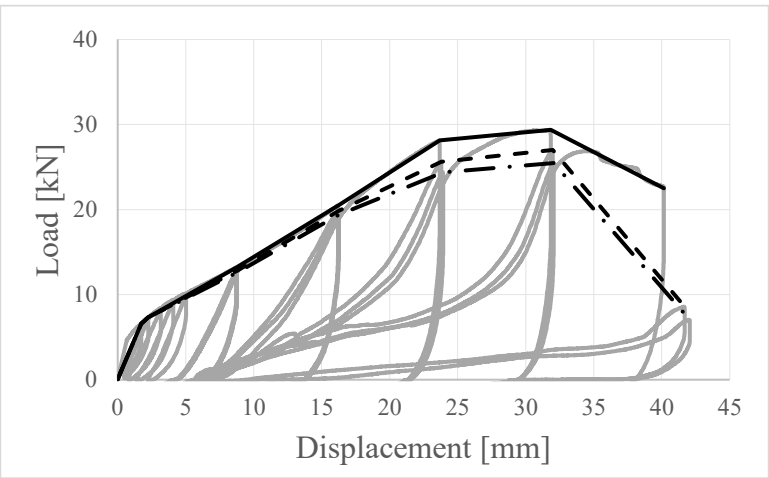

Figure A-32: load-displacement curve of test A-P-T-C-1

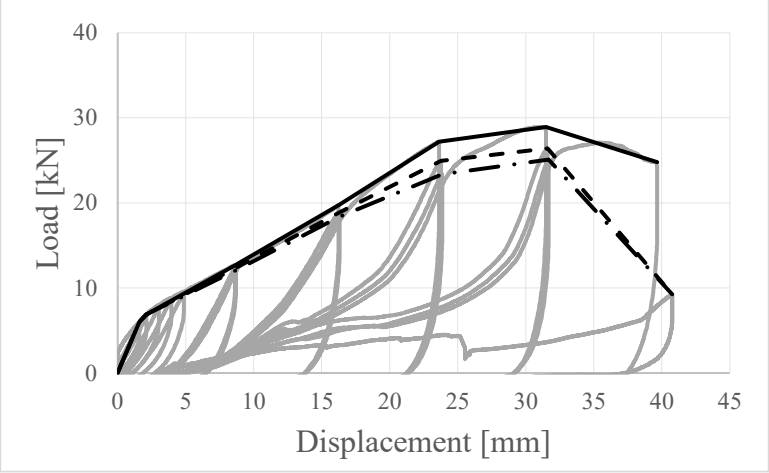

Figure A-33: load-displacement curve of test A-P-T-C-2

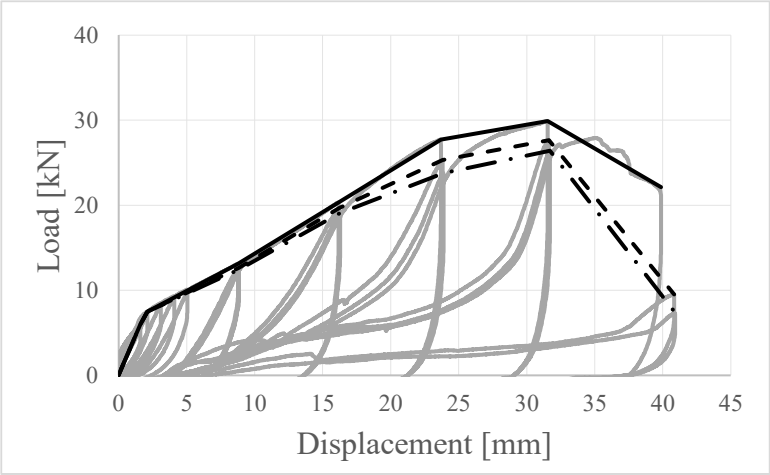

Figure A-34: load-displacement curve of test A-P-T-C-3

A.3.3. Fully nailed under shear

A.3.3.1 Monotonic

Table A-11: Mechanical properties of fully nailed TCN200 angle bracket under monotonic shear

Parameter	Unit	A-F-S-M-1	A-F-S-M-2	A-F-S-M-3	Mean	CoV
F_{max}	[kN]	67.96	69.13	71.64	69.58	2.71
$v_{F,max}$	[mm]	22.86	24.90	22.78	23.51	5.11
v_u	[kN]	36.18	36.23	33.50	35.30	4.42
$F_{y,EEEP}$	[mm]	61.74	63.16	64.28	63.06	2.02
$v_{y,EEEP}$	[mm]	10.49	11.43	11.20	11.04	4.41
$k_{e,EEEP}$	[kN/mm]	6.20	6.21	6.16	6.19	0.41
$D_{m,EEEP}$	[-]	2.39	2.57	2.41	2.46	3.94
$F_{y,trilinear}$	[kN]	57.42	58.72	62.09	59.41	4.05
$v_{y,trilinear}$	[mm]	9.73	10.56	10.79	10.36	5.38
$k_{e,trilinear}$	[kN/mm]	5.90	5.56	5.75	5.74	2.95
$D_{m,trilinear}$	[-]	3.72	3.43	3.10	3.42	8.99

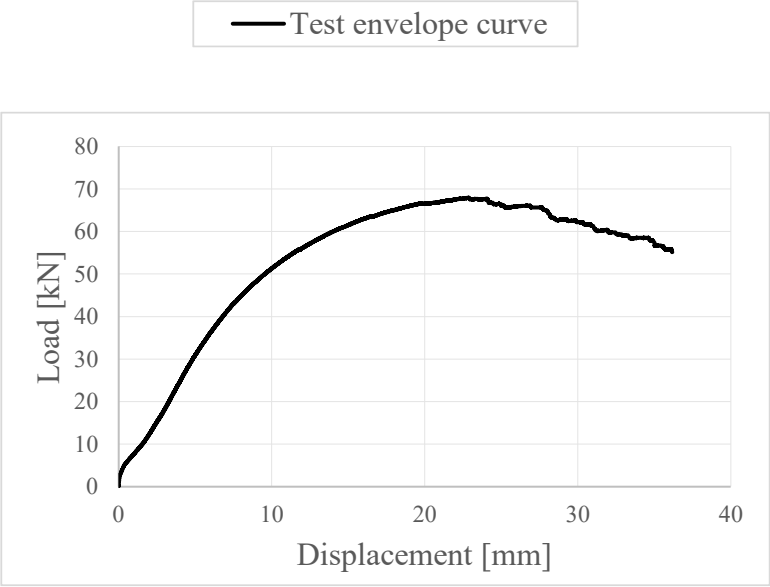

Figure A-35: load-displacement curve of test A-F-S-M-1

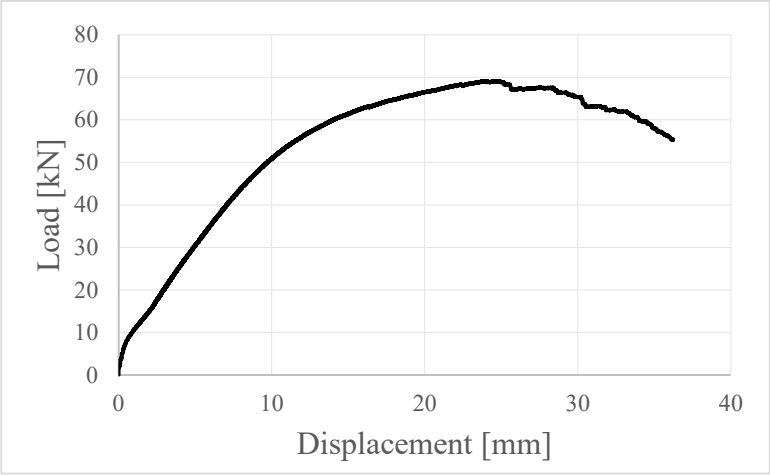

Figure A-36: load-displacement curve of test A-F-S-M-2

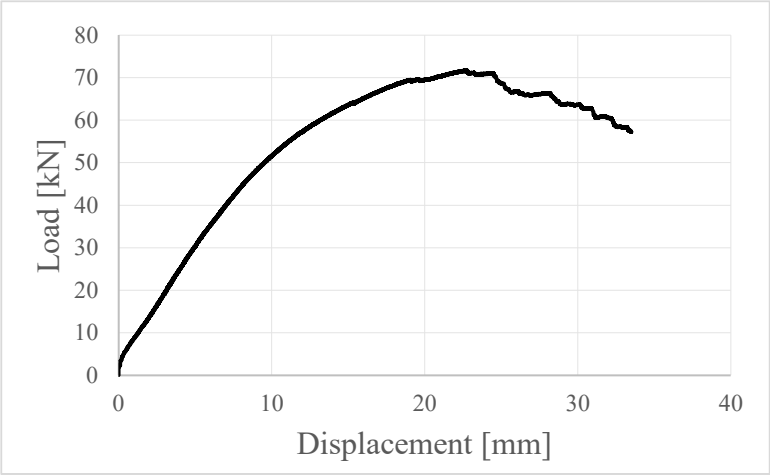

Figure A-37: load-displacement curve of test A-F-S-M-3

A.3.3.2 Cyclic

Table A-12: Mechanical properties of fully nailed TCN200 angle bracket under cyclic shear

Parameter	Unit	A-F-S-C-1	A-F-S-C-2	A-F-S-C-3	Mean	CoV
F_{max}	[kN]	66.03	64.53	68.35	66.31	2.90
$v_{F,max}$	[mm]	21.40	19.34	20.69	20.48	5.12
v_u	[kN]	35.84	33.50	35.11	34.82	3.45
$F_{y,EEEP}$	[mm]	61.15	60.43	64.91	62.16	3.87
$v_{y,EEEP}$	[mm]	10.56	13.65	14.93	13.05	17.22
$k_{e,EEEP}$	[kN/mm]	5.77	4.98	4.75	5.17	10.35
$D_{c,EEEP}$	[-]	3.39	2.45	2.35	2.73	21.03
$F_{y,trilinear}$	[kN]	55.42	59.59	63.54	59.52	6.82
$v_{y,trilinear}$	[mm]	9.57	13.48	14.64	12.57	21.16
$k_{e,trilinear}$	[kN/mm]	5.79	4.42	4.34	4.85	16.84
$D_{c,trilinear}$	[-]	3.75	2.48	2.40	2.88	26.24
ΔF_{1-3}	[%]	18.16	18.73	20.34	19.08	5.93
$v_{eq,1}$	[%]	12.93	13.94	13.28	13.38	3.83
$v_{eq,3}$	[%]	10.37	11.76	11.51	11.21	6.61

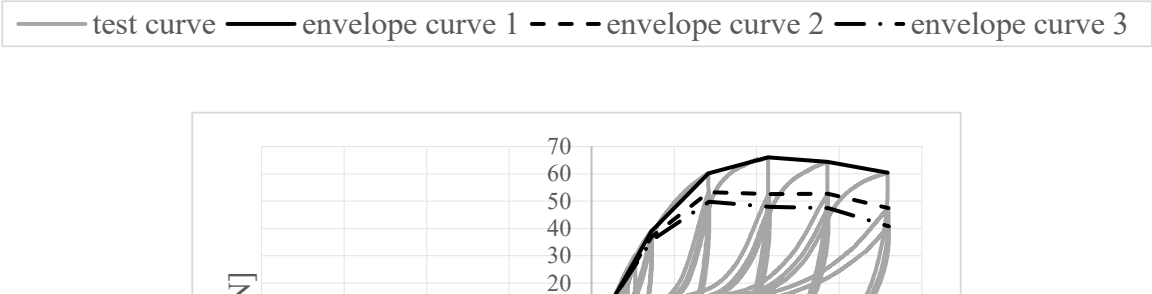

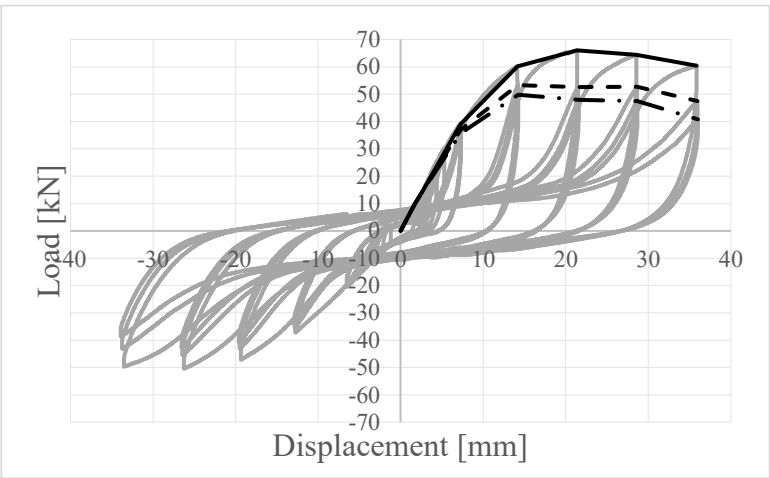

Figure A-38: load-displacement curve of test A-F-S-C-1

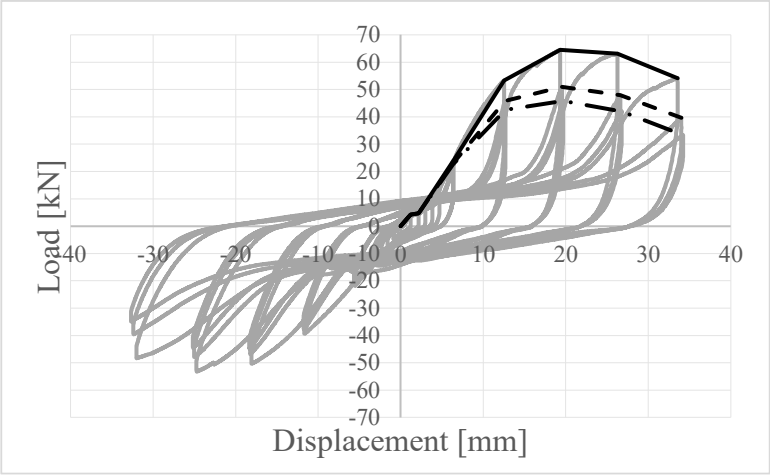

Figure A-39: load-displacement curve of test A-F-S-C-2

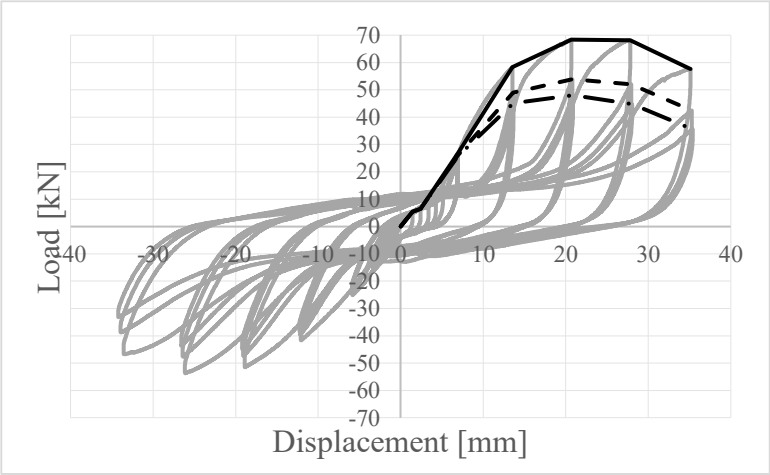

Figure A-40: load-displacement curve of test A-F-S-C-3

A.3.4. Partially nailed under shear

A.3.4.1 Monotonic

Table A-13: Mechanical properties of partially nailed TCN200 angle bracket under monotonic shear

Parameter	Unit	A-P-S-M-1	A-P-S-M-2	A-P-S-M-3	Mean	CoV
F_{max}	[kN]	54.78	49.32	47.33	50.48	7.65
$v_{F,max}$	[mm]	23.00	24.63	18.32	21.98	14.89
v_u	[kN]	27.70	34.25	30.63	30.86	10.63
$F_{y,EEEP}$	[mm]	50.37	45.76	43.25	46.46	7.78
$v_{y,EEEP}$	[mm]	11.68	11.58	9.28	10.85	12.54
$k_{e,EEEP}$	[kN/mm]	4.31	4.42	5.21	4.65	10.56
$D_{m,EEEP}$	[-]	2.37	2.59	2.55	2.51	4.70
$F_{y,trilinear}$	[kN]	48.43	44.30	41.95	44.89	7.31
$v_{y,trilinear}$	[mm]	11.19	11.18	8.97	10.45	12.21
$k_{e,trilinear}$	[kN/mm]	4.33	3.96	4.67	4.32	8.25
$D_{m,trilinear}$	[-]	2.48	3.06	3.41	2.98	15.87

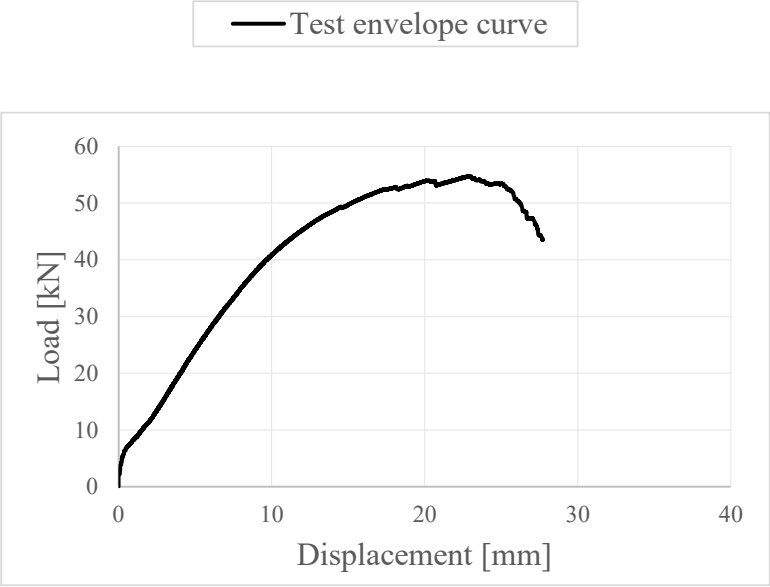

Figure A-41: load-displacement curve of test A-P-S-M-1

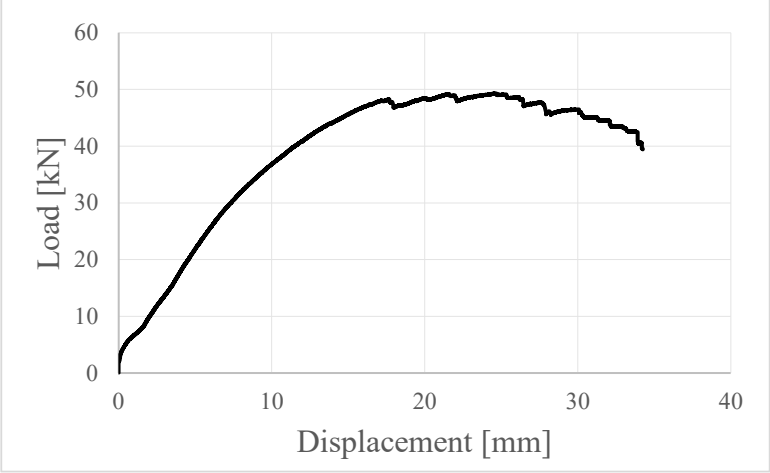

Figure A-42: load-displacement curve of test A-P-S-M-2

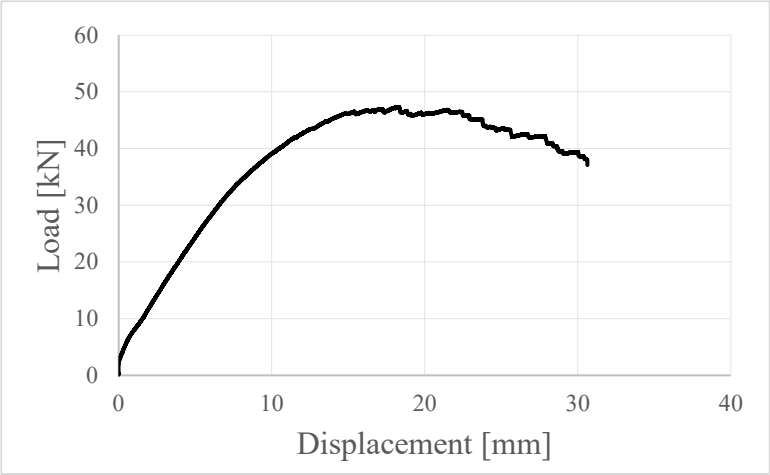

Figure A-43: load-displacement curve of test A-P-S-M-3

A.3.4.2 Cyclic

Table A-14: Mechanical properties of partially nailed TCN200 angle bracket under cyclic shear

Parameter	Unit	A-P-S-C-1	A-P-S-C-2	A-P-S-C-3	Mean	CoV
F_{max}	[kN]	50.75	49.33	52.03	50.70	2.66
$v_{F,max}$	[mm]	18.44	18.50	24.60	20.51	17.26
v_u	[kN]	29.93	29.78	30.97	30.23	2.16
$F_{y,EEEP}$	[mm]	45.44	46.02	49.77	47.08	4.98
$v_{y,EEEP}$	[mm]	8.18	12.35	16.89	12.47	34.92
$k_{e,EEEP}$	[kN/mm]	5.46	3.62	2.89	3.99	33.08
$D_{c,EEEP}$	[-]	3.66	2.41	1.83	2.63	35.40
$F_{y,trilinear}$	[kN]	40.64	45.33	49.77	45.24	10.09
$v_{y,trilinear}$	[mm]	7.30	12.16	16.89	12.11	39.58
$k_{e,trilinear}$	[kN/mm]	7.30	3.73	2.95	4.66	49.80
$D_{c,trilinear}$	[-]	4.10	2.45	1.83	2.79	41.94
ΔF_{1-3}	[%]	13.33	16.49	19.85	16.56	19.68
$v_{eq,1}$	[%]	12.45	13.32	13.69	13.15	4.84
$v_{eq,3}$	[%]	9.81	10.77	11.15	10.58	6.50

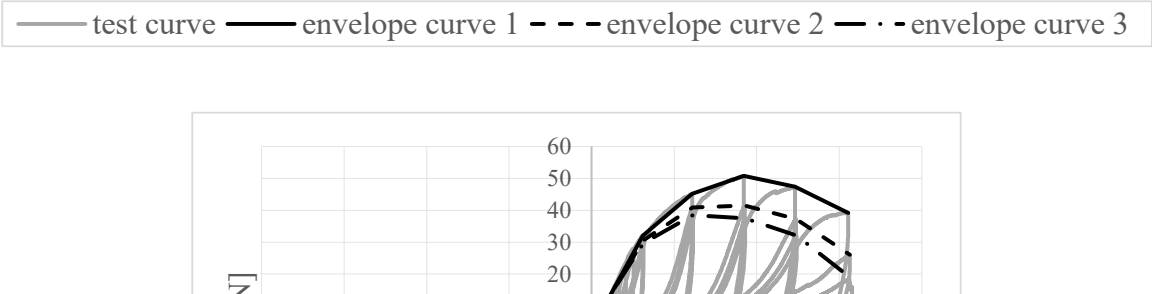

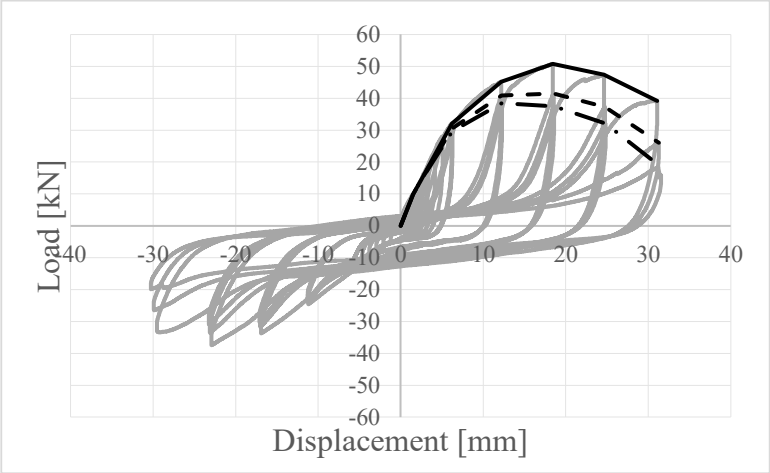

Figure A-44: load-displacement curve of test A-P-S-C-1

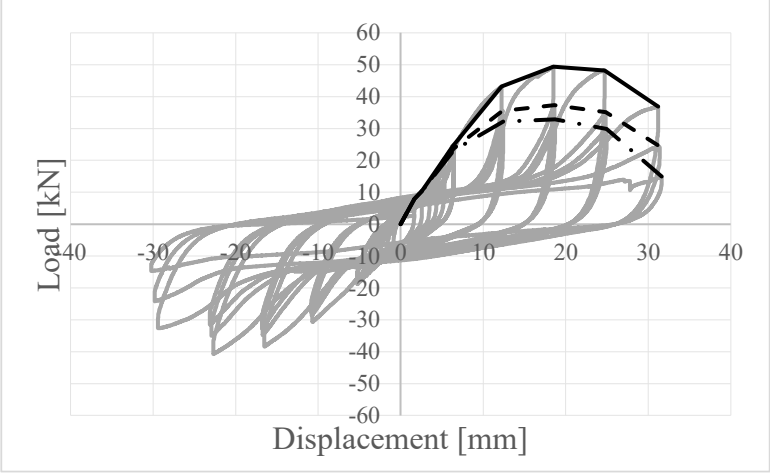

Figure A-45: load-displacement curve of test A-P-S-C-2

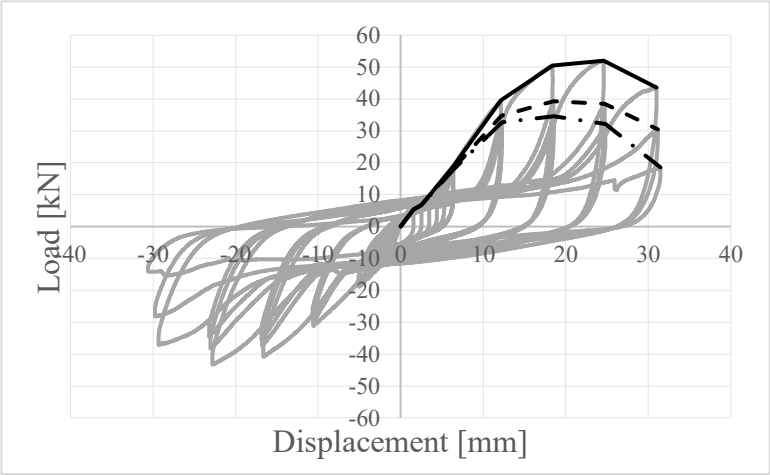

Figure A-46: load-displacement curve of test A-P-S-C-3

A.4. Panel-to-panel connections

A.4.1. HBS 8 × 80 screws under shear

A.4.1.1 Monotonic

Table A-15: Mechanical properties of HBS 8 × 80 screws panel-to-panel connections under monotonic shear

Parameter	Unit	P-8-S-M-1	P-8-S-M-2	P-8-S-M-3	Mean	CoV
F_{max}	[kN]	7.75	7.31	7.36	7.47	3.24
$v_{F,max}$	[mm]	44.88	40.06	44.70	43.21	6.32
v_u	[kN]	57.06	53.94	56.25	55.75	2.90
$F_{y,EEEP}$	[mm]	6.73	6.23	6.33	6.43	4.05
$v_{y,EEEP}$	[mm]	9.65	10.24	10.58	10.16	4.63
$k_{e,EEEP}$	[kN/mm]	0.70	0.61	0.60	0.63	8.52
$D_{m,EEEP}$	[-]	5.91	5.27	5.32	5.50	6.51
$F_{y,trilinear}$	[kN]	4.58	4.44	4.56	4.52	1.69
$v_{y,trilinear}$	[mm]	6.38	6.95	7.31	6.88	6.78
$k_{e,trilinear}$	[kN/mm]	0.72	0.64	0.62	0.66	7.60
$D_{m,trilinear}$	[-]	8.94	7.76	7.70	8.13	8.61

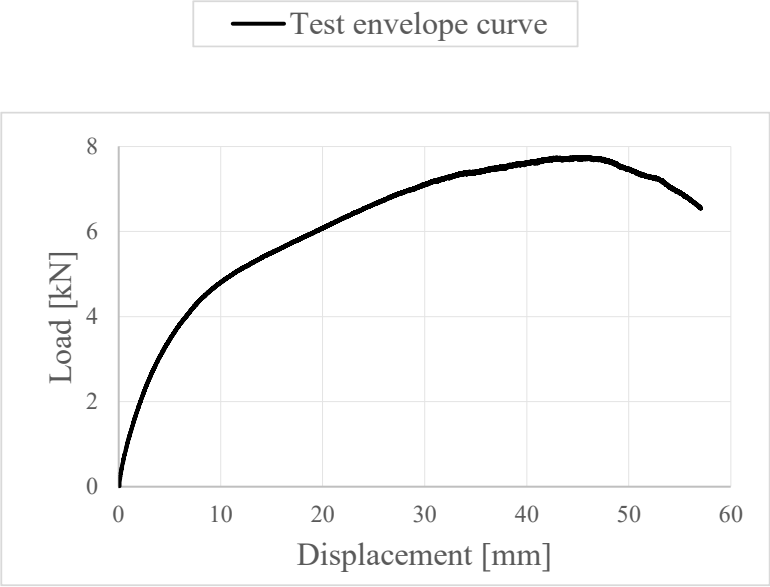

Figure A-47: load-displacement curve of test P-8-S-M-1

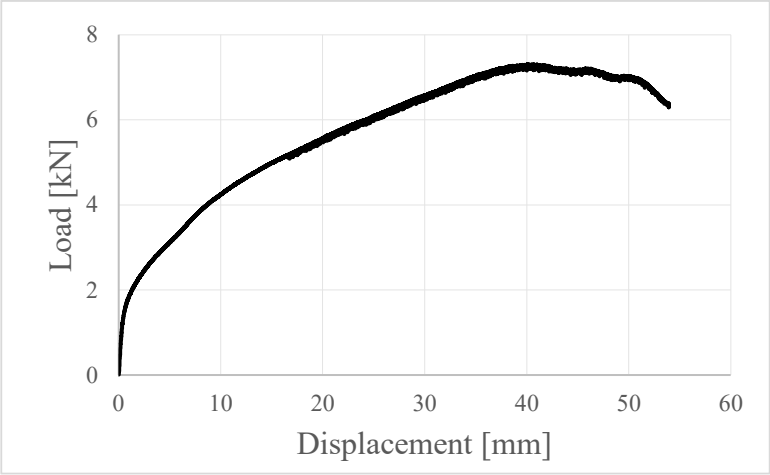

Figure A-48: load-displacement curve of test P-8-S-M-2

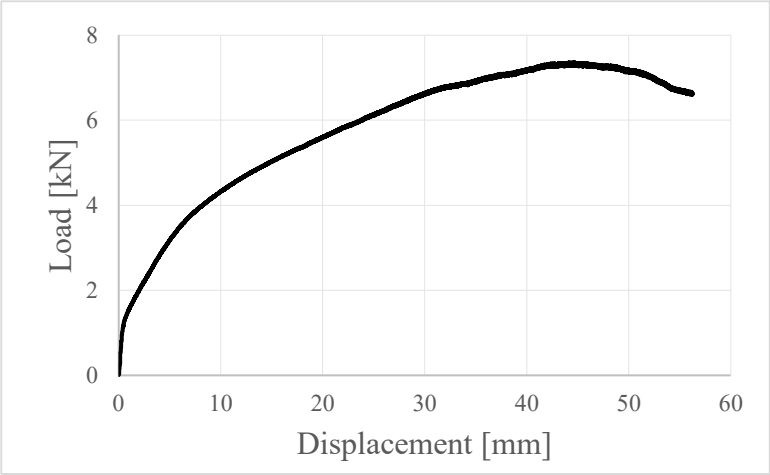

Figure A-49: load-displacement curve of test P-8-S-M-3

A.4.1.2 Cyclic

Table A-16: Mechanical properties of HBS 8 × 80 screws panel-to-panel connections under cyclic shear

Parameter	Unit	P-8-S-C-1	P-8-S-C-2	P-8-S-C-3	Mean	CoV
F_{max}	[kN]	7.09	7.57	7.48	7.38	3.41
$v_{F,max}$	[mm]	42.60	44.39	32.74	39.91	15.73
v_u	[kN]	45.09	51.49	42.99	46.53	9.52
$F_{y,EEEP}$	[mm]	6.10	6.37	6.33	6.27	2.30
$v_{y,EEEP}$	[mm]	6.07	9.92	8.03	8.01	24.02
$k_{e,EEEP}$	[kN/mm]	0.92	0.60	0.74	0.75	21.33
$D_{c,EEEP}$	[-]	7.42	5.19	5.35	5.99	20.80
$F_{y,trilinear}$	[kN]	4.24	4.46	4.41	4.37	2.62
$v_{y,trilinear}$	[mm]	4.06	6.76	5.42	5.41	24.95
$k_{e,trilinear}$	[kN/mm]	1.05	0.66	0.81	0.84	23.11
$D_{c,trilinear}$	[-]	11.11	7.62	7.93	8.89	21.76
ΔF_{1-3}	[%]	3.03	2.35	1.53	2.30	32.58
$v_{eq,1}$	[%]	11.60	14.84	15.28	13.91	14.44
$v_{eq,3}$	[%]	8.29	7.90	11.01	9.07	18.65

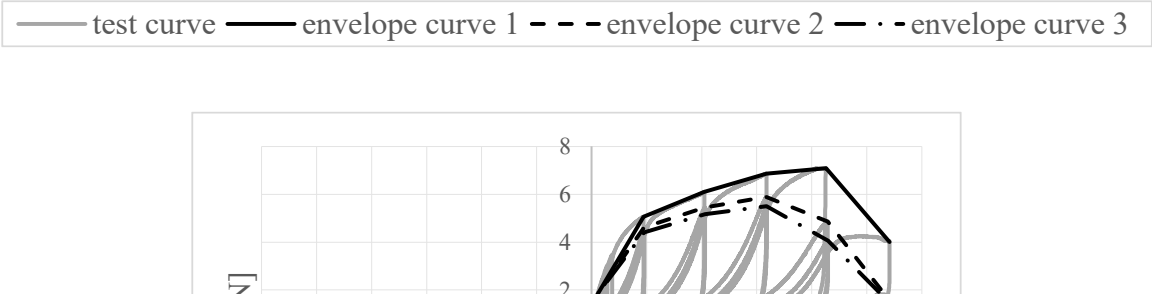

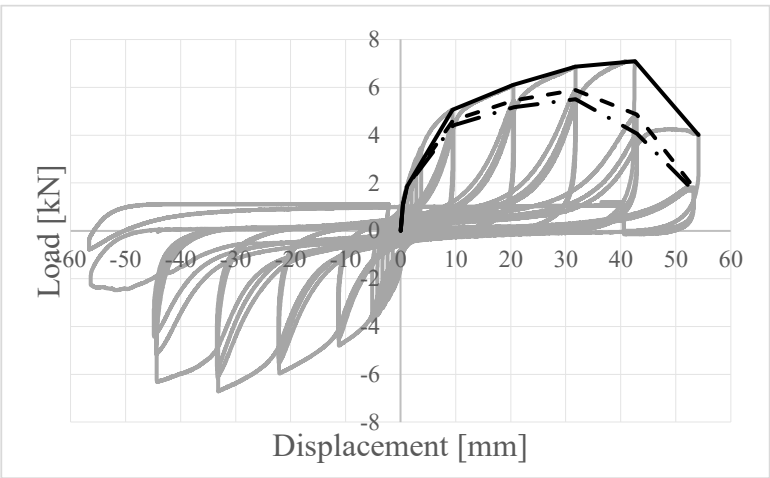

Figure A-50: load-displacement curve of test P-8-S-C-1

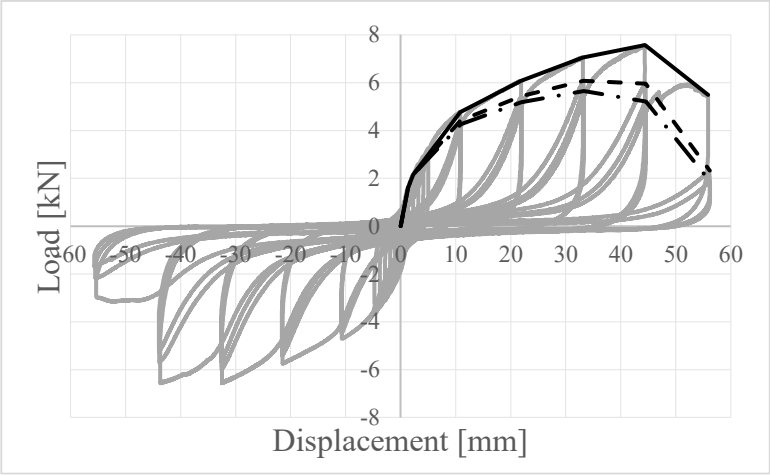

Figure A-51: load-displacement curve of test P-8-S-C-2

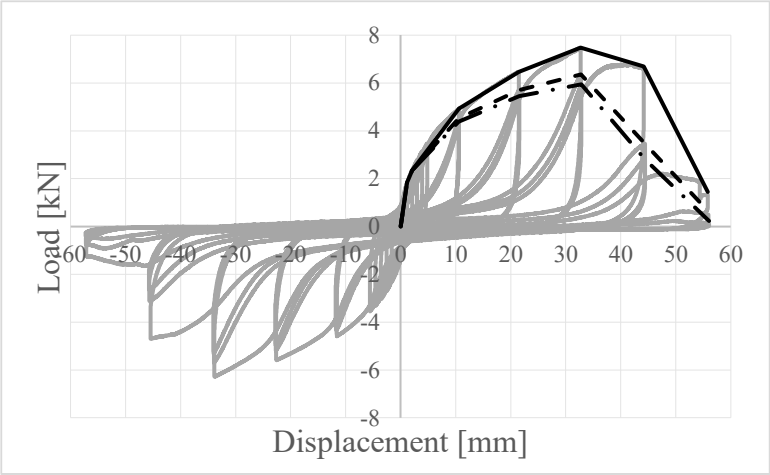

Figure A-52: load-displacement curve of test P-8-S-C-3

A.4.2. HBS 6 × 70 screws under shear

A.4.2.1 Monotonic

Table A-17: Mechanical properties of HBS 6 × 70 screws panel-to-panel connections under monotonic shear

Parameter	Unit	P-6-S-M-1	P-6-S-M-2	P-6-S-M-3	Mean	CoV
F_{max}	[kN]	5.37	5.52	5.95	5.61	5.43
$v_{F,max}$	[mm]	27.80	29.86	30.86	29.51	5.29
v_u	[kN]	45.59	37.73	45.54	42.95	10.52
$F_{y,EEEP}$	[mm]	4.69	4.63	4.97	4.76	3.79
$v_{y,EEEP}$	[mm]	5.82	5.27	3.93	5.01	19.38
$k_{e,EEEP}$	[kN/mm]	0.81	0.88	1.26	0.98	25.03
$D_{m,EEEP}$	[-]	7.83	7.16	11.58	8.86	26.90
$F_{y,trilinear}$	[kN]	3.24	3.08	2.89	3.07	5.76
$v_{y,trilinear}$	[mm]	3.79	3.29	2.08	3.05	28.86
$k_{e,trilinear}$	[kN/mm]	0.86	0.94	1.39	1.06	27.23
$D_{m,trilinear}$	[-]	12.03	11.47	21.93	15.14	38.85

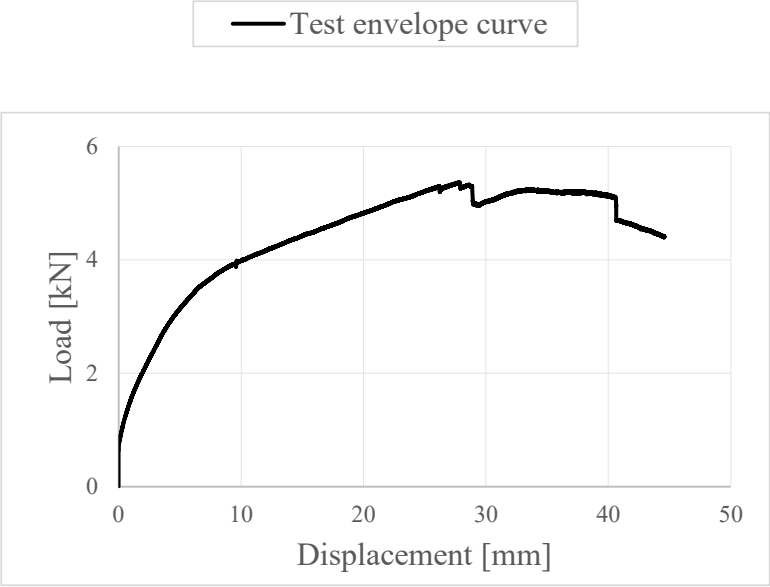

Figure A-53: load-displacement curve of test P-6-S-M-1

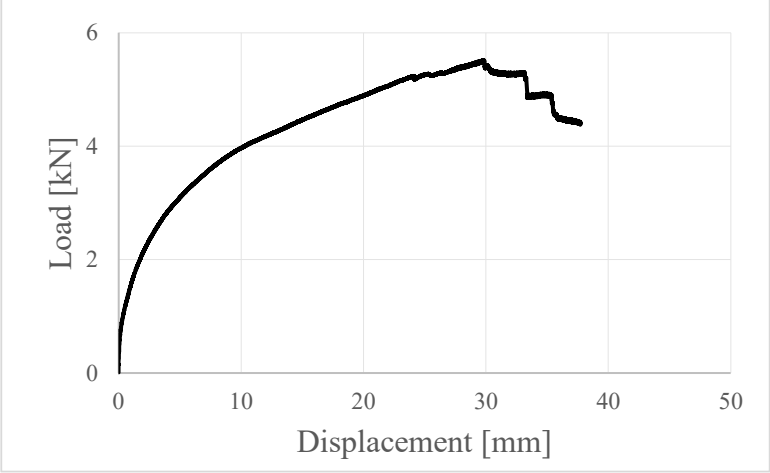

Figure A-54: load-displacement curve of test P-6-S-M-2

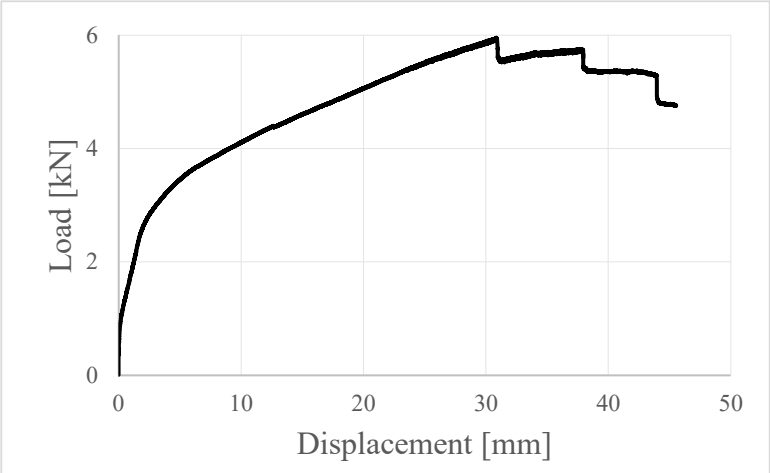

Figure A-55: load-displacement curve of test P-6-S-M-3

A.4.2.2 Cyclic

Table A-18: Mechanical properties of HBS 6 × 70 screws panel-to-panel connections under cyclic shear

Parameter	Unit	P-6-S-C-1	P-6-S-C-2	P-6-S-C-3	Mean	CoV
F_{max}	[kN]	4.55	4.43	4.57	4.52	1.64
$v_{F,max}$	[mm]	16.34	16.70	24.14	19.06	23.10
v_u	[kN]	24.58	23.80	27.07	25.15	6.80
$F_{y,EEEP}$	[mm]	4.04	3.19	3.09	3.44	15.17
$v_{y,EEEP}$	[mm]	6.26	5.30	4.63	5.40	15.20
$k_{e,EEEP}$	[kN/mm]	0.63	0.60	0.67	0.63	5.25
$D_{c,EEEP}$	[-]	3.93	4.49	5.85	4.76	20.79
$F_{y,trilinear}$	[kN]	3.21	3.85	3.92	3.66	10.70
$v_{y,trilinear}$	[mm]	4.95	6.41	5.94	5.77	12.90
$k_{e,trilinear}$	[kN/mm]	0.65	0.60	0.63	0.63	4.12
$D_{c,trilinear}$	[-]	4.96	3.71	4.56	4.41	14.41
ΔF_{1-3}	[%]	0.74	0.66	1.54	0.98	50.00
$v_{eq,1}$	[%]	23.66	22.43	17.69	21.26	14.82
$v_{eq,3}$	[%]	12.52	12.71	10.14	11.79	12.15

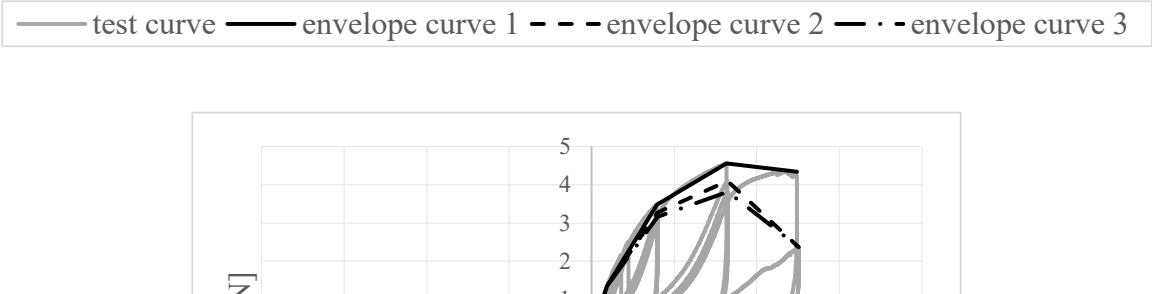

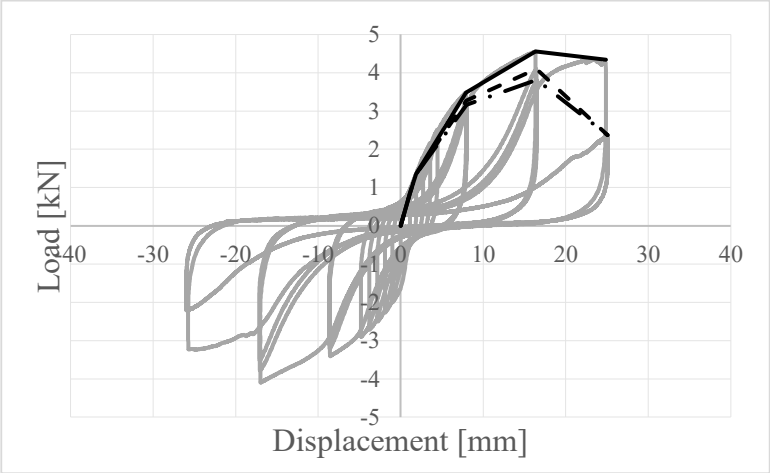

Figure A-56: load-displacement curve of test P-6-S-C-1

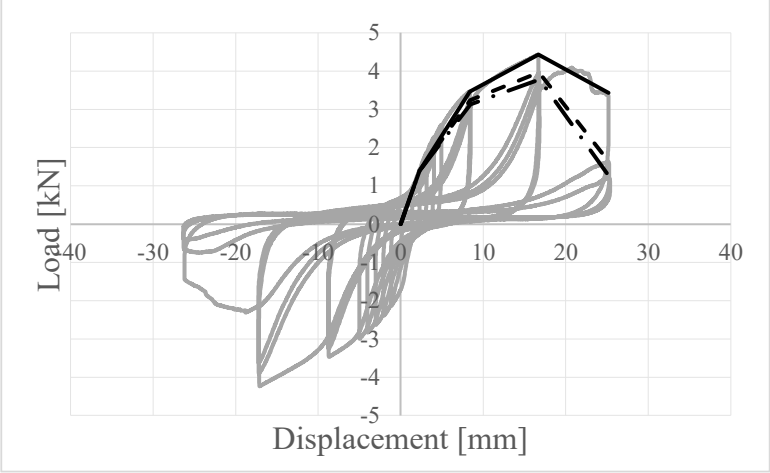

Figure A-57: load-displacement curve of test P-6-S-C-2

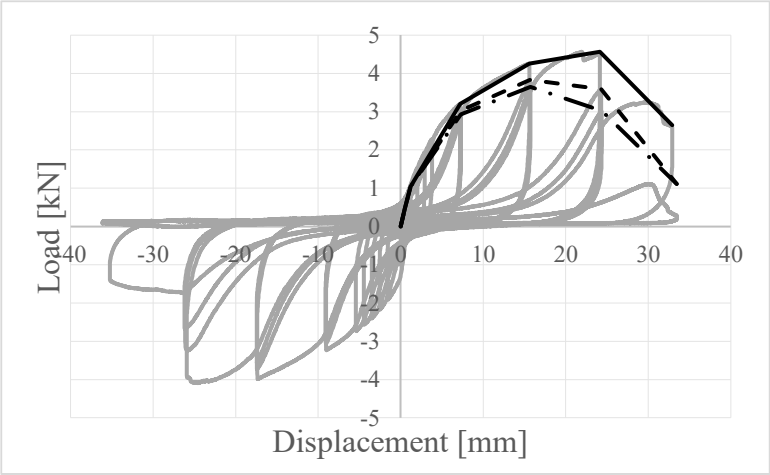

Figure A-58: load-displacement curve of test P-6-S-C-3

A.4.3. Galvanized spiral 3.4 × 63.5 nails under shear

A.4.3.1 Monotonic

Table A-19: Mechanical properties of galvanized spiral nail 3.4 × 63.5 nail panel-to-panel connections under monotonic shear

Parameter	Unit	P-3.4-S-M-1	P-3.4-S-M-2	Mean	CoV
F_{max}	[kN]	2.57	2.58	2.57	0.29
$v_{F,max}$	[mm]	32.97	36.91	34.94	7.98
v_u	[kN]	43.01	53.55	48.28	15.44
$F_{y,EEEP}$	[mm]	2.15	2.13	2.14	0.74
$v_{y,EEEP}$	[mm]	4.27	4.25	4.26	0.31
$k_{e,EEEP}$	[kN/mm]	0.50	0.50	0.50	0.43
$D_{m,EEEP}$	[-]	10.07	12.60	11.34	15.74
$F_{y,trilinear}$	[kN]	1.26	1.13	1.20	7.66
$v_{y,trilinear}$	[mm]	2.36	2.20	2.28	4.98
$k_{e,trilinear}$	[kN/mm]	0.53	0.51	0.52	2.68
$D_{m,trilinear}$	[-]	18.24	24.37	21.30	20.34

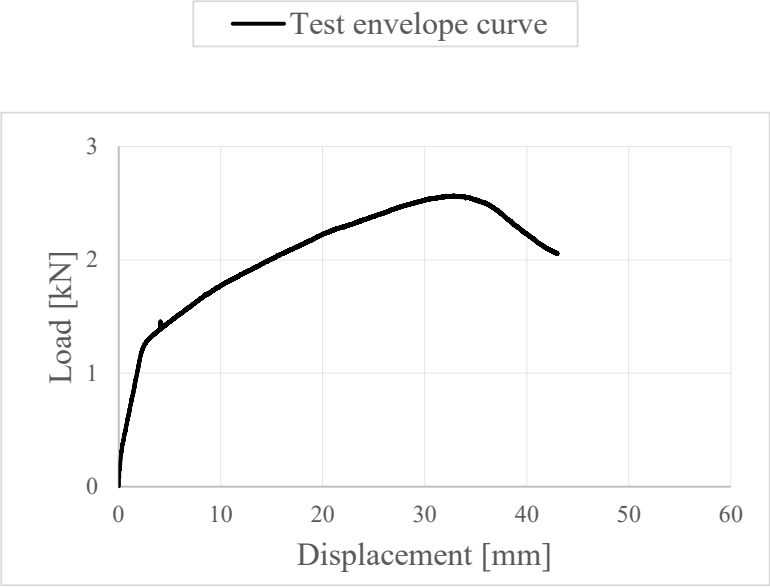

Figure A-59: load-displacement curve of test P-3.4-S-M-1

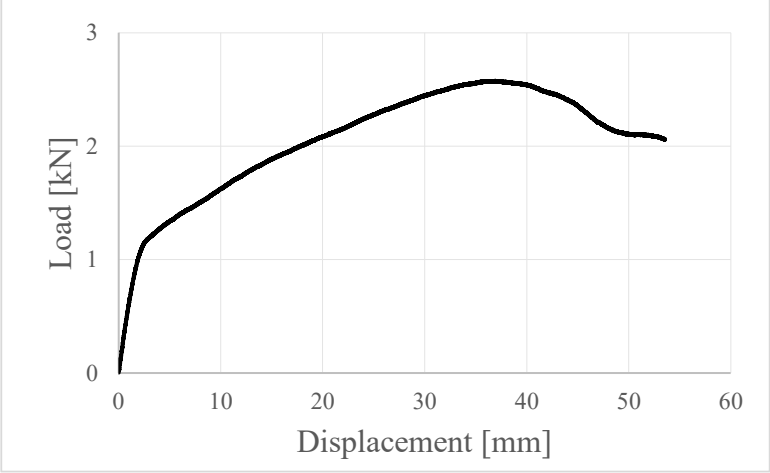

Figure A-60: load-displacement curve of test P-3.4-S-M-2

A.4.3.2 Cyclic

Table A-20: Mechanical properties of galvanized spiral nail 3.4 × 63.5 nail panel-to-panel connections under cyclic shear

Parameter	Unit	P-3.4-S-C-1	P-3.4-S-C-2	P-3.4-S-C-3	Mean	CoV
F_{max}	[kN]	2.27	2.06	2.23	2.19	5.17
$v_{F,max}$	[mm]	19.76	19.46	19.36	19.52	1.07
v_u	[kN]	20.71	22.78	29.73	24.41	19.37
$F_{y,EEEP}$	[mm]	1.77	1.58	2.06	1.80	13.30
$v_{y,EEEP}$	[mm]	3.32	5.37	13.11	7.27	71.04
$k_{e,EEEP}$	[kN/mm]	0.52	0.28	0.15	0.32	58.96
$D_{c,EEEP}$	[-]	6.23	4.24	2.27	4.25	46.66
$F_{y,trilinear}$	[kN]	1.08	1.34	2.07	1.50	34.05
$v_{y,trilinear}$	[mm]	2.00	4.53	13.17	6.57	89.22
$k_{e,trilinear}$	[kN/mm]	0.54	0.30	0.16	0.33	58.72
$D_{c,trilinear}$	[-]	10.38	5.02	2.26	5.89	70.13
ΔF_{1-3}	[%]	1.51	1.18	0.83	1.17	28.90
$v_{eq,1}$	[%]	34.60	26.50	21.26	27.45	24.48
$v_{eq,3}$	[%]	31.48	20.84	18.06	23.46	30.20

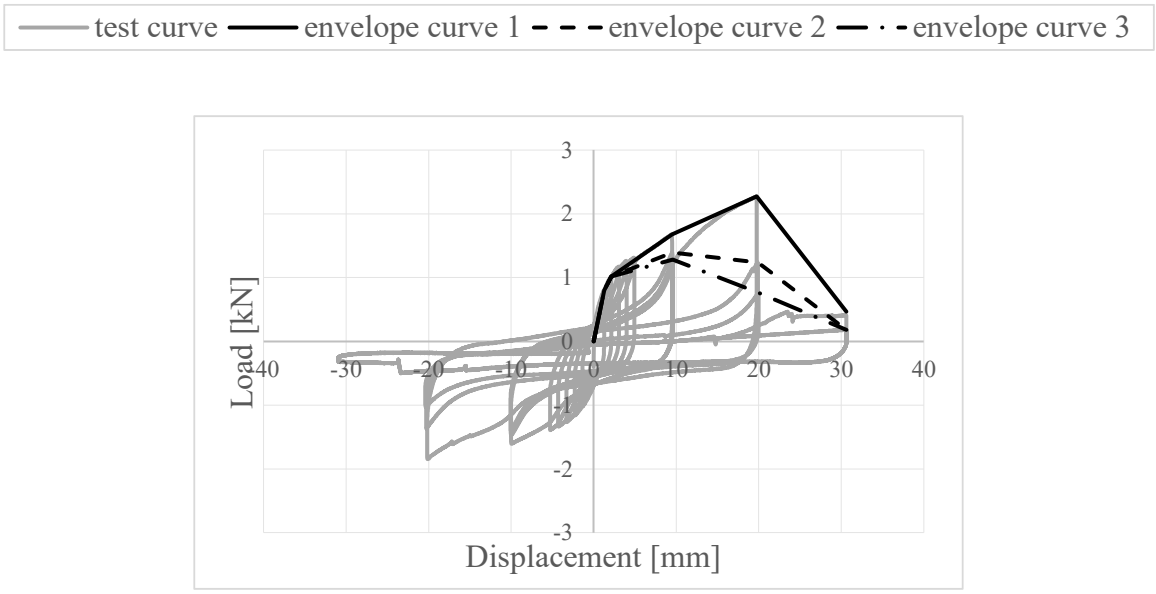

Figure A-61: load-displacement curve of test P-3.4-S-C-1

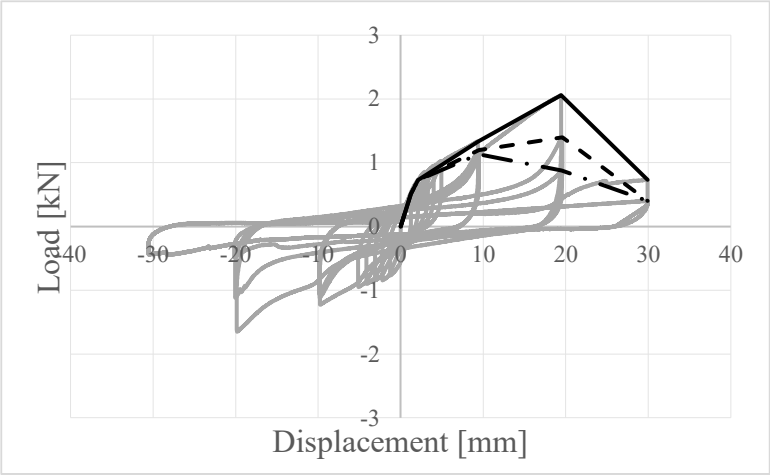

Figure A-62: load-displacement curve of test P-3.4-S-C-2

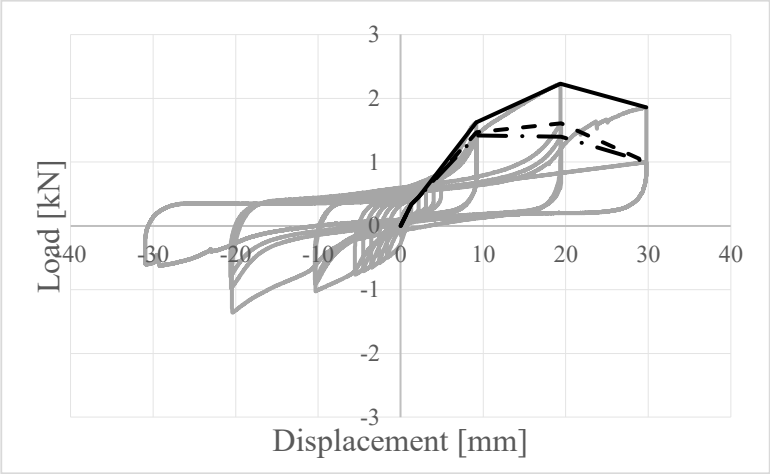

Figure A-63: load-displacement curve of test P-3.4-S-C-3

Appendix B - Details of shearwall tests set-up and mesh sensitivity analysis

B.1. Test set-ups

In this section, the details of shearwall level test-ups and information, outlined in Chapter 6, are presented. Figure A-1 illustrates the test set-up used for a three-panel wall without angle brackets to present the attachments and steel sections, denoted as S_1-S_4. In the case of walls with angle brackets (walls #6-#12), the sliding support, S1, was ignored, while for walls with two panels (#11) and four panels (#12) two and four fitted bolts and top plates, S2, respectively, were used.

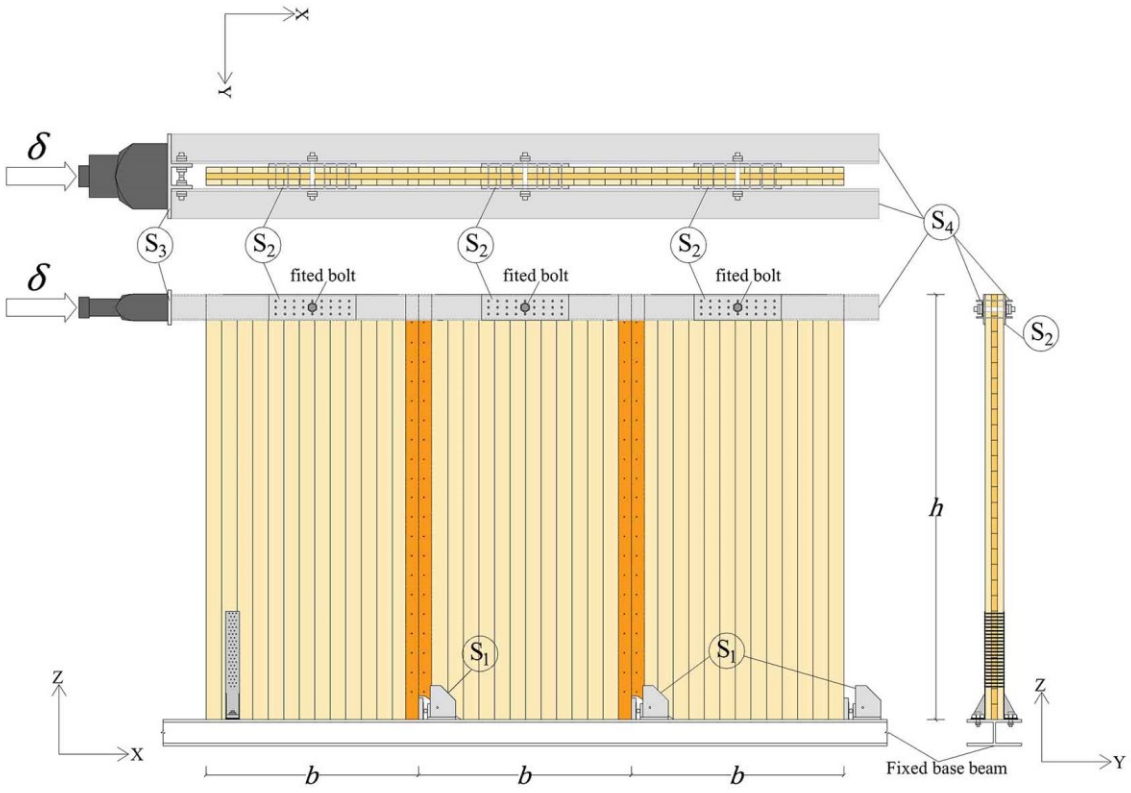

Figure B-1: Test configuration of shearwalls without angle brackets

Figure A-7-Figure B-5 illustrate the details of S_1-S_4.

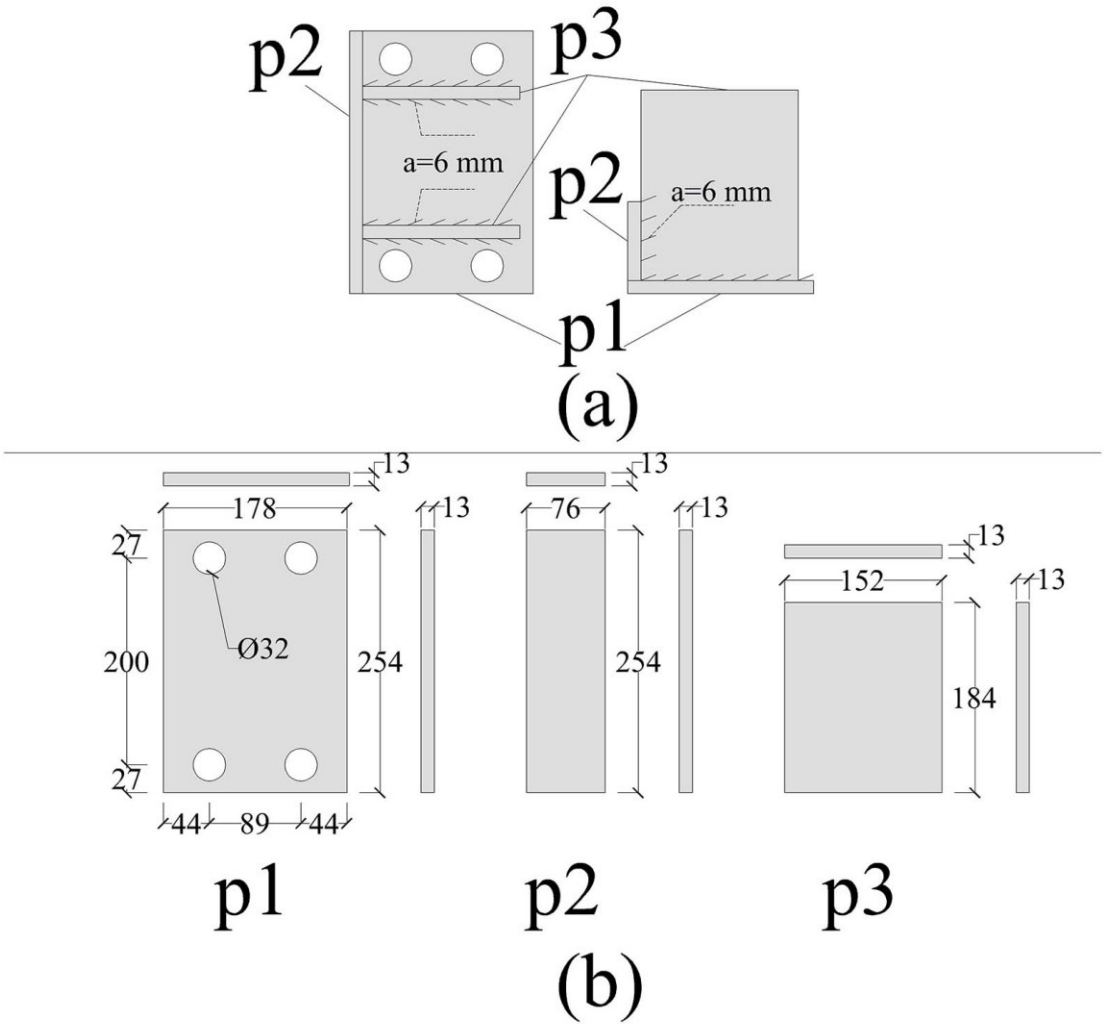

Figure B-2: sliding steel support used in shearwall-level test set-ups (S_1): (a) assembled support and (b) steep plates used in the assembly

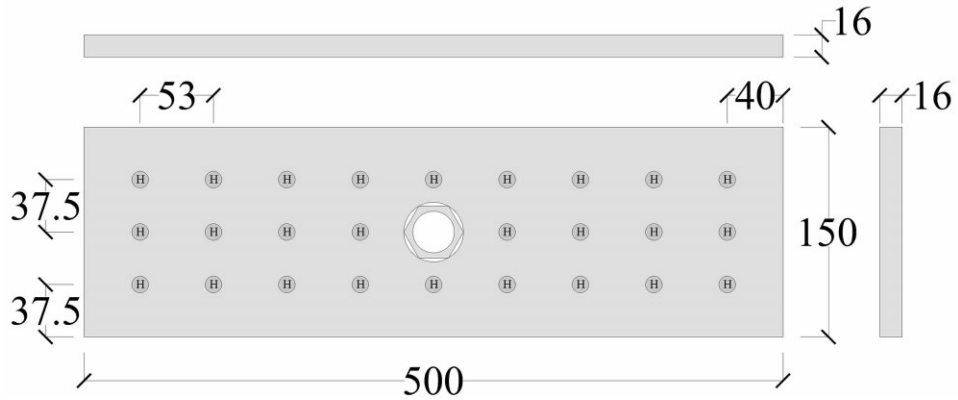

Figure B-3: Top plates used in shearwall-level test set-ups (S_2)

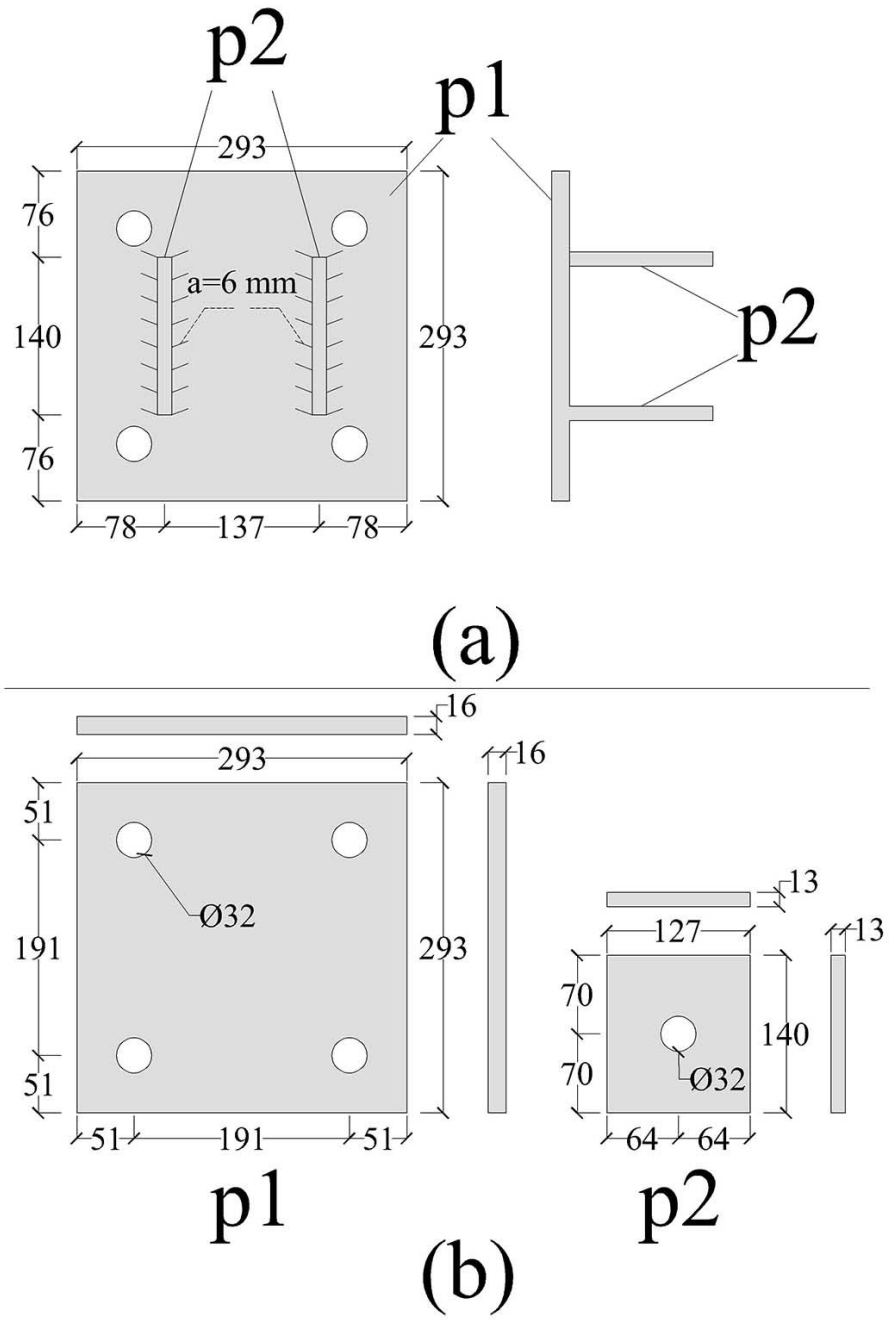

Figure B-4: E-shape steel section used in shearwall-level test set-ups (S_3) : (a) assembled section and (b) steep plates used in the assembly

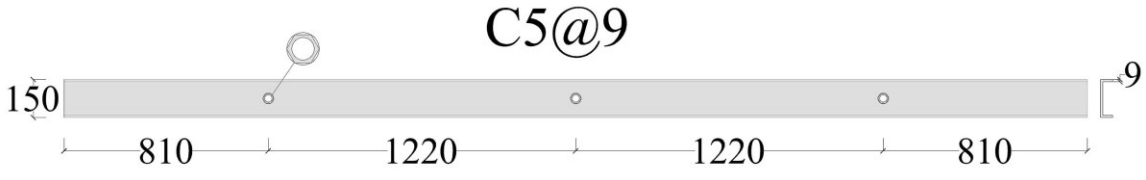

Figure B-5: Steel channels used in shearwall-level test set-ups (S_4)

Figure A-6 shows the denoted names of CLT panels (i.e., P_1-P_8) used in shearwall-level tests: (a) walls #1-#5, (b) walls #6-#10, (c) wall #11, and (d) wall #12. The details of each panel (P_1-P_8), including dimensions and cut sizes, are presented in Figure B-7.

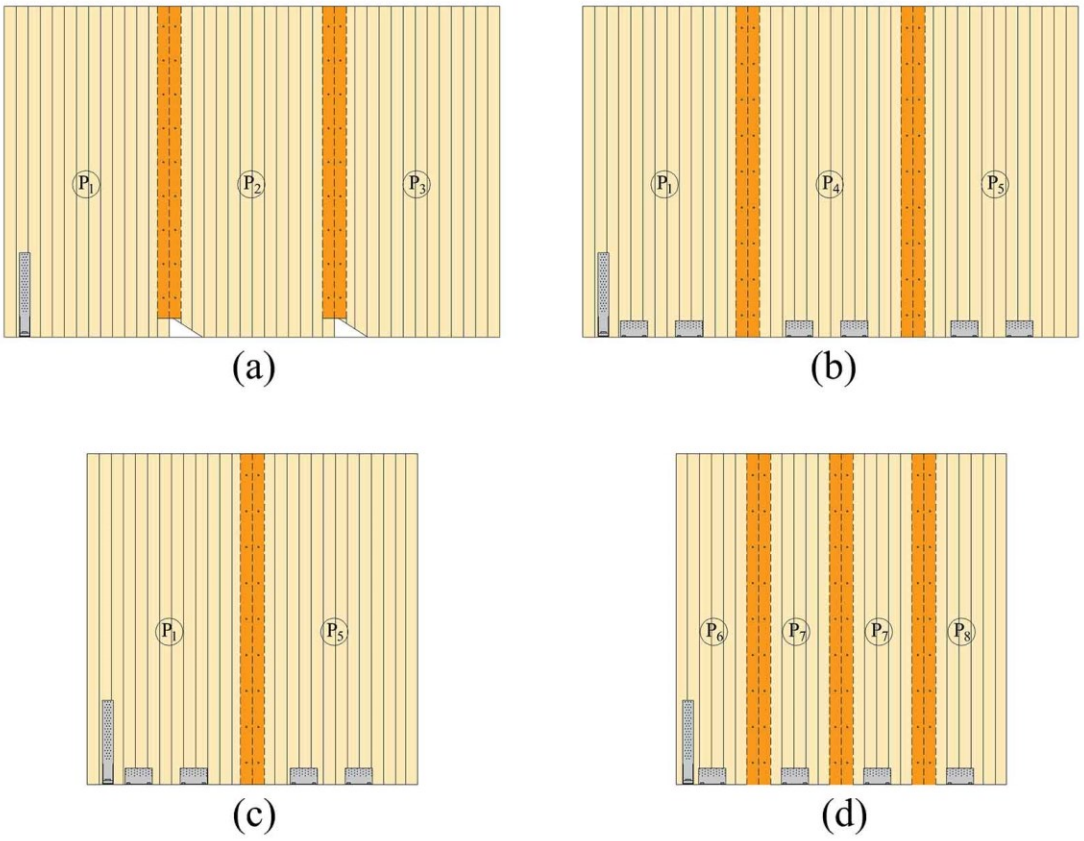

Figure B-6: The names of CLT panels used in shearwall-level tests

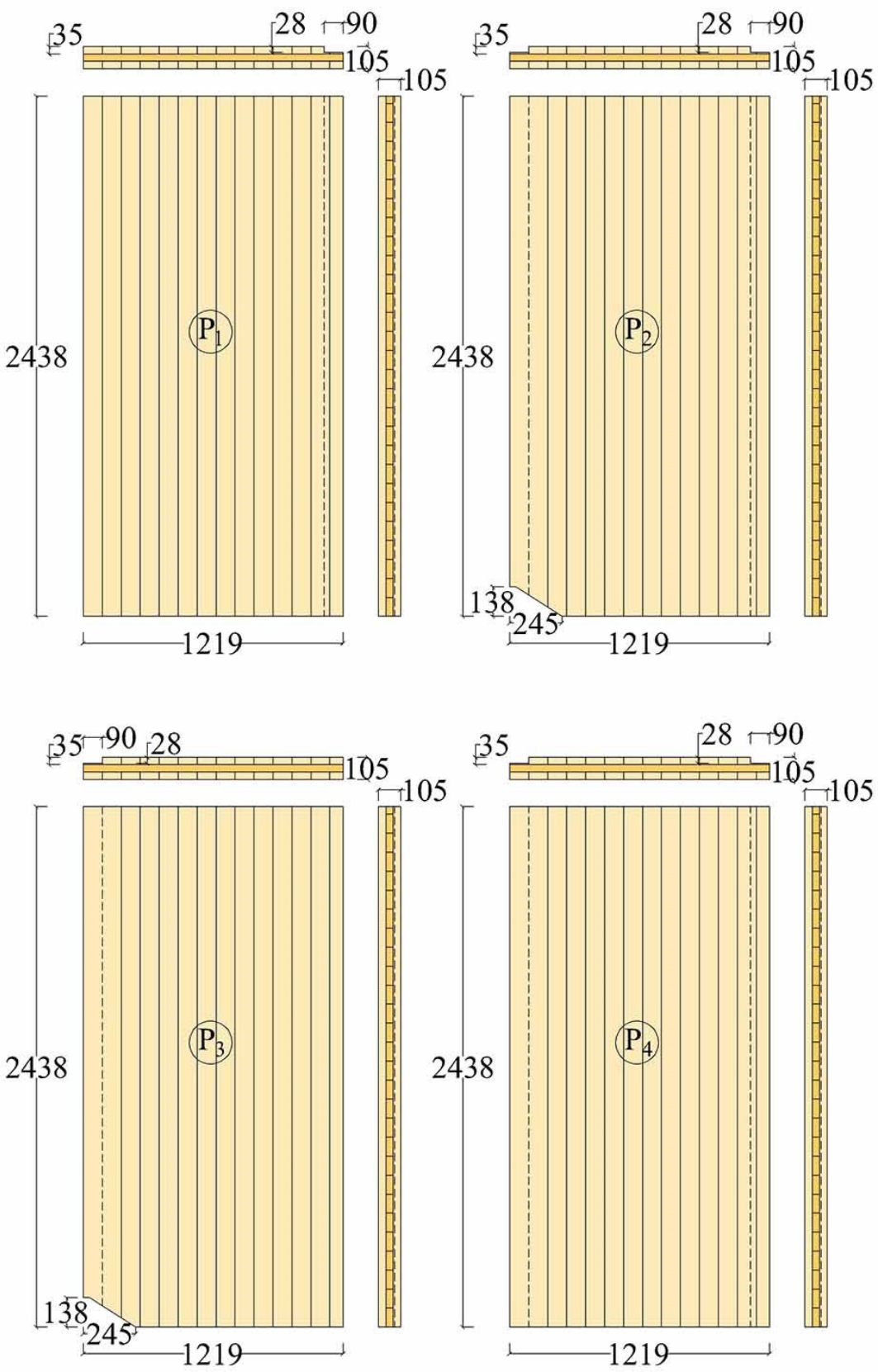
35
28
90
105
105
2438
P1
1219
35
28
90
105
105
2438
P2
138
245
1219
35
90
28
105
105
2438
P3
138
245
1219
35
28
90
105
105
2438
P4
1219

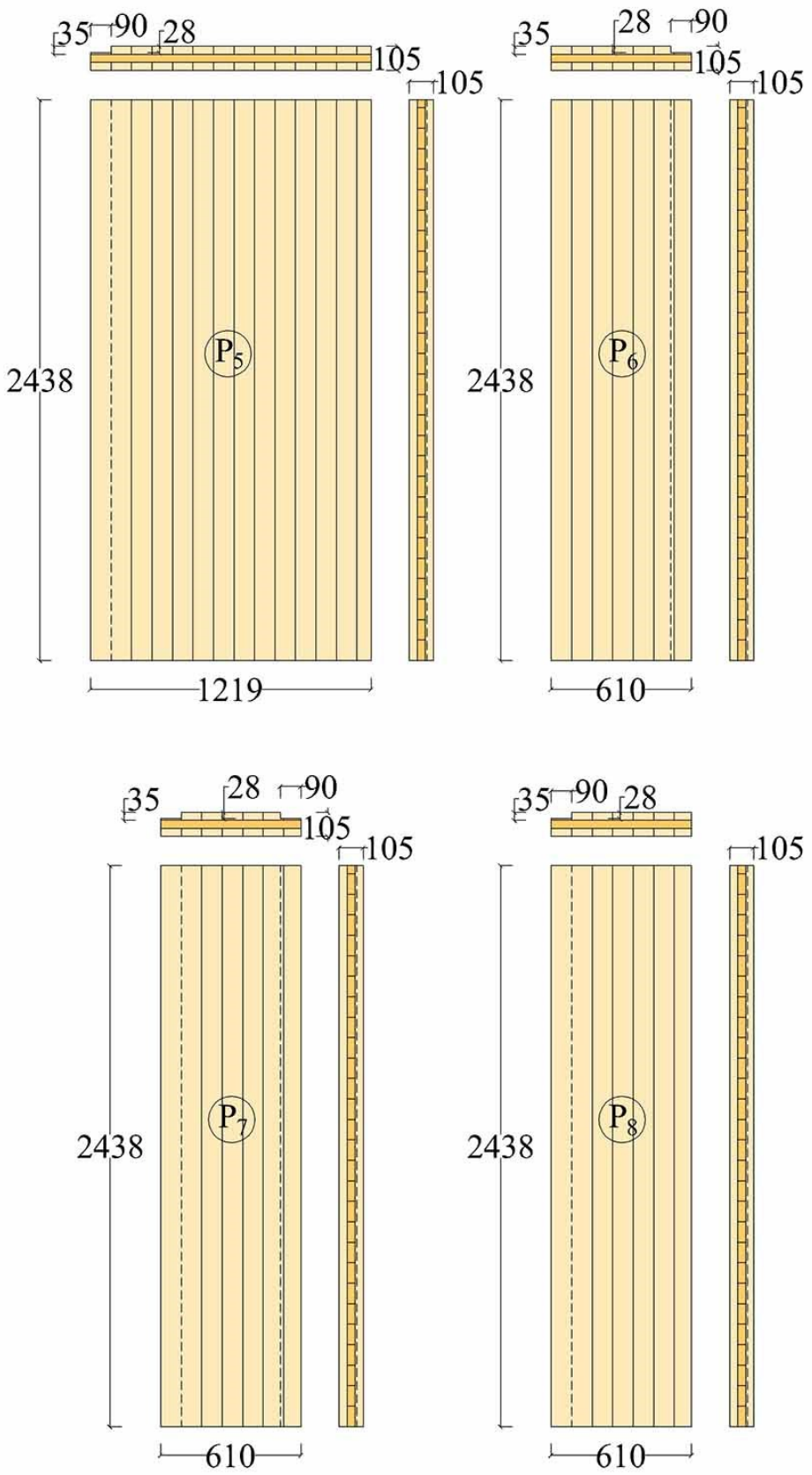

Figure B-7: The details of CLT panels used in shearwall-level tests

B.2. Mesh sensitivity analysis

The purpose of this section is to present the mesh sensitivity analysis to demonstrate the applicability of the 61×61 mm mesh size used in Chapter 7. Figure B-8-to Figure B-12 illustrate the load-displacement curves of wall #1 with mesh size of 61×61 mm versus 49×49 mm, 76×76 mm, 122×122 mm, 203×203 mm, and 244×244 mm, respectively. The perfect match between different mesh sizes indicates the accuracy of the mesh size used. Table B-1 presents the discrepancy between 61×61 mm and other mesh sizes, denoted as ξ. The results indicated a difference of 1.2% for 49×49 mm and 0.7% for 244×244 mm mesh sizes. Although the results showed that mesh size 244×244 mm could also be utilized with high accuracy, 61×61 mm was employed in order to model multiple panel-to-panel connections and the accurate position of the mechanical brackets.

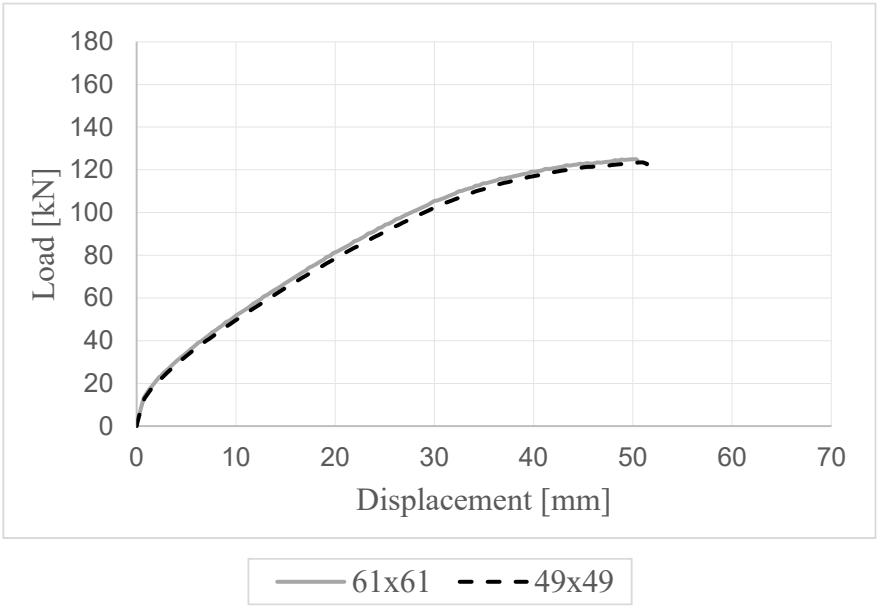

Figure B-8: Load-displacement curves of wall #1 with mesh sizes of 49×49 mm and 61×61 mm

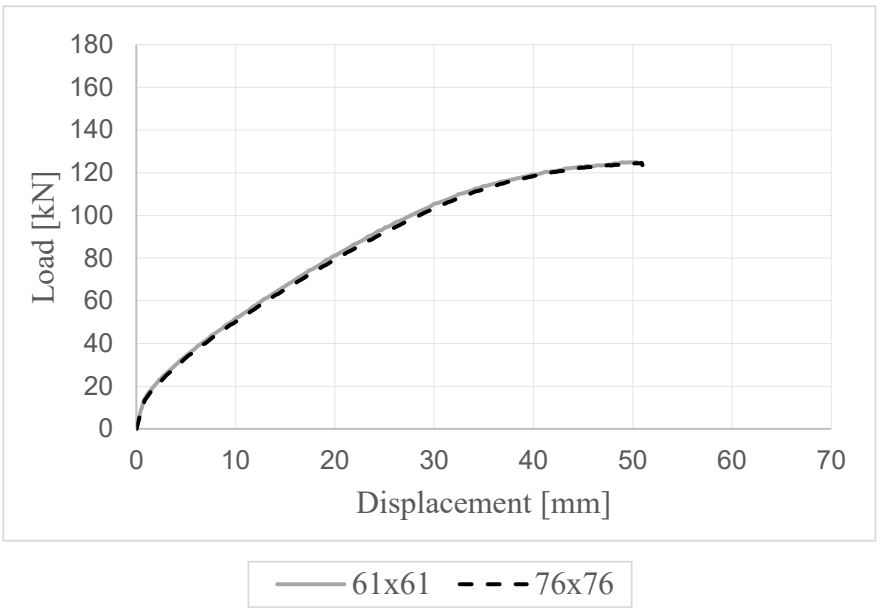

Figure B-9: Load-displacement curves of wall #1 with mesh sizes of 61×61 mm and 76×76 mm

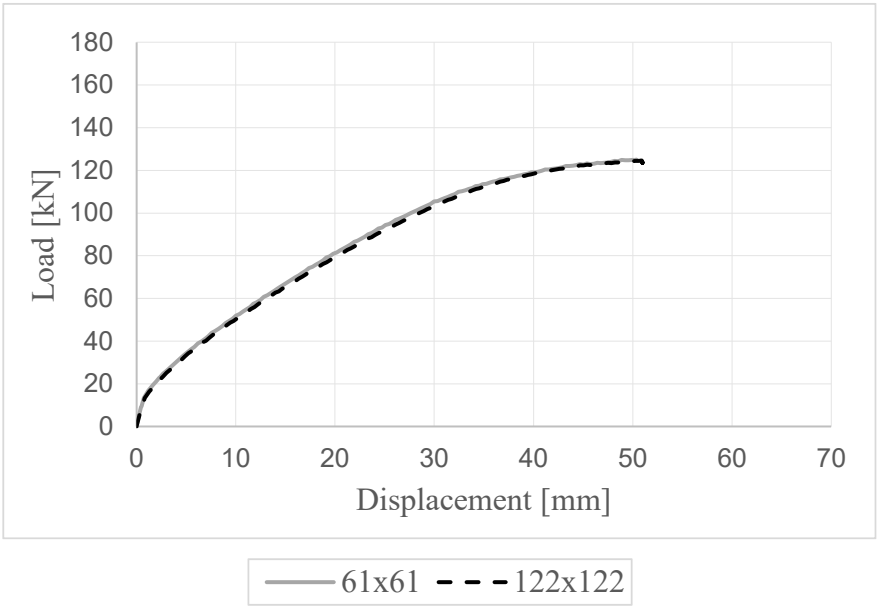

Figure B-10: Load-displacement curves of wall #1 with mesh sizes of 61×61 mm and 122×122 mm

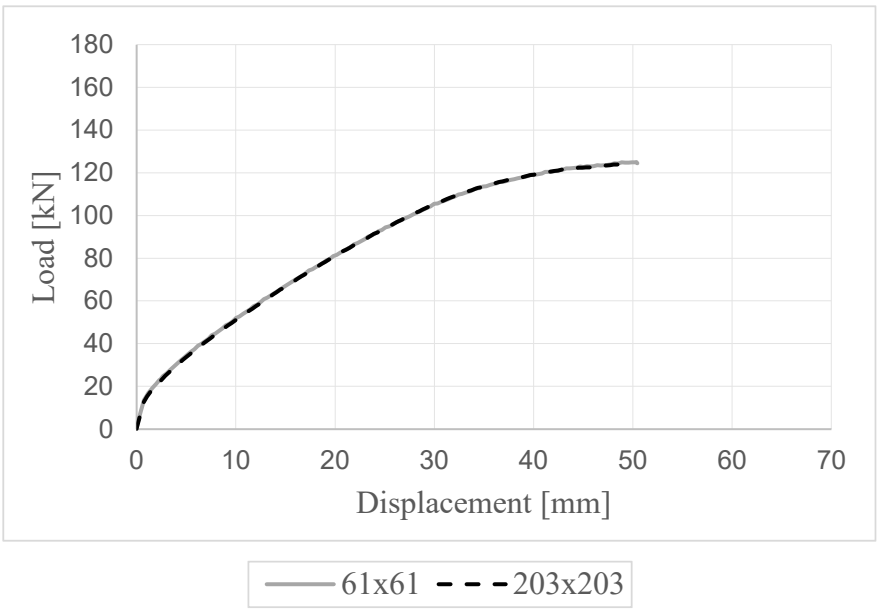

Figure B-11: Load-displacement curves of wall #1 with mesh sizes of 61×61 mm and 203×203 mm

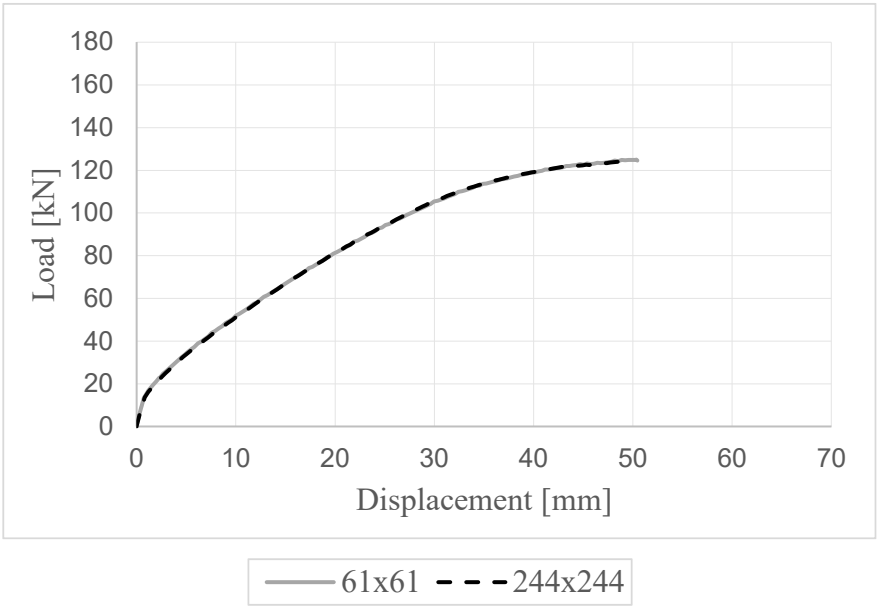

Figure B-12: Load-displacement curves of wall #1 with mesh sizes of 61×61 mm and 244×244 mm

Table B-1: The difference in maximum lateral strength of wall #1 considering various mesh size

Size (mm)	$\mathbf{49 \times 49}$	$\mathbf{76 \times 76}$	$\mathbf{122 \times 122}$	$\mathbf{203 \times 203}$	$\mathbf{244 \times 244}$
$\boldsymbol{\xi}$	1.2%	0.4%	0.4%	0.6%	0.7%

Appendix C - Applicability of interpolation between CP and SW

This section provides the results from various analyses on different CLT shearwall configurations in Intermediate (IN) kinematic mode to demonstrate the applicability of interpolation between proposed expressions for Coupled-panel (CP) and Single-Wall (SW) against the results obtained from expressions for IN available in the literature (Casagrande et al., 2018). Ten different shearwalls were studied by varying the number of panels from three to seven. Each shearwall was analyzed three times by changing the connections configurations and their properties to achieve IN mode very close to either CP or SW or in the middle of two, resulting in a total of thirty analyses. The mechanical properties of connections and configurations are selected based on the experimental tests on connections summarized in Table C-1. Two variables are evaluated, CLT shearwall factored rocking resistance, $R_{w,r}$, and the lateral stiffness due to the rocking K_R. The associated equations can be found in Casagrande et al. (2018)

Table C-1 presents the difference between the interpolation and IN expressions. K_R shows lower difference than $R_{w,r}$, with the highest average of 3.12% difference among the three behaviours. The highest average of difference of 8.12% was achieved for $R_{w,r}$.

Table C-1: The difference in $R_{w,r}$ and K_R between interpolation and IN expressions

Cases	Close to CP		Close to SW		Intermediate	
	$R_{w,r}$	K_R	$R_{w,r}$	K_R	$R_{w,r}$	K_R
1	0.26%	0.43%	12.56%	8.80%	7.42%	0.17%
2	0.02%	0.57%	9.97%	8.37%	3.03%	0.52%
3	0.22%	1.87%	6.83%	5.52%	3.40%	0.78%
4	0.17%	0.43%	3.48%	2.70%	0.35%	1.30%
5	0.73%	1.43%	13.73%	0.33%	6.52%	0.78%
6	0.43%	1.93%	10.51%	0.83%	5.68%	0.32%
7	1.92%	2.76%	12.27%	0.50%	6.91%	0.51%
8	2.88%	3.65%	6.30%	0.58%	0.71%	0.93%
9	0.36%	0.11%	3.75%	2.66%	6.01%	0.49%
10	10.15%	4.88%	1.82%	0.89%	9.17%	0.00%
Average	1.71%	1.81%	8.12%	3.12%	4.92%	0.58%

The results show that interpolation could predict the results reasonably well, even in cases with a high number of panels (e.g., seven). It is noteworthy to mention that the interpolation results provide conservative values in most cases, especially the cases with higher differences, such as 13.73%. The non-conservative results were with less than 3.40% differences in most cases.